J. FARRELL

Hyperbaric Welding of Duplex Stainless Steel Pipelines Offshore

School of Industrial and Manufacturing Science

Ph.D. Thesis

J. FARRELL

Hyperbaric Welding of Duplex Stainless Steel Pipelines Offshore

School of Industrial and Manufacturing Science

Ph.D. Thesis

CRANFIELD UNIVERSITY

School of Industrial and Manufacturing Science

Ph.D. Thesis

1996

J FARRELL

Hyperbaric Welding of Duplex Stainless Steel Pipelines Offshore

Supervisor: Dr J Spurrier

January 1996

ABSTRACT

Three duplex stainless steels (Avesta 2205, Sandvik SAF2507 and Zeron 100) were successfully welded automatically at a range of pressures from 1 to 32bar.

The gas tungsten arc (GTA) welding process was chosen as it allows a high degree of control to be exercised during welding. Initial autogenous bead on plate welds established the effects of pressure on the welding process and allowed the process parameters to be determined for subsequent experiments. Analysis of the effects of pressure on the weld thermal cycle showed that at higher pressures the precipitation of phases deleterious to the weld quality was less likely than at ambient pressure. It was also found that the arc melting efficiency increased as the pressure increased, which was taken into account when the process parameters for the joints were selected.

A V-butt design with a "land" on each side was chosen for the joints to counteract any tendency for the welding arc to wander at higher welding pressures. The root welds were performed using pulsed current welding techniques to overcome the difficulties in achieving consistent penetration that were encountered when welding at lower pressures. It was found that by employing standard welding consumables commonly used for welding duplex steels at ambient pressure satisfactory austenite-ferrite phase balances could be achieved in the weld metal at all pressures. Metallographic examination of the welds showed that the joints did not have any microstructural complications that were related to pressure and mechanical testing revealed that, in terms of impact toughness, the weld metal and heat affected zone (HAZ) performed as well as, if not better than, the parent plate material.

This work shows that welding of duplex stainless steels using the hyperbaric welding method is a viable option for subsea operations up to a depth of at least 320m, automated hyperbaric welding being advantageous at depths greater than 40m.

ACKNOWLEDGEMENTS

I would like to thank my supervisor Dr John Spurrier for his guidance throughout the experimental work and the preparation of this thesis. Many thanks are due to my colleagues from the welding group at Cranfield, particularly Ian Richardson and William Cave without whose patient assistance the welding would have not been possible.

I would also like to thank Matthew and my family for their endless support and encouragement throughout the duration of this work.

DEDICATION

For Mum and Dad.

CONTENTS

LIST OF FIGURES

4.13 The influence of pressure on the weld bead penetration in duplex stainless steels.

4.14 The influence of pressure on the arc melting efficiency in duplex stainless steels.

4.15 Development of sigma phase in Avesta 2205 during isothermal heat treatment at 850°C.

4.16 Development of sigma phase in Sandvik SAF2507 during isothermal heat treatment at 850°C.

4.17 Development of sigma phase in Zeron 100 during isothermal heat treatment at 850°C.

4.18 The influence of heat treatment time at 850°C on the hardness of (a) Avesta 2205, (b) Sandvik SAF2507, (c) Zeron 100 materials.

4.19 The influence of pressure on the heat input required to achieve a satisfactory root weld in the duplex stainless steel joints.

4.20 The influence of pressure on the time spent in the sigma phase forming temperature range for each weld pass for a duplex stainless steel weld.

4.21 The profiles of the Avesta 2205 joints welded at pressures up to 32bars.

4.22 The 1.54kJ/mm heat input root weld of the Avesta 2205 joint welded at 1bar showing the fine grained weld metal.

4.23 Root Detail of the Avesta 2205 joint welded 1bar (heat input, 1.54kJ/mm) showing intergranular porosity between the austenite grains.

4.24 Reheated weld metal in the 1.00kJ/mm heat input Avesta 2205 joint welded at 1bar.

4.25 Fine grained austenite in the reheated weld metal of the 1.00kJ/mm heat input Avesta 2205 joint welded at 1bar.

4.26 The Widmanstätten and acicular structure of the austenite in the reheated weld metal of the 1.00kJ/mm heat input Avesta 2205 joint welded at 1bar.

4.27 Large primary ferrite grains in the Sandvik 22.8.3L weld metal in the cap of the 1.00kJ/mm heat input Avesta 2205 joint welded at 1bar.

4.28 Ferrite growth adjacent to the fusion line of the 1.00kJ/mm heat input Avesta 2205 joint welded at 1bar.

4.29 Detail of the precipitates (chromium nitrides) in the HAZ of the 1.00kJ/mm heat input Avesta 2205 joint welded at 1bar.

4.30 Complete penetration in the 0.27kJ/mm heat input root weld of the Avesta 2205 joint welded at 32bars.

4.31 The fine grained microstructure of the austenite with Widmanstätten sideplates in the 0.27kJ/mm heat input root weld of the Avesta 2205 joint welded at 32bars.

4.32 The reheated weld metal of the 0.66kJ/mm heat input Avesta 2205 joint welded at 32bars showing finer primary ferrite grains than in the joint welded at 1bar.

4.33 The predominantly fine grained acicular structure of the austenite in the reheated weld metal of the 0.66kJ/mm heat input Avesta 2205 joint welded at 32bars.

4.34 Widmanstätten and acicular structure of the austenite in the cap weld metal of the 0.66kJ/mm heat input Avesta 2205 joint welded at 32bars.

4.35 The ferrite growth region in the HAZ of the 0.66kJ/mm heat input Avesta 2205 joint welded at 32bars.

4.36 HAZ detail of the of the 0.66kJ/mm heat input Avesta 2205 weld performed at 32bars showing fewer precipitates than in the joint welded at 1bar.

4.37 Grain boundary precipitates in the 1.30kJ/mm heat input root weld of the Avesta 2205 joint welded at 4bars.

4.38 The profiles of the Sandvik SAF2507 joints welded at pressures up to 32bars.

4.39 Poor root penetration and large grained microstructure in the 1.50kJ/mm heat input root weld of the Sandvik SAF2507 joint welded at 1bar.

4.40 Chromium nitride precipitates in the 1.50kJ/mm heat input root weld of the Sandvik SAF2507 joint welded at 1bar.

4.41 Chromium nitride precipitates in the 1.50kJ/mm heat input root weld of the Sandvik SAF2507 joint welded at 1bar.

4.42 Fine grained structure delineating the weld passes in the reheated weld metal of the 1.00kJ.mm heat input Sandvik SAF2507 joint welded at 1bar.

4.43 Austenite and chromium nitride precipitates in the reheated weld metal of the 1.00kJ.mm heat input Sandvik SAF2507 joint welded at 1bar.

4.44 Sandvik 25.10.4L weld metal at the cap of the 1.00kJ.mm heat input Sandvik SAF2507 joint welded at 1bar.

4.45 Austenite formation in the cap weld metal of the 1.00kJ.mm heat input Sandvik SAF2507 joint welded at 1bar.

4.46 Significant chromium nitride precipitation in the HAZ of the 1.00kJ.mm heat input Sandvik SAF2507 joint welded at 1bar.

4.47 Complete penetration at the 0.34kJ/mm heat input root weld of the Sandvik SAF2507 joint welded at 32bars.

4.48 Fine grained microstructure free of defects in the 0.34kJ/mm heat input root weld of the Sandvik SAF2507 joint welded at 32bars.

4.49 Weld passes delineated by the fine grained structure in the reheated weld metal of the 0.67kJ/mm heat input Sandvik SAF2507 joint welded at 32bars.

4.50 Fine austenite grains formed intragranularly in the reheated weld metal of the 0.67kJ/mm heat input Sandvik SAF2507 joint welded at 32bars.

4.51 Sandvik 25.10.4L weld metal in the cap of the 0.67kJ/mm heat input Sandvik SAF2507 joint welded at 32bars.

4.52 Detail of the Sandvik 25.10.4L weld metal in the cap of the 0.67kJ/mm heat input Sandvik SAF2507 joint welded at 32bars.

4.53 Chromium nitride formation in the HAZ of the 0.67kJ/mm heat input Sandvik SAF2507 joint welded at 32bars, despite a fast cooling rate.

4.54 Chromium nitride precipitates in the HAZ around the cap of the 0.75kJ/mm heat input Sandvik SAF2507 joint welded at 16bars.

4.55 The profiles of the Zeron 100 joints welded at pressures up to 32bars.

4.56 Poor joint fit up and lack of fusion in the 1.32kJ/mm heat input root weld of the Zeron 100 joint welded at 1bar.

4.57 Widmanstätten and acicular austenite in the 1.32kJ/mm heat input root weld of the Zeron 100 joint welded at 1bar.

4.58 Fine grained austenite and coarser ferrite delineating the weld passes in the reheated weld metal of the 1.02kJ/mm heat input Zeron 100 joint welded at 1bar.

4.59 Austenite formation predominantly at the primary ferrite grain boundaries in the cap weld metal of the 1.02kJ/mm heat input Zeron 100 joint welded at 1bar.

4.60 Detail of austenite in the form of Widmanstätten side plates in the cap of the 1.02kJ/mm heat input Zeron 100 joint welded at 1bar.

4.61 Chromium nitride precipitates in the HAZ of the 1.02kJ/mm heat input Zeron 100 joint welded at 1bar.

4.62 Chromium nitride precipitates and evidence of sigma phase formation at the grain boundaries in the HAZ of the 1.02kJ/mm heat input Zeron 100 joint welded at 1bar.

4.63 Complete penetration in the root of the 0.27kJ/mm heat input root weld Zeron 100 joint welded at 32bars.

4.64 Fine austenite grains within a ferrite matrix in the 0.27kJ/mm heat input root weld of the Zeron 100 joint welded at 32bars.

4.65 Austenite forming as fin grains rather than as Widmanstätten side plates in the reheated weld metal of the 0.27kJ/mm heat input Zeron 100 joint welded at 32bars.

LIST OF TABLES

4.3 The arc stabilities and arc voltages for the initial autogenous bead on plate welds on Zeron 100.

4.4 The partition coefficients for the parent plate and autogenous weld metal of the three materials.

4.5 The hardness survey results for the Sandvik 22.8.3L (Avesta 2205) weld metals.

4.6 The hardness survey results for the Sandvik 25.10.4L (Sandvik SAF2507) weld metals.

4.7 The hardness survey results for the Metrode Zeron 100X (Zeron 1005) weld metals.

4.8 The hardness survey results of the Avesta 2205 welds.

4.9 The hardness survey results of the Sandvik SAF2507 welds.

4.10 The hardness survey results of the Zeron 100 welds.

1. INTRODUCTION

1. Introduction

The aim of this work was to develop satisfactory hyperbaric welding processes and procedures for achieving high quality, reproducible welds in duplex stainless steel pipes. Such pipes are finding increased usage in subsea engineering, particularly for the transportation of sour products and are predicted to become more widely used in the future.

Stainless steels are used in the offshore industry because of their improved corrosion resistance compared with structural steels, particularly for the transportation of sour gas or oil. Current duplex stainless steels characteristically contain 4.5-7.5% nickel, 20-25% chromium and low levels of carbon. They typically have a two phase ferritic-austenitic microstructure. Their strength is provided by the solution hardened ferrite matrix and fine grain size; during manufacture the heat treatment is controlled to ensure that the fine grain size is maintained. Standard duplex and super duplex steels cover a range of microstructures, the properties of these alloys depending mainly on the balance between the two phases. Any form of heat treatment, including weld thermal cycles, influences the morphology of these steels and will influence the mechanical and corrosion properties of the heat affected zone in welded joints.

Normal practice for the welding of subsea pipelines is the hyperbaric method. This involves surrounding the weld area with a waterproof habitat from which the water is evacuated by filling the habitat with gas that is maintained in hydrostatic equilibrium with the water outside. The pressure of the gas in the chamber is equivalent to one atmosphere for every 10 metres that the welding site is below the surface. Environmental pressure affects the characteristics of all arc welding procedures, particularly arc stability and thermal efficiency. In addition to this the thermal conductivity of the gas in the habitat increases as the pressure is increased, thus resulting in enhanced cooling rates for the weld metal and heat affected zone.

Consequently it was not possible to predict whether the parameters used to successfully weld duplex stainless steels at one atmosphere would produce satisfactory welds at higher pressures. Therefore, it was necessary to determine the effects of pressure on the welding procedure and the microstructure and properties of duplex stainless steels in order to determine the correct welding parameters.

2. LITERATURE SURVEY

2. Literature Review

2.1 Introduction

In order to appreciate the problems that may be encountered in the hyperbaric welding of duplex stainless steels an understanding of both the hyperbaric welding process and the microstructure and properties of duplex stainless steels must be reached. This literature survey aims to review the influence of pressure upon the arc welding process with particular attention being paid to the gas tungsten arc welding process. Duplex stainless steels have properties which are highly sensitive to their microstructure, as a result particular attention will be paid to the microstructure and any process, such as welding, which influences it.

2.2 The Gas Tungsten Arc Welding Process

Gas tungsten arc welding relies upon the arc generated between a non-consumable electrode and the workpiece to produce the energy required for fusion. The arc and the workpiece are protected by an inert shielding gas. Filler metal may or may not be added to the fused material. This process is highly controllable, the process parameters being determined by several mechanisms. A general discussion of the basic physical mechanisms occurring in the arc will now be presented, followed by a summary of the main arc process variables.

2.2.1 The Gas Tungsten Welding Arc

2.2.1.1 The Structure of the Gas Tungsten Arc

The physics of the GTA welding arc has been covered in great detail by others[1,2], but a brief description of its basic structure and properties will now be given.

An arc is generated by a flow of electrical current between two electrodes in a gas or vapour. This requires removal of electrons from the material of one electrode, conduction through the ionised gas and absorption at the opposite electrode. In the case of the gas tungsten arc, the negative electrode or cathode is usually a tungsten rod with its end ground to a point, the positive electrode is a metal surface and the gaseous conductor is typically a noble gas, such as argon.

The electric welding arc can be divided into three distinct regions: the cathode fall zone, the arc column and the anode fall zone. The cathode fall region extends out from the tungsten cathode surface to a distance of $\approx 10^{-6}$m. The small size of this zone has limited diagnostic studies although theoretical models give approximate descriptions of the mechanisms occurring in this region. In the cathode fall zone electrons are emitted from the electrode due to the high electric field strength (by field emission) or the high temperature (thermal emission). In welding electrodes the predominant mechanism is through thermal emission. The high temperature is maintained by positive ions colliding with the electrode and their kinetic energy being converted to heat energy. The anode fall zone is the region of the arc separating the anode surface from the plasma column. In the anode fall zone the electrons are accelerated towards the positively charged anode where heat is produced as they give up their kinetic energy. Both the anode and the cathode fall zones are typified by their high electric field strengths and high thermal energies.

The arc column extends from the cathode fall zone to the anode fall zone. As the arc column has low electric field strength, the mean free path of the charged particles is too short to produce ionising collisions. As a result the production of charge carriers is by thermal ionisation. The minimum arc plasma temperature required to maintain sufficient ionisation of the shielding gas is around 10,000°C in GTAW arcs. Above this temperature the degree of ionisation increases rapidly with increasing temperature. Most of the current is carried by electrons because of their high mobility: ions only account for 0.4% and 1.2% of the current carrying capacity in argon and helium arcs respectively. As the arc column is electrically neutral, electrons are continually fed into the welding arc by the external welding power supply circuit. The arc column is constricted due the interaction of the arc current with its self-induced magnetic field giving the arc a property known as stiffness, the name reflecting its ability to resist deflection.

2.2.1.2 Arc Initiation

There are several methods of starting the welding arc. The simplest of these is the touch strike mechanism. Touch striking is possible in both manual and automatic welding. The electrode is brought into contact with the workpiece and then withdrawn rapidly; the short circuit heats the electrode sufficiently to allow thermionic emission to start when the electrode is withdrawn. In manual welding this method depends upon the skill of the operator to avoid contamination and overheating of the electrode.

Programmed touch striking overcomes these problems. In this method, once a short circuit occurs the system allows a small current to flow. As the electrode is withdrawn the subsequent increase in arc voltage is monitored and the main current supply is turned on.

Initiation can also be performed by causing a spark to jump from the cathode to the anode. Very large d.c. voltages are required to initiate the arc in this way, so this method is restricted to automatic operating systems to protect the welder from the danger of electrocution. High frequency, high voltage arc initiation can also be used and is not dangerous to the operator. This method may produce inconsistent results depending on the compatibility of the power supply and the striking system. Additionally the high frequencies may interfere with radio waves and the mains electricity, which in turn may affect any electronic equipment used in the welding environment[3].

2.2.2 GTAW Process Variables

2.2.2.1 Heat Input or Process Power

Most commonly the heat input of a weld is expressed as the amount of heat supplied to the weld per unit length and is defined as:-

Equation 2.1

$$q = \eta \frac{V * I}{v}$$

where:-

V is the arc voltage

I is the welding current

v is the weld speed.

η is the arc efficiency which takes into account any energy losses from the arc column due to convection or conduction

For GTAW, η is usually in the range 0.2-0.5. When a heat input is quoted in the literature the efficiency term is generally ignored.

discontinuous weld beads[3]. Decreasing the arc angle increases the arc voltage. This is most likely due to plasma climb, where the arc length increases as the arc reaches further up the conical section of the electrode tip[7].

2.2.2.6 Shielding Gas

The primary requirements for a shielding gas are to sustain a stable arc and to protect both the tungsten electrode and the weld pool from contamination by the surrounding atmosphere[3,8]. In order to meet the first requirement, the ionisation potential of the gas must be sufficiently low so that the arc can be struck and maintained at a reasonably low arc voltage. Secondly, the thermal conductivity must not be high as this causes the arc column to contract resulting in loss of stability.

In addition to the criteria mentioned above, a shielding gas can also be used to control the weld bead profile and the weld mechanical properties. The penetration and the fusion area can be controlled by choosing the gas according to the voltage required to maintain the arc, i.e. controlling the heat input to the weld[3,9]. Also, a gas containing reducing or oxidising elements may be utilised depending upon the requirements of the material being welded.

The properties of the common constituents of the shielding gases used for GTAW have been discussed by others[3,8,9]. A summary of their key properties is presented.

Argon is an inert monatomic gas, which produces an easily struck and stable arc due to its low ionisation potential and low thermal conductivity.

Helium is a low density, inert, monatomic gas which requires a higher arc voltage than an argon arc of similar arc length and current due to its higher thermal conductivity and ionisation potential. Helium is more expensive than argon; however, the higher welding speeds that can be obtained, due to its producing a hotter burning arc can compensate for this in some cases. Pure helium is not used commonly; it is usually employed in a mixture with argon to obtain a gas with a combination of the shielding properties.

Hydrogen is a slightly reducing gas, which when added to argon or helium increases the arc voltage and hence the heat input of the arc. Gas mixtures containing hydrogen produce a cleaner weld due to their reducing nature. Hydrogen additions are not recommended for welding of high alloy steels because of the risk of hydrogen cracking.

Nitrogen is an unreactive, diatomic gas which dissociates in the arc. When it re-associates at the workpiece it produces more heat energy than a monatomic gas, making it beneficial for the welding of high thermal conductivity materials. It is not recommended for use in ferritic materials where it may result in porosity.

The properties of these shielding gas constituents are shown in Table 2.1.

2.3 Underwater Welding Processes

This research project used the GTAW process in a hyperbaric welding environment. Before the effects of pressure on the GTAW process are discussed, the various means of welding underwater will be reviewed. A brief review of the welding processes used in a hyperbaric environment will also be presented.

The simplest method of underwater welding is wet welding using the manual metal arc process (MMA). In MMA welding the arc is maintained between a coated consumable "stick" electrode and the workpiece, the shielding being provided by the gas and slag produced as the coating decomposes. The presence of water may have several negative effects on both the process and the weld material's performance. A poor arc may be obtained from the high cooling rates encountered at the edges of the arc due to the presence of water. Additionally, the cooling rate may result in non uniform bead shape and regions of hardness in the weld metal and heat affected zone[10]. The inexhaustible supply of hydrogen from the dissociation of the water and the high cooling rates encountered may help to trap hydrogen in the weld metal which may lead to hydrogen cracking. Porosity may also occur, which although it may not be a problem in itself, may hide other defects during non destructive examination of the weld[11].

The problems associated with wet welding can be overcome by welding in a dry environment. In one atmosphere welding the weld process is as simple as for non underwater welding. To perform one atmosphere welds a pressure chamber is constructed around the area to be welded and the water is evacuated using pressurised gas which is then returned to atmospheric pressure after the chamber is sealed. The chamber has to be of robust construction in order to withstand the pressure differential between the surrounding water and the gas in the chamber. The construction of the chamber also becomes further complicated due to the requirement that the diver must be able to access the chamber without encountering pressures above one atmosphere. Despite the advantage of the welding process being

relatively simple in the one atmosphere environment, the forward planning and the high cost of this type of welding limit its use to projects where the requirements are known well in advance.

A simpler alternative to one atmosphere welding from an engineering viewpoint is dry hyperbaric welding. In this case the area to be welded is surrounded by a chamber from which the water is evacuated by filling it with a gas at a slightly higher pressure than the surrounding water. Usually the bottom of the chamber is left open to the sea which allows easy access by the welders. However, the increased pressure does affect the arc welding performance and metallurgical properties, which in turn influence the procedure chosen at different depths.

2.3.1 Hyperbaric Welding Processes

2.3.1.1 Manual Metal Arc Welding

The most widely used process for hyperbaric welding is manual metal arc welding[11]. Its stability and hence its suitability, is determined mainly by the composition of the electrode flux coating, basic electrodes giving the best performance at elevated welding pressures. As with wet MMA welding, the dissolution of hydrogen in the weld metal and HAZ is a problem. This may be exaggerated by the decomposition of the flux if the electrodes are stored in the humid atmosphere of the hyperbaric chamber. This problem can be overcome and consistently good welds can be obtained by correct storage of the electrodes. An alternative to the MMA process is the flux cored process, which instead of a stick electrode, employs a continuous hollow wire filled with a flux, and so removes the inconvenience of the frequent need to change the electrode as in MMA. Problems with insufficient shielding encountered at higher pressures can be alleviated by the use of additional gas shielding.

2.3.1.2 Gas Metal Arc Welding (GMAW)

GMA welding, where the arc is maintained between a consumable wire electrode and the workpiece, has become more controllable at high pressure since the development of transistor based power supplies, and since it does not require cleaning of the weld between passes it can be employed as an automatic process. Problems originally encountered with arc stability can now be overcome by close control of the power supply characteristics. The welding consumable diameter must be limited as larger diameters may result in arc instability. Reduction in the concentration of the active gas elements directly in

proportion with the increase in pressure reduces the tendency for spatter to form[10].

2.3.1.3 Hyperbaric GTA Welding

At one atmosphere GTA welding is considered to be a high precision, low deposition rate process. Provided that the influence of pressure on the GTA welding arc properties and the workpiece thermal response are considered, the high degree of precision and control that are possible at one atmosphere can be maintained over a range of pressures. The main effects of pressure on the GTA welding process will now be considered.

2.3.2 The Influence of Pressure on the GTAW Process

In section 2.2 the GTAW process was discussed. The influence of pressure on the process has been studied by several researchers. The particular influences that are thought to be relevant to this research project will now be presented.

2.3.2.1 Arc Voltage

It has been reported[12-15] that the arc voltage increases with pressure. The anode and the cathode fall voltages generally do not exhibit behaviour dependent on the pressure. It is the column voltage which is dependent on the welding pressure, following a relation of the form shown in equation 2.3.

Equation 2.2

$$V = V_0 + I.E_1.\left(\frac{P}{P_0}\right)^n$$

where V is the arc voltage at the operating pressure

V_0 is the arc voltage at atmospheric pressure and zero arc length

I is the arc length

E_1 is the electric field strength at atmospheric pressure.

P and P_0 are the operating pressure and atmospheric pressure respectively.

The exponent n is generally supposed to be approximately 0.5 although calculated values have ranged between 0 and 1[13]; Suga[14,15] has established its dependence on arc length.

$$n = 0.53\ I^{-0.31} \quad (15)$$

$$n = 0.64\ I^{-0.25} \quad (14)$$

If all other welding parameters are kept constant, this increase in voltage leads to an increase in process power with increasing pressure. As a result, this effect must be taken into consideration when deciding the process variables to be used when undertaking GTA welding at elevated pressures.

2.3.2.2 Arc Stability

It has been observed that the arc stability decreases as ambient pressure increases[13,15,16]. There are two main mechanisms by which arc instability can be initiated. Firstly, instability can be brought about by a transition of the shielding gas flow from laminar to turbulent flow. This occurs in the pressure range of 5-8bar[13] causing the arc to wander with greater frequency and greater amplitude as the pressure is increased. This can be controlled to a certain extent by decreasing the mass flow rate of the gas[13]. Fulfilling this condition requires that the volumetric flow rate is decreased at a rate inversely proportional to the increase in pressure; however, this eventually results in the shielding efficiency being reduced unacceptably. The increased turbulence in the outer regions of the shielding gas results in constriction of the arc. It has been found that application of magnetic fields to the arc can have a useful stabilising effect [13,16], alternating fields being particularly beneficial in stabilising the resultant voltage fluctuations[16].

Secondly, arc instability is caused by electrode erosion. Erosion also increases as the pressure is increased [13,16,17]. As the arc constricts with increasing pressure the cathode spot shrinks, which results in the temperature of the electrode tip increasing in order to fulfil thermionic emission requirements, which in turn results in higher electrode erosion. Factors, such as increased welding current and welding in a helium atmosphere have also been found to enhance electrode erosion[15]. Larger diameter electrodes, smaller electrode included angles and replacing the thoria in the electrode with lanthanum oxide have been found to be beneficial in reducing erosion[17,18].

2.3.2.3 Weld Bead Characteristics

The characteristics of the weld bead depend upon the efficiency and the stability of the welding process, which in turn depends upon the pressure. As the welding pressure is increased, the weld bead penetration is increased by a factor of approximately two over the first twenty bars for argon arcs[13-16,18]. Small increases in the bead width have also been observed in the same studies with an associated increase in weld fusion area. Suga and Hasui[14,15] found that this increase in penetration resulted in the critical current required for the welding of thin plate being reduced significantly as the pressure was increased, the change being most significant for helium arcs. Yada[18] has suggested that the increase in penetration could be due to the increase in process power caused by the higher arc voltages that accompany an increase in pressure. Allum[13] measured the arc melting efficiency, which takes into account changes in process power using a formula of the type shown below. He found that the efficiency increases by up to a factor of two over the first few bars, and then remains unchanged or even decreases at higher pressures.

Equation 2.3

$$z\% = \frac{v.A.Q_m}{V.I}\%$$

where z is the arc melting efficiency

v is the weld traverse speed

A is the cross sectional area of the weld bead

Q_m is the energy required to raise the temperature of unit volume of the plate material to it's melting point and to melt it.

V is the arc voltage.

I is the welding current

Arc instabilities, which increase with increasing pressure, have been found to produce uneven weld bead shapes due to arc wander[13,14,16]. Application of magnetic fields to the welding arc reduces arc wander and thus gives better control of the bead shape[13,16]. Application of a static magnetic field tends to produce an unsymmetrical, although stable, weld bead shape, the best results have been obtained by using an alternating magnetic field[16]. However, one adverse effect of applying a magnetic field to the welding arc is to reduce the penetration slightly[13].

2.3.2.4 Weld Properties

Several researchers have studied the effects of pressure on the GTA welding process and have reported the influence of pressure on the mechanical properties as part of this work[13-15,18]. The results did not indicate any significant deterioration of the mechanical properties although the presented test schedules were not comprehensive.

2.4 Duplex Stainless Steels

2.4.1 Introduction

Duplex stainless steels (DSS) are defined as a group of steels that have a two phase ferritic - austenitic microstructure. Both phases must contain the minimum chromium content required to make them stainless and be present in large separate volumes of approximately equal volume fraction. DSS have several advantages when compared with standard austenitic grades, including higher mechanical strength, better corrosion resistance (especially to stress corrosion cracking) and lower price due to the reduced nickel content.

Duplex stainless steels can be classified by their Pitting Resistance Equivalent (PRE) values. These give an indication of their resistance to pitting based on their chemical composition. Conventionally PRE values are given by the formula:-

Equation 2.4

$$PRE = \%Cr + 3.3\%Mo + 16\%N$$

By using the PRE values duplex stainless steels can be divided into four distinct sub-groups :-

- The standard duplex grade UNS S31803 which contains 22%Cr, 5%Ni, 3%Mo, 0.17%N which has recently had its corrosion resistance improved by increasing the nitrogen content. The corrosion resistance of this alloy group is in between that of the austenitic grade AISI 316 and the 5-6%Mo super austenitic.
- The super duplex grades which contain 25%Cr, 6-7%Ni, 3-4%Mo, 0.25-0.27%N with possible additions of Cu and/or W. These have pitting resistance equivalents of more than 40 and were especially developed for marine, chemical, and oil recovery applications where a combination of mechanical strength and corrosion resistance in very aggressive

environments is required. The corrosion resistance of these grades is equivalent to that of the super austenitic grades.

- The low cost molybdenum free grades containing 23%Cr, 4%Ni, 0.15%N which are alternatives to the austenitic grades AISI 304 and 316.
- Grades which contain 25%Cr with varying amounts of molybdenum and nickel. These have pitting resistance equivalents in the range 30 - 39.

A summary of the compositions of commonly available duplex alloys is given in Table 2.2. The role of the major alloying elements is reviewed in Table 2.3.

Duplex stainless steels have numerous uses that depend mainly on their corrosion resistance[20-41]. Their equivalent corrosion resistance and greater mechanical strength when compared with austenitic grades makes them ideal replacements for austenitic stainless steels in oil and gas production[20,21,27,34,36,38,39,41]. This is especially true as these resources are depleted and exploration requires that the steels are used in increasingly aggressive environments. Duplex stainless steels are also used extensively in chemical plant[20,25,29,32,33,41] and the food industry[20,27] where their high pitting resistance is advantageous. Other uses range from nuclear plant[20,22], flue gas desulpurisation plants[23,24], through to yacht keels[29] and domestic hot water heaters[41]. The present uses of duplex stainless steels are summarised in Table 2.4.

The properties of DSS depend greatly on maintaining the phase balance of the ferrite and austenite. The phase balance and microstructure are known to be affected by heat treatment, such as that experienced during welding. The effects of heat treatment on the microstructure will now be reviewed along with an indication of the influences on the materials properties.

2.4.2 Microstructure of Wrought Products

Duplex stainless steels consist of a two phase mixture of face centred cubic (f.c.c.) γ-austenite and body centred cubic (b.c.c.) δ-ferrite, usually showing a rolling texture. Alloys containing approximately equal volume fractions of ferrite and austenite are produced by work hardening, followed by solution annealing in the two phase region of the phase diagram and quenching with simultaneous control of the chemical composition. The microstructural balance of duplex stainless steels can be predicted on a simple scale by the use of a pseudo binary Cr-Ni-68%Fe phase diagram (Figure 2.1). However, the presence of other alloying elements complicates matters,

leading to the use of empirical formulae based upon the ability of each element to stabilise either ferrite or austenite.

Annealing of duplex stainless steels and other hot working operations are normally performed in the temperature range 1000-1200°C. The upper limit may be as high as 1300°C in super duplex stainless steels. Above this temperature oxidation problems may occur. Below the lower limit, brittleness may be induced due to the formation of precipitates. In addition to ferrite and austenite, a number of other phases can be formed when the material is subjected to elevated temperatures that do not exceed 1000°C. These are mainly due to the instability of the δ-ferrite and are, on the whole, undesirable. The deleterious phases are summarised in Table 2.5 and in Figure 2.2, and will now be treated in greater detail.

2.4.2.1 Sigma Phase (σ)

The sigma phase is probably the most important of the secondary phases formed in DSS due to its negative effect on the corrosion resistance and toughness properties of the material[42-52]. Sigma is formed from iron, chromium and molybdenum in the δ-ferrite when the material is subjected to temperatures in the range 600-950°C, the most rapid formation occurring between 700-900°C. Typically it is nucleated on the austenite-ferrite grain boundaries and at $Cr_{23}C_6$ precipitates on δ/δ grain boundaries[44], consuming chromium and molybdenum as it grows into the ferrite[44,46]. More austenite is usually formed around the σ in the ferrite which has been depleted in chromium and molybdenum since these ferrite stabilising elements are effectively removed from solution. Elements which promote the formation of σ are typically those that stabilise ferrite (Cr,Mo,W,Si) by decreasing the amount of time required for its formation. Charles[44] demonstrated that in the cases of molybdenum and tungsten the effect is also to increase the temperature range over which σ is able to form[44]. In the same study the influence of copper was also observed and found not to be significant.

The rate and extent of formation of σ are controlled by the concentration of the σ forming elements such as chromium and molybdenum; this implies that σ phase formation is likely to occur more readily in super duplex stainless steels where concentrations of these elements are much higher. It has also been observed by Maehara[45] that elements such as nickel that promote the formation of austenite, can also increase the rate at which σ

forms while reducing the volume fraction that forms in total. This phenomenon can be attributed to a higher nickel content which increases the amount of austenite formed, hence, reducing the volume fraction of ferrite present and leading to a higher concentration of chromium and molybdenum in the ferrite. As there is less available ferrite to transform, the total volume fraction of σ is reduced.

In addition to the role of the alloying elements on the formation of σ, the effect of straining and heat treatment has been studied by Maehara et al[46] and Josefsson et al.[47]. Straining due to hot work, cold work or quenching accelerates the formation of σ,. Cold working, which is the most severe, even produces σ in the austenite grains[46]. It was found that increasing the solution heat treatment temperature reduced the amount of σ formed by increasing the volume fraction of the ferrite and thus diluting the σ forming elements in the ferrite[47]. Maehara et al[46] confirmed these results and also stated that remelting, such as occurs in welding, reduces the amount of σ formed as a consequence of homogenisation of the ferrite.

The deleterious effects of σ on the corrosion resistance of DSS were studied by Potgeiter[48]. It was observed that both the corrosion and pitting potentials for 2205 DSS were reduced with increasing σ volume fraction, although Nilsson et al[52] found that the loss of corrosion resistance could also be due to chi phase which forms simultaneously (See section 2.4.2.4). It was also seen that corrosion was restricted to the ferrite, particularly the regions around the σ phase that had been depleted of chromium and molybdenum. Embrittlement due to σ phase was evident by a 50% reduction of impact toughness at levels of σ as low as 1%; while "complete embrittlement" (where the impact toughness was reduced to virtually zero) occurred at concentrations of 10% in work by Nilsson et al[52] Norstrom et al[49].

2.4.2.2 Chromium Nitrides

The effects of chromium nitrides are an important consideration due to the increased amounts of nitrogen used in current grades of DSS. There are two types: the more common hexagonal Cr_2N and the cubic CrN. Cr_2N can be formed intragranularly as elongated precipitates due to rapid cooling from high temperatures or intergranularly during isothermal heating in the temperature range 700-900°C. The latter form produces a simultaneous precipitation of secondary austenite and has been related to loss of localised pitting resistance. The only reported occurrence of the cubic CrN was that by

Hertzmann et al[50] in the heat affected zones of SAF 2205; however, there were no adverse effects on the toughness or corrosion properties.

2.4.2.3 Secondary Austenite

Secondary austenite is formed when the duplex structure is effectively quenched from a high temperature at which the equilibrium fraction of δ ferrite is higher. The transformation can occur over a wide temperature range by any of the following mechanisms:-

- The eutectoid transformation $\delta \rightarrow \sigma + \gamma$ which is aided by the rapid diffusion possible along σ/γ grain boundaries. This occurs in the 700-900°C temperature range where σ destabilises the ferrite by reducing its chromium and molybdenum content.
- At temperatures above 650°C where diffusion is more rapid, Southwick and Honeycombe[51] found Widmanstätten precipitates. These precipitates had a higher nickel content than the surrounding material, indicating that the transformation was diffusion assisted and obeyed the usual Kurdjimov-Sachs relationships.
- Below temperatures of 650°C, Southwick and Honeycombe[51] reported a martensite shear type transformation. This transformation occurred isothermally and there was no difference in composition between the austenite and the ferrite matrix suggesting that no diffusion occurred.

The austenite that forms at grain boundaries has been found to be low in chromium especially when Cr_2N precipitates simultaneously. This explains why pitting sometimes occurs even though the concentration of σ is considered to be rather low.

2.4.2.4 Chi Phase (χ)

The intermetallic phase, χ usually forms in the same temperature range as σ but is not as common. Work by Nilsson et al[52] demonstrated that the nose of the C curve on the TTT diagram appears at lower temperatures than that of σ. The χ phase consumes chromium and molybdenum from the ferrite and has a composition of approximately 50%Fe, 25%Cr, 20%Mo, balance Mn/Ni, thus reducing the corrosion resistance of the surrounding material. Although its presence is largely overshadowed by σ, loss of pitting resistance

can be attributed to χ and the resultant secondary austenite in conditions where σ could not be present, such as below the C curve for σ formation in SAF 2507.

2.4.2.5 R Phase

R phase is a molybdenum rich intermetallic which was first observed by Hochmann et al[53] and forms in the temperature range 550-700°C. Nilsson and Lui[54] estimated that the composition was approximately 31%Fe, 25%Cr, 6%Ni, 34%Mo, 4%Si in 2205 weld metal. Poorer toughness and critical pitting temperatures were associated with its formation in the same work. Both intergranular and intragranular precipitates have been observed. The intergranular type is thought to be more important with respect to a reduction in pitting resistance as it may contain up to 40% Mo, thus depleting the surrounding material.

2.4.2.6 π Phase

Work by Nilsson and Liu[54] found a molybdenum rich phase after isothermal heat treatment at 600°C. The composition of the phase was 28%Fe, 35%Cr, 3%Ni, 34%Mo, and its structure was shown to be cubic. π is precipitated within grains and like R phase contributes to embrittlement and pitting corrosion.

2.4.2.7 Carbides

There are two types of massive carbides that can form in duplex stainless steels: M_7C_3 forms in the temperature range 950-1050°C, and $M_{23}C_6$ forms below 950°C. These precipitates have been observed at all types of grain boundaries[43,51] although the most common site is at the δ/α phase boundaries. These precipitates are not as critical in DSS as in austenitic stainless steels. The ferrite present in DSS assists diffusion into the area surrounding the precipitate, thus maintaining the chromium content above the 13% required for corrosion protection.

2.4.2.8 Other Precipitates

Copper rich DSS may exhibit a tendency to precipitate copper particles from ferrite when it becomes supersaturated at lower temperatures[55]. Soylu

and Honeycombe[56] studied the refinement of DSS and found that copper particles precipitated from the ferrite acted as nucleation sites for the formation of austenite.

Redjaïma et al[42] found another precipitate (τ) which formed between 550-650°C. They did not link this phase with any changes in the material's properties.

2.4.2.9 475°C Embrittlement

475°C embrittlement is caused by a miscibility gap in the Fe-Cr system. This leads to iron rich α and chromium rich α′ forming, which can occur by either nucleation and growth or by spinodal decomposition. The elements chromium, molybdenum and copper, which super duplex stainless steels are rich in have been found to promote the formation of α′[44,57]. Nickel also indirectly promotes its formation of α‘ as it partitions the chromium and molybdenum to the ferrite, although it does limit the amount that can be formed overall[56].

2.4.3 Mechanical Properties

The typical tensile properties of specimen duplex grades compared with a ferritic and an austenitic steel are shown in Table 2.6.

It can be seen that the duplex grades have superior properties when compared with standard austenitic grades of equivalent corrosion resistance. In particular, the yield strength is approximately twice that of the austenitic steel grades. The tensile strength is also much higher, and the elongation properties are good, allowing weight and capital savings to be made due to the thinner sections required for load bearing.

Charles[44] reviewed the possible mechanisms responsible for the higher mechanical strengths of the duplex stainless steels:-

- Interstitial solid solution strengthening, e.g. by carbon and nitrogen.
- Substitutional solid solution strengthening e.g. by chromium and molybdenum.
- Grain refinement due to two phases being present and stopping mutual growth during heat treatment.

- Hardening due to the possible presence of secondary austenite.
- The presence of ferrite which is harder than austenite of a similar composition.

Usually, the tensile strength of the alloy would be determined by the softer of the two phases, approximately following a law of mixtures. However, in nitrogen alloyed duplex stainless steels the austenitic phase can be as strong as the ferritic phase. This is due to interstitial solid solution strengthening as nitrogen is partitioned in the austenite. Wahlberg and Dunlop[58] found that for UNS S31803 type DSS, overall contents of 0.2%N led to higher microhardness values for the austenitic phase than for the ferritic phase. This was as a result of the nitrogen content of the austenite being 0.38%. There is a practical limit, after which further additions in nitrogen make little improvement in strength, this is around 0.12%N in a standard duplex steel. Super duplex grades have yet higher strengths when compared with standard duplex grades. As the grain sizes are similar, the increased strength can be attributed to the solid solution strengthening properties of chromium, molybdenum, and nitrogen.

Duplex stainless steels have toughness properties that lie in between those of austenitic and ferritic stainless steels. Charles[44] reported that the fracture toughness of DSS was satisfactory at temperatures as low as -60°C. It can be seen that super duplex grades have lower toughness than standard duplex grades.

The service temperatures of DSS must be restricted to below 300°C. This is due to the reduction in toughness that occurs when ferrite decomposes producing various precipitates. This feature was investigated by Hochman et al[53] who found that embrittlement occurred in two distinct temperature ranges. Loss of toughness in the range 600-900°C was attributed to the formation of σ phase, whilst below 500°C there was 475°C embrittlement. Between these temperatures embrittlement was still apparent but it required a longer time to develop. The formation of other phases, such as Cr_2N and χ, have also been shown to cause embrittlement in the absence of σ phase[54]. Therefore, in order to retain good toughness, it is important that any heat treatment should be followed by cooling that is sufficiently fast to avoid formation of these phases.

The fatigue and corrosion fatigue properties have been reviewed by Johnsson and Groth[59]. They concluded that the superior fatigue limit found in duplex steels was a result of their higher yield and tensile strengths. The maximum stress at the fatigue limit was also discovered to be of the same

order of magnitude as the yield strength of the material under passive conditions. When the materials were tested in a corrosive environment it was found that the fatigue limit was reduced, whilst still retaining the fatigue strength. However, Charles[55] reported that for materials whose PRE values were greater than 40, the fatigue limit in seawater conditions was the same as in air.

2.4.4 Corrosion Properties

Pipelines used for the transportation of crude oil and gas are subjected to corrosive media containing a mixture of chlorides, carbon dioxide and hydrogen sulphide. The severity of the medium is dependent upon the partial pressures of these components in the water, hence at increased pressures the aggression of the medium increases. Carbon dioxide produces a sweet medium, with acidic pH values; these usually result in stress corrosion cracking (SSC). Duplex steels are usually susceptible to SSC, but as hydrogen sulphide is not commonly found in North Sea applications they can be used there[60]. In addition to the presence of H_2S and CO_2, some circumstances may lead to the introduction of oxygen into the system, e.g. during maintenance work. This results in the electrode potential being increased so that it lies in the region where localised corrosion may occur.

The resistance of duplex stainless steels to pitting corrosion and crevice corrosion depends upon the passivating properties of chromium and molybdenum which are preferentially partitioned in the ferrite phase. Thus, unless the austenite is highly alloyed with nitrogen it has a reduced corrosion resistance. The pitting resistance equivalent (PRE),(equation 2.3), is a good indication of the alloy's resistance to localised corrosion. There is good correlation between the PRE value and the critical pitting temperature of duplex alloys[34].

Duplex stainless steels exhibit excellent resistance to chloride stress corrosion cracking; however, in environments containing H_2S they do not perform as well. Bernhardsson[61] proposed that this was because of the ferrite phase being subject to hydrogen absorption. Attempts have been made to establish reliable test methods to determine the safety of duplex steels in service, but due to the lack of service data for comparison the materials can only be given a relative ranking[62]. The most conservative test found in this work was one involving slow strain rate testing. This produced plastic straining which was considered to be the worst case scenario to be found in service.

Selective corrosion of either of the two phases in duplex steels does not occur under normal circumstances. In very aggressive environments the material can be forced into the active state resulting in dissolution of the less noble species[61].

Sensitisation occurs most commonly in austenitic stainless steels after heat treatment in the range 600-1000°C, or after welding. It is caused by chromium carbides forming at grain boundaries, thus depleting the material immediately around the carbides of chromium and reducing the corrosion resistance. In duplex stainless steels the ferrite allows easier diffusion of chromium through its matrix, resulting in a wider region of less severely depleted material. Nilsson et al[52] also speculated that the lower carbon content of duplex stainless steels contributed to a reduced likelihood of carbide formation occurring.

2.5 Welding of Duplex Stainless Steels

In the previous section the microstructure and properties of duplex stainless steels were examined. Particular attention was paid to the influence of exposure to elevated temperatures with regard to changes in microstructure. The thermal cycling experienced during welding is more complicated than the isothermal heat treatments used in the work discussed earlier. For this reason a review of the work centred specifically on welding will now be presented. In addition to the control of the effects of the weld thermal cycle other developments in controlling the weld properties, such as consumable development will be presented.

2.5.1 Microstructural Evolution of the Weld Metal and Heat Affected Zone

When duplex stainless steels solidify in a weld pool, epitaxial grains of ferrite grow from the high temperature HAZ. The resulting weld metal is initially ferrite, having coarse columnar grains growing from the edges of the weld and some equiaxed grains near to the centre. Austenite is formed intergranularly as the last material solidifies and also intragranularly during cooling. The extent of austenite formation is dependent upon both the composition and the cooling rate, a slow cooling rate between 1250-800°C being favourable.

Adjacent to the weld metal is the region of the HAZ where some partial melting has occurred. The extent of this region depends upon the amount of segregation at grain boundaries. Sulphur and phosphorus contribute to the

formation of low melting point films, which enable deeper penetration along the grain boundaries, the easiest route being along the δ/δ grain boundaries. The presence of low melting point films and residual stresses at low temperatures may cause liquation cracking to occur. Atamert and King[63] suggested minimising the degree of ferritisation and the amount of impurities to limit this problem.

During hot working of duplex stainless steels, ferrite sub-grain boundaries are formed. In the ferrite grain growth region of the HAZ these are coarsened rapidly at first. The amount of ferrite grain growth that occurs is less in alloys containing higher amounts of carbon and nitrogen. The final ferrite grain size is increased as the heat input is increased and as the plate thickness is decreased. Austenite grains in this region of the HAZ decompose only partially, due to the thermal gradients encountered in the HAZ during welding. The remaining γ particles pin the ferrite grain boundaries and restrict the amount of ferrite grain growth that can occur.

At a further distance from the weld metal is the partially transformed zone. In this region a limited δ+γ→δ transformation occurs upon heating; this reaction is suppressed by the presence of austenite stabilising elements such as carbon and nitrogen. On cooling the reverse reaction occurs, the fastest transformation being above temperatures of 1000°C. The austenite content is increased by a lower cooling rate in the 1250-800°C temperature range. The grain size of the parent plate is also important, as is the inclusion content, since a greater inclusion content provides more sites for the precipitation of austenite.

2.5.1.1 The Effect of Reheating on the Weld Microstructure

The phase balance between austenite and ferrite depends on the weld metal composition and the thermal cycles experienced. In multipass welds the microstructure of the weld metal and HAZ are determined by the extent of reheating occurring from subsequent welds. A schematic diagram representing the positions of the microstructural regions that can occur as a result of reheating is shown in Figure 2.3.

In region B, adjacent to the weld metal (A), the peak temperature lies below the solidus but above the complete ferritisation temperature. This temperature is high enough for the material to completely transform to ferrite on heating. On cooling partial transformation to austenite occurs; however, the volume fraction formed is reduced, leaving an austenite denuded zone next to the fusion boundary. Atamert et al[64] found that this region did not occur in low

heat input welds due to limited time for the transformation to ferrite being available in the weld thermal cycle.

In region C, the temperature does not reach that required for complete ferritisation, but is high enough to allow some transformation to austenite to occur. The driving force for this transformation is the ferrite content after the first weld being higher than would be achieved under equilibrium conditions. The austenite that forms on reheating is acicular and forms intragranularly, the volume fraction achieved can reach 70%. In region D the temperature may enter the $\gamma+\delta$ area on the phase equilibrium diagram, but the time at this temperature during a weld thermal cycle is not sufficient for this transformation to occur.

2.5.2 Welding Consumables

Initially the compositions of welding consumables for DSS were matched to the parent plate material. When consumables were developed for UNS S31803 it was found that this was unsatisfactory as there was low toughness in the weld metal due to a high ferrite level. This was overcome by employing filler metals with higher nickel contents to promote the formation of austenite.

Bower et al[65] studied a wide range of consumables for UNS S31803 covering MMA, GTA, GMA, SMAW processes with different compositions. They found that most of the consumables produced acceptable welds with respect to tensile, bend impact, intergranular corrosion, crevice corrosion, and stress corrosion properties. One consumable that produced unacceptable welds provided an austenite content of only 18-31%. This result was related to the $Ni_{(eq)}$:$Cr_{(eq)}$ ratio (as in the Schaeffler diagram[66], Figure 2.4) of the consumable which was only 0.42 in this case, compared to 0.59 for the best performing consumable of those tested. The $Ni_{(eq)}$:$Cr_{(eq)}$ ratio is a guide to the ability of the consumables to produce austenite in the weld metal, where $Ni_{(eq)}$ and $Cr_{(eq)}$ are given by:-

Equation 2.5

$$Ni_{(eq)} = \%Ni + 30(\%C + \%N) + 0.5\%Mn$$

Equation 2.6

$$Cr_{(eq)} = \%Cr + \%Mo + 1.5\%Si + 0.5\%Nb$$

It was concluded that a $Ni_{(eq)}$:$Cr_{(eq)}$ ratio of around 0.5 for the consumable could be used as guidance for obtaining good weld metal properties.

Nitrogen is important to produce a good phase balance of ferrite and austenite and for supporting the corrosion resistance of DSS. The weldability of DSS is also improved[67] when there are increased levels of nitrogen in the weld metal and/or parent plate. Therefore compensation must be made to counter the tendency for the weld metal to lose nitrogen to the shielding gas during welding. Bonnefois et al[68] considered the methods available for introducing nitrogen to the weld metal, including the use of higher nitrogen contents in the welding consumables. It was thought to be straightforward in the cases of covered electrodes and flux cored wires, but in the case of solid wire for GTAW and GMA, the amount of nitrogen that can be added is limited as it affects the hot rolling properties of the wire.

In super duplex stainless steel welds one of the most important considerations is the corrosion resistance. Fager[69] reviewed the development of consumables for the super duplex grade UNS S31803. He concluded that the chromium, molybdenum and nitrogen contents must be kept as high as possible to maintain good corrosion properties. Also, the ferrite content must be neither too low or too high. If it is too low, then chromium and molybdenum is concentrated in the ferrite and there is the danger of intermetallic phases being formed at low heat inputs. If it is too high, there is the possibility of secondary austenite forming in the grains.

2.5.3 Welding Procedure and Parameters

Duplex stainless steels are usually delivered in the quenched and annealed condition, providing a fine grained microstructure. During a weld thermal cycle, structural changes occur that affect the properties of the welded joint. The weld metal microstructure and properties can be controlled by the choice of the right welding consumable. The HAZ properties depend upon the microstructure and composition of the parent plate and upon the weld thermal cycle. The latter is a function of the welding parameters, hence for a given composition of parent plate care must be taken to utilise the right conditions.

Upon heating, transformation to ferrite occurs at temperatures above about 1000°C. In welding the degree of transformation depends upon the peak temperature during welding (characterised by the distance from the fusion boundary for a given thermal cycle). On cooling austenite reforms at the ferrite

grain boundaries and also intragranularly if the $Ni_{(eq)}$:$Cr_{(eq)}$ ratio of the base metal is favourable. The amount of austenite that reforms is dependent upon the high temperature cooling rate, a low cooling rate being favourable; these conditions are provided by a high heat input weld. However, longer times at high temperatures encourage grain growth of ferrite in the HAZ resulting in loss of toughness. Also, slow cooling times enable the precipitation of deleterious phases such as the sigma phase. On the other hand, low heat inputs result in faster cooling rates which suppress the formation of austenite in both the weld metal and HAZ. Therefore, a compromise of welding parameters must be reached to achieve a satisfactory weld. This has been covered extensively in previous work and will be reviewed next.

Gooch[70] observed that in the range 0.6-1.6 kJ/mm, the heat input did not significantly affect the HAZ structure in terms of grain size or austenite content; however, larger heat inputs increased the width of the region of the HAZ heated above the austenite-ferrite transformation temperature. It was stated that in high power density welding processes, such as electron beam welding, the transformation temperature may be raised to higher temperatures. However, in high chromium content alloys the HAZ region bordering the fusion zone may become fully ferritic, and because of the rapid cooling rates encountered in this case, the transformation back to austenite is repressed. van Nassau et al[71] studied data relating the cooling rates experienced in the HAZ and the amount of austenite formed. Cooling times of 8-30s were recommended for the 800-500°C temperature range

Studies of the effects of heat input upon the weld properties recommend both low heat inputs to maintain good HAZ properties, and high heat inputs to maintain good weld metal properties. Faucher and Gilbert[72]) observed that low heat inputs (causing rapid cooling) produced high ferrite contents in the weld metal causing reduced toughness, while high heat inputs promoted the formation of ferrite in the HAZ in welds of UNS S31803. Yasuda et al[73] also found that a higher heat input was beneficial to the corrosion and toughness properties of the weld metal. A study of the effects on weld properties of a range of heat inputs up to 3.0kJ/mm for GTA welds and 6.0kJ/mm for submerged arc welds, also concluded that an increased heat input was beneficial to the toughness and pitting resistance of the weld.

Lundqvist and Norberg[74] recommended that the heat input should be kept above a minimum level of 0.5kJ/mm in UNS S31803 and UNS S32304 in order to reduce the amount of ferrite in the weld metal and hence increase its toughness. Also, the maximum interpass temperature of 150°C, previously recommended to minimise phase formation by reducing the cooling time, was

considered to be irrelevant as the time required to form sigma in these alloys is several minutes. However, van Nassau[71] surveyed welding techniques for duplex and super-duplex alloys and recommended that cold-pass techniques should always be employed to limit the formation of σ in multi-pass welds.

Studies on the effects of welding on the properties of super-duplex stainless steels by Stekly et al[75] and Atamert and King[63] concluded that low heat inputs were beneficial to the HAZ properties. It was observed that low heat inputs (0.5kJ/mm) dramatically reduced the amount of $\delta+\gamma\rightarrow\delta$ transformation that took place. In high nitrogen (super-duplex) alloys containing more than 0.25%N the transformation temperature was increased to 1300°C and the grain growth of ferrite was suppressed by the nitrogen in the parent plate. Also, low heat inputs were found to suppress the precipitation of carbides and nitrides, as the supersaturation of ferrite in both interstitial and substitutional alloying elements was prevented. When high heat input welds were used, the amount of austenite that reformed on cooling was found to be dependent not only on the cooling rate but also on the ferrite grain size and the inclusion content. The baseplate inclusion content of super duplex alloys is low, so the amount of intragranular precipitation of austenite was reduced. As a result of this, and the slow cooling rate associated with higher heat inputs, the precipitation of other phases such as chromium nitrides was encouraged within the ferrite grains.

The different heat input requirements to achieve optimum properties of the weld metal and HAZ from the heat input employed pose a problem. However, as the weld metal properties can be determined adequately by the use of the appropriate welding consumable, it would seem that the solution is to use a lower heat input to achieve adequate HAZ properties. In multi-pass welds the root run is reheated by each subsequent pass, therefore it would be beneficial if the austenite content of the root run is optimised. To avoid excessive precipitation of secondary phases in the root run Gooch[76] recommended that the use of a low energy root run followed by much higher energy filling passes should be avoided. Therefore, it would seem that a medium energy heat input root run of around 1.5kJ/mm should be used with subsequent passes employing a slightly lower energy. To achieve satisfactory cooling rates an interpass temperature of around 150°C should be maintained. This approach has been adopted by this research project.

2.5.4 Shielding Gases

Generally shielding and backing gases based on argon are used for the welding of DSS. In pure argon there may be problems due to nitrogen being lost from the weld metal during welding. This can be detrimental to the weld properties as it results in less austenite being formed and a lower corrosion resistance in the austenite. The benefits in maintaining austenite levels by additions of nitrogen to the welding gases have been well documented[68,70,71,73,76-79]. Creffield et al[77] also reported that the maximum allowable heat input to achieve austenite formation in the weld metal could be raised as a result of using nitrogen in the shielding gas. This is probably due to nitrogen raising the $\delta+\gamma\rightarrow\delta$ transformation temperature, thus permitting austenite to form at higher temperatures on cooling. The addition of 1-2%N_2 to the shielding gas seems to be the optimum level for achieving both the desired weld metal properties and maintaining the arc stability[68,79].

The addition of hydrogen to the shielding gas has also been studied due to beneficial effects upon the weld pool fluidity. Lundqvist and Norberg[74] found that this did not cause any problems in UNS S31803 as it has a low sensitivity to hydrogen embrittlement. van Nassau and Bekkers[71] considered the use of hydrogen to be inadvisable due to the possibility of delayed crack formation in high ferrite content welds.

2.6 Hyperbaric Welding of Stainless Steels

Various authors have studied the response of materials when welded under hyperbaric conditions[80,81]. Habrekke and Berge[80] studied the behaviour of C-Mn and stainless steels. Particular attention was paid to the level of oxygen contamination in the welding environment. The allowable level of oxygen contamination must be decreased as the pressure is increased in accordance with Dalton's law of partial pressures. An example was given where the allowable amount of 500ppm. for a surface weld is reduced to 45p.p.m. at 100 m.s.w. (metres sea water), ie., at an ambient pressure of 11bar. To ensure that oxygen pick-up was minimised, purging the weld area with helium was recommended prior to welding. Ralstone and Malone[81] facilitated this by surrounding the weld area with a clear plastic tent which was purged with argon.

The recommended shielding gas for GTA welding was a 70%He 30%Ar mixture[80,81]. Habrekke and Berge[80] noted that this allowed a 30-40A reduction in welding current to achieve acceptable penetration. The efficiency of the

shielding gas was tested by welding in an atmosphere with oxygen contents of up to 900p.p.m., there was no increase in the degree of oxygen pick-up. During hyperbaric short circuit GMA welding of duplex stainless steel the amount of oxygen absorption by the weld was shown to increase as the oxygen content of the shielding gas was increased[82]. In the same study the amount of nitrogen absorption did not appear to be related to the shielding gas content.

Ralstone and Malone[81] reported that the mechanical properties of the hyperbarically welded joint in their study, were on the whole, acceptable. However, this cannot be verified as the full results for the duplex stainless steel joints were not reported. The only significant reported result was that from the hardness survey in which some areas of the weld did not meet the requirement of a maximum Hv10 Vickers hardness value of 300 imposed by the sponsors of the work. The authors noted that this was probably due to excessive requirements being imposed on relatively new materials. This would seem to be a justifiable statement as the hardness values for material of the type UNS S31803 are around Hv10 235 before any welding operation is carried out.

2.7 Summary of Literature Review

The relative advantages of underwater welding processes were discussed briefly in order to determine the relevance of the hyperbaric process to this work. The influence of pressure on the GTA welding process was reviewed. The arc voltage is known to increase with the pressure at which welding is performed. This is relevant to choosing the controllable welding parameters in order to achieve an acceptable heat input to the weld. Additionally the stability of the GTA weld process has been shown to deteriorate as the ambient pressure is increased, the component of this due to electrode erosion being dependent on the welding current. Therefore, it will be necessary to determine whether the welding arc will remain stable for a sufficient length of time at the current being used, for all the pressures at which welding will be performed. Also, the stability may cause arc wander which may in turn result in fluctuations in the weld bead shape. There is evidence that the melting efficiency of the welding arc may increase as the pressure is increased, this requires investigation so that changes to the weld parameters at higher pressures can be made to achieve a constant weld bead profile.

From the review of the microstructure and properties of duplex stainless steels it is clear that the composition and microstructure must be tightly controlled in order to maintain the properties of these materials. Problems can be caused when the austenite/ferrite phase balance is changed so that the smaller volume fraction of the two phases falls below 30%. Additional problems can be caused by the precipitation of secondary phases such as sigma phase which form after heat treatment or welding. Unacceptable reductions in the toughness and corrosion resistance may be caused as a result.

These problems were considered by researchers when welding procedures at atmospheric pressure were determined. The recommended heat inputs for welding at atmospheric pressure are between 0.5-2.0kJ/mm. The minimum value is to ensure that sufficient austenite formation occurs, the higher limit is to ensure that excessive ferrite grain growth in the HAZ does not occur and to minimise the precipitation of secondary phases. The consumables for duplex stainless steels match the composition of the parent plate, with the exception of the austenite stabilising element nickel which is overmatched by around 2% to ensure that sufficient austenite formation in the weld metal. Some researchers have recommended adding nitrogen to the shielding gas in order to overcome problems with nitrogen loss from the weld pool during welding. This would not be a simple process for hyperbaric welding as active gas contents have to be reduced at higher pressures according to Daltons law of partial pressures[80]. Therefore in hyperbaric welding control of the weld nitrogen content would be best controlled by increased nitrogen contents in the consumables.

Finally workers have recommended that a helium rich shielding gas be employed so that lower welding currents can be used. This would also be in the interests of the divers safety, as it would lower the risk of argon contamination.

3. EXPERIMENTAL

3. Experimental

3.1 Introduction

The main objective of this study was the development of successful welding processes and parameters for hyperbaric welding of duplex stainless steels. The literature surveyed has shown that in order to achieve this objective, the work must be approached from two directions. Firstly, the influence of pressure on the GTA welding process is known to produce changes in properties such as arc voltage, arc efficiency and stability. Secondly, the reaction of duplex stainless steels to welding processes is known to be mainly dependent on the thermal cycle encountered. Therefore, the changes in arc characteristics, specifically when dealing with duplex stainless steels, and the changes in weld thermal cycle had to be studied, before the production of welded joints could be undertaken successfully.

The experiments of this project were split into four sections to reflect the step by step approach to determining the behaviour of duplex stainless steels when welded hyperbarically. The initial experiments were autogenous bead on plate welds to determine the arc stability and changes to arc voltage over the range of welding pressures. The second set of experiments were also autogenous bead on plate welds, where the thermal cycles were determined by monitoring the output of thermocouples embedded in the weld specimen. The positions of the thermocouples were determined after examination of the welds produced in the first set of experiments. At the same time as these experiments were performed an investigation into the production of sigma phase was carried out to determine whether the thermal cycles encountered would cause the precipitation of sigma phase.

After examining the behaviour of the GTA process and the duplex stainless steel under hyperbaric conditions the work progressed to the production of welded joints. The third set of experiments was to evaluate the weld joint design, particularly with respect to the production of the root welds. The final set of experiments was the production of welded joints for each material at a range of pressures and subsequent evaluation of their properties.

3.2 Materials, Equipment and Procedures

3.2.1 Materials

Three duplex stainless steel alloys were chosen for this study. Avesta 2205 (UNS S31803) was chosen to represent the most common material currently in wide use. Sandvik SAF2507 (UNS S32750) and Weir Materials Zeron 100 (UNS S32760) were chosen to represent the newer super duplex grades that are expected to become more widely used. The composition, form and properties of these materials are shown in Tables 3.1-3.3. Matching welding consumables were chosen for these materials, the compositions and properties of these are shown in Tables 3.4-3.5.

3.2.2 The Hyperbaric Welding Facility

3.2.2.1 The Hyperbaric Chamber

A detailed description of the hyperbaric welding chamber was given by Richardson[82]. A brief summary will now follow.

The hyperbaric chamber is 1.3m long and has a circular section of 0.43m diameter and can be pressurised up to 100bars. The external shell can be unclamped from the end flange to allow easy access to the internal working frame that is connected to the end flange. The workframe (shown in Figure 3.1) supports the dual (y and z) axis torch manipulator and the single (x) axis work table that are all driven by d.c. servo motors. The chamber has three observation ports, two were opposite each other along the transverse (y) axis and one at the end of the chamber viewing along the longitudinal (x) axis.

3.2.2.2 Gas Supplies

Commercial grade gases were used for both shielding and chamber pressurisation. A 75%helium 25%argon premixed gas mixture was used for the shielding gas, argon was used for the pressurisation gas. During welding, the shielding gas flow rate was monitored using a Platon float and gap flow meter, the flow rate was set at a needle valve close to the flow meter inlet. The flow meters had been calibrated previously[82], the flow rate being given by the relation:-

Equation 3.1

$$W = a.s.\left(\frac{\rho_{Ar}}{P.\rho_{gas}}\right)^{0.5}$$

where a is the calibration constant of the flow meter

s is the setting on the flow meter

ρ_{Ar} and ρ_{gas} are the density of the chamber gas (argon) and the shielding gas respectively.

P is the chamber pressure in bars.

In this study the shielding gas was a mixture so its density was calculated by applying the law of mixtures to the densities of the individual gas components. The calibration constant for the shielding gas flow meter was 2.5 in this case.

3.2.2.3 The Welding Torch

The GTA welding torch used for this investigation was a hybrid torch adopted for the hyperbaric chamber from a BOC TA 151A TIG welding torch with a 9.5mm gas shroud fitted. All spare parts for the torch were standard BOC parts. The torch was attached to a piece of Tufnol which in turn was attached to the torch axis manipulator allowing easy removal of the torch.

3.2.2.4 Welding Power Supply

The welding power supply used throughout the welding trials was a GEC AWPH350sr model. This is a series regulated type supply with a maximum current of 350A and a maximum voltage of 110V. Further details of this welding current supply have been given elsewhere[82].

3.2.2.5 Control and Monitoring Systems

All control systems were managed by computer. Throughout all welding trials the control of the power supply and the torch vertical (z) axis was through a control system developed under the direction of Norsk Hydro for deep water welding operations[82]. The user interface of this system was an IBM AT computer which stored weld information and executed the control program. The longitudinal and transverse axes movements were controlled by a menu driven program on another computer that also had the facility to perform weaving movements during the weld[83].

The voltage and current readings were monitored from indicators on the power supply. Thermal cycle measurements, where relevant, were by connection of R type thermocouples to the weld specimen; the output of these was monitored and recorded by a further personal computer with an integrated Amplicon PC26 analogue input board.

3.2.3 Procedures

3.2.3.1 Metallurgical Examination

Specimens for optical microscopy and scanning electron microscopy were all hot mounted in conducting Bakelite resin and ground and polished on a Beuhler Mastermet automatic polisher. For optical microscopy the specimens were electrolytically etched in 10% oxalic acid at a potential of 6V for approximately 30s.

Specimens for transmission electron microscopy were sliced from the bulk material using a Beuhler Isomet 2000 cut-off saw. Discs of 3mm diameter were cut from these using a spark eroder, these were then ground until they were approximately 200μm thick and thinned and electropolished in a twin jet polishing unit using 20% perchloric acid, 10% glycerol, and 70% ethanol at 0°C and 45V.

3.2.3.2 Mechanical Testing

Hardness surveys were performed on the weld metal and on the HAZ of the welded joints according to BS7191:1989. Charpy V-notch impact tests according to BS131: Part 2 were carried out on specimens cut from the weld metal and HAZ at a range of temperatures down to -100°C using a mixture of methylated spirits and liquid nitrogen to cool the specimens.

3.3 Initial Experiments

The initial weld trials were autogenous (that is, no additions of filler material were made) bead on plate welds. The welds were performed on all three of the test materials at a range of pressures up to 32bar in order to determine whether the arc remained stable at higher pressures. The change in arc voltage with pressure was also noted so that the process variables could be determined to achieve a given heat input for future welds. The welding process variables for this set of experiments are shown in Tables 3.6 and 3.7. Table 3.6 shows the welding process variables that remained constant throughout all of the welding experiments in this research project.

After welding, the specimens were sectioned and prepared for metallographic examination (see section 3.2.3.1). The weld bead profiles were examined so that the positions of the thermocouples to be used in the thermal cycle experiments could be determined.

Due to the lack of success in achieving a satisfactory weld bead profile in the first part of this work, a further experiment was performed. In this experiment all of these welds were performed at a pressure of 1bar only in order to prevent waste of material. Two currents and a range of welding speeds were used. The welding parameters are shown in Table 3.8. The specimens were sectioned and prepared for metallographic examination as before.

3.4 Thermal Cycle Monitoring

The thermal cycle monitoring experiments were performed on specimens of all three sample materials. Autogenous beads on plate welds using 1kJ/mm and 2kJ/mm heat inputs were performed at six pressures up to 32bar. The welding conditions used for these welds are shown in Table 3.9.

Prior to welding, four holes were drilled on the underside of the specimen along the centre line to accommodate the thermocouples. The depths of the holes were varied so that the thermocouple positions were at distances between approximately 2.5 and 4mm below the weld surface. The variation in depth was to ensure that at least one thermocouple would be positioned in the HAZ. The thermocouples were secured in place by using a thermocouple welder. The thermocouples were then connected to the monitoring equipment described in section 3.1.2.5. The specimens were bolted to the work table via two spacers approximately 25mm thick placed at

each end, this was to prevent the thermocouples being short circuited on the work table.

When the welding was performed the monitoring equipment delayed logging the data from the thermocouples until the temperature from any of the thermocouples first exceeded 50°C.

3.5 Sigma Phase Formation Evaluation

This experiment was performed in order to determine whether sigma phase formation would be a problem in the welded joints. Specimens of each material were isothermally heat treated at 850°C for various times up to 6 hours. Immediately after removal from the furnace the specimens were water quenched. They were then prepared for metallographic examination, and hardness tests were performed on each specimen.

3.6 Joint Design Evaluation

The joint design to be used on the hyperbarically welded joints was based upon a standard single V-butt joint preparation but with the addition of a 2mm thick "land". This design can be seen in Figure 3.2. The addition of the land to the joint preparation was to prevent the arc from wandering up the sides of the joint at higher pressures, particularly in the critical root welding phase. In this particular set of experiments the materials used for the joint evaluation were a standard mild steel for the joint and an austenitic stainless steel filler material to prevent waste of the duplex stainless steel materials.

Only the root runs were laid in these experiments as it was thought that the filling weld passes would be straightforward to achieve and not essential to the investigation at this point. The heat inputs used for the welds were based on a value of 1.5kJ/mm at a pressure of 1bar. Adjustments were made to the process parameters at higher pressures to compensate for the changes in arc melting efficiency that occur when welding at higher pressures. To ensure complete fusion was achieved in the root a transverse weaving pattern was used which oscillated with an amplitude of 1.5mm and a frequency 1.2mm/s around the weld centreline. The automatic voltage control (A.V.C.) on the power supply was activated so that the voltage could be easily maintained at the levels assumed when the process parameters were calculated. The weld parameters used for these welds are shown in Table 3.10.

3.7 Production and Evaluation of Duplex Stainless Steel Joints

For the duplex stainless steel welded joints the joint preparation was exactly the same as that evaluated in the previous section of the experimental details. Two identical joints were prepared at each pressure for each material, these were mounted simultaneously in the chamber side by side. Prior to welding the joints were fixed together using tack welds at either end and midway along the length of the weld. The joints were then welded to three strongbacks of approximately 2.5cm square section positioned at either end and mid-way along the length of the weld. The strongbacks had two purposes. Firstly, they held the welds in place and controlled the degree of warping. Secondly, the strongbacks held the welds away from the worktable and thus prevented the joints being welded to the table. The thermal cycles of the welds were monitored using a single thermocouple attached mid-way along the length.

The first attempts at welding the duplex stainless steel joints were at a pressure of 1bar. The parameters used were the same as for the joint design evaluation experiments which were based on the parameters found in the literature. However, problems were encountered in achieving adequate fusion in the root using these parameters. Adjustments were made to the welding current, weld speed, wire feed rate, land thickness and root gap in order to achieve acceptable penetration. Eventually, a pulsed welding arc and no weave was used, the land thickness was reduced to 1.5mm. The modified joint design is shown in Figure 3.3. Once a successful root weld had been achieved the joint was filled.

The joints at higher pressures were welded with less difficulty. Adjustments to the parameters used for the 1 bar weld were made to account for the changes in arc characteristics at higher pressures. These adjustments were in the form of lower current levels and higher welding speeds as the pressure was increased. The parameters used for the welded joints are shown in Tables 3.11-3.13.

When the joints were completed they underwent metallurgical examination and mechanical testing as described in sections 3.2.3.1 and 3.2.3.2.

4. RESULTS

4. Results

The effects of pressure on the GTA welding process and factors likely to influence the welding properties of duplex stainless steels were surveyed separately in Section 2. In Section 3 an experimental programme was outlined which was to determine the specific effects of the hyperbaric process on the welding of duplex stainless steels. The results of this programme will now be presented in the same chronological order.

4.1 Initial Experiments

The first set of experiments in this study were to determine the effects of pressure on the arc stability and arc voltage when welding duplex stainless steels specifically. These welds were autogenous bead on plate welds using two welding currents and constant speed at a range of pressures up to 32bars. It was found that the arc did not become unstable at higher pressures and that the arc voltage for a given welding current increased as the pressure was increased. These results are presented in Tables 4.1-4.3, the influence of pressure on the arc voltage is shown graphically in Figure 4.1.

These welds were sectioned and examined to determine the influence of pressure on the weld penetration so that the positions of thermocouples for thermal cycle monitoring could be determined. However, it was found that these welds suffered from low penetration as shown in Figure 4.2. This was thought to be as a result of the heat inputs for the welds being somewhat lower than those recommended for atmospheric welding by the surveyed literature. Microstructural examination of the welds showed a highly ferritic structure as typified by Figure 4.3. As a result a second set of experiments, at atmospheric pressure only, were performed to determine the welding parameters that would give satisfactory weld bead profiles. These welds showed improved penetration as shown in Figure 4.4. Microanalysis of typical weld metals for each material showed that the partitioning of the main alloying elements between the austenite and ferrite phases differed from the equilibrium state of the parent plate as shown in Table 4.4.

4.2 Thermal Cycle Experiments

For the thermal cycle experiments two nominal heat inputs of 1kJ/mm and 2kJ/mm were chosen for the autogenous bead on plate welds at a range

of pressures up to 32bars. This enabled the effects of both the pressure and the heat input on the thermal cycle of each material to be assessed to assist in determining the welding parameters for the welded joints. Analysis of the thermal cycles of the welds showed that faster cooling times were achieved by either using a lower heat input or welding at a higher pressure. This is presented in Figures 4.5-4.7. Specific analysis of the influence of pressure and heat input on the cooling times through the austenite forming temperature range and the sigma phase forming temperature range is shown in Figures 4.8-4.9.

The influence of pressure on the weld bead profile was thought to be important as it would assist in determining how the welding parameters for a joint at atmospheric pressure should be changed when welding at higher pressures. It was found that the penetration and to some extent the width of the weld bead increased as the pressure increased for a given heat input as illustrated in Figures 4.10-4.12, the increase in penetration with pressure is shown in Figure 4.13. Pressure is known to increase the arc voltage for a given welding current, hence it was not known whether the observed increase in the weld bead cross sectional area was due to this or an increase in the arc melting efficiency. Figure 4.14 illustrates the influence of pressure on the arc melting efficiency, the term for arc melting efficiency being taken from Allum[13] and which takes into account the increase in arc voltage with pressure.

4.3 The development of sigma phase in the specimen alloys

The previous experiment on thermal cycle measurements on autogenous bead on plate welds enabled the cooling times to be determined for each pressure through the temperature ranges where precipitations of secondary phases are thought to occur. In order to predict whether sigma phase would form in the specimen alloys in these timescales, it was necessary to determine as accurately as possible the exact time at which sigma phase precipitation becomes detectable by optical microscopy and in terms of changes to mechanical properties. This was done by heat treating samples of the alloys for various times in the sigma phase forming range and subsequently performing metallographic examinations of the specimens. It was hoped that as part of this work that a simple mechanical test, for example, a hardness test, could be employed to indicate the levels of sigma phase present in a weld. A similar, although indirect, comparison had already been proved by Thorvaldsson et al[43] where impact energy and hardness as a function of heat treatment time were plotted on the same graph. This may

possibly allow the simple estimation of the extent of sigma phase in future welds and indicate which of these may have unsatisfactory levels of embrittlement. The results of the present experiments on individual alloys will now be presented below.

4.3.1 Avesta 2205

Figure 4.15 shows examples of microstructures for the alloy Avesta 2205. Photograph (a) shows the as received condition, whilst photographs (b-g) are after heat treatment at 850°C. The untreated material has the typical microstructure of a duplex stainless steel, containing 50% austenite in a ferrite matrix. There are no precipitates obvious in this condition. After 15 minutes at 850°C the first signs of sigma precipitation can be seen at the ferrite/austenite grain boundaries (Figure 4.15(b)) and not at the sites of $Cr_{23}C_6$ precipitates on ferrite/ferrite grain boundaries as stated by other experimentalists[44]. The amount of sigma phase at this level of heat treatment would appear to be less than 1%, indicating that very little embrittlement would have occurred. It can be seen in Figure 4.15 (c-g) that the level of sigma phase increases as the duration of the heat treatment is increased which is as expected. The levels of precipitation found at 30 minutes and 1 hour are still less than 10%, but after two hours at 850°C a greater amount of precipitation is obvious. No specimens show indications of secondary phase precipitation in the austenite. This would be expected as the levels of sigma forming elements, such as chromium and molybdenum, are lower in the austenitic phase and diffusion of the required elements is more difficult in this phase due to its close packed structure.

The hardness surveys on the untreated and heat treated material show that the hardness increases as the time of heat treatment increases (Figure 4.18(a). The initial increase is low, reflected by the low levels of sigma phase seen in Figure 4.15(b-c). Between 30 minutes and 2 hours of heat treatment there appears to be a rapid increase in the hardness reflected by the increase in the amount of precipitation seen in Figure 4.15(d-e). At times over 2 hours the rate at which hardness increases with time of heat treatment is lowered, probably due to the sigma forming process nearing completion, although it is apparent that there still remains a slight positive gradient on the curve at this point, indicating that there is still the possibility of further sigma phase formation if heat treatment is continued for longer terms. However it may be that the material is significantly embrittled at this point and therefore any increase in hardness would not necessarily mean that the material was

becoming further embrittled. It is the hardness level of the material at the point which it first becomes brittle that is the important parameter.

4.3.2 Sandvik SAF 2507

The Sandvik SAF 2507 alloy shows a greater tendency to form sigma phase upon heat treatment. It can be seen in Figure 4.16(b) that heat treating this material at 850°C for only 15 minutes leads to a noticeable precipitation of sigma phase both at the δ/γ grain boundaries and at some δ/δ grain boundaries. The presence of precipitates at the δ/δ grain boundaries indicates that the sigma phase precipitation may have been preceded by the precipitation of some $Cr_{23}C_6$ precipitation at these points. After 30 minutes it would appear that almost all of the ferrite has been affected. This is confirmed in Figure 4.16(d) which shows little sign of an increase in sigma phase content after heat treatment for 1 hour. The only change in the microstructure after this point is the apparent precipitation of sigma phase at the austenite sub-grain boundaries. The driving force, in the first instance, for the faster precipitation of sigma phase in this alloy is the increased concentration of sigma forming elements in the SAF 2507 alloy compared with the Avesta 2205 alloy, i.e., an extra 4% Cr and 0.8%Mo which will mainly be concentrated in the ferrite.

The influence of this sigma phase formation on the mechanical properties and the progression of sigma phase formation in this alloy are characterised by the change in hardness with time (Figure 4.18(b)). It can be seen that after 15 minutes heat treatment at 850°C there is a slight increase in hardness. At 30 minutes there is a rapid increase in hardness as would be expected from the large amount if sigma phase formation shown in Figure 4.16(c). After 30 minutes there does not seem to be any more significant increase in the hardness, in fact after 2 hours it would seem that the hardness-time of heat treatment curve has levelled out indicating that the sigma phase precipitation within the ferrite is complete. This confirms the information obtained from Figure 4.16(d-g).

4.3.3 Zeron 100

As Zeron 100 is a super duplex stainless steel, it would be expected to behave in the same manner as the SAF 2507 alloy. It can be seen in Figure 4.17 that this is generally the case, with the exception of the microstructure after 15 minutes. Here it appears that a large proportion of the ferrite has been converted to sigma phase. For heat treatment times of 30 minute or above the precipitation of sigma phase in the ferrite is complete. Again the only change appears to be the formation of some precipitates at the austenite sub-grain

boundaries. As with the SAF 2507 alloy, the increased rate of sigma phase precipitation compared with the Avesta 2205 is almost certainly due to the higher concentration of sigma forming elements. In the case of the Zeron 100 the increase in concentration of sigma forming elements is augmented by the inclusion of a small amount of tungsten in the composition of the material.

The graph of hardness against heat treatment time (Figure 4.18(c)) once again shows a small increase in hardness after a heat treatment time of 15 minutes as with the SAF 2507. However, in this case, with knowledge of the microstructure, it would be expected that the initial increase in hardness would be higher. As with the SAF 2507 there is no significant increase in hardness for heat treatment times of 30 minute or above, with the curve levelling out after heat treatment times greater than 1 hour, indicating that again the precipitation of sigma phase has effectively concluded.

4.3.4 Summary

These experiments have determined that it is possible to induce the precipitation of sigma phase by isothermal heat treatment in the alloys examined in this programme. At heat treatment times greater than 15 minutes, the formation of sigma phase is a problem in all of the alloys chosen for the current work. As predicted by the literature survey, the super duplex alloys which contain greater amounts of chromium and molybdenum produced sigma phase sooner and more extensively than the relatively low alloying element content Avesta 2205 material in the time periods examined. As the experiment did not include a heat treatment time lower than 15 minutes the exact time at which sigma phase starts to precipitate in the higher alloyed materials was not determined.

It is obvious that the hardness increases as the sigma phase precipitates, a slight increase being apparent after 15 minutes at the heat treatment temperature. However, in this work, no attempts were made to relate this increase to any loss of the material's toughness. It should be noted, however, that the maximum value of hardness achieved due to this heat treatment is greater in the two super duplex alloys than in the standard duplex grade Avesta 2205. The Zeron 100 achieved a maximum hardness value of around 400 HV10 compared with the maximum values of around 300 HV10 attained by the Avesta 2205 material. The higher hardness value may be related to the super duplex materials being able to produce a greater concentration of sigma phase compared with the standard duplex alloy.

4.4 The Preparation of Duplex Stainless Steel Joints

Initial evaluation of the weld joint design using mild steel parent plate and stainless steel welding consumables indicated that the joint design was adequate. The presence of the "land" prevented the arc from wandering up the sides of the joint, and it was found that by making simple adjustments to the welding parameters, optimum fusion in the root weld could be achieved.

When attempting to weld the duplex stainless steels using this weld joint design and welding parameters, difficulties were encountered. The nature and possible causes of these problems will be discussed in Section 5. Variation of the welding parameters eventually led to parameters that could be used to achieve acceptable root welds. Analysis of the parameters showed that there was a relation between the heat input required to achieve fusion in the root weld and the pressure at which welding was performed. This is illustrated in Figure 4.19.

The results presented in Section 4.2 show that the cooling times through the temperature range at which sigma phase formation is thought to occur were reduced as the pressure was increased. In the duplex stainless steel joints, the number of weld passes required to complete a joint was increased as the pressure was increased. This was due to the way in which the welding parameters were adjusted to account for any pressure related differences in welding efficiency. It was therefore a concern that the reduction in cooling time for a single weld pass may be negated by the cumulative effects of a greater number of weld passes. Analysis of the cooling times for each weld pass, as shown in Figure 4.20 demonstrated that this was not the case.

4.5 Analysis of Duplex Stainless Steel Joints

Examination of the joints was performed on a macro and micro scale shown in Figures 4.21-4.71. Analysis of the form of the joints, shown in Figures 4.21, 4.38, 4.55, suggested that the weld quality improved as the pressure was increased, albeit from a purely aesthetic point of view. Detailed examination of the microstructures of the welds was performed and is shown in Figures 4.22-4.37, 4.39-4.54, 4.56-4.71. These micrographs concentrate mainly on the welds performed at the extremes of the pressure range studied, although some examples of anomalies from welds performed at other pressures are presented. Full descriptions and discussion of the microstructures are included in the discussion section of this work.

The mechanical properties of the welds were examined. The results are limited to the hardness properties and the impact toughness properties. The hardness of the weld metals and the HAZ of the three materials are shown in Tables 4.5-4.10. The impact toughness properties are presented in Figures 4.72-4.74.

5. DISCUSSION

5. Discussion

This discussion is split into sections which reflect the chronological order in which the work was performed. However, the first two sections cover the material used in the work and some of the pervading difficulties encountered with the practical methods employed. Dealing first with these topics which are common to the whole of the work, enable the subjects covered in the subsequent sections to be discussed and understood more clearly.

5.1 Materials

The materials chosen for this research programme represented both the established standard duplex stainless steel alloys and the newer super duplex grades, both of which are used in oil and gas extraction. A complementary discussion of the relative merits of each type of duplex grades will be found in the literature survey, but a brief résumé of the specific properties of the alloys used will now be given.

Avesta 2205 is the representative of the standard duplex alloys with nominally 22% chromium and 5% nickel. Its PRE value of 34.5 enables its use in applications such as pressure vessels[21,40], pipelines[21,35], reactor coils[23], and cargo tanks[27]. It can be seen in Table 3.3 that this alloy contains a higher nitrogen level than the earlier grades, which gives it higher strength through hardening of the austenitic phase. The welding of this type of alloy at one atmosphere is well documented and extensive guidance for atmospheric welding is available. However the application of hyperbaric welding has only been studied briefly and therefore it was considered an urgent requirement to examine the behaviour of this alloy when it is welded hyperbarically. Previous work[44,45] at atmospheric pressure (1bar) has shown that the precipitation of deleterious secondary phases requires the alloy to be maintained in the precipitation temperature range for at least 3-5 minutes. When welded the cooling times through the appropriate temperature range are much shorter, typically around a maximum of 20s. When it is known that hyperbaric atmospheres reduce cooling times[13], precipitation of secondary phases was not anticipated to be a problem in this particular case.

The newer super duplex alloys Sandvik SAF2507 and Zeron 100 have very similar compositions and therefore have very similar PRE values of 42.7 and 41.5 respectively and at the outset of this project, were being considered

for more widespread use in pipelines. Therefore this work aimed to study the parameters controlling the welding process and properties produced, based on welding conditions likely to be encountered in service, and hence to assess the viability and scope for increased usage of these alloys. These alloys not only have greater corrosion resistances but higher strengths also. This is due mainly to the higher alloy contents, particularly the nitrogen which, as stated earlier, is a known strengthener of the weaker phase austenite[44,58]. However there are negative aspects to the higher alloy content, the main one being the greater tendency for secondary phases to be precipitated. In fact the time required to detect sigma phase precipitations in the requisite temperature range is reduced to around 3 minutes in super duplex grades. This is one area where, at the outset of this project, it was thought that hyperbaric welding would be superior to atmospheric welding as its accelerated cooling rate would possibly eliminate these precipitations.

5.2 Limitations and Difficulties with Equipment and Procedures

The computer controlled monitoring and control systems used when welding were essential to this work. With the welding procedures in the hyperbaric chamber three people were required to perform the welding work. One person operated the computers which controlled the welding arc and the movement of the axes, another person monitored and controlled the shielding gas flow rate, the chamber pressure and the wire feed speed, the final person observed the weld and directed the wire consumable into the correct area of the weld pool. The procedure would have been simpler if the wire feed speed, shielding gas flow rates and chamber pressure had also been computer controlled. This would have allowed the welding to be performed by two persons instead of three.

It was thought to be important that the welds produced at 1atmosphere were performed in the chamber for comparative purposes. The majority of problems encountered with the welding process were limited to the welds performed at one atmosphere. Of these problems, two are worthy of note. When two joints were mounted in the chamber simultaneously it was difficult for the wire feed operator to observe the weld as it was not in the direct line of the end observation port. Visibility was also impaired, at high pressures especially, when the joint became hot and caused convection of the gas

immediately adjacent to the joint, an effect similar to the heat haze seen just above ground level on a hot summer's day. Another problem that was encountered was when the consumable was being fed into the weld pool. Occasionally, the wire became so hot that it melted onto the contact tip which disrupted the wire feed mechanism and, as a result, led to the weld run being abandoned. A solution to this problem for future work of this kind could be to locate the contact tip away from the weld pool, but this may cause control of the wire to be lost. Alternatively, the motor of the wire feed mechanism could be upgraded so that when the wire started to melt back into the contact tip it could be prevented from sticking to the contact tip.

No problems were encountered with the optical examination of the duplex stainless steels following the initial trials to determine satisfactory etchant and electrochemical conditions. Identification of the phases present in the weld by energy dispersive microanalysis with a scanning electron microscope was difficult. The electron beam voltages of around 20kV required to generate sufficient X-ray counts from the elements in the duplex stainless steels in spot mode, meant that it was impossible to guarantee that the volume of material sampled contained only the phase observed on the surface of the specimen. Monte Carlo simulations have shown that the electron beam voltages used result in the volume sampled penetrating 2-3μm into the material[84]. This was particularly problematic for very small grains or precipitates whose visible areas were only 2μm across. Attempts were made to carry out X-ray microanalysis using a transmission electron microscope. However, despite several attempts in the time available the optimum level of thinning and electropolishing on the specimen was not established. Attempts frequently resulted in the specimen being thinned too much, causing the precipitates to fall out of the specimen, probably due to the material around the precipitates being preferentially removed. This would seem to indicate that the precipitates were sigma phase as it is known that the material around sigma phase precipitates commonly suffers from a loss of corrosion resistance due to the localised loss of chromium and molybdenum[52].

5.3 Initial Experiments

The initial experiment determined that the GTA welding arc would remain stable at all pressures and established the influence of pressure on the arc voltage for a GTA welding arc when the anode was a duplex stainless steel. The results of the first bead on plate welds performed at pressures of 1-32bar are shown in Tables 4.1-4.3. The influence of pressure on the arc

voltage in this work is shown graphically in Figure 4.1. The voltage relationships predicted by equation 2.1 for pure argon[6] and pure helium[15] arcs are also shown in equation 2.1. Although there is some variation in the arc voltages achieved in this experiment, it is still obvious that the use of the shielding gas containing helium increases the arc voltage above that obtained from a pure argon shielding gas. It can be seen that the influence of pressure on the arc voltage for the helium/argon shielding gas is similar to that predicted for pure helium and pure argon arcs. As the aim of these initial experiments were to determine the weld bead penetration and not to study the influence of pressure on the welding arc, insufficient data were obtained to quantify the relationship with an empirical equation.

Although the arc remained stable, the arc voltages were not as high as initially anticipated resulting in low heat input values. The heat inputs achieved (Tables 4.1-4.3) by the welds at atmospheric pressure were in the range of 0.3-0.5kJ/mm. These values were lower than those recommended in the reviewed literature. Hence, the resulting weld bead penetrations were disappointing. All of the resulting weld bead profiles were wide and shallow as exhibited in Figure 4.2. Although the voltage increased with pressure as discussed earlier, thus causing the heat input to be increased, the weld penetrations were still low. Another effect of low heat inputs predicted by the literature survey is the production of a mainly ferritic structure in the weld metal, which also occurred in the initial bead on plate welds in the current work as shown in Figure 4.3. The weld metal microstructure clearly shows large primary ferrite grains with some austenite formed intergranularly. There is no visible evidence of any austenite forming within the ferrite grains, indicating that the cooling rate from these low heat input welds was too high to allow much diffusional growth. The use of a filler metal overalloyed in nickel would have improved the phase balance a little but it would probably not have produced a completely satisfactory weld. If the conditions used for these were used for a welded joint it would have resulted in poor toughness properties[72-74] and poor corrosion resistance[73]. These experiments therefore support the view that a minimum heat input in excess of 0.5kJ/mm is required for welding these steels at atmospheric pressure[74].

In view of these disappointing penetration results, a second set of experiments was performed at a pressure of one bar only. Knowledge of arc voltage achieved from the previous experiment was used to obtain a range of heat inputs closer to those recommended by the literature. This enabled a suitable set of parameters for the thermal cycle experiments to be determined. The weld bead profile in Figure 4.4 is clearly an improvement on the previous

example. The weld metal microstructures were still mainly ferrite, indicating that the addition of filler metal is required to achieve a satisfactory phase balance. Table 4.4, shows the distribution of the main alloying elements between the ferrite and austenite in the weld metal and the parent plate. The partition coefficients of the alloying elements between the ferrite and austenite in the weld metal deviate from those of the equilibrium structured parent plate material, particularly with respect to the molybdenum content. In all cases the molybdenum content in the austenite is higher in the weld metal than the parent plate material, increasing the passivity of the austenite and thus making preferential corrosion of this phase less likely. However, it must be noted that this increase in corrosion resistance is at the expense of the weld metal toughness which is reduced due to the high ferrite content.

5.4 Thermal Cycle Measurements

The aim of this set of experiments was to determine the influence of pressure on the weld thermal cycle in duplex stainless steels. This was to establish whether any of the deleterious secondary phases discussed in the literature survey would be likely to form in the welded joints prepared under hyperbaric conditions.

5.4.1 The influence of pressure on the weld thermal cycle

The influence of both pressure and heat input on the cooling characteristics of a weld are shown in Figures 4.5-4.7. Increasing the heat input from 1kJ/mm to 2kJ/mm clearly increases the total cooling time from the melting point to a temperature of 300°C, where no transformations are likely, by more than a factor of three, a point to be considered when choosing heat input values to minimise the production of secondary phases such as sigma phase. Conversely, increasing the pressure to 32 bar reduces the cooling time to between one quarter and one third of its value at 1bar. This would suggest that the probability of secondary phase formation would be reduced as the pressure is increased, and that using an increased heat input at higher pressures would be possible. However, it is worth noting that even at 32bar, the total cooling time for a 2kJ/mm heat input weld is still greater than that of a 1kJ/mm weld performed at 1bar. This is shown in Figure 4.7.

Analyses were performed to determine the influence of pressure on the cooling times through two temperature ranges, 1200-800°C thought to be of significance for the formation of primary austenite and 800-500°C where deleterious secondary phases such as sigma phase, are likely to occur. These

results are shown in Figures 4.8-4.9. It can be seen that the most significant reduction in cooling time with pressure for both temperature ranges occurs for the 2kJ/mm heat input welds. The cooling times in the 1200-800°C temperature range are significantly greater for the 2kJ/mm heat input weld implying that this heat input would produce the most favourable austenite contents as stated in previous work[72-74]. However it would be unwise to rely on a high heat input to produce the required weld metal microstructure, as the cooling time in the temperature range 1200-800°C is highly influenced by increases in pressure. The widely used method of employing a filler metal overalloyed in nickel would appear to be the simplest means of ensuring sufficient austenite formation when using the hyperbaric welding process.

The cooling times for the 2kJ/mm heat input welds are also much higher in the 800-500°C temperature range than for the 1kJ/mm heat input welds, and are once again more influenced by increases in pressure. Although the cooling time for the 2kJ/mm heat input welds were significantly reduced at higher pressures, they were still long enough to permit possible secondary phase precipitation, particularly when the cumulative effects of multipass welds are considered. The 1kJ/mm heat input welds produce cooling times in the range of 10-15s, indicating that the lower heat input would not cause significant secondary phase formation in the HAZ. This is the method that was recommended by Gooch[76] to minimise sigma phase formation. This would imply that a low heat input weld should be used to minimise the amount of secondary phase precipitation, and that attainment of the optimum amount of austenite in the weld metal should be pursued by some other means. The most reliable method of achieving this would be by choosing the correct consumable.

5.4.2 The influence of pressure on the weld bead geometry

Increased pressure produces greater penetration and fusion areas as shown in Figure 4.10-4.12. The increase in penetration as shown in Figure 4.13 was in the range 20-40% for the 1kJ/mm heat input over the first 20bar and 40-80% for the 2kJ/mm heat input compared with a 100% increase for argon arcs and a 30% increase for helium arcs reported in the literature[5,14,15,18]. There is a possibility that the behaviour of the helium/argon gas mixture may be closer to pure helium at lower currents, tending to move towards the behaviour of an argon arc at higher currents. The weld bead shapes shown in Figure 4.10-4.12 appear to be symmetrical implying that the

arc was not wandering and that no external means, such as an applied magnetic field would be required to stabilise its behaviour.

In addition to the increase in penetration there is evidence of a slight increase in weld bead width as observed in previous work[5,14,15,18]. The overall increase in weld bead area has previously been accredited to the increase in voltage increasing the heat input to the weld [18] and also to the increase in arc melting efficiency [5]. In this work attempts were made to maintain the heat input levels as the pressure was increased. This was facilitated by increasing the welding speed to compensate for the increase in arc voltage. Hence, in the current work, it would seem that the increase in fusion area with pressure is due to an overall increase in arc efficiency. Allum[13] used an expression to calculate the arc melting efficiency based upon the fusion area, heat input and an estimated value of the energy required to raise a given volume of the parent plate material to its melting point and to melt it. When this expression is applied to the weld fusion areas achieved with the present work a graph of efficiency against pressure (Figure 4.14) is produced. From these diagrams it may be concluded that the increase in fusion area is closely linked to an increase in arc melting efficiency and this is most likely to be the controlling parameter. In order to perform the welds at increased pressures using parameters based upon those recommended for welding at one atmosphere it would seem that it is also necessary to compensate for the increase in efficiency when choosing the weld parameters for the welds at higher pressures.

5.5 Production and Properties of Welded Joints

5.5.1 Production of Joints

The welding parameters that were used to evaluate the weld joint design were selected for the initial full welded joints. As with the previous experiments the 1bar weld was to be performed first as welding of duplex stainless steels at 1bar was well documented and any problems encountered would therefore be easily overcome. However great difficulty was encountered in producing the first root weld for the welded joints. None of the literature surveyed had reported any problems in welding duplex stainless steels although some industrialists had verbally reported problems. As the problems with obtaining a root weld were so great in this work, it was assumed that the problem must be due to attempting to weld the steels automatically. As none

of the surveyed literature had specified whether it was automatic or manual welding that was used, it could be assumed that previous work had used manual welding to produce welded joints.

The main problem encountered in trying to achieve a root weld in the duplex alloys was in getting sufficient penetration. This was caused by the material warping when it was being welded causing the joint to close up before the arc reached it. Warping is commonplace in austenitic stainless steels and was expected, to a certain extent, in duplex stainless steels. It was hoped that the strongbacks which were attached to the joints to hold them in the correct position prior to welding would be strong enough to prevent warping from occurring. Attempts to overcome the problems of the weld closing up by increasing the process power in order to melt more material in the root were unsuccessful. Here, even minute increases to the welding current caused the root to burn through which led to catastrophic loss of control of the welding arc leading to abortion of the run. This occurred frequently in the initial stages, rapidly depleting the supply of weld preparations as well as causing significant delays in the intended experimental programme.

The welds parameters used to test the joint profile included a weaving arc. The weave pattern was modified along with the welding parameters a number of times before the weaving arc movement was abandoned. Eventually pulsing the welding arc current was attempted and seemed to produce more promising behaviour. Attempts to refine the pulse parameters to achieve optimum penetration were only partially successful so it was decided to abandon the pursuit of a consistently satisfactory root run as it did not appear to be a worthwhile exercise in the time available. Once the first joint had been completed at a pressure of 1bar, the parameters for welding at pressure were modified to account for the influence of pressure on the welding process, based on data from the earlier trials. It was found that achieving full penetration on the root at higher pressures was much easier than at 1bar.

The reason for the difficulty in achieving satisfactory root weld parameters at 1bar has not yet been identified. The phenomenon known as cast to cast variation in austenitic steel was considered. Here when elements such as sulphur, oxygen or silicon are reduced due to the presence of trace elements such a aluminium, calcium and selenium low weld penetration can occur. Since this would have been a consistent problem throughout all of the attempts to perform the root weld, it is unlikely to be the reason for the unpredictable behaviour in this case.

Despite the problems that were encountered in achieving the root weld at 1bar, the parameters used in this work are a good basis for an investigation to determine the optimum welding parameters. There does appear to be a power law relationship between the heat inputs that were used to achieve the root welds and pressure as shown in Figure 4.19. Analysis of these data have provided the following relationship:

Equation 4.1

$$q = 1.81\left(\frac{P}{P_0}\right)^{-0.56}$$

where q is the heat input

P is the pressure

P_0 is atmospheric pressure.

Due to the difficulties encountered in obtaining the root welds, there was insufficient time to expand on the work to obtain an operating envelope of parameters within which a joint could be welded satisfactorily. However this relationship may prove to be useful in future work if the parameters for welding at 1bar can be first determined.

5.5.2 The thermal cycle history of the welded joints

The influence of pressure on the weld thermal cycle for a single run autogenous bead on plate weld was discussed in section 5.4.1. It was stated that by increasing the pressure from 1bar to 32bar, the total cooling time could be reduced by two thirds and the times spent in the temperature ranges at which secondary phases are known to form were also reduced. However, it is not possible to predict the thermal cycle behaviour of the full welded joints, for reasons that will now be discussed.

The way in which the welding parameters were adapted to account for the influence of pressure on the welding process meant that the joints welded at higher pressures required more welding passes to fill them. To compensate for the increase in voltage and increase in arc melting efficiency that occurs as the pressure of welding is increased, the weld travel speed was increased accordingly. As the wire feed rate remained constant with time, the amount of welding consumable deposited on each weld pass was reduced as the pressure was increased. Hence, the number of weld runs required to complete a joint was increased as the pressure was increased. The cumulative effect of

a greater number of weld runs may have negated the influences of faster cooling for individual runs. The thermal cycle data were analysed and it was found that increasing the number of weld runs did not increase the amount of time spent in a temperature range where secondary phases are likely to form. This is shown graphically in Figure 4.20 where the time spent in the 800-500°C temperature range is plotted for each weld run for joints completed at 1, 8, and 32bars. However it may be argued that this is specific to the material around the root weld where the thermocouples were positioned. To prove this theory it would be necessary to expand this work by obtaining thermal cycle data for other areas of the weld.

5.5.3 The microstructure of the welded joints

This work studied the effects of welding at six different pressures on three separate alloys. Obviously, it would be a laborious process to discuss each individual weld in turn, especially as the differences in progressing from pressure to pressure may be small. Therefore each alloy will now be discussed individually, primarily taking note of the changes in microstructure caused by changes in pressure, and secondarily noting any differences that occur due to the different alloy compositions.

5.5.3.1 Avesta 2205

In the first instance the microstructure of the Avesta 2205 weld performed at a pressure of 1bar will be discussed. The microstructure of the weld performed at 32 bar will then be addressed and the differences in microstructure between the weld carried out at these two extremes in pressures will then be examined, together with any notable aspects of the welds performed at the intervening pressures.

It can be seen in Figures 4.21(a) and 4.22 that there was incomplete fusion on the root weld at 1bar. This could have been caused by several factors including the problems with achieving full penetration and geometric mis-match in the joint fit up. In Figure 4.22 the microstructure seems to consist of dark regions in the laid down weld metal: these are not precipitates but fine grained material. All of the weld metal appears to consist of coarse primary grains which have been refined by further weld passes reheating the non equilibrium structure. Within the large primary ferrite grains there are some Widmanstätten side plates of austenite visible at low magnifications. There is also a region in the centre of the first pass that on first appearances has a fine grained austenitic structure. This would normally imply that the material would have a high toughness. However, although the mainly austenitic structure is

confirmed at higher magnifications (Figure 4.23), it also appears that some of the ferrite has transformed to sigma phase even though the time spent in the sigma phase forming temperature range for this weld was less than one minute. The precipitation of sigma phase in this case could have been assisted by the thermal stresses present when welding, as it is already known that prior cold work can contribute to the precipitation of sigma phase. Although the volume fraction of sigma phase is low, it is still likely reduce the toughness[43,49,52] and the corrosion resistance[47,48,52] in this region. Unfortunately the large volume fraction of austenite observed in this area probably consists of the low grade secondary austenite that is low in the passivating elements chromium and molybdenum, which would mean that this area would be susceptible to corrosive attack[51].

The boundaries between the weld passes can be seen at low magnifications (Figure 4.24). This is mainly due to the reheating effects of successive weld passes on the weld metal. The microstructure of the reheated region consists of primary ferrite grains with austenite at the grain boundaries and some austenite growing into the ferrite grains. Finer austenite grains are produced on further transformation giving an acicular type structure within the grains that presents itself as dark regions at low magnifications (Figure 4.25) but which can be resolved at higher magnifications (Figure 4.26). The acicular austenite will have improved the toughness but as it is likely to be deficient in chromium and molybdenum it will have a slightly reduced corrosion resistance compared with that of weld metal that has not been reheated[64]. The brighter regions seen at low magnifications, forming a border between subsequent weld beads, are in fact similar to the region of ferrite growth commonly seen in the HAZ of duplex welds. Here, the temperatures reached during the weld thermal cycle have been sufficient to cause complete ferritisation of the material and the cooling rates have been too fast to allow a measurable amount of transformation to austenite to occur[64]. The phase balance is obviously difficult to measure for such small grain sizes but is estimated to be around 50% ferrite. On the whole, the combination of small grains and even phase balance in the reheated weld metal imply that the mechanical properties should be very good, perhaps approaching those of the parent plate material.

The cap weld beads (Figure 4.26) are made up of large ferrite grains with only small amounts of austenite forming at the grain boundaries and a little intragranular precipitation. It is apparent that the cap welds have not had the benefit of reheating by subsequent passes that the previous runs have, and therefore, this non-equilibrium structure predominates. This may of course be fortuitous from the point of view that the occurrence of deleterious

precipitates is low, but on the other hand the high ferrite content, large grained cap material will have a low toughness compared with the rest of the weld. Therefore it could be an area of weakness as it would allow an easier route for the propagation of surface initiated cracks.

At the fusion line and HAZ (Figure 4.28) the grains are noticeably coarser than in the reheated regions of the weld metal. The region of ferrite growth adjacent to the weld metal, as described by Atamert and King[63], is the only area where there is a change in the bulk microstructure. At positions further away from the fusion line there are what appear to be large precipitates when viewed at low magnifications. These can be resolved into areas of smaller precipitates in the ferrite (Figure 4.29), their identity has not been positively determined due to the difficulties discussed in section 5.2, but due to their position and form they are most likely to be chromium nitrides[75]. In addition to these precipitates there is some evidence of sigma formation at the δ/γ grain boundaries. As with the sigma formation in the weld metal, the thermal exposure times experienced by the HAZ are lower than those required to cause precipitation in the parent plate material, hence the action of thermal stresses are thought to be responsible for the enhanced precipitation. The presence of sigma phase and chromium nitrides indicate that the toughness[43,47,49,52] and corrosion resistance[47,48,52,75] will be reduced in the HAZ.

There is full penetration of the root on the 32 bar weld. It is obvious that the filler metal has penetrated completely (Figure 4.30) whereas in the lower pressure welds complete penetration only consisted of limited fusion in the root. As with all of the other welds the dark-etching areas seen on the low magnification photographs can be resolved into a finer structure at higher magnifications. When compared with the microstructure of the root material of the lower pressure welds, it can be seen that the microstructure of the 32bar (Figure 4.31) weld is much finer than that of the 1 bar weld whilst still retaining a similar balance of austenite and ferrite in similar morphologies. In fact there are no signs of any secondary phases being present in the root weld metal in this particular case. It would be expected in view of these favourable microstructural conditions that both the mechanical and corrosion properties of the root area of this weld would be superior to those of the lower pressure welds.

In the middle of the 32bar weld metal (Figure 4.32), which once again consists of mainly reheated material, the faster cooling rates experienced due to the increased pressure result in a finer microstructure. The primary grains that first form upon cooling (Figure 4.33) are finer than those achieved at lower

pressures, as would be expected for a faster cooling rate. The weld beads are smaller than those of the one atmosphere weld due to less material being laid down each time, but also their shapes are more balanced than in the one atmosphere joint. In addition to the primary grains being finer the microstructure within the grains is also finer, with the morphology moving to a more acicular type at lower pressures which contained more Widmanstätten type microstructure. This refinement in the microstructure means that the mechanical properties of the welds performed at higher pressures should be superior to those of the lower pressure welds.

As higher pressures produce faster cooling rates, it would be expected that the capping welds would have a more ferritic structure than the welds at lower pressures, resulting in slightly lower toughness, particularly as the cap welds do not benefit from the positive effects of reheating by subsequent weld passes. However it can be seen that for the 32bar weld (Figure 4.34) this is not the case. The higher austenite content is shown in the form of more Widmanstätten sideplates and more acicular austenite nucleating intragranularly in the ferrite grains, producing cap material of higher toughness than that of the 1bar welds. If a shielding gas containing active gas ingredients that promote the formation of austenite had been used, this phenomenon would have been easily explained. However the shielding gas used was an inert gas and therefore should not have affected the microstructure at all. This may be an area which requires further investigation in future projects.

The extent of the coarse grained HAZ of the 32bar weld (Figure 4.35) is effectively the same as that of the one atmosphere and other low pressure welds, whilst it's microstructure is in fact finer than that of the lower pressure welds. It may be possible that the finer microstructure is due to the higher cooling rates encountered when welding at higher pressures. In work performed at 1bar, Atamert and King[63] observed that the extent of the coarse grained HAZ decreased as the heat input of the weld was decreased. In this work the heat input was decreased and the cooling rate increased as the pressure was increased, which, on this basis, should have led to some reduction in the extent of the ferrite growth region. It is possible that the cumulative heating effects of the greater number of weld passes required to fill the joints at higher pressures were responsible for maintaining the size of the coarse grained HAZ. Again there are some precipitates present in the HAZ at greater distance from the fusion zone as shown in Figure 4.36, but on the whole their volume fraction is lower than that achieved at lower pressures, which once again implies that the weld properties of the 32bar weld are more favourable.

As the pressure progresses from 2 to 16 bars there is an overall increase in the weld quality (Figure 4.21). The weld beads seem to adopt a more uniform appearance at the higher pressures. The main change is seen in the penetration of the root welds which are improved considerably at pressures over 4 bar. Even below 4 bars the root welds have better fusion than the 1 bar weld although this may be due to better weld fit up. It must be noted that full penetration is not achieved at the lower pressure, which may be due to excessive warping in the joint prior to fusion. A feature in the 4 bar (Figure 4.37) weld root is the presence of considerable grain boundary precipitates which will make the weld susceptible to corrosion in this area, and may result in stress corrosion cracking in the HAZ if the weld root is exposed to excessive stress. In the welds performed at 8 and 16bar there is complete penetration in the root, with an appreciable underbead being achieved at 16bar. It would seem, therefore, that the root weld properties are improved as the welding pressure is increased.

5.5.3.2 Sandvik SAF 2507

In the root weld Figures (4.38(a) and 4.39) of the 1bar weld of SAF2507 there is more penetration than for the corresponding weld of the Avesta 2205 material although it does not appear to be complete. Once again, this is due to the mis-match in the joint fit up. Even at low magnifications it can be seen that the grains in the root appear to be larger than in the corresponding Avesta 2205 weld. This is confirmed at higher magnifications (Figures 4.40-4.41). It can be seen that precipitates are present in the weld metal once more. Judging from their shape, colour and location and from the literature [44,46] these are not sigma phase as in the case of the corresponding Avesta 2205 weld, but chromium nitrides. This would be expected when comparing the compositions of these two materials as the SAF 2507 has both more chromium and nitrogen available to form this precipitate. As with sigma phase, this phenomenon is undesirable due to its effect upon the corrosion resistance of the material, and must be avoided if possible.

The reheated region exhibits a very similar microstructure to that found in the corresponding Avesta 2205 weld. Again, the weld bead boundaries are shown as bright lines at low magnifications (Figure 4.42), whilst the darker regions are representative of the areas with finer microstructures which have undergone transformation upon reheating by subsequent weld passes. In the case of the SAF 2507 weld, however, this finer microstructure appears to have a larger grain size than previously with some very fine grains forming

intragranularly (Figure 4.43). These appear to be surrounded by blocky precipitates similar in appearance to those found in the root weld and are most likely to be chromium nitrides once more.

The cap material has a vastly different appearance from that of the Avesta 2205 welds. It can be seen that the primary grain size is a great deal smaller than seen previously (Figure 4.44). At higher magnifications (Figure 4.45) it can also be seen that there is a greater proportion of austenite in this material. The cooling rates are essentially identical for the welds on these two steels, and so it is likely to be caused by the increased concentrations of austenite formers such as nickel and nitrogen. The smaller grain size and higher austenite content of the cap weld in this material signify that it is likely to have a higher toughness than the corresponding region in the Avesta 2205 weld.

A common factor in the Sandvik SAF 2507 welds is that they all contain chromium nitride precipitates in the HAZ from the root weld up to the cap weld. This can be seen as the lighter shaded "shadows" adjacent to the weld metal in Figure 4.38. This phenomenon, exclusive to these welds, is almost certainly due to the higher concentrations of both chromium and nitrogen in the parent material, although careful selection of the welding parameters in future welds would also probably assist in minimising this effect. Examination of the remaining microstructures in these areas (Figure 4.46) reveals that there is no other sign of transformation in the bulk microstructure around the precipitates, this would indicate that the choice of welding parameters is not the sole reason for the precipitation but that the composition was a deciding factor.

In the weld performed at 32bar (Figures 4.38(f) and 4.47) there is complete penetration in the root weld as for the Avesta 2205 weld at the same pressure. However in this case the underbead is not as large. At higher magnifications (Figure 4.48) the microstructure of the root is revealed to be essentially the same as for the lower pressure welds but finer, although there are no precipitates in the weld metal. Both of these phenomena would be expected due to the faster cooling rate achieved at higher pressures. In the case of the chromium nitride precipitates it would appear that the formation of precipitates in the root weld of the 1bar weld could have been avoided with the selection of more appropriate welding parameters.

At low magnifications the reheated weld metal seen in Figure 4.49 shows the same microstructure as the corresponding one atmosphere area. However if examined more closely it can be seen that there are fewer precipitates in the weld metal than seen previously. The grain sizes are also

smaller than before (Figure 4.50), consistent with the higher cooling rates caused by the higher pressure. The cap material appears to have the same microstructure (Figure 4.51) as the weld performed at one atmosphere, but at higher magnifications (Figure 4.52) it is apparent that there are slight differences in the morphology. The small grains of austenite that formed intragranularly in the primary ferrite grains appear to be aligned to the grain boundaries at an angle similar to the side plates growing from the grain boundaries. This implies a crystallographic influence on the growth direction.

There are precipitates in the HAZ of the 32bar weld (Figure 5.53) similar to those found in the corresponding region of the 1 bar weld. This would seem to indicate that the welding parameters used for the lower pressure weld were not the primary cause of the precipitation, as the faster cooling rates experienced by the 32bar joint still produced precipitates. As discussed previously, the determining factor in causing this precipitation is almost certainly the higher chromium and nitrogen content of the Sandvik SAF 2507 alloy. Hence, to prevent the precipitation of chromium nitrides in the HAZ of welds at all pressures the alloy content should be carefully monitored to ensure that the levels of these elements are not excessive.

As with the Avesta 2205 material, the root weld quality in the SAF2507 joints improves as the pressure is increased. In fact there is complete penetration for all the welds carried out at pressures above 1bar. Unlike the Avesta 2205 material, there are no apparent changes in microstructure that occur as the welding pressure is increased. It is worth noting that the chromium nitride precipitates found in the HAZ of the welds carried out at 1 and 32bar are present in every weld (Figure 4.54), implying that the corrosion resistance of all the welds in SAF 2507 will suffer from loss of corrosion resistance.

5.5.3.3 Zeron 100

It is obvious from Figure 4.55(a) that there has been no penetration whatsoever in the 1bar weld. It can also be seen that any problems that may be due to the welding process and parameters have been aggravated by very bad joint fit up, and, it is impossible to discern whether full penetration would have been achievable if the joint had been properly prepared. There is some fusion of the parent plate material but this is restricted to one side of the joint. The other side of the joint has undergone sufficient heating by the root weld to produce some chromium nitrides in the parent plate material (Figure 4.56), a

problem that in common with the SAF 2507 material is due to the increased nitrogen and chromium contents found in this alloy. At higher magnifications (Figure 4.57) it is clear that the microstructure of the root weld metal in this alloy is very similar to that found in the alloys discussed earlier, being an even balance of austenite and ferrite, with the austenite being in the form of both Widmanstätten sideplates growing from the grain boundaries, and smaller acicular type grains within the ferrite crystals. It is possible that there may be some precipitates forming at the grain boundaries of the ferrite and smaller grains of austenite. If this is the case it may be that the austenite is secondary austenite, which has a lower corrosion resistance, formed as a direct result of the precipitation of deleterious phases such as sigma phase.

Once again the boundaries of the weld passes are delineated by bands of ferrite grains in the microstructure, which appear as lighter colours at lower magnifications (Figure 4.58). The microstructure consists of larger side plates of austenite growing into the ferrite and some smaller grains which have obviously formed as a result of reheating by subsequent weld passes. There is no discernible difference in the microstructure of the reheated regions found in this alloy compared and the two alloys discussed previously.

The phase balance of 1bar cap weld (Figures 4.59, 4.60) lies between that of the corresponding welds in Avesta 2205 and SAF 2507. The majority of the austenite phase formation in this case has occurred at the ferrite grain boundaries and has grown into the ferrite as sideplates. There are some regions of smaller precipitates between the sideplates but these seem to be aligned at the same orientation to the grain boundaries. When comparing the reheated weld metal microstructure and the cap materials microstructure, it is clear that in this case there is a great deal of refinement of the material when it is reheated.

In the HAZ of the 1bar weld there are a large number of precipitates approximately 4-5mm away from the fusion line (Figure 4.61). On first consideration these appear to be just chromium nitrides as in the welds of Avesta 2205 and SAF 2507, but when examined closely, it is clear that sigma phase is present at the ferrite/austenite grain boundaries (Figure 4.62). This is unwelcome as it means that in addition to the loss of corrosion resistance caused by the chromium nitrides, the material's toughness is also reduced by the presence of sigma phase.

During the latter stages of preparation of the 32bar weld in Zeron 100 problems with the wire feed mechanism occurred as described in section 5.2. It was not always immediately apparent when a weld was being performed at

which point the wire feed mechanism malfunctioned. As a result some regions underwent unnecessary heating which will have caused more deleterious precipitations and hence reduced the mechanical performance and the corrosion resistance of the weld metal and HAZ. When this weld was performed the supply of prepared weld profiles had been exhausted and it was hoped to repeat this weld at a later time, however there was insufficient time to do this and so the properties of this joint will now be discussed.

As with all of the other welds performed at higher pressures, the weld performed on Zeron 100 at 32bar has complete fusion in the root weld (Figures 4.55(f) and 4.63). In this weld however, the microstructure appears to be different having less austenite than the weld at 1bar. The austenite that is present is in the form of fine grains (Figure 4.64). It is unlikely that this has been caused by the effects of excessive reheating during the latter stages of preparation of this weld as it can be seen from all the previously discussed welds that the reheating effects of the later weld passes would not have extended this far. However, the higher cooling rate associated with welding at higher pressures may have retarded the formation of austenite in this weld.

The effects of more weld thermal cycles and the faster cooling rate appear to have had a similar effect on the microstructure of the reheated weld metal (Figure 4.65). Here the austenite is mainly in the form of fine intragranular precipitates which form during subsequent weld passes as opposed to the Widmanstätten sideplate microstructure which is formed on the first weld pass. As in the previously discussed welds this austenite will have lower concentrations of chromium and molybdenum and therefore have a slightly lower corrosion resistance than freshly deposited weld metal.

The cap weld consists of primary ferrite grains that are smaller than the lower pressure welds due to the faster cooling rate (Figure 4.66). The austenite formed in the cap is mainly fine grained acicular type austenite, which seems to have formed in bands. These bands are orientated to the grain boundaries at similar angles to that of the Widmanstätten sideplates (as seen in Figure 4.67). The finer grains in the austenitic structure is obviously another manifestation of the higher cooling rate.

The HAZ contains less chromium nitride and fewer of the sigma grain boundary precipitates than the lower pressure weld (Figure 4.68). As in the case of all of the other welds performed at higher pressures this is due to the faster cooling rates associated with higher pressures and is advantageous to both the toughness properties and corrosion resistance of the HAZ.

As the pressure used during welding is increased from 2 to 16 bars the appearance of the Zeron 100 welds improve as with the previously discussed alloys. All of the welds carried out at pressures above 1bar have complete penetration on the root and acceptable microstructures. The weld performed at 2bar pressure is an exception as it has clusters of precipitates which are most likely to be chromium nitrides in the root material (Figure 4.69). Another anomaly is the weld performed at 8bar which appears to have a line of precipitates aligned across the root weld (Figure 4.70). At higher magnifications it is clear that these precipitates are located on a prior ferrite grain boundary (Figure 4.71). This grain boundary could have become aligned in this way as a result of the arc being positioned off to the side of the joint at this particular point.

5.5.3.4 Summary of Microstructural Changes

In the three materials investigated, it is obvious that the appearance of the weld improves as the pressure is increased. The precise reason for this is unknown. The increase in cooling rate would account for the microstructural improvements, but not necessarily for the improvements in the weld bead geometries. In fact, earlier work[13,16] suggested that the symmetry of the weld bead is lost as the pressure is increased without the use of an external stabilising process.

The phase balance in the weld metals of the three materials have not been adversely affected by the increased cooling rates at higher pressures. Any effects of faster cooling have been compensated for by the reheating of the weld metal by subsequent weld passes. Whether the austenite formed as a result of reheating is secondary austenite has not been confirmed. X-ray microanalysis was not really feasible on such a fine grained structure so another form of analysis or test must be used for future work.

In all of the materials investigated, it has been shown that welding at higher pressures produces welds with less precipitates. Previous work has shown that exposure to high temperatures increases the tendency for precipitates to form. Thus, it must be concluded that the higher cooling rates experienced as a result of increased pressure are the main driving force behind the improvement in quality of the weld microstructure.

5.5.4 Mechanical Properties of the Welds

5.5.4.1 Hardness Survey Results

There is often an upper limit placed on the hardness by codes relating to the welding of pipeline steels. For example, in the Statoil specification quoted in the literature[81], the requirement for welds in pipeline steels is that no part of the HAZ or weld metal should have a hardness greater than 285HV10. This requirement is to give an indication whether hydrogen sulphide stress corrosion cracking could take place. In the case of duplex stainless steels this level may be too conservative as the hardness of the parent plate material is in the range of 230-260HV10 in the untreated state. In fact Lundqvist and Norberg[74] stated that the level of 285HV has been translated from an often quoted value of 28HRC, which for the weld metal of a duplex stainless steel of the same type as Avesta 2205 has been shown to be equivalent to 350HV. This will be considered when the results of the hardness tests are discussed.

The hardness values of the weld metal in the welded joints are shown in Tables 4.5-4.7. Generally they are below the 300HV10 level with the exception of some of the Zeron 100 welds which only just rise above this level. There is inconclusive evidence that the super duplex alloys have higher weld metal hardness values than the standard duplex alloys, probably due to the higher alloying content of the super duplex welding consumables, particularly chromium and molybdenum. The difference in the weld thermal cycles experienced by the root and the cap areas of the weld may lead to higher ferrite and precipitate contents in the root region, and therefore it would be expected that a difference in the hardness values would be found. However in these welds there is no clear evidence to support this theory. It is possible that any increased tendency to form secondary phases in the root area are cancelled out by the beneficial effect of successive thermal cycles. This would also apply to the middle of the weld metal, which may undergo reheating treatments, and consequently may not exhibit any difference in hardness from other areas of weld metal.

The hardness values of the HAZ of the Avesta 2205 welds are shown in Table 4.8. All of the values were below 300 HV10, probably due to the lower concentrations of the ferrite stabilising elements such as chromium in the standard duplex alloys. There is no evidence of the pressure at which the welds were made affecting the hardness values found in the HAZ, although there is evidence that the HAZ of the cap area is not as hard as that of the root area, This is probably due to the root being exposed to more thermal cycles, which would increase the tendency for ferrite growth or secondary

phase precipitation. The HAZ in the welds of SAF 2507 (Table 4.9) were all harder than the Avesta 2205; the hardness values exceeding 300HV10 in many places. This would be expected as this alloy has higher concentrations of the ferrite stabilising elements that are also thought to be responsible for the greater tendency of super duplex alloys to precipitate secondary phases. As with the Avesta 2205 material there is some evidence that the HAZ around the cap area is not as hard as that of the root, and also there may be an improvement in the hardness values of the welds performed at higher pressures due to the increased cooling rate experienced by these welds. As seen in Table 4.10, the Zeron 100 welds also have some hardness values above 300. This is to be expected as the materials composition is very similar to that of the SAF 2507 material. In this case, however, there is no evidence of the pressure at which the welds were performed affecting the hardness values found in the HAZ.

Due to the effects of pressure on the cooling rate of welds it may be argued that the extent of the HAZ in the welds decreasing with increasing welding pressure, and hence any increases in hardness in the HAZ, should also be reduced for the higher pressure welds. However in the case of these welds, as the pressure is increased the number of weld passes required to complete the weld also increases. This is due to the way in which the welding parameters were deliberately altered to compensate for the effects of pressure on the welding process. Hence, it may be that any changes in cooling rate experienced by the material due to changes in pressure are negated by the increased number of weld thermal cycles experienced. In the weld metal the increased number of weld passes may not have adversely affected its properties due to the high level of primary austenite, but in the case of the HAZ it may cause the formation of unwanted precipitates.

5.5.4.2 Charpy Impact Tests

The results of the Charpy impact tests on the parent plate, weld metal and HAZ of each material are shown in Figures 4.72-4.74. The results of the tests performed on the parent plate material of the three alloys gave results similar to those found in the surveyed literature for the Avesta 2205 and Zeron 100 materials. However the SAF 2507 material gave very low values in the as supplied condition. To determine whether this was due to any age hardening effects the tests were repeated on some material which had undergone an annealing heat treatment at 1050°C for ten minutes. It can be seen that there is a little improvement in the Charpy impact toughness but it still remains very

low. Therefore it is more likely that the low values are due to the orientation of the test piece in the parent plate material, which is a traverse specimen notched so that the crack would propagate longitudinally with respect to the pipe axis. The low toughness of the SAF 2507 parent plate material must be taken into consideration when the results of the impact tests on the HAZ of the welds are assessed.

The weld metal of the Avesta 2205 welds (Figure 4.72(b)) generally does not exhibit any indication of undergoing any ductile to brittle transition at the temperatures tested, apart from the welds performed at 2 and 4 bar. These seem to have reduced toughnesses at lower temperatures although a ductile to brittle transformation does not occur. There is some evidence that the impact toughness values of the welds performed at higher pressures are higher than those at lower pressures, although this is not conclusive. It must be noted that the toughness values of the weld metal are higher than those of the parent plate material, which must be taken as a positive indication of the improvement in weld metal microstructure. This is most likely due to the overmatching of the welding consumables with respect to nickel. All of the welds have Charpy impact toughness values above 150J at -40°C, thus exceeding the requirement at this temperature by over 100J. The toughness values for the super duplex alloys SAF 2507 (Figure 4.73(b)) and Zeron 100 (Figure 4.74(b)) are not as high as those of the Avesta 2205 alloy although they do exceed the requirement of 27J. In the case of the SAF 2507 weld metal the toughness values far exceed the depressed values obtained from the parent plate. Conversely, the Zeron 100 weld metal does not perform as well as the parent plate material. It would seem that the weld metal Charpy values are determined mainly by the composition of the consumable. As the super duplex alloys are more heavily alloyed in the ferrite forming elements chromium and molybdenum than the standard duplex alloys, the positive effects of overmatching with the austenite stabilising element nickel may be negated and the toughnessof the weld metal reduced accordingly. As with the Avesta 2205 material, increases in the pressure at which the welds are performed reduce the tendency for the material to show any sign of undergoing a ductile to brittle transition. There is one exception to this, which is the Zeron 100 weld performed at 32bars This was expected to be a poor quality weld before any examination took place due to the problems encountered with the wire feed mechanism during welding.

The HAZ Charpy specimens (Figures 4.72(c), 4.73(c), 4.74(c)) were all 7.5mm thick so it could be argued that a 1.33 scaling factor should be applied to the resulting values. However, this would ignore the effects of specimen

size on the toughness values so the scaling factor will be ignored in this instance. Generally the HAZ Charpy impact results of the welds exhibited a lot of scatter and no relationship between pressure and impact toughness behaviour can be seen for any of the alloys. This does not mean, however, that the pressure does not affect the impact toughness. As with the hardness values, it may be that the influence is concealed by the possible cumulative effects of successive weld thermal cycles. The Avesta 2205 material has the best impact performance in both the weld metal and the HAZ. The SAF 2507 and the Zeron 100 both perform relatively poorly although the results for the SAF 2507 HAZ are much improved compared with those of the parent plate material. In conclusion it must be noted that all the HAZ results from the full scale ambient and hyperbaric welds exceed the suggested 35J at -40°C[85] and so must be judged as mechanically sound welds.

5.5.4.3 Summary of Mechanical Property Results

As the pressure at which welding was performed was increased it was expected that there may be a slight deterioration in the mechanical properties of the joints. It was assumed that the hardness of the weld metal would increase and it's toughness decrease as the higher cooling rates encountered would be expected to reduce the proportion of austenite in the weld metal. However, the microstructures of the welds performed at higher pressures showed no tendency to have high ferrite contents. This is also apparent from the results of the mechanical testing programme. There was no loss of impact toughness or increase in hardness that could be attributed to welding at increased pressures in any of the duplex steels in the project. Where any poor results were obtained for welds performed at higher pressures it was apparent that these were superior properties to those obtained in the corresponding weld performed at 1bar, and that the problem lay with the material and not with the welding process.

6. CONCLUSIONS

6. Conclusions

1. Three duplex stainless steels have been successfully automatically welded at a range of pressures from 1 to 32 atmospheres. A thorough review of the literature has indicated that this has not been achieved before.

2. Gas tungsten arc welding was used because of the high degree of process control that was required. It was found that by using standard GMA welding consumables for atmospheric welding, as recommended by the literature, it was possible to achieve an adequate austenite-ferrite phase balance at all pressures. As a result, no consumable development is considered to be necessary.

3. Pulsed current welding techniques were necessary to overcome problems with inconsistent penetration in the root weld which were thought to be due to problems with weld pool fluidity and heat distribution.

4. A V-butt design with a 2mm wide x 1.5mm thick 'land' on each side was found to minimise the variations in welding parameters, particularly the arc voltage, due to the high pressure phenomenon of arc wander.

5. Although welds have been successfully produced at lower pressures, the operating envelope for the weld parameters becomes very small, and problems with burn through are more prevalent in the root runs.

6. Manual welding techniques appear to be more successful for pressures of 1-4 atmospheres, whilst automatic welding is advantageous for welding at pressures above 4 atmospheres (depths of more than 40 metres).

7. Analysis of the weld thermal cycles showed that the cooling times from peak temperatures decreased as the pressure was increased, thus reducing the tendency for deleterious secondary phases to precipitate. This was confirmed by metallographic examination of the test welds which did not exhibit any pressure-related microstructural complications. This is important if the process is to be considered industrially viable.

8. Evaluation of the mechanical properties of the welded joints revealed that the impact toughness of the weld metal of the Avesta 2205 joints exceeded that of the parent plate material. High values were also attained for the HAZ. In the super duplex materials the impact toughness of the HAZ was as good as, if not better than, that of the parent plate material, and was exceeded by the impact toughness of the weld metal.

Fully automated GTA welding has been shown to be viable at water depths above approximately 40m, on both the standard 2205 duplex grades, which are currently widely used in offshore environments, and also on the more recently developed super duplex grades, that are thought to be candidate materials for use in more aggressively corrosive environments. This work implies that automated GTA is viable for offshore applications, as when the water depth is increased it becomes more attractive in terms of cost and safety to use automated welding procedures.

REFERENCES

REFERENCES

1. American Welding Society. *Welding Handbook, Vol. 1 (Fundamentals of Welding), 7th edition.*

2. J.F. Lancaster. Energy distribution in argon-shielded welding arcs. *British Welding Journal* ***1*** *(September 1965), 412-426.*

3. J. Ziljp. Heat transport during gas tungsten arc welding. *Ph.D. These, Delft Technical University, 1990.*

4. J. Norrish. *Advanced Welding Processes, Institute of Physics Publishing, 1992.*

5. W.F. Savage, E.F.Nippes, I.K. Agusa. Effect of arc force on defect formation in GTA welding. *Welding Journal Research Supplement* ***58*** *(July 1979), 212s-224s.*

6. C.J. Allum. Power dissipation in the column of a TIG welding arc. *Journal of Physics D (Applied Physics) Vol. 16, No. 11 (Nov. 1983) 2149-2165.*

7. W.F. Savage, S.S. Strunck, Y. Ishikawa. The effect of electrode geometry in gas tungsten arc welding. *Welding Journal Research Supplement,* ***44*** *(Nov. 1965), 489s-496s.*

8. W. Lucas. Shielding gases for arc welding. Part 1. *Welding and Metal Fabrication,* ***60*** *(June 1992),218-225.*

9. American Welding Society. *Welding Handbook, Vol. 2 (Arc and Gas Welding and Cutting, Brazing and Soldering), 7th edition.*

10. I.M. Richardson. Underwater arc welding - a survey of process behaviour. *Welding Review* ***8*** *(Feb. 1989), 11-20.*

11. N. Bailey. Welding underwater - a metallurgical appraisal. *Proceedings of the First International Offshore and Polar Engineering Conference, Edinburgh, 11-16th August 1991.*

12. H. Fulfs, A. Kataounis. Heat flow in argon tungsten arcs and workpiece thermal response at pressures up to 6MPa. *Proceedings of the First International offshore and Polar Engineering Conference, Edinburgh, 11-16th August 1991.*

13. C.J. Allum. Characteristics and structure of high pressure (1-42bars) gas tungsten arcs. *Ph.D. Thesis, Cranfield Institute of Technology, 1983.*

14. Y. Suga, A. Hasui. The effect of argon pressure on the TIG welding arc. *Transactions of the Japanese Welding Society* ***20*** *(October 1989), 119-125.*

15. Y. Suga, A. Hasui. Effects of helium pressure on characterics of TIG arcs and mechanical properties of welds. *Transactions of the Japanese Welding Society, **21** (April 1990), 24-30.*

16. Y. Suga. The effect of magnetic field stabilisation on TIG arc welding under hyperbaric conditions. *Proceedings of the First International offshore and Polar Engineering Conference, Edinburgh, 11-16th August 1991.*

17. Y Suga, H. Matsumoto. Effect of ambient pressure on erosion of some types of tungsten electrodes in hyperbaric welding. *Proceedings of the First International offshore and Polar Engineering Conference, Edinburgh, 11-16th August 1991.*

18. M. Yada, T. Onuma, T. Matsumoto, S. Kanaeko, R.Abe. Investigation of TIG welding in a pressurised helium atmosphere. *Welding International, **6**, (5), 372-377.*

19. F. Yang, F Schmelzer, M. Koçak. Analysis of hyperbaric weldments. *Welding '90, Proceedings of the International Conference on Welding Technology, Materials and Fracture, Geesthact, Germany, 22-24th October 1990.*

20. D.L.A. Fruytier. Industrial experiences with duplex stainless steels related to their specific properties. *Proceedings of the Conference Duplex Stainless Steels '91, Beaune, France, 28-30th October 1991.*

21. C. Duret-Thual, J.L. Moiron. Duplex stainless steel wirelines for use in H_2S containing aqueous chloride environments. *Proceedings of the Conference Duplex Stainless Steels '91, Beaune, France, 28-30th October 1991.*

22. C. Coussement, D Fruytier. An industrial application of duplex stainless steel in the petrochemical industry: a case study, failure analysis and subsequent investigations. *Proceedings of the Conference Duplex Stainless Steels '91, Beaune, France, 28-30th October 1991.*

23. R.L. Richard. Duplex stainless steel 25Cr. For FGD applications. *Proceedings of the Conference Duplex Stainless Steels '91, Beaune, France, 28-30th October 1991.*

24. G.H. Wagner, R. Münster. Application of "duplex" stainless steels in the chemical process industry and environmental protection plants. *Proceedings of the Conference Duplex Stainless Steels '91, Beaune, France, 28-30th October 1991.*

25. M. Loze, O. Agasse, P. Richard, F. Haegel. Behaviour of Uranus 52N exchangers in chemical industry. *Proceedings of the Conference Duplex Stainless Steels '91, Beaune, France, 28-30th October 1991.*

26. B. Leffler. Marine transportation of chemicals : an application for duplex stainless steels. *Proceedings of the Conference Duplex Stainless Steels '91, Beaune, France, 28-30th October 1991.*

27. L. Fassina. Duplex stainless steels: A versatile answer to application needs. *Proceedings of the Conference Duplex Stainless Steels '91, Beaune, France, 28-30th October 1991.*

28. G. Gawless, P. Gröger. Practical experience in manufacturing parts of chemical plants in 22 05 03 CrNiMoN duplex stainless steel. *Proceedings of the Conference Duplex Stainless Steels '91, Beaune, France, 28-30th October 1991.*

29. I. Ward. Experience with duplex stainless steels in Australia and New Zealand. *Proceedings of the Conference Duplex Stainless Steels '91, Beaune, France, 28-30th October 1991.*

30. A. Wensley, C. Reid. Duplex stainless steels in the paper and pulp industry. *Proceedings of the Conference Duplex Stainless Steels '91, Beaune, France, 28-30th October 1991.*

31. E.-M. Horn, S. Savakis, G. Schmidtt, I. Lewanowski. Performance of duplex stainless steels in caustic solutions. *Proceedings of the Conference Duplex Stainless Steels '91, Beaune, France, 28-30th October 1991.*

32. J.P. Ardouard, P. Soulignac. Duplex stainless steels for phosphoric acid plants. Corrosion properties and in service experience. *Proceedings of the Conference Duplex Stainless Steels '91, Beaune, France, 28-30th October 1991.*

33. A. Andreaus, R. Cicciarelli, J Schönofer. Evaluation of a duplex steel for a chemical production plant. *Proceedings of the Conference Duplex Stainless Steels '91, Beaune, France, 28-30th October 1991.*

34. V.J. Diggs, W.D. Busko, A.M. Schillmoller. The role of duplex stainless steels in the oil and gas industry. *Proceedings of the Conference Duplex Stainless Steels '91, Beaune, France, 28-30th October 1991.*

35. F. Blanchard. Duplex stainless steel tubing and casing for sour gas wells. *Proceedings of the Conference Duplex Stainless Steels '91, Beaune, France, 28-30th October 1991.*

36. M. Barteri, D. Condanni, M. Marangoni, B. Vincentini. Material selection of "T-block" conditions. *Proceedings of the Conference Duplex Stainless Steels '91, Beaune, France, 28-30th October 1991.*

37. M. Barteri, G. Rondelli, L. Scoppio and A. Tamba. Cold working and compositional effect on the performance of duplex stainless steels for OCTG. *Proceedings of the Conference Duplex Stainless Steels '91, Beaune, France, 28-30th October 1991.*

38. R. Contini, R. Cavalloti, L. Renaud. UR52N$^+$ super duplex stainless steel: offshore application. *Proceedings of the Conference Duplex Stainless Steels '91, Beaune, France, 28-30th October 1991.*

39. G. Warburton, M. Spence, A.W. Stevenson. The use of Zeron 100 super duplex stainless steels in the fabrication of thick walled pressure vessel.

Proceedings of the Conference Duplex Stainless Steels '91, Beaune, France, 28-30th October 1991.

40. B. Bazzoni, M. Celant, T. Pastore, P. Pedefferi, G. Sala. Duplex stainless steel bi-metallic strip for reinforced soils. *Proceedings of the Conference Duplex Stainless Steels '91, Beaune, France, 28-30th October 1991.*

41. H. L. Groth, M.L. Erbing, J. Olsson. Design ideas and case studies utilizing duplex stainless steels. *Proceedings of the Conference Duplex Stainless Steels '91, Beaune, France, 28-30th October 1991.*

42. A. Redjaïma, G. Metauer, M. Gantois. Decomposition of delta ferrite in a Fe-22Cr-5Ni-3Mo-0.03C duplex stainless steel. A morphological and structural study. *Proceedings of the Conference Duplex Stainless Steels '91, Beaune, France, 28-30th October 1991.*

43. T. Thorvaldsson, H. Eriksson, J. Kutka, A. Salwén. Influence of microstructure on mechanical properties of a duplex stainless steel. *Proceedings of the Conference Stainless Steels '84.*

44. J. Charles. The duplex stainless steels: materials to meet your needs. *Proceedings of the Conference Duplex Stainless Steels '91, Beaune, France, 28-30th October 1991.*

45. Y. Maehara, Y. Ohmori. Sigma phase formation and hot ductility of δ-ferrite/austenite duplex stainless steels. *The Sumito Search, No. 1, November 1985, 147-154.*

46. Y.Maehara, N. Fujino, T. Kunitake. Effects of plastic deformation and thermal history on σ phase precipitation in duplex phase stainless steels. *Transactions of the Iron and Steel Institute of Japan, 1983, **23**, 247-255.*

47. B. Josefsson, J.-O. Nilsson, A. Wilsson. Phase transformations in duplex stainless steels and the relationship between continuous cooling and isothermal heat treatment. *Proceedings of the Conference Duplex Stainless Steels '91, Beaune, France, 28-30th October 1991.*

48. J. H Potgeiter. Influence of σ phase on general and pitting corrosion resistance of SAF 2205 duplex stainless steel. *British Corrosion Journal, **27**, (3), 219-223.*

49. L.A. Norstrom, S. Petersson, S. Nordin. Sigma phase embrittlement in some ferritic-austenitic stainless steels. *Z. Worktofftech, **12**, (1981), 229-234.*

50. S. Hertzmann, W. Roberts, M. Lindenmo. Microstructure and properties of nitrogen alloyed duplex stainless steel after welding treatments. *Proceedings of the Conference Duplex Stainless Steels '91, Beaune, France, 28-30th October 1991.*

51. P.D. Southwick, R.W.K. Honeycombe. Decomposition of ferrite to austenite in 26%Cr-5%Ni stainless steel. *Metal Science **14** (July 1980), 253-261.*

52. J.-O. Nilsson, A. Wilsson, B. Josefsson, T. Thorvaldsson. Relationship between pitting corrosion, toughness and microstructure for isothermally heated super duplex stainless steel. *Proceedings of the Conference Applications of Stainless steels '92, Stockholm, Sweden, 9-11th June 1992.*

53. J. Hochmann, A. Desestret, P. Jolly, P Mayoud. *Metaux Corrosion Industrie, **2** (1974), (591-592),404.*

54. J.-O. Nilsson, P. Lui. Aging at 400-600°C of submerged arc welds of 22Cr-3Mo-8Ni duplex stainless steel and its effect on toughness and microstructure. *Materials Science and Technology, **7**, (9), September 1991, 853-862.*

55. J. Charles, Super duplex stainless steels: structure and properties. *Proceedings of the Conference Duplex Stainless Steels '91, Beaune, France, 28-30th October 1991.*

56. B. Soylu, R.W.K. Honeycombe. Microstructural refinement on duplex stainless steels. *Materials Science and Technology, **7**, (2), February 1991, 137-145.*

57. M. Guttman. Intermediate temperature aging of duplex stainless steel. A review. *Proceedings of the Conference Duplex Stainless Steels '91, Beaune, France, 28-30th October 1991.*

58. G. Wahlberg, G.L. Dunlop. Nitrogen strengthening of duplex stainless steels. *Proceedings of the Conference Stainless Steels '87, York, 1987.*

59. R.E.Johansson, H.L. Groth. Corrosion fatigue and fatigue data for duplex stainless steels. *Proceedings of the Conference Duplex Stainless Steels '91, Beaune, France, 28-30th October 1991.*

60. J.M. Drugli, T. Rogne. Corrosion testing and evaluation of required weld quality for duplex stainless steels for transport of oil and gas. *Proceedings of the Conference Stainless Steels '92, Stockholm, Sweden, 9-11th June 1992.*

61. S. Bernhardsson. The corrosion resistance of duplex stainless steels. *Proceedings of the Conference Duplex Stainless Steels '91, Beaune, France, 28-30th October 1991.*

62. M.-J. Scholfield, S.M. Wilhelm, J.W. Oldfield. Application for various stress corrosion cracking test techniques: validity and relevance to practice. *Proceedings of the Conference Duplex Stainless Steels '91, Beaune, France, 28-30th October 1991.*

63. S. Atamert, J.E. King. Super duplex stainless steels. Part 1. Heat affected zone microstructures. *Materials Science and Technology, **8** (10), October 1992, 896-911.*

64. S Atamert, R.C. Reed, J.E. King. Modelling of duplex stainless steel weld deposit microstructures. *Proceedings of the Conference Duplex Stainless Steels '91, Beaune, France, 28-30th October 1991.*

65. E.N. Bower, J.W. Fielder, K.J. King. The characteristics of HyResist 22/5 duplex stainless steel welds using commercially available consumables. *3rd International Conference on Welding and Performance of Pipelines, London, 18-21st November 1986.*

66. A.L. Schaeffler, Constitution diagram for stainless steel weld metal. *Metal Progress, 56 (11), p680 and p680-B.*

67. B. Bonnefois, J. Charles, F. Dupoiron, P. Soulignac. How to predict welding properties of duplex stainless steels?. *Proceedings of the Conference Duplex Stainless Steels '91, Beaune, France, 28-30th October 1991.*

68. B. Bonnefois, P. Soulignac, J. Charles. Some aspects of nitrogen introduction to the weld pool. *Proceedings of the Conference Duplex Stainless Steels '91, Beaune, France, 28-30th October 1991.*

69. S.-A. Fager. Design of consumables for the welding of super duplex stainless steel. *Proceedings of the Conference Duplex Stainless Steels '91, Beaune, France, 28-30th October 1991.*

70. T.G. Gooch. Weldability of ferritic-austenitic stainless steels. *Proceedings of the Conference Duplex Stainless Steels, St. Louis. 25-28th October 1982.*

71. L. Van Nassau, K. Bekkers, J. Hilkes, H.Meelker. Welding duplex and super duplex piping systems and components. *Proceedings of the Conference Joining/Welding 2000, The Hague, The Netherlands, 1-2nd July 1991.*

72. D. Faucheur, D. Gilbert. Welding of austenitic ferritic (duplex) stainless steels. *Proceedings of the Conference Duplex Stainless Steels '86, The Hague, The Netherlands, 26-28th October 1986.*

73. K. Yasuda, K. Tamaki, S. Nakomo, K. Kobayashi, N. Nishiyama. Metallurgical characteristics of weld metals and corrosion performance of girth weld joints of duplex stainless steel pipes. *Proceedings of the Conference Duplex Stainless Steels '86, The Hague, The Netherlands, 26-28th October 1986.*

74. B. Lundqvist, P. Norberg. Weldability aspects and weld joint properties of duplex stainless steels. *Welding Journal* ***67, (7), 1988.***

75. J.J.K. Stekly, J.-L. Scandella, K.A. Salmon. Effect of welding techniques on the properties of super duplex stainless steels. *Proceedings of the Conference Duplex Stainless Steels '91, Beaune, France, 28-30th October 1991.*

76. T.G. Gooch. Corrosion resistance of welds in duplex stainless steels. *Proceedings of the Conference Duplex Stainless Steels '91, Beaune, France, 28-30th October 1991.*

77. G.K. Creffield, M.H. Cole, R. Paciej, W. Huang, S. Urmston. Nitrogen containing gases for GTAW of duplex stainless steel. *Proceedings of the*

Conference Offshore Mechanical and Arctic Engineering, Glasgow, U.K., 20-24th June 1993.

78. P.C. Gough, J.C.M. Farrar. Factors affecting weld root run corrosion performance in duplex and super duplex pipework. *Proceedings of the Conference Duplex Stainless Steels '91, Beaune, France, 28-30th October 1991.*

79. A.W. Stevenson, P.C. Gough, J.C.M. Farrar. The weldability of super duplex alloys-welding consumables and procedure development. *Proceedings of the Conference Joining/Welding 2000, The Hague, The Netherlands, 1-2nd July 1991.*

80. T. Habrekke, J.O. Berge, I. Hillersoy. The behaviour of C-Mn and stainless steels when welding under hyperbaric conditions. *Proceedings of the Second (1992) International Offshore and Polar Engeineering Conference, San Fransisco, USA, 14-19th June 1992.*

81. R.B. Malone, J.M.D. Ralston. Hyperbaric welding of exotic steel pipeline. *Proceedings of the 11th Conference Offshore Mechanical and Arctic Engineering, Calgarry, Alberta, Canada, 7-12th June 1992.*

82. I.M Richardson. Properties of the constricted gas tungsten (plasma) welding arc at elevated pressures. *Ph.D Thesis, Cranfield Institute of Technology, 1991.*

83. W.R. Cave. Private communication.

84. M.F. Thornton. Private communication.

85. B. Lundqvist, P. Norberg, K Olsson. Influence of different welding conditions on mechanical properties and corrosion resistance of Sandvik SAF 2205 (UNS S31803). *Sandvik Steel Publication S-91-45-ENG.*

FIGURES

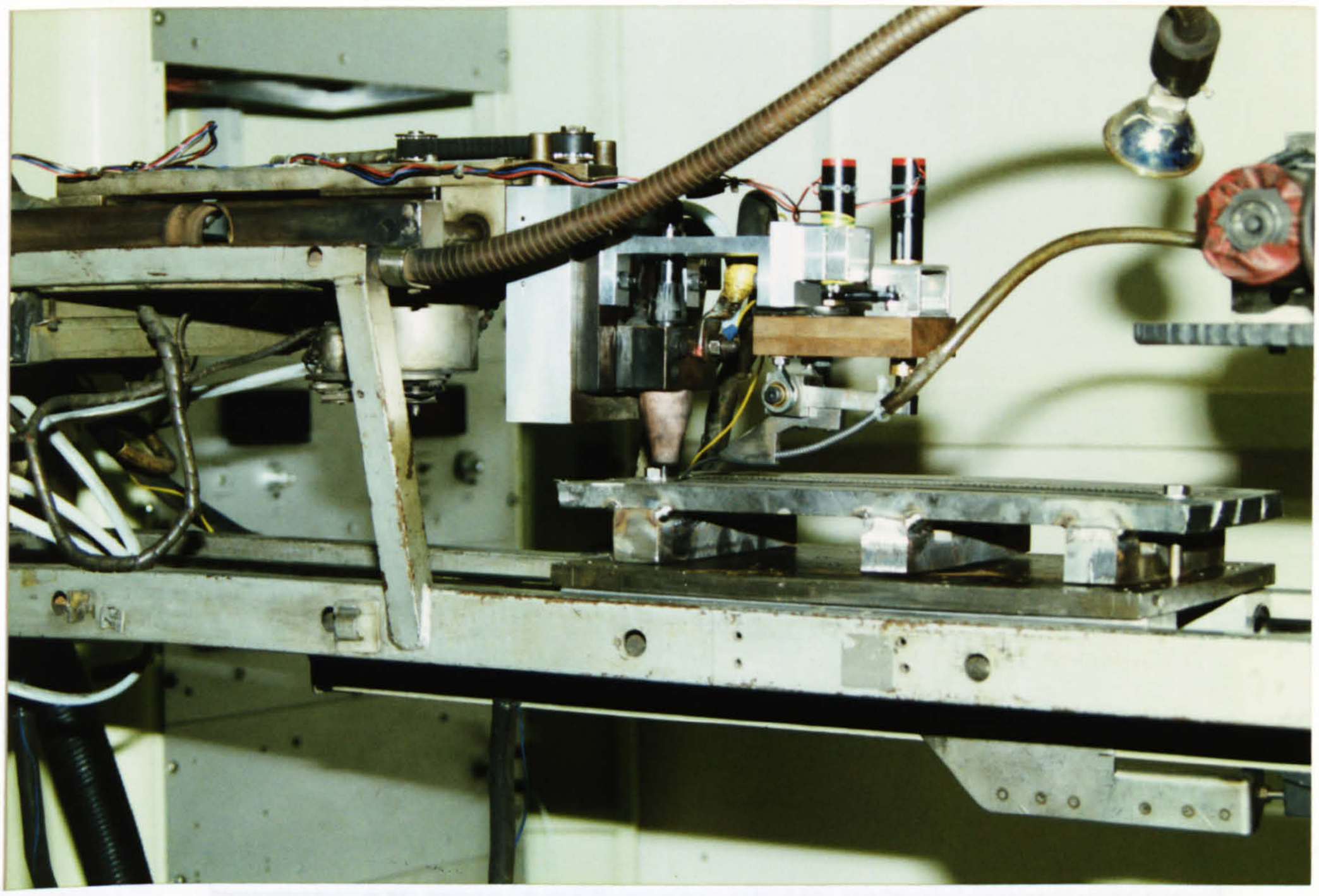

Figure 3.1: The hyperbaric chamber workframe showing the welding torch and wire feed assembly, ready to perform a weld.

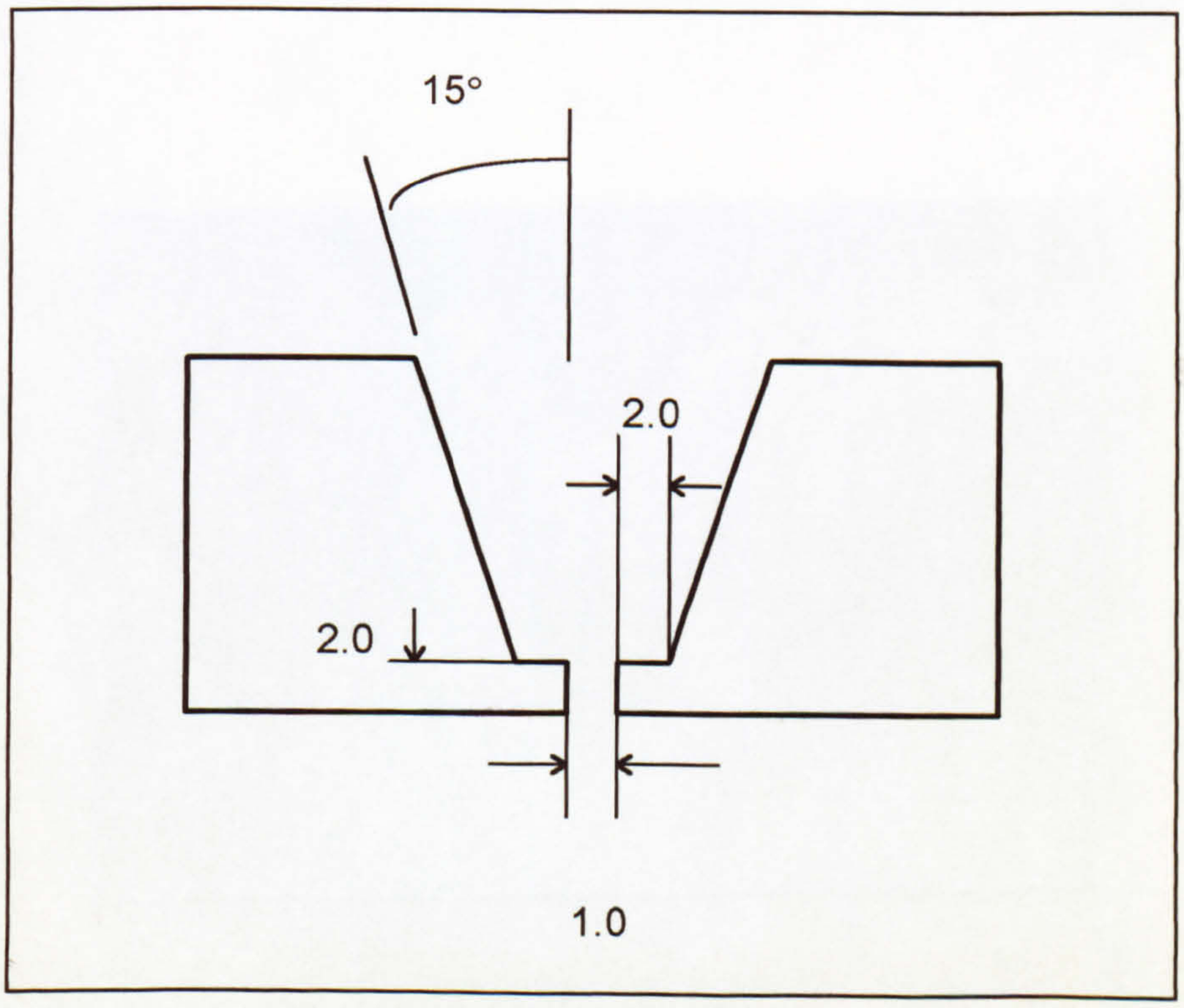

Figure 3.2: The original weld joint design. (Dimensions in mm).

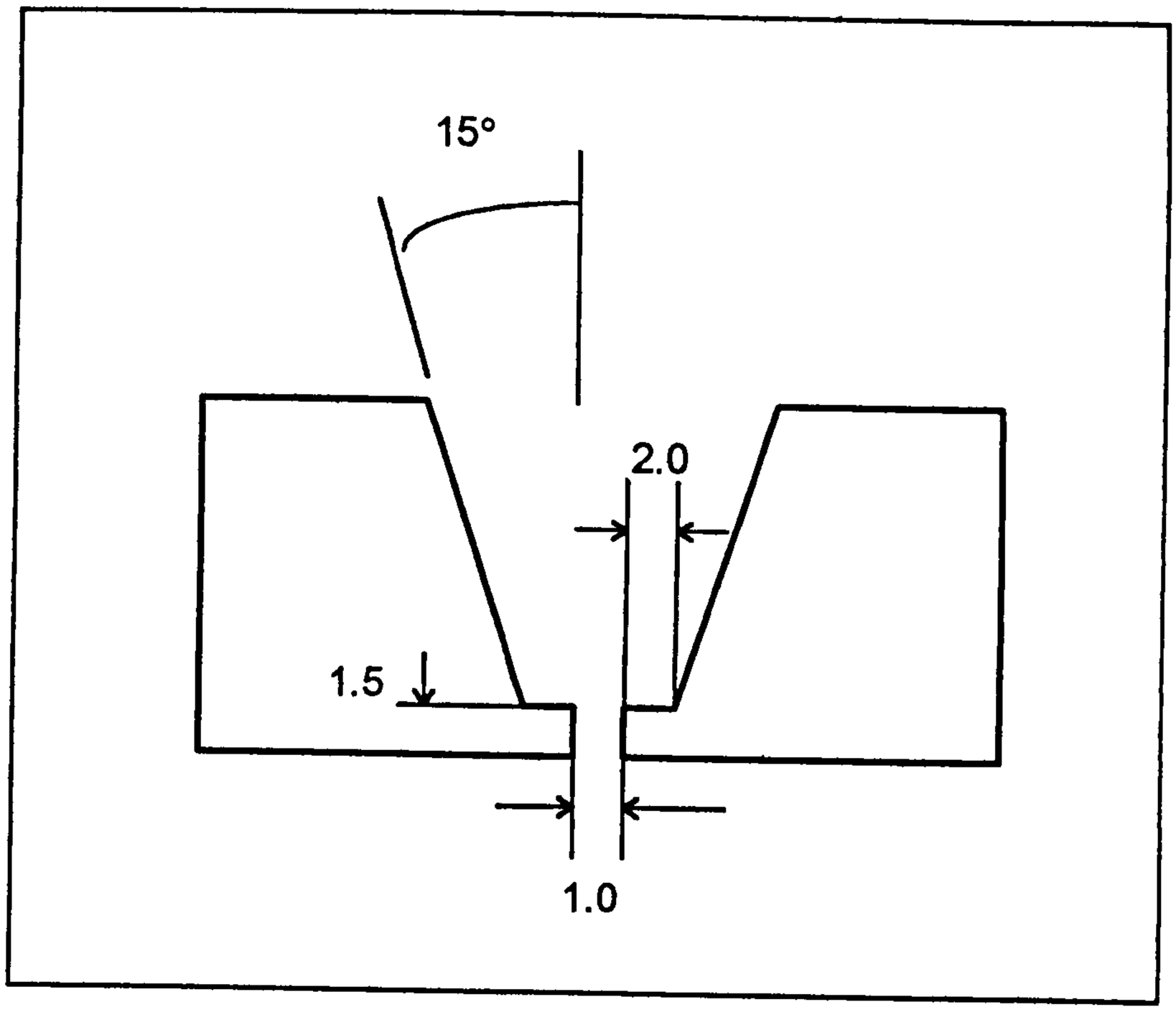

Figure 3.3: The modified weld joint design showing the thinner "land". (Dimensions in mm).

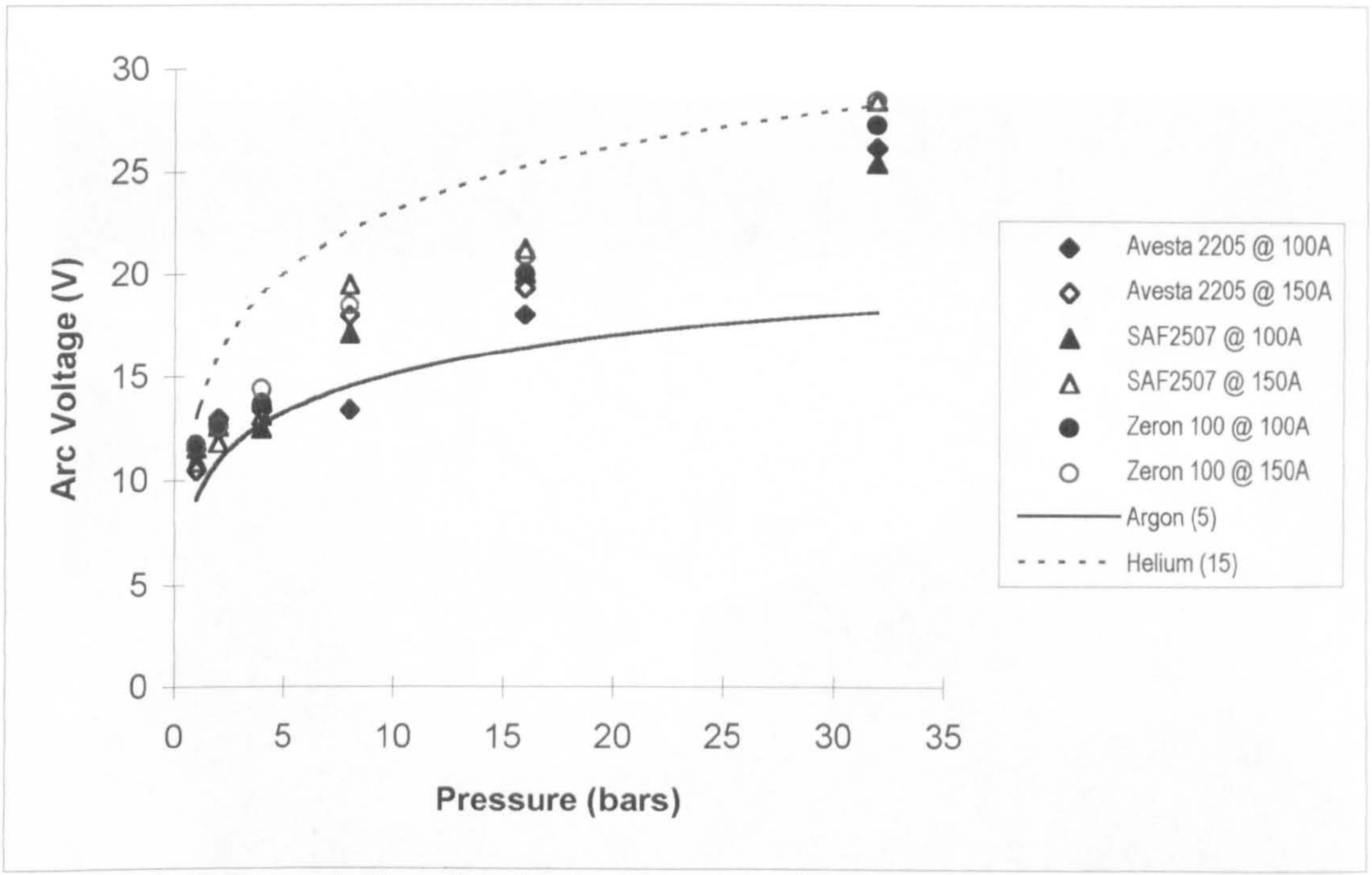

Figure 4.1: The relationship between arc voltage and pressure for the autogenous GTA bead on plate welds.

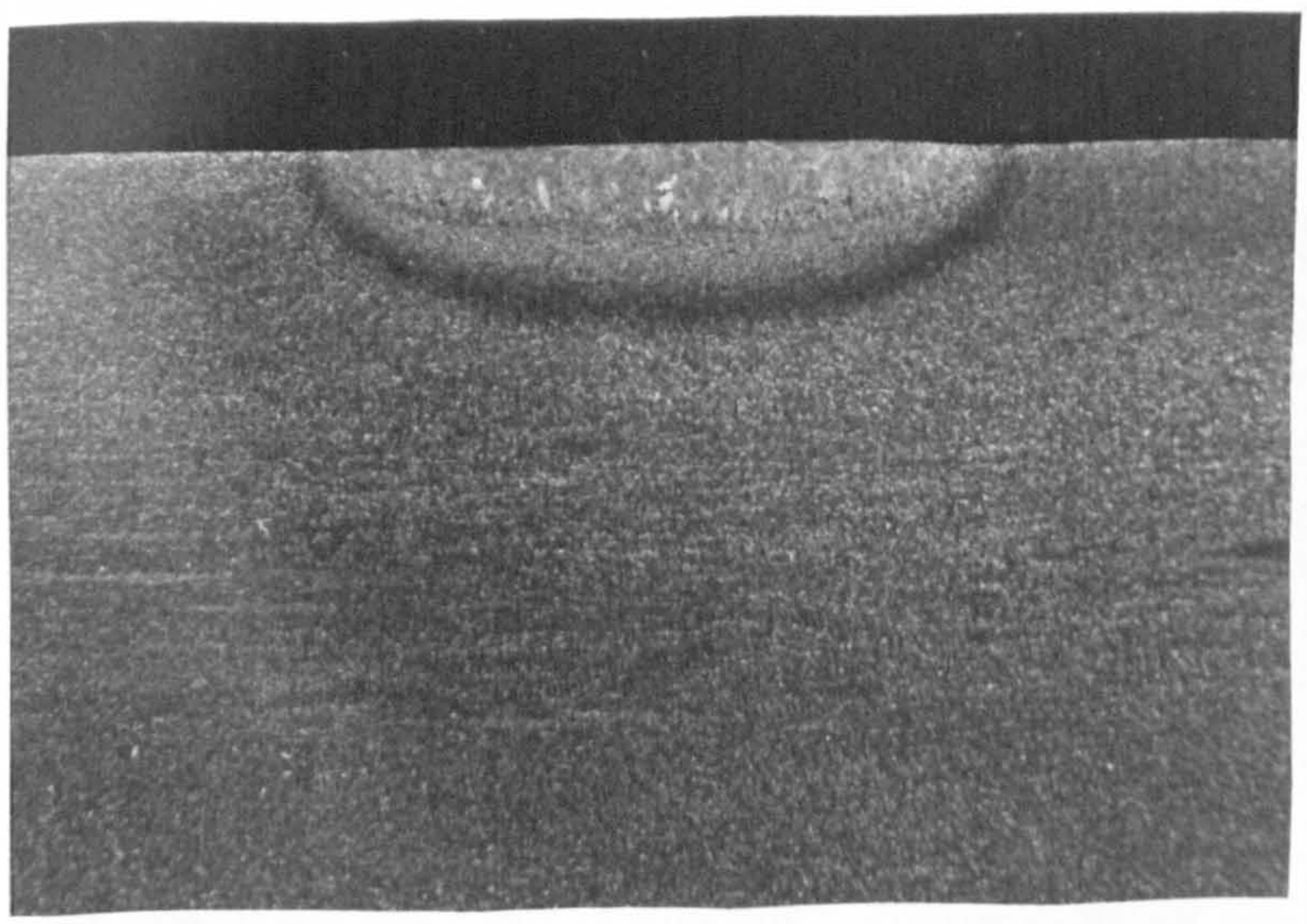

Figure 4.2: The weld bead profile of a 0.57kJ/mm Zeron 100 autogenous bead on plate weld performed at 1bar (x5).

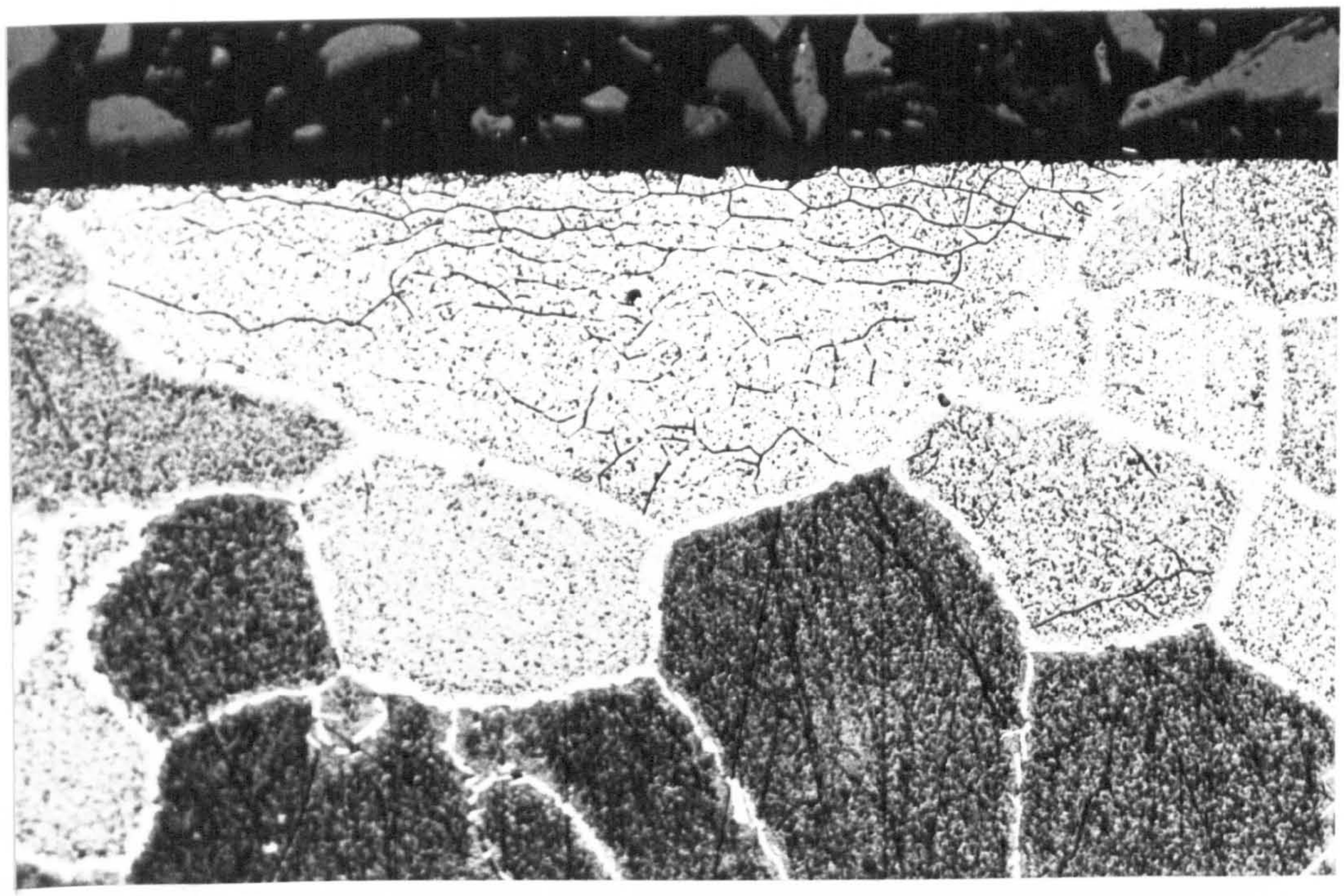

Figure 4.3: The mainly ferritic weld microstructure of a 0.39kJ/mm heat input autogenous bead on plate weld in Zeron 100 (x200).

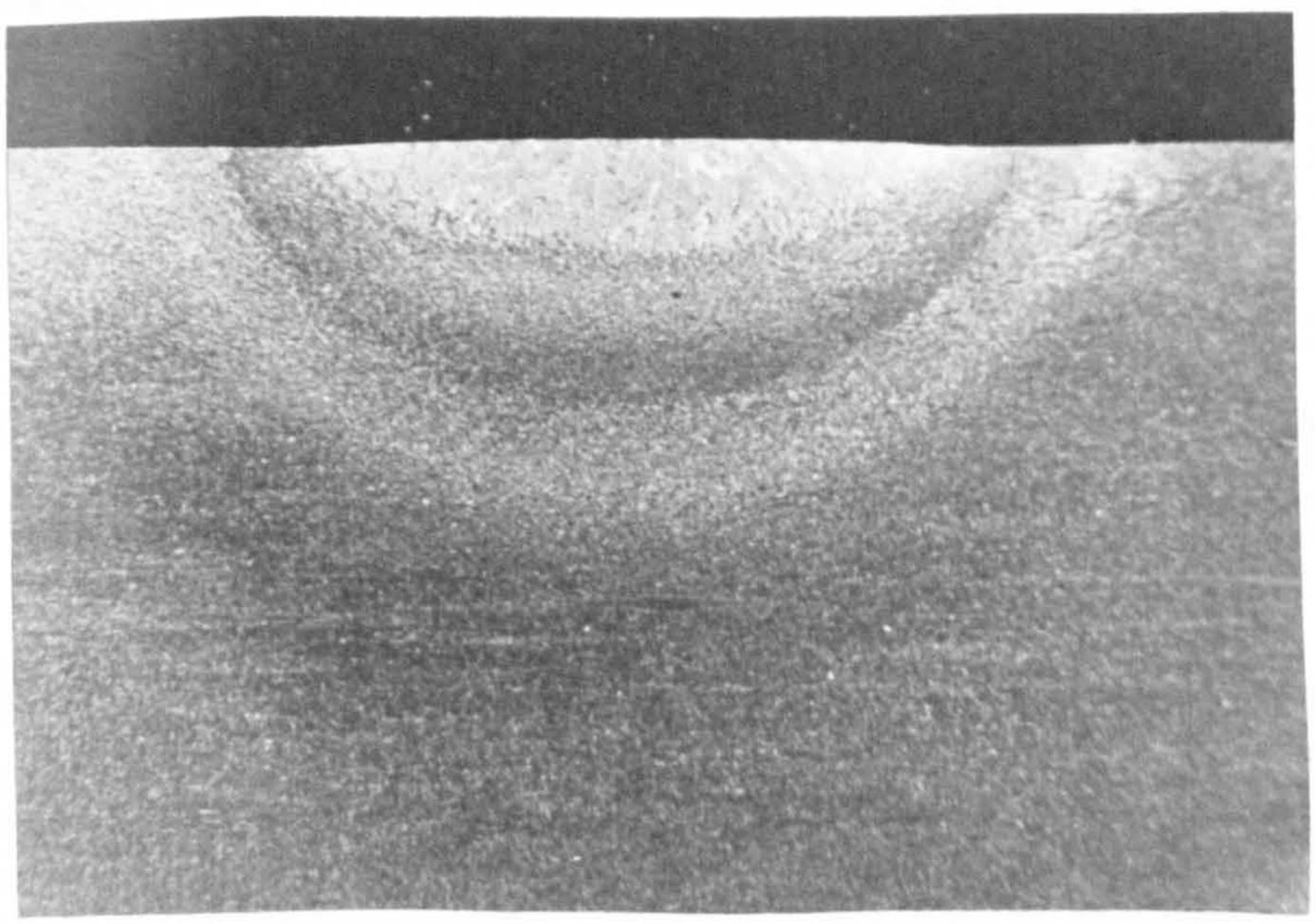

Figure 4.4: The weld bead profile of the 1.23kJ/mm Zeron 100 autogenous bead on plate weld at 1bar (x5).

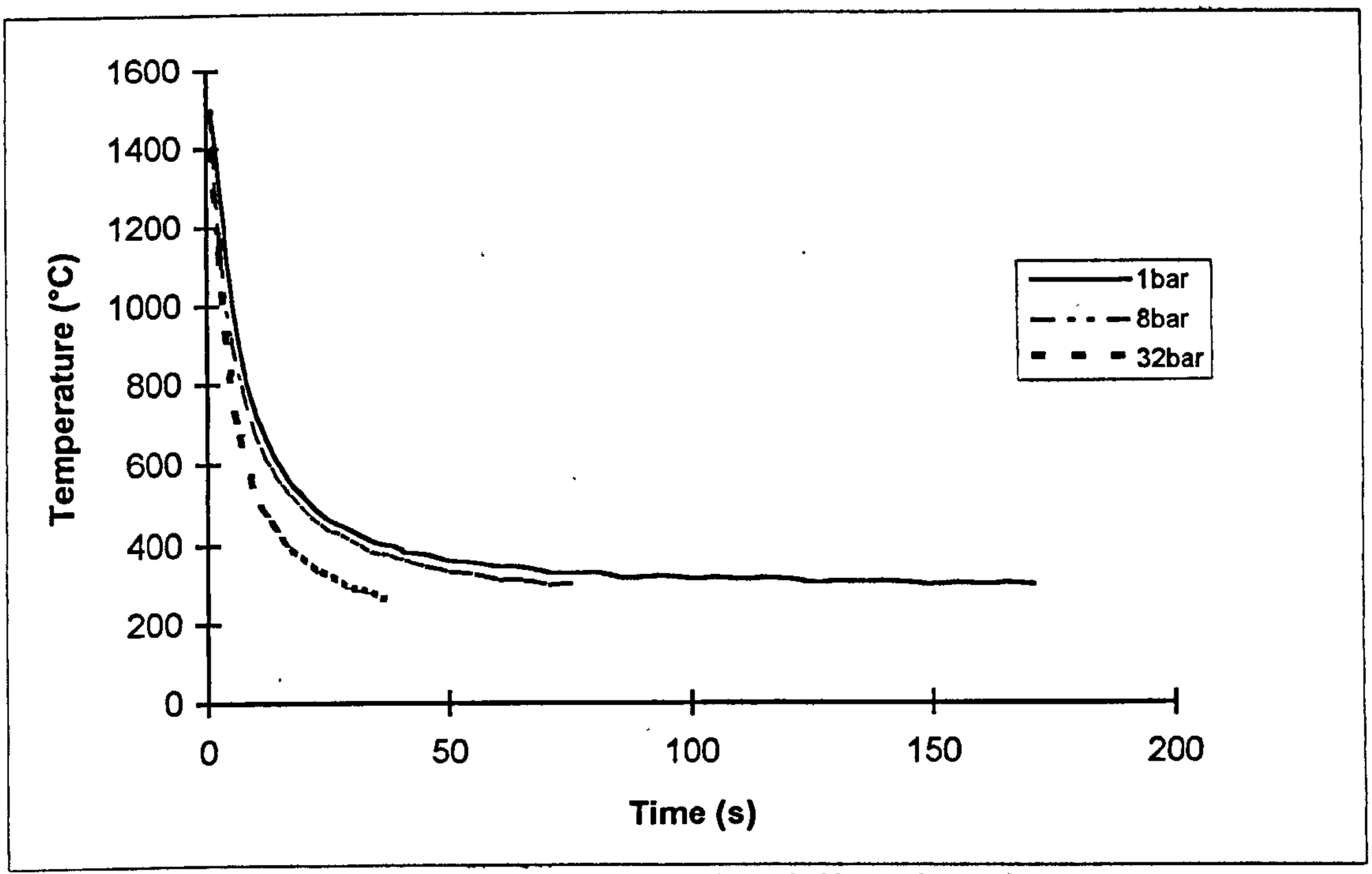

Figure 4.5: The cooling charateristics of a 1kJ/mm heat input autogenous bead on plate weld on a duplex stainless steel at a range of pressures.

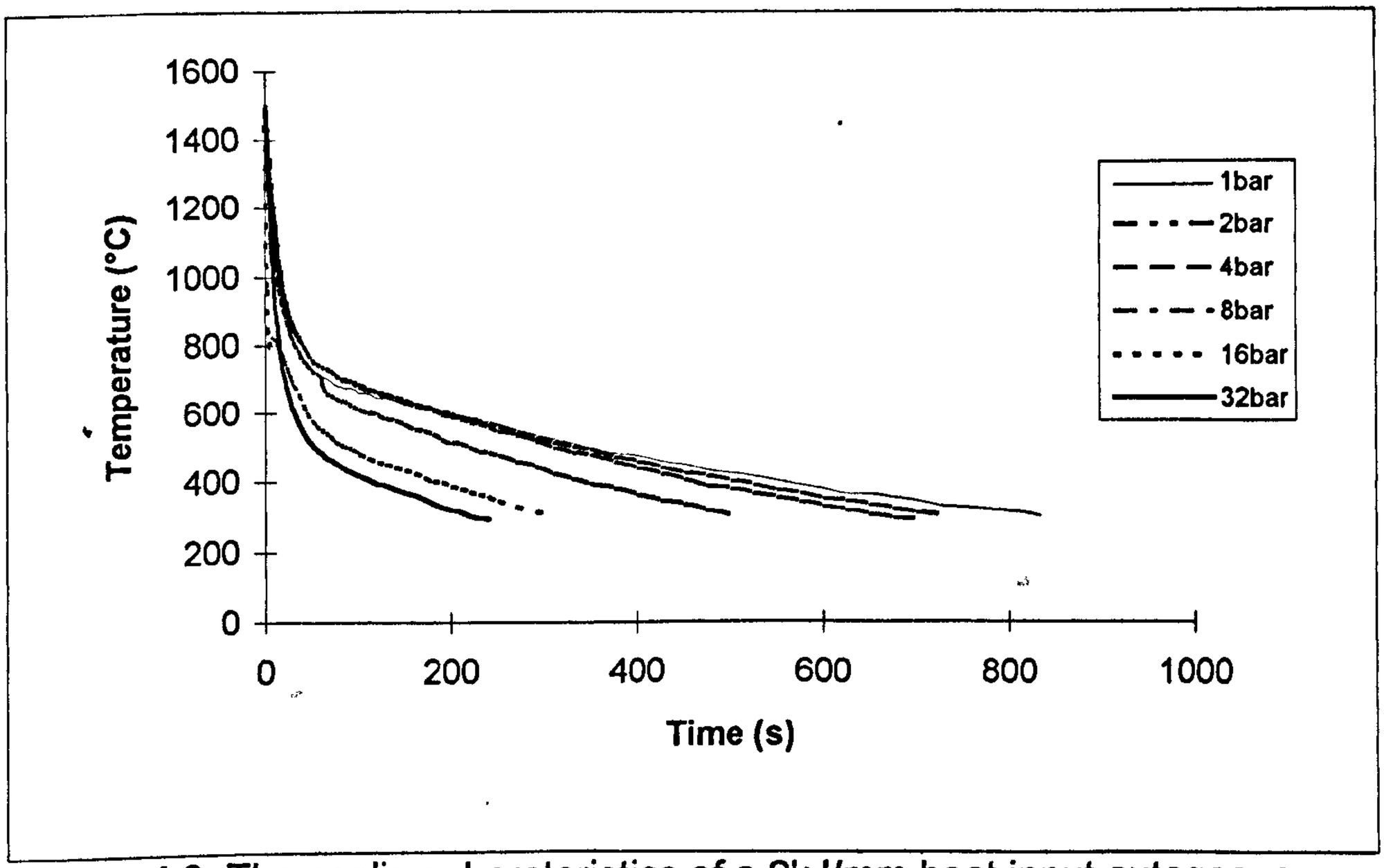

Figure 4.6: The cooling charateristics of a 2kJ/mm heat input autogeous bead on plate weld on a duplex stainless steel at a range of pressures.

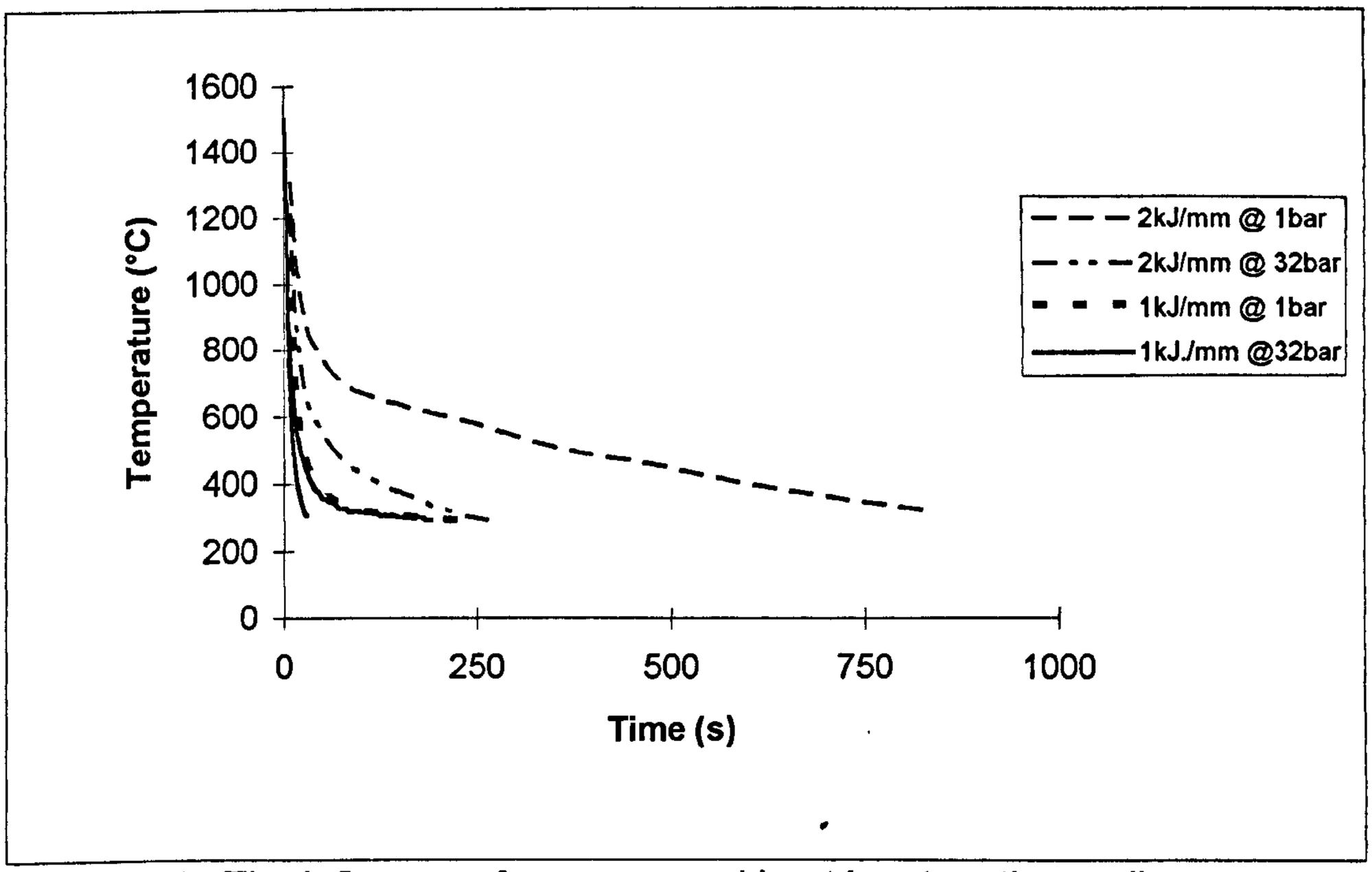

Figure 4.7: The influence of pressure and heat input on the cooling charaterisitics of autogenous bead on plate welds in duplex stainless steels.

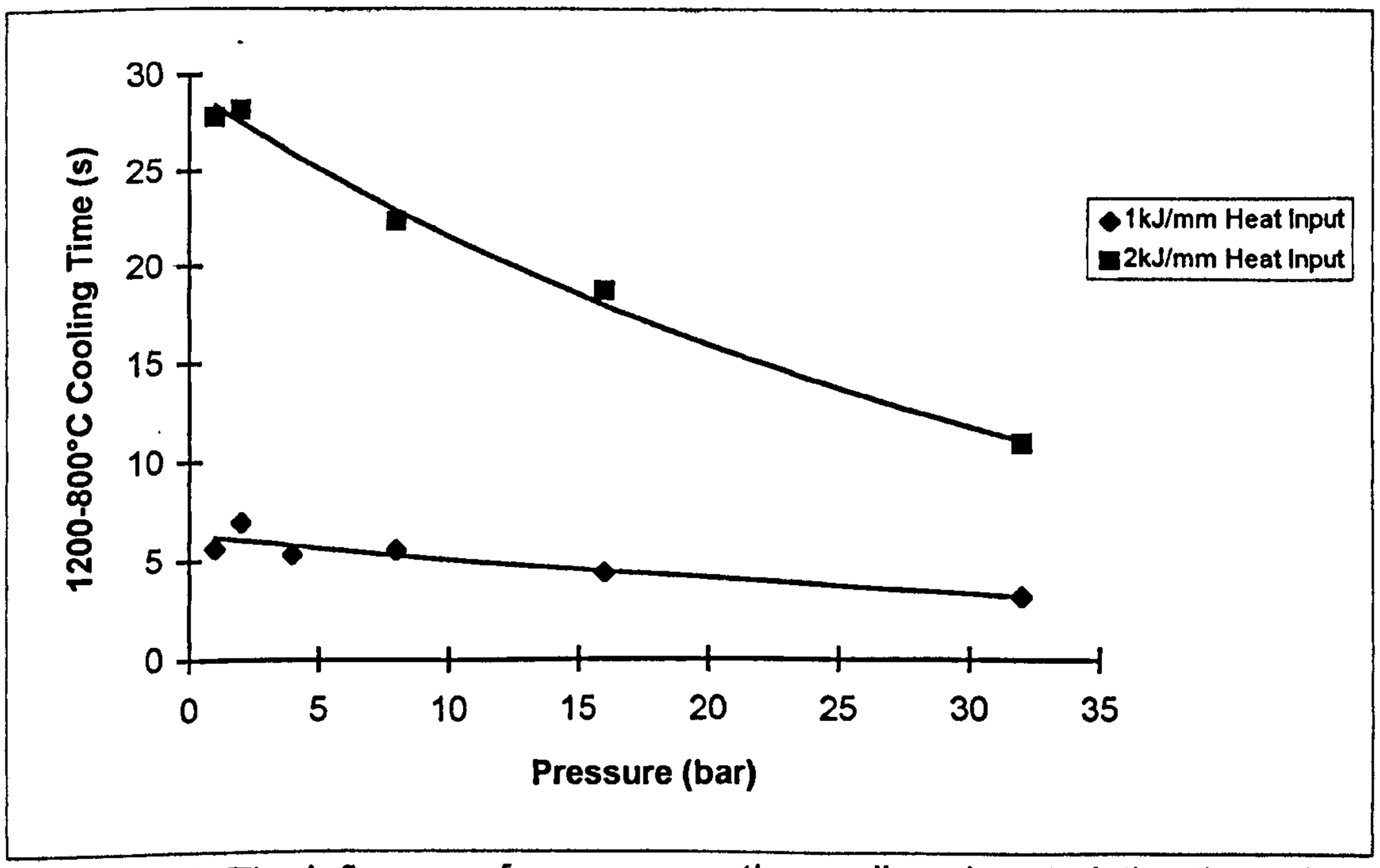

Figure 4.8: The influence of pressure on the cooling charateristics through through the 1200-800°C temperature range.

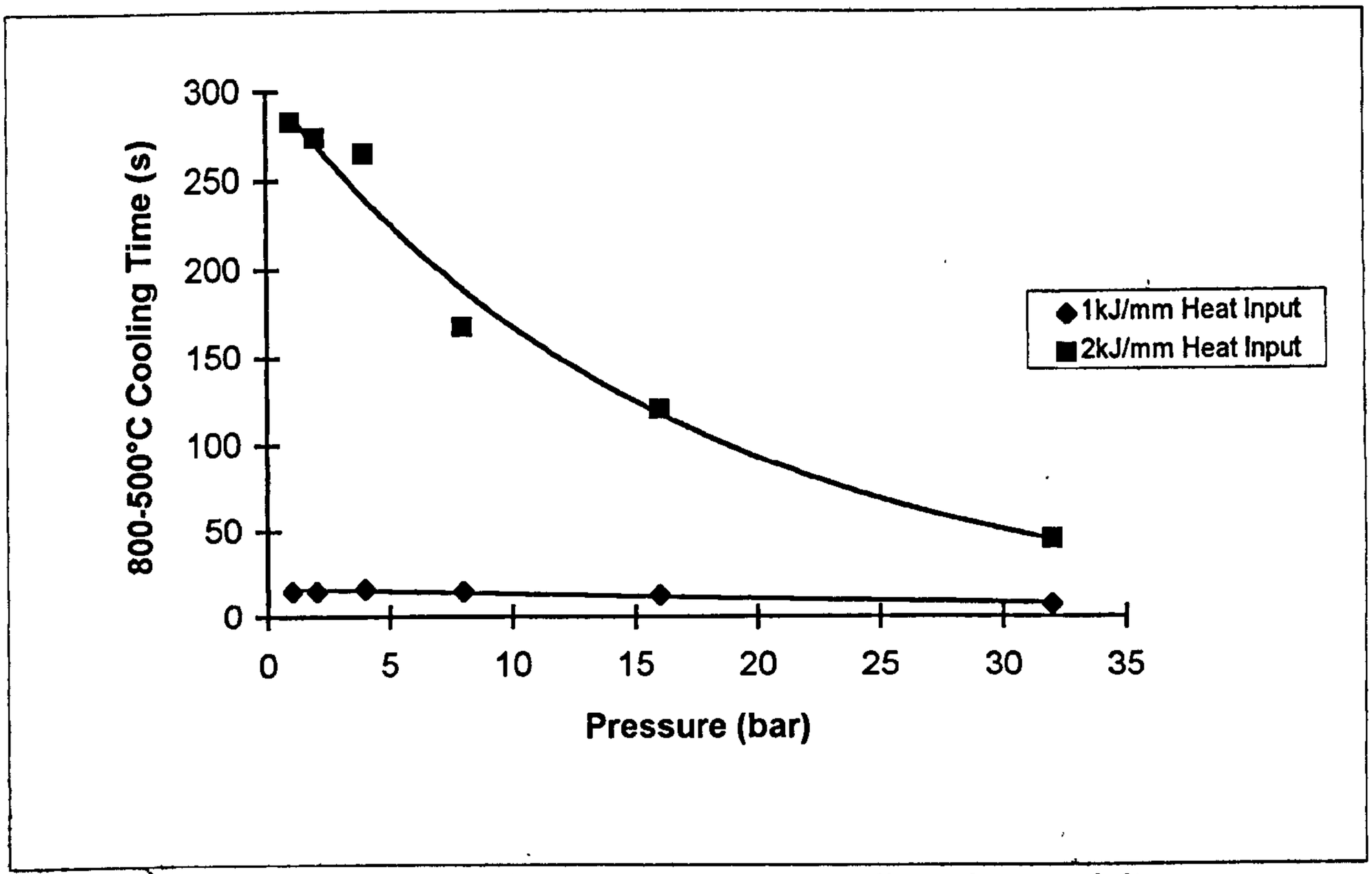

Figure 4.9: The influence of pressure on the cooling charaterisitcs through the 800-500°C temperature range.

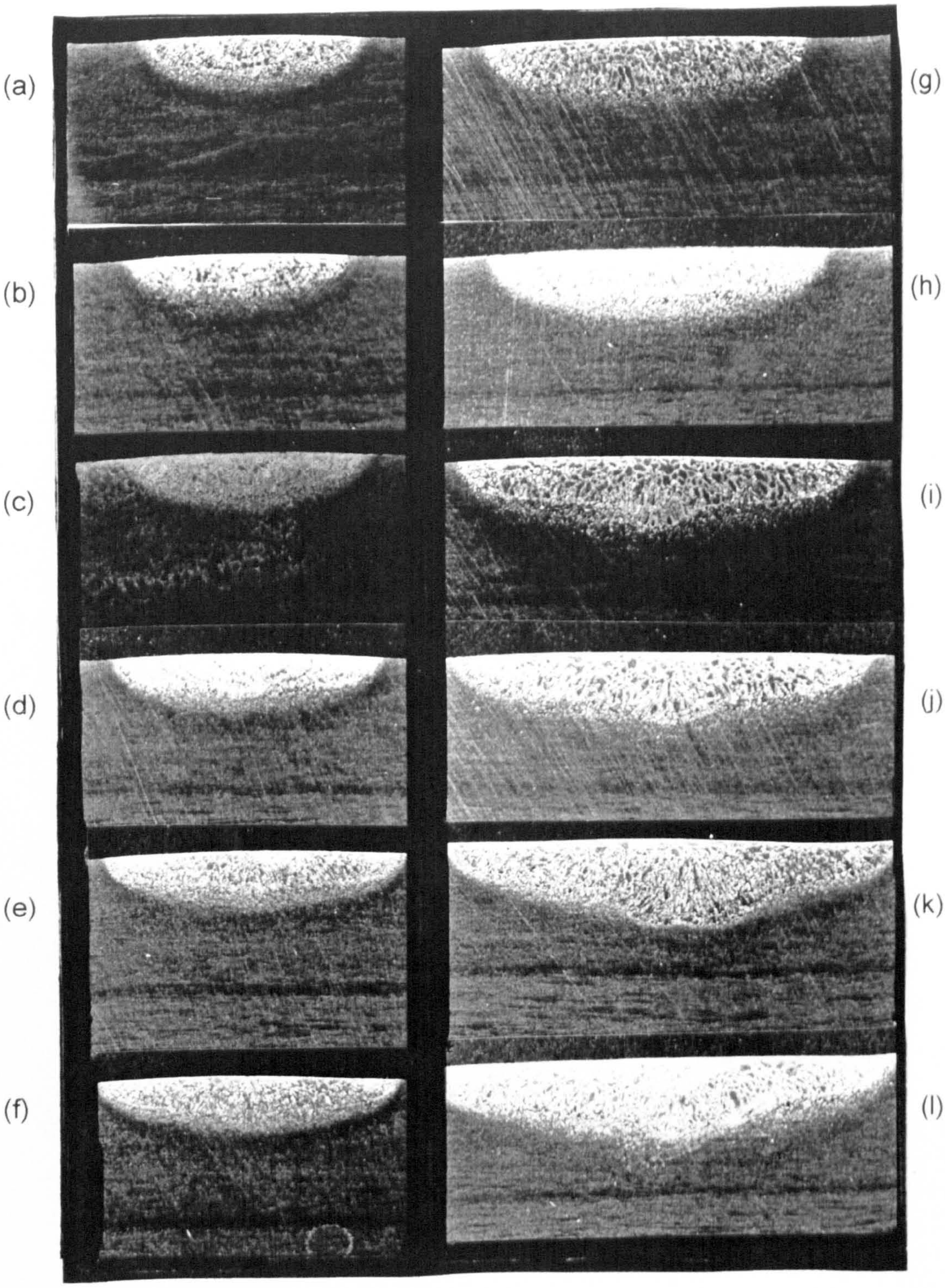

Figure 4.10: Weld bead profiles of autogenous bead on plate welds in Avesta 2205 (x3). (a-f) 1kJ/mm heat input, 1, 2, 4, 8, 16, 32bars; (g)-(l) 2kJ/mmheat input, 1, 2, 4, 8, 16, 32bars.

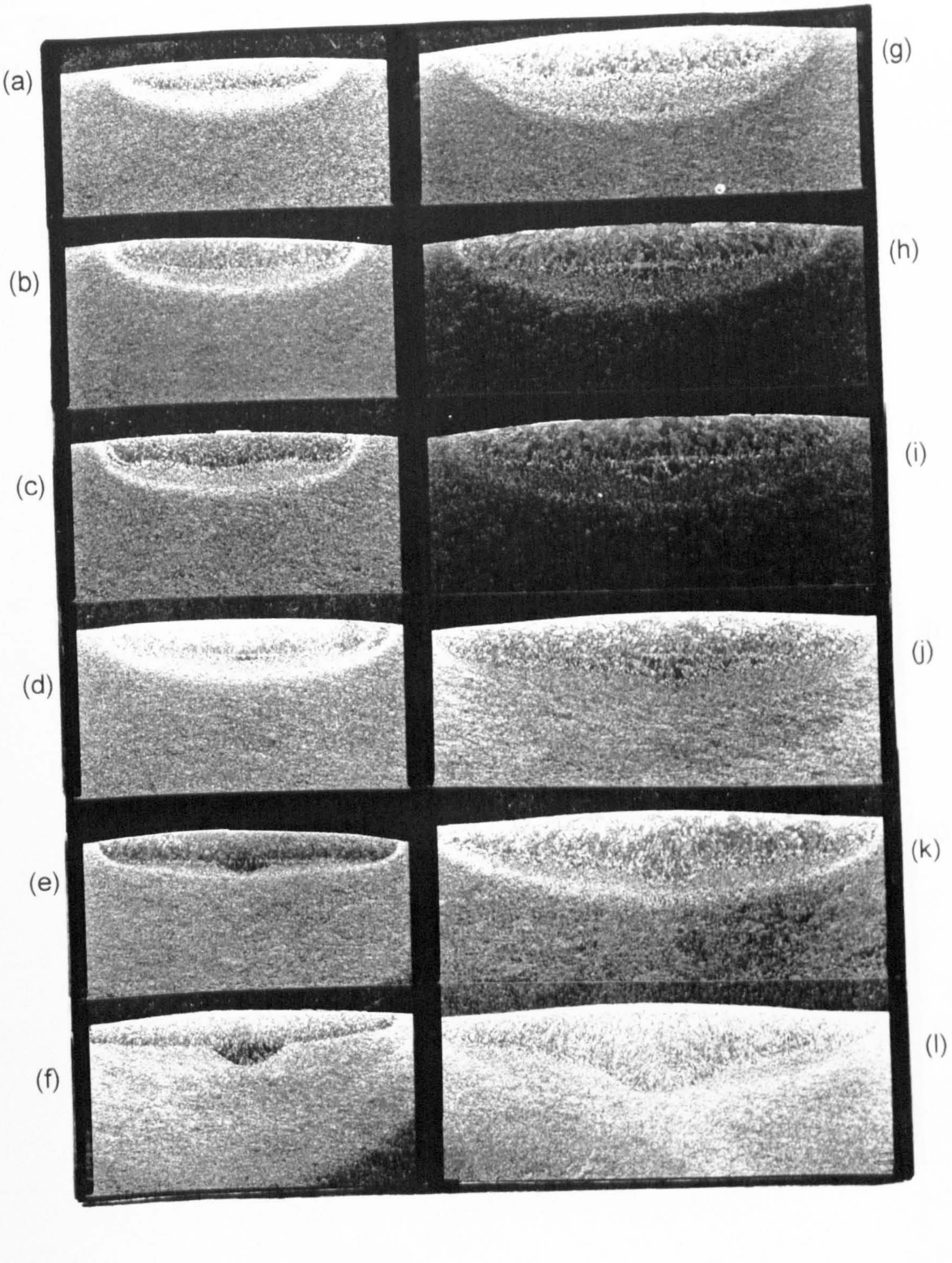

Figure 4.11: Weld bead profiles of autogenous bead on plate welds in Sandvik SAF2507 (x3). (a-f) 1kJ/mm heat input, 1, 2, 4, 8, 16, 32bars; (g)-(l) 2kJ/mm heat input, 1, 2, 4, 8, 16, 32bars.

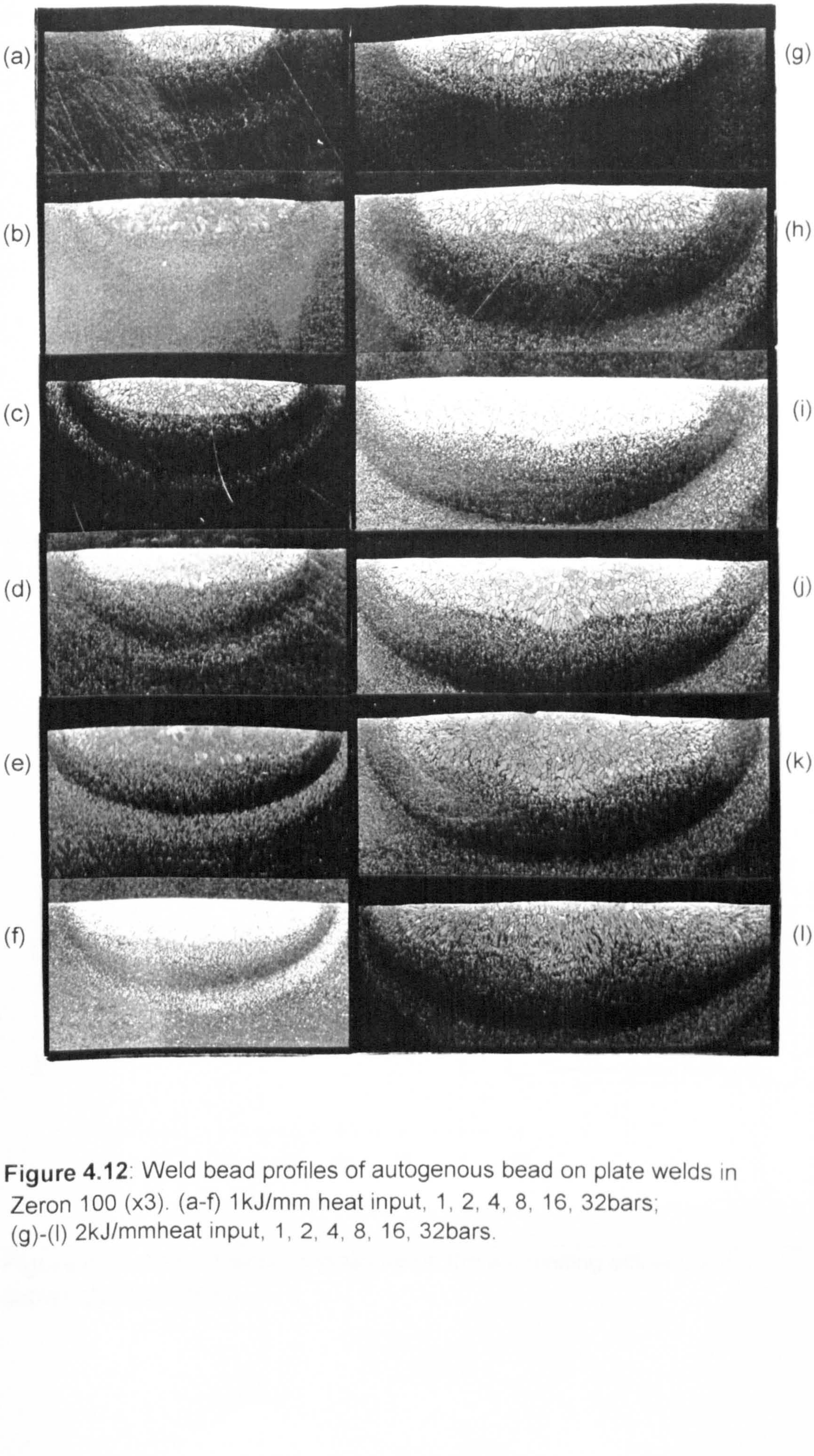

Figure 4.12: Weld bead profiles of autogenous bead on plate welds in Zeron 100 (x3). (a-f) 1kJ/mm heat input, 1, 2, 4, 8, 16, 32bars; (g)-(l) 2kJ/mmheat input, 1, 2, 4, 8, 16, 32bars.

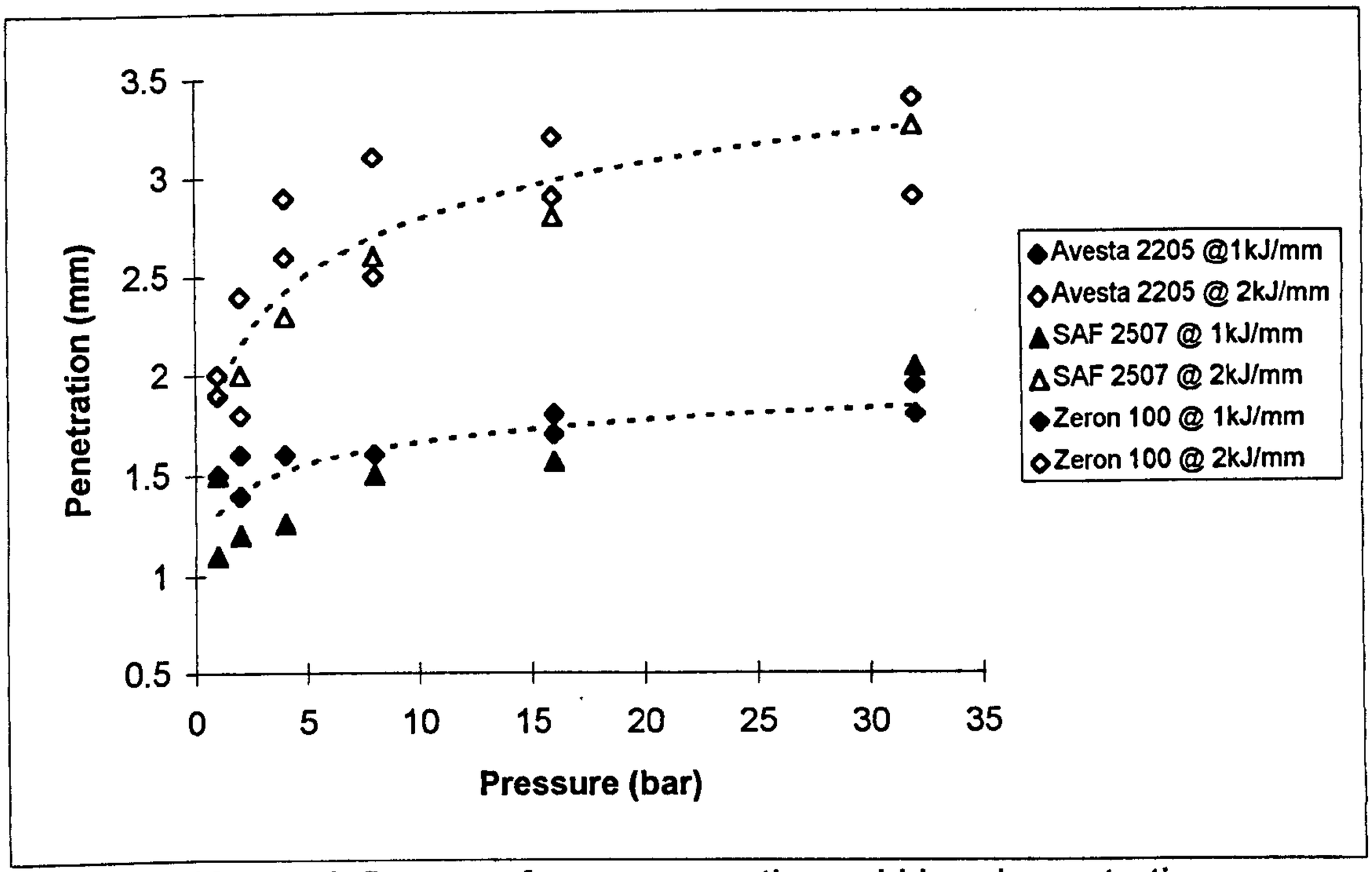

Figure 4.13: The influence of pressure on the weld bead penetration in duplex stainless steels.

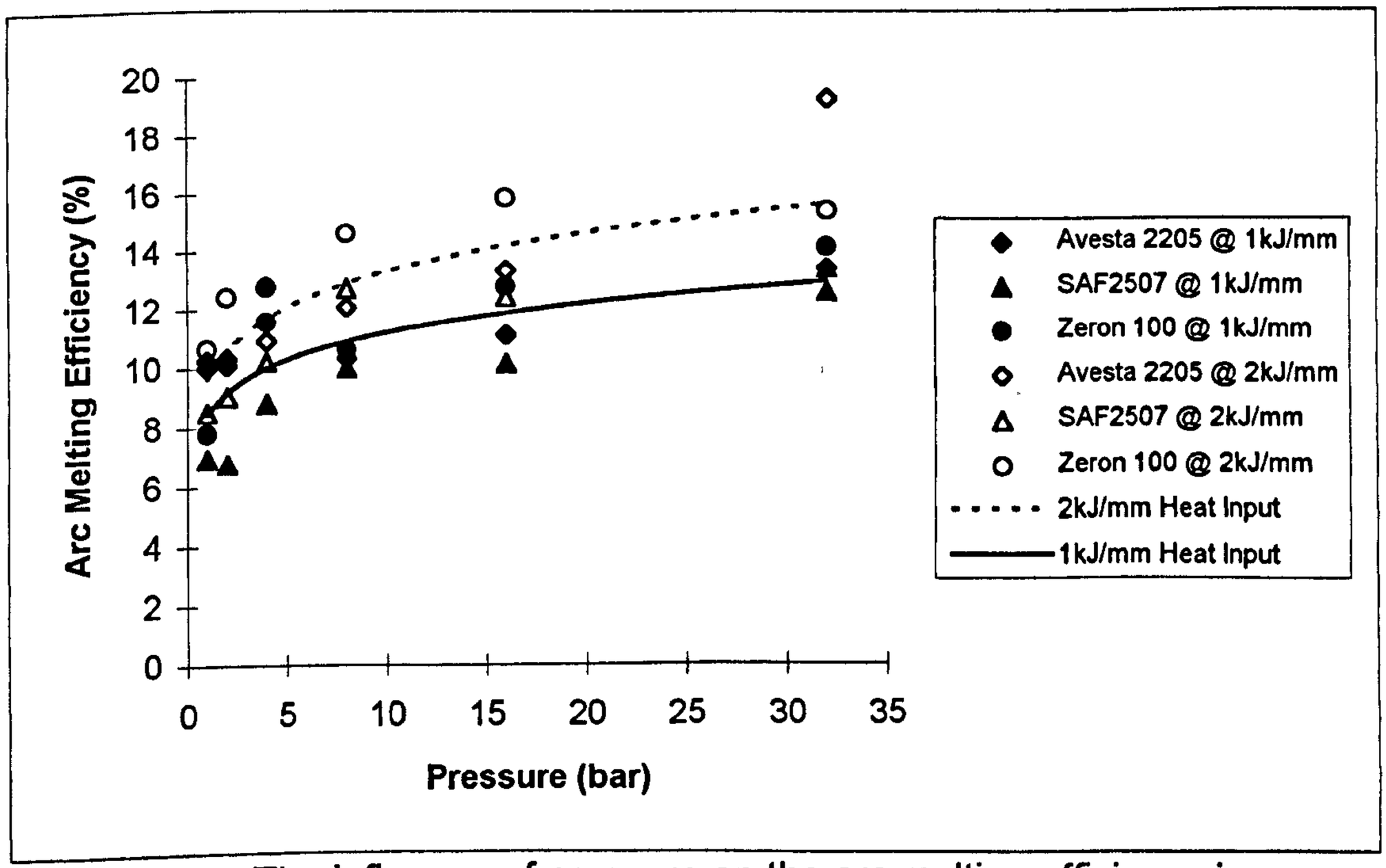

Figure 4.14: The influence of pressure on the arc melting efficiency in duplex stainless steels.

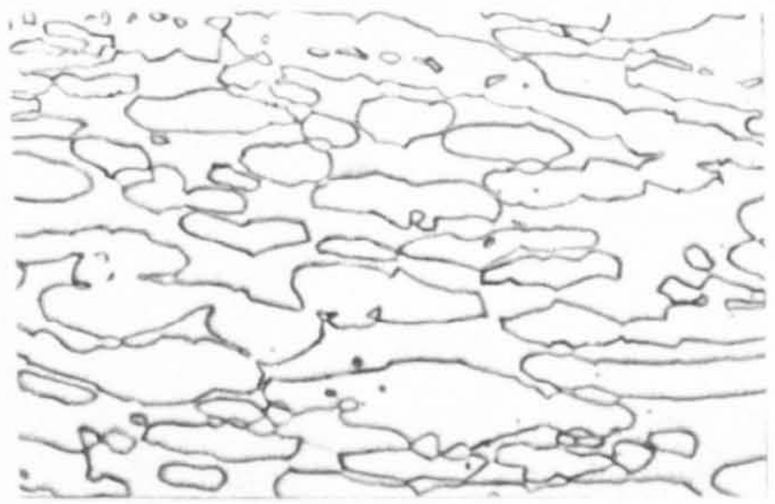

No treatment

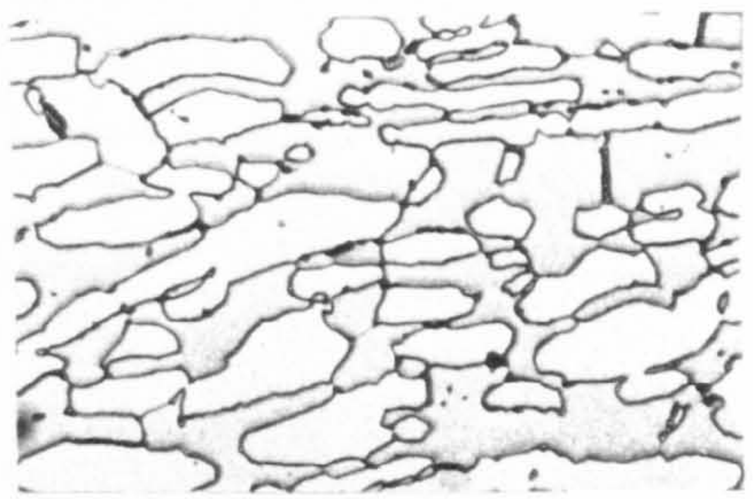

15 minutes

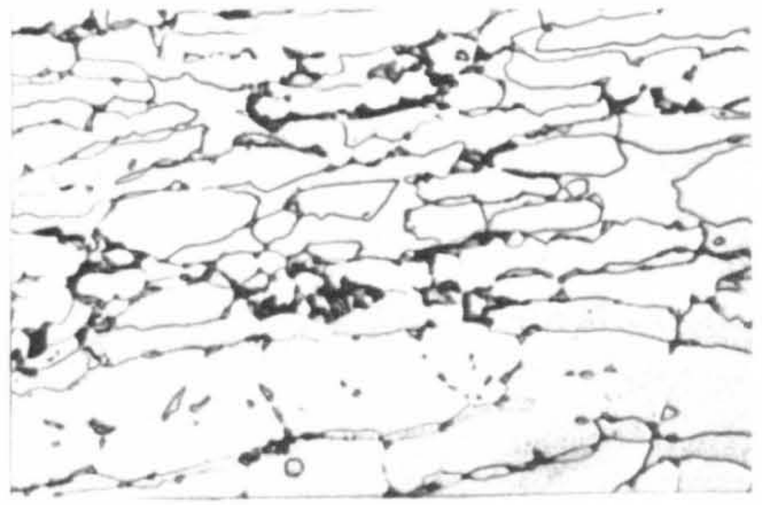

30 minutes

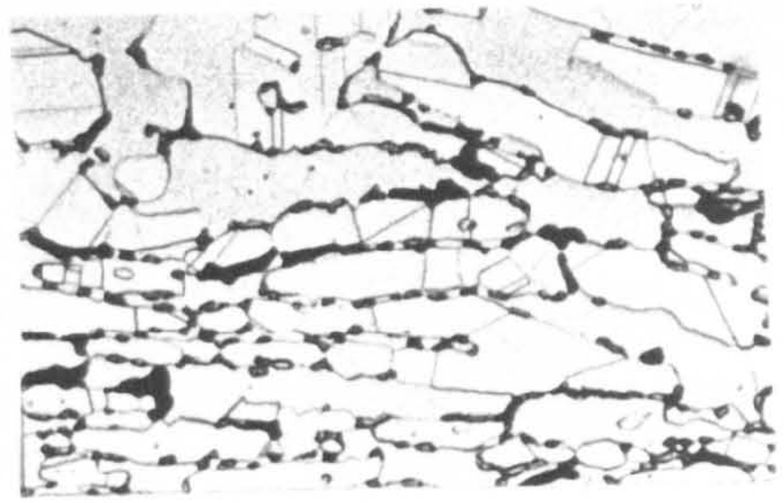

1 hour

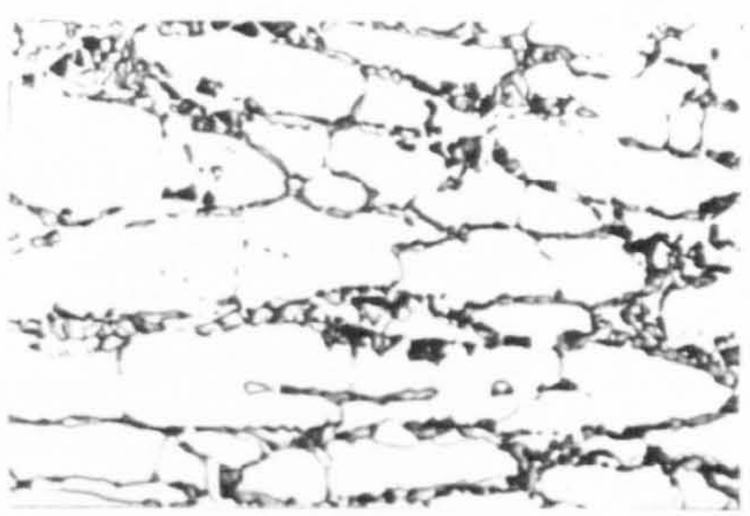

2 hours

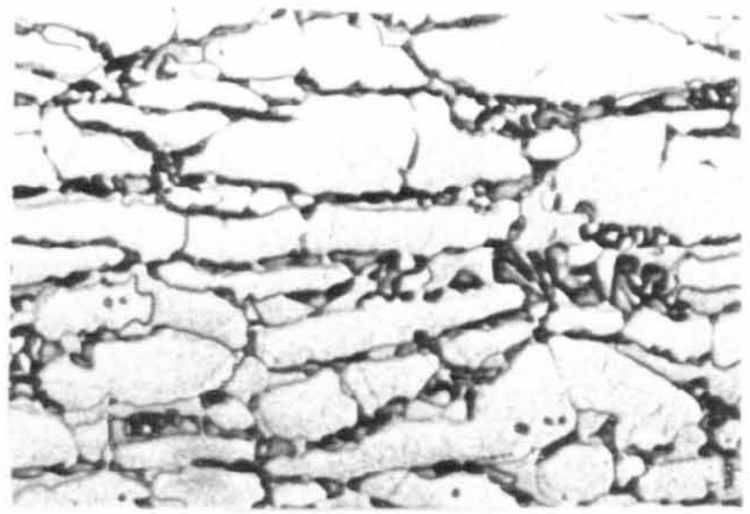

4 hours

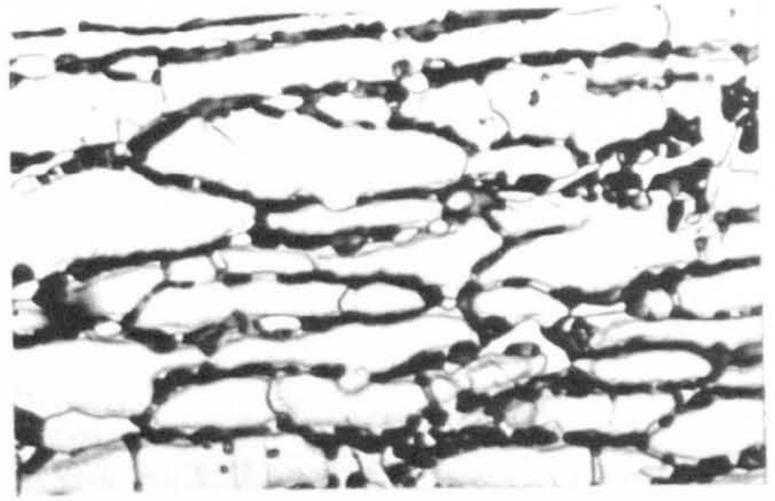

6 hours

Figure 4.15: Development of sigma phase in Avesta 2205 during isothermal heat treatment at 850°C (x400). The austenite is the lighter shaded of the two phases, the ferrite gradually decomposes to sigma phase.

No treatment

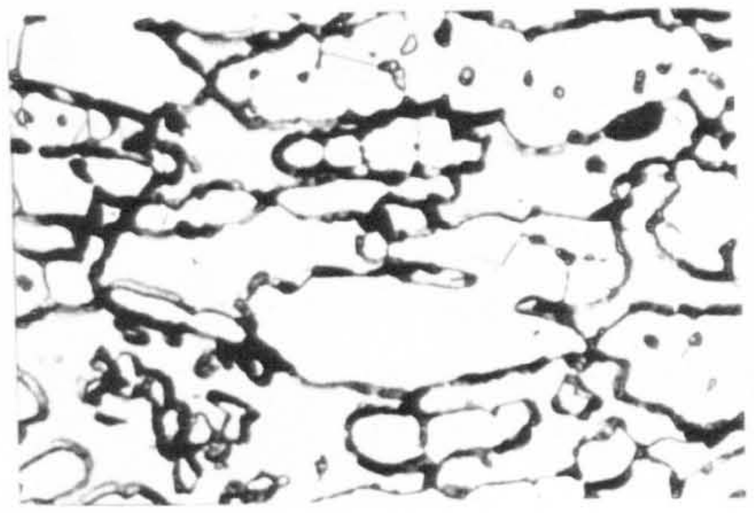

15 minutes

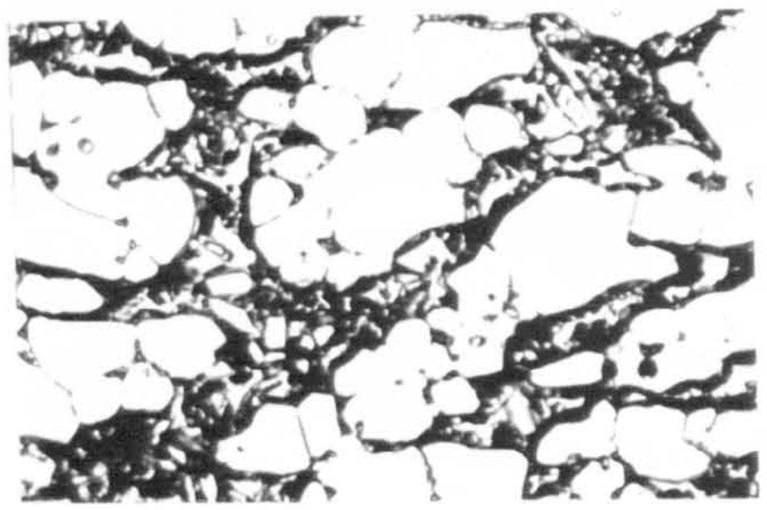

30 minutes

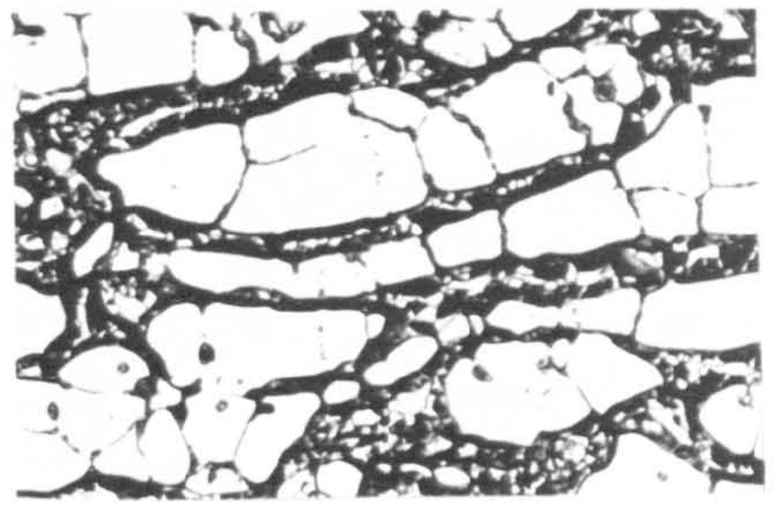

1 hour

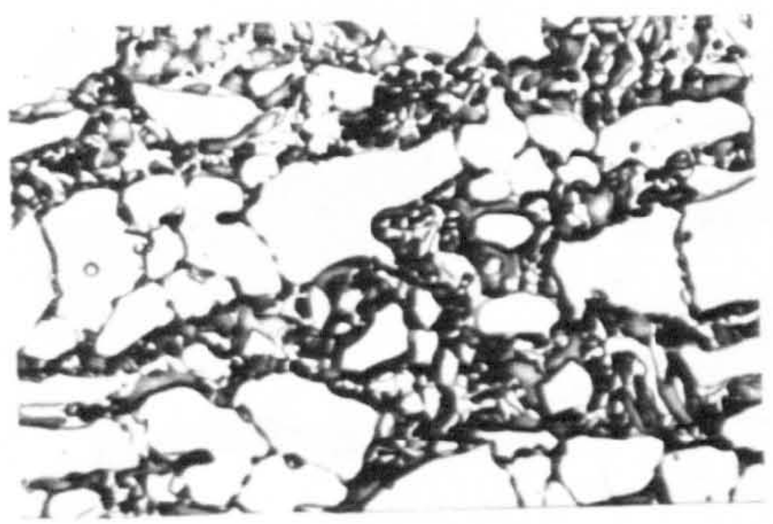

2 hours

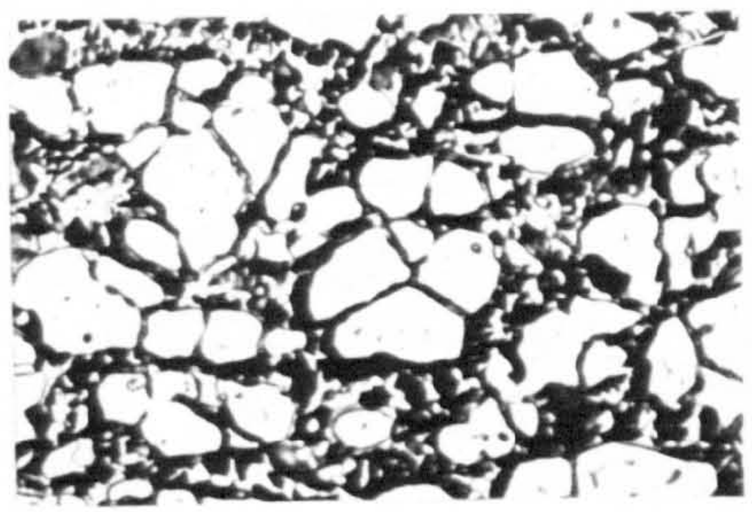

4 hours

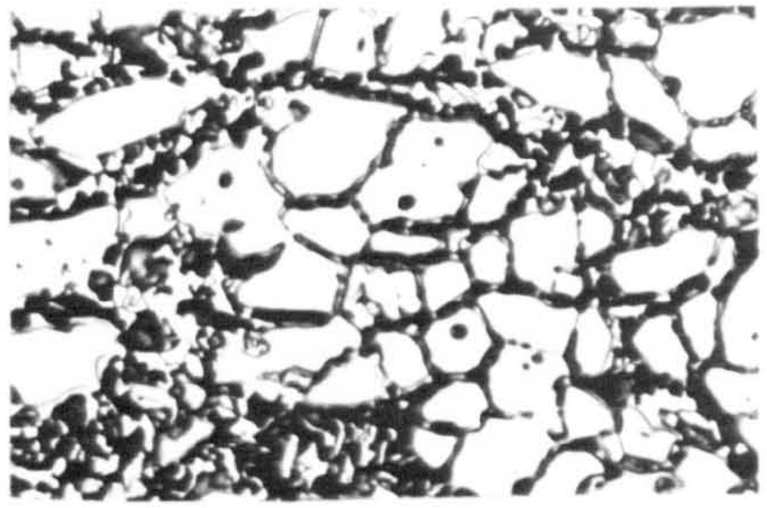

6 hours

Figure 4.16: Development of sigma phase in Sandvik SAF2507 during isothermal heat treatment at 850°C (x400).

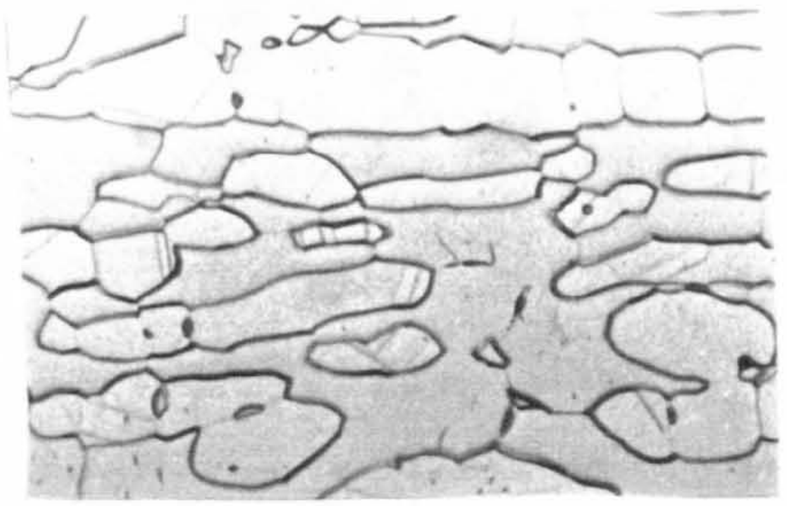

No treatment

15 minutes

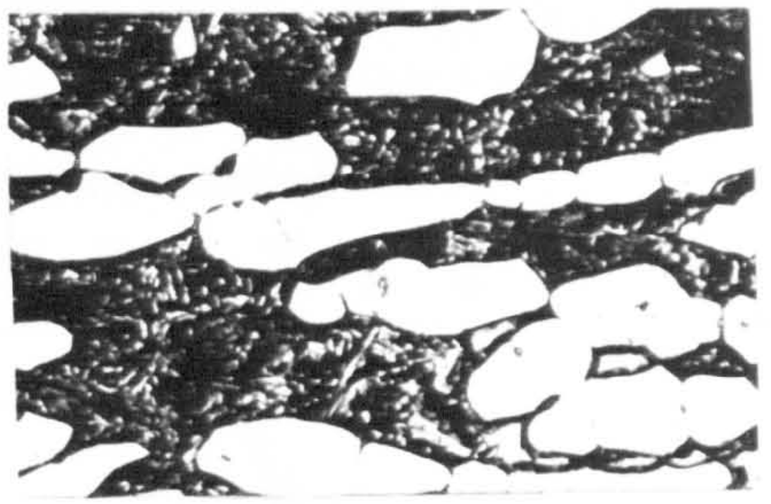

30 minutes

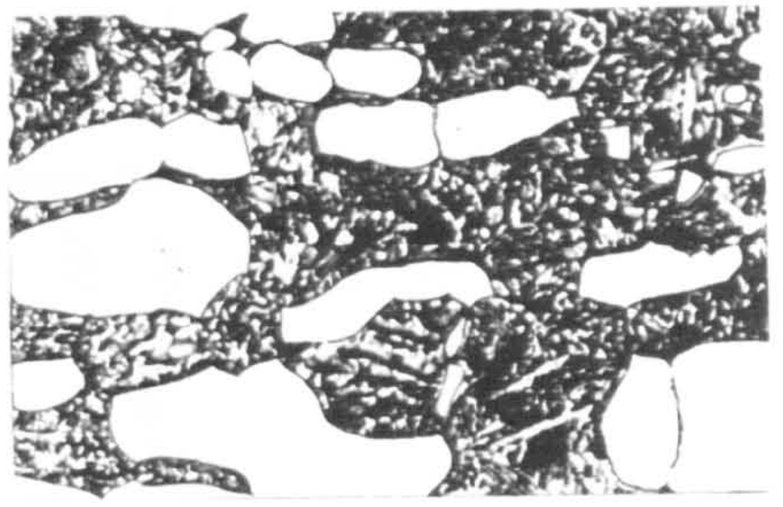

1 hour

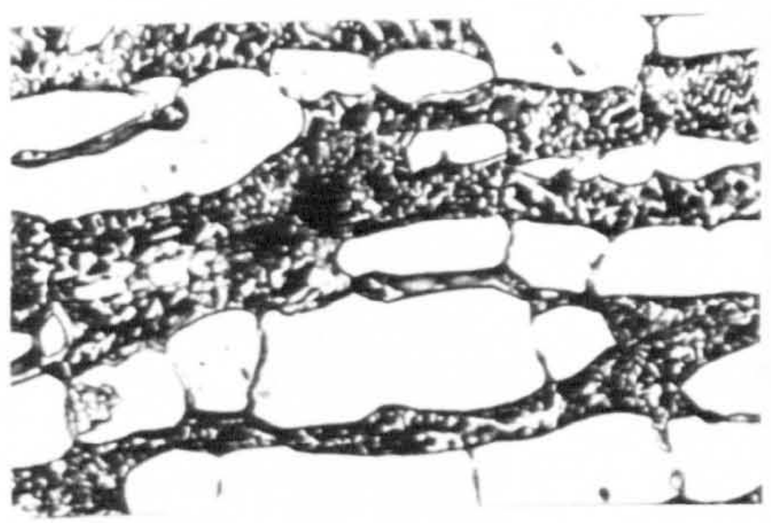

2 hours

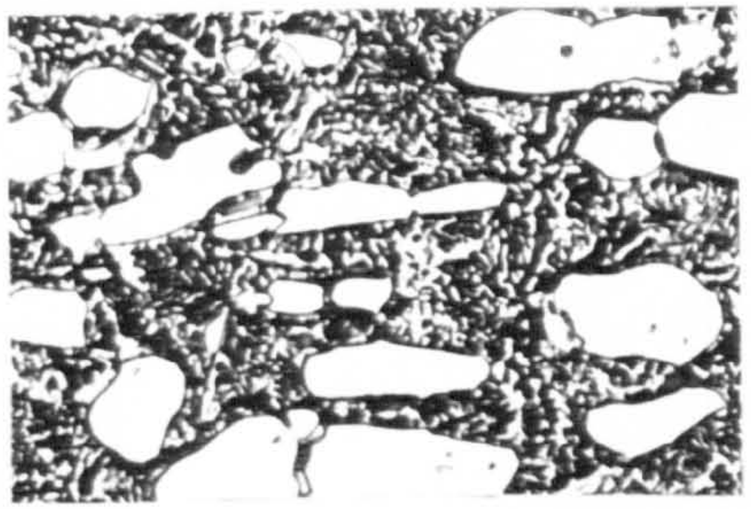

4 hours

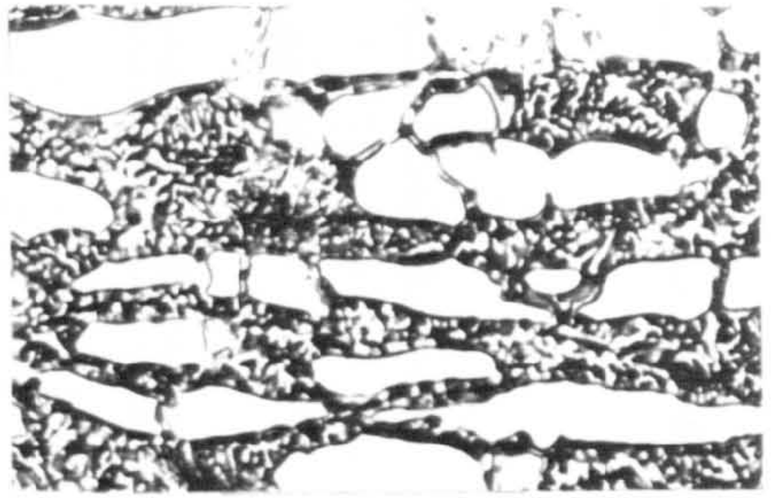

6 hours

Figure 4.17: Development of sigma phase in Zeron 100 during isothermal heat treatment at 850°C (x400).

(a)

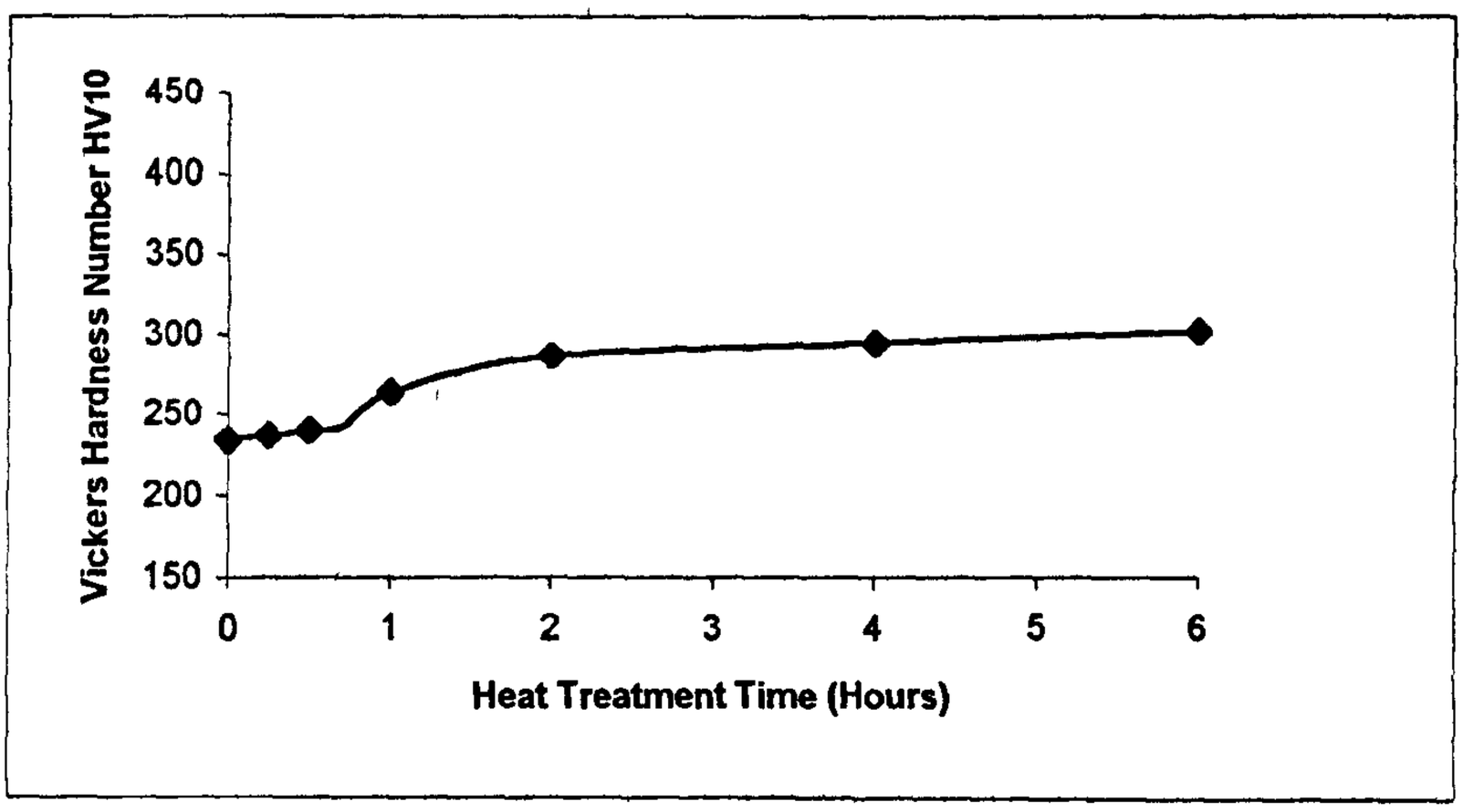

(b)

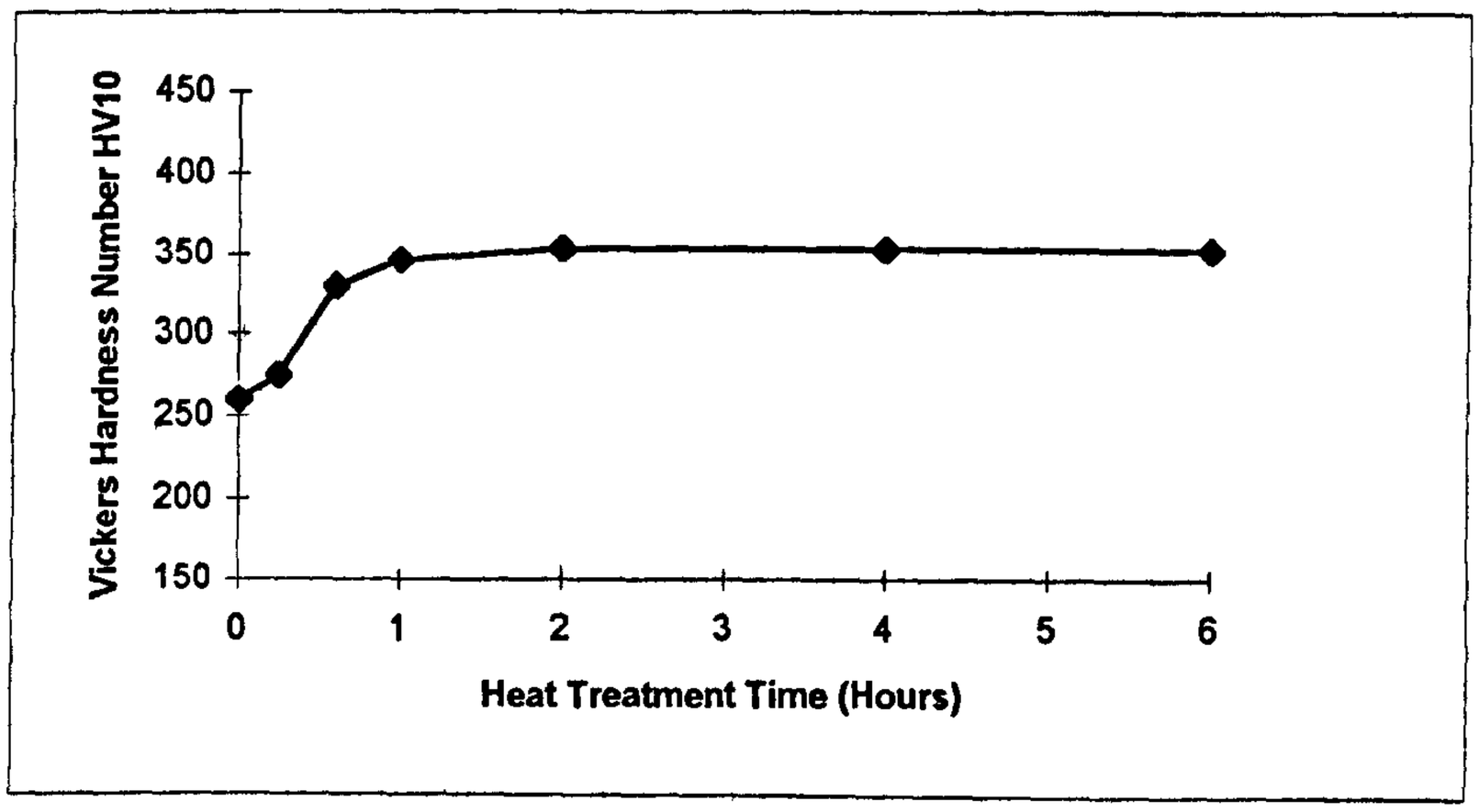

(c)

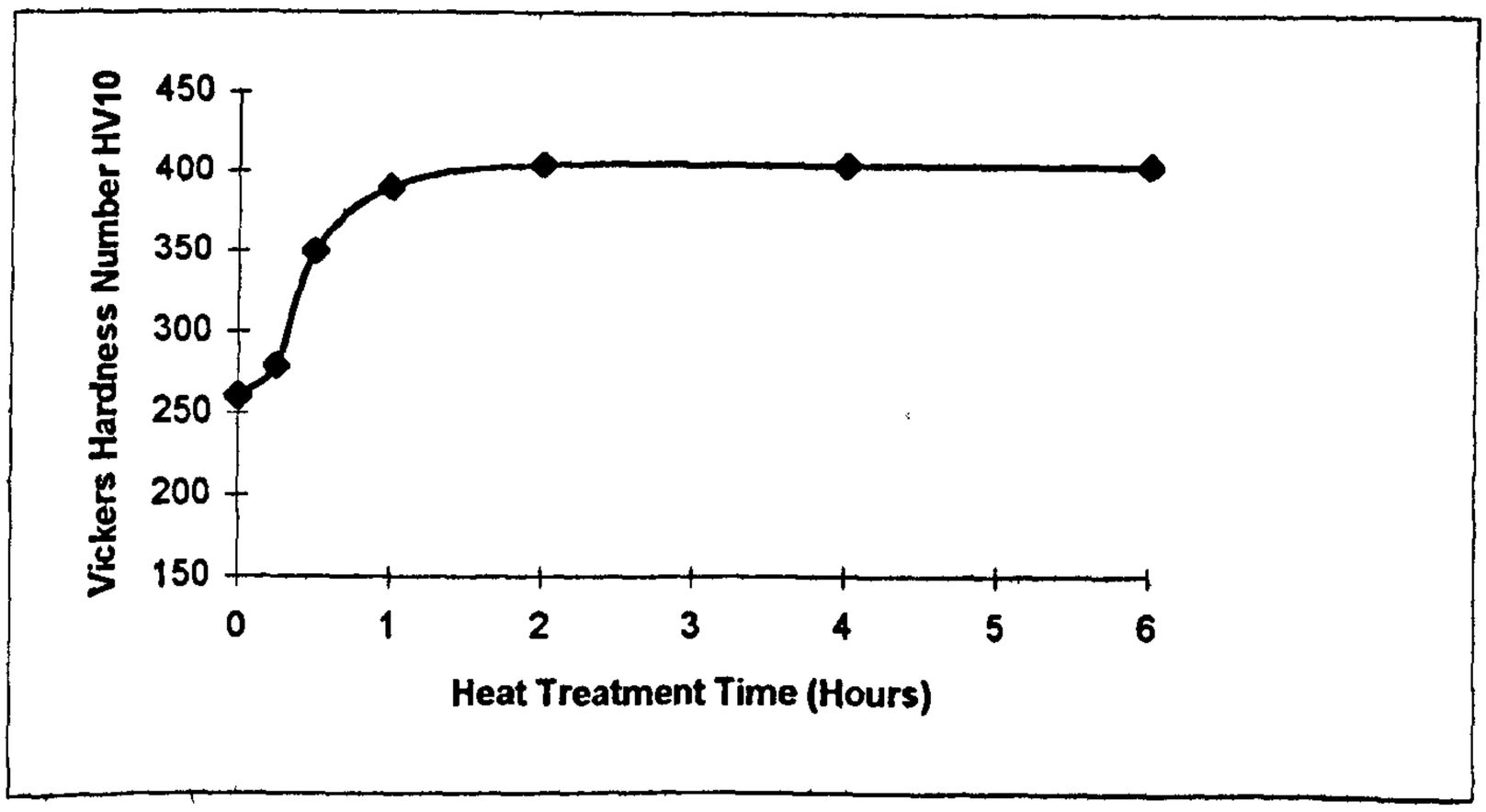

Figure 4.18: The influence of heat treatment time at 850°C on the hardness of the (a) Avesta 2205, (b) Sandvik SAF2507, (c) Zeron 100 materials.

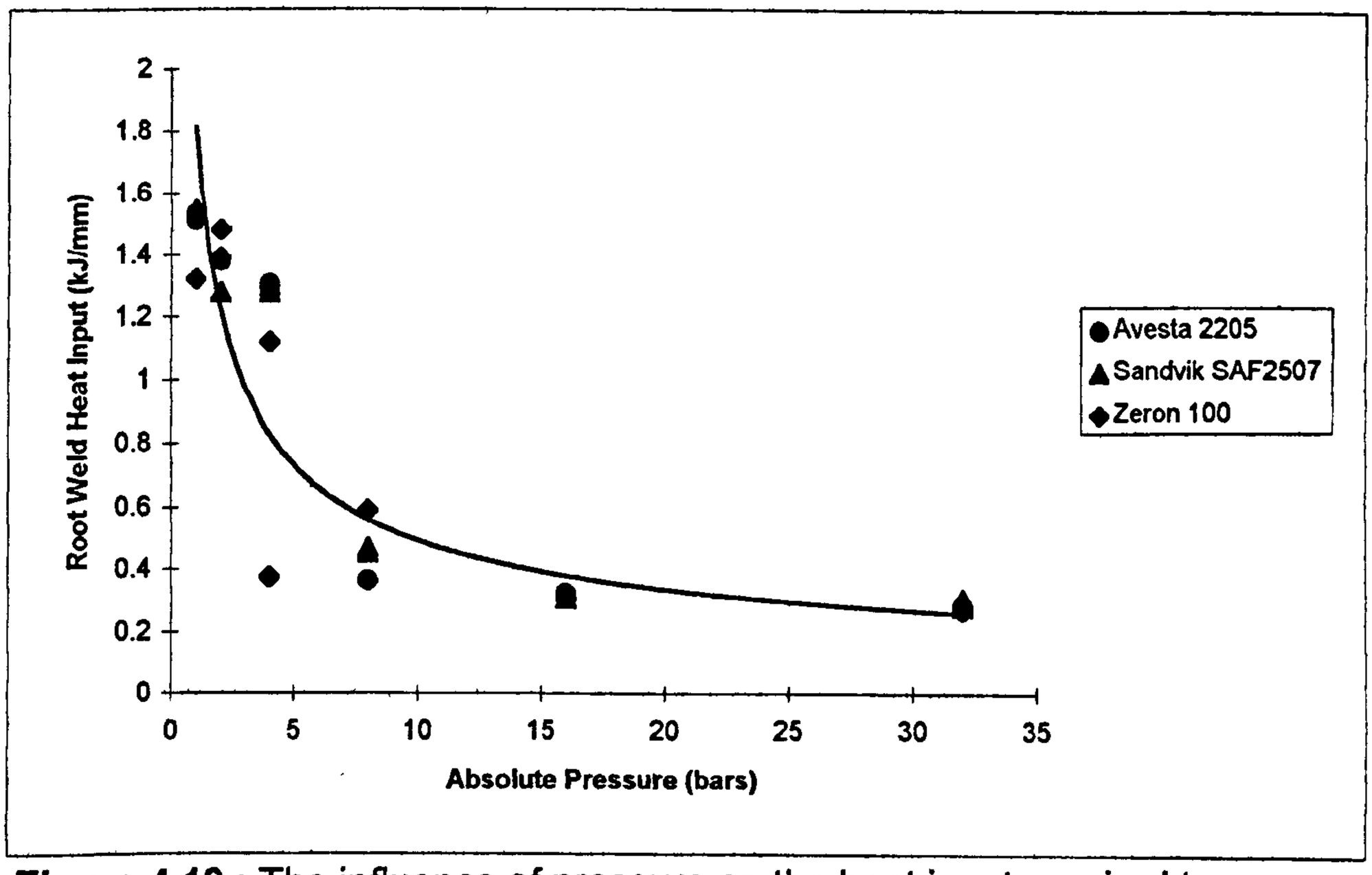

Figure 4.19 : The influence of pressure on the heat input required to achieve a satisfactory root weld in the duplex stainless steel joints.

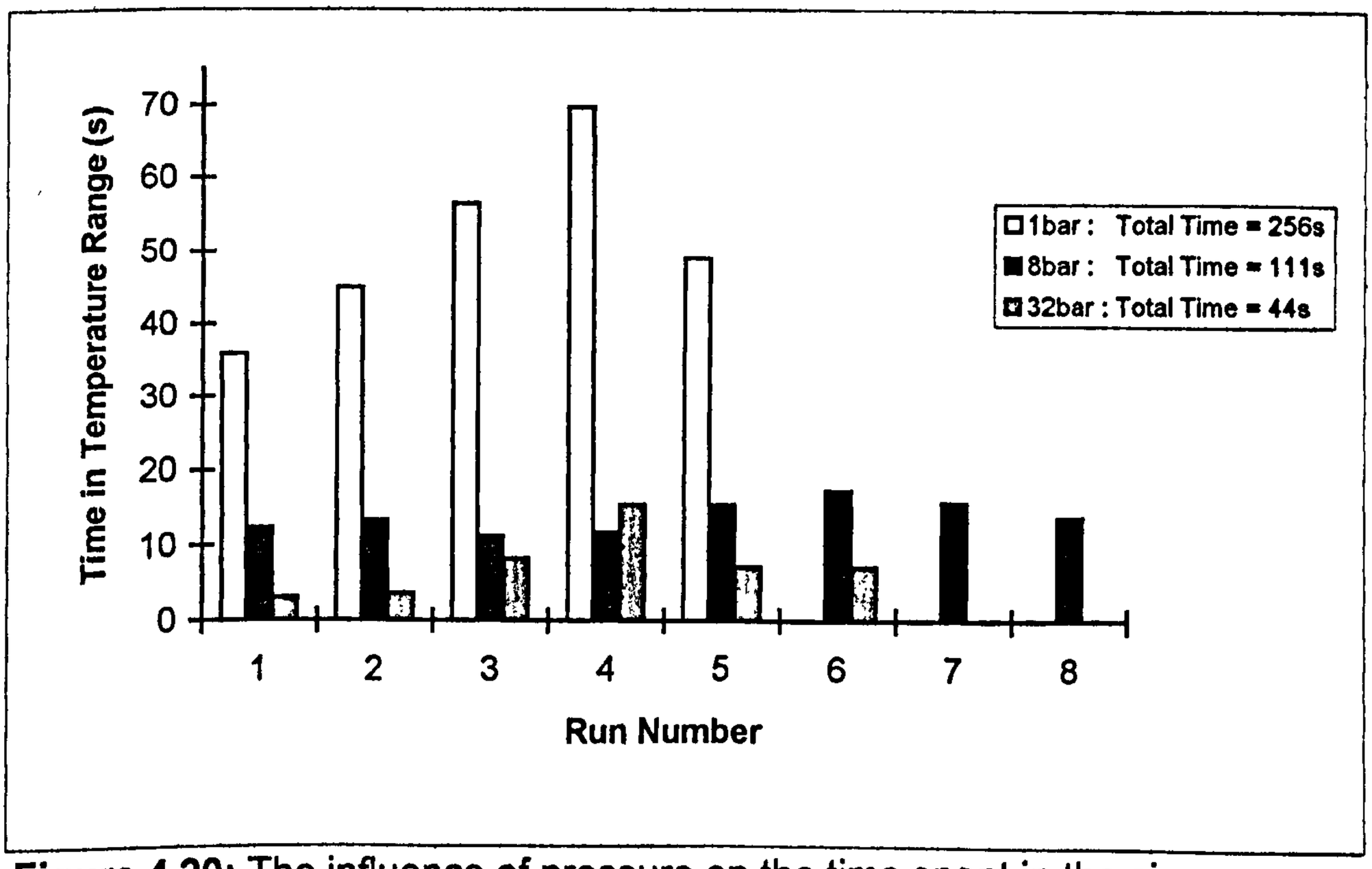

Figure 4.20: The influence of pressure on the time spent in the sigma phase forming temperature range for each weld pass for a duplex stainless steel weld.

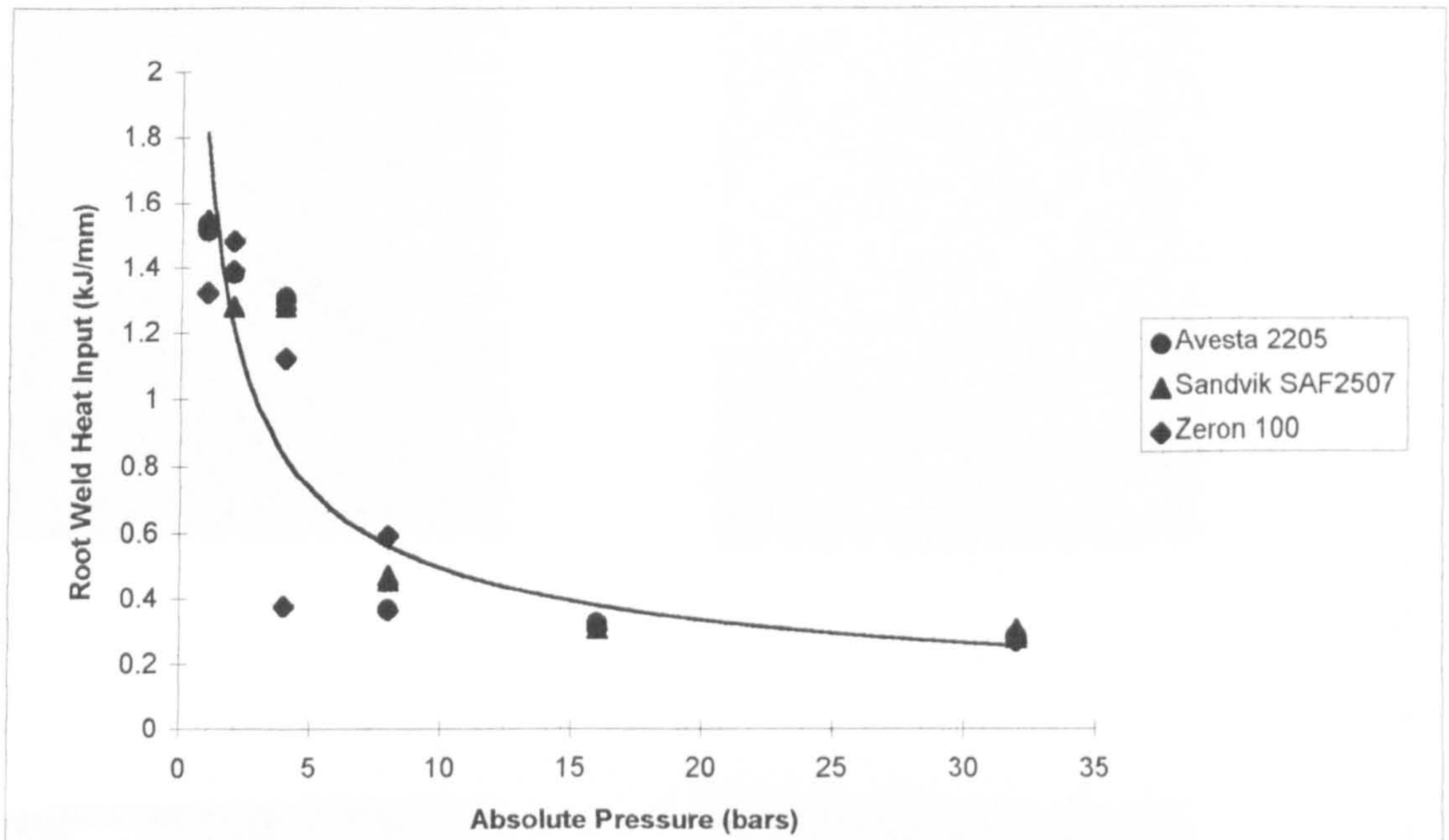

Figure 4.19 : The influence of pressure on the heat input required to achieve a satisfactory root weld in the duplex stainless steel joints.

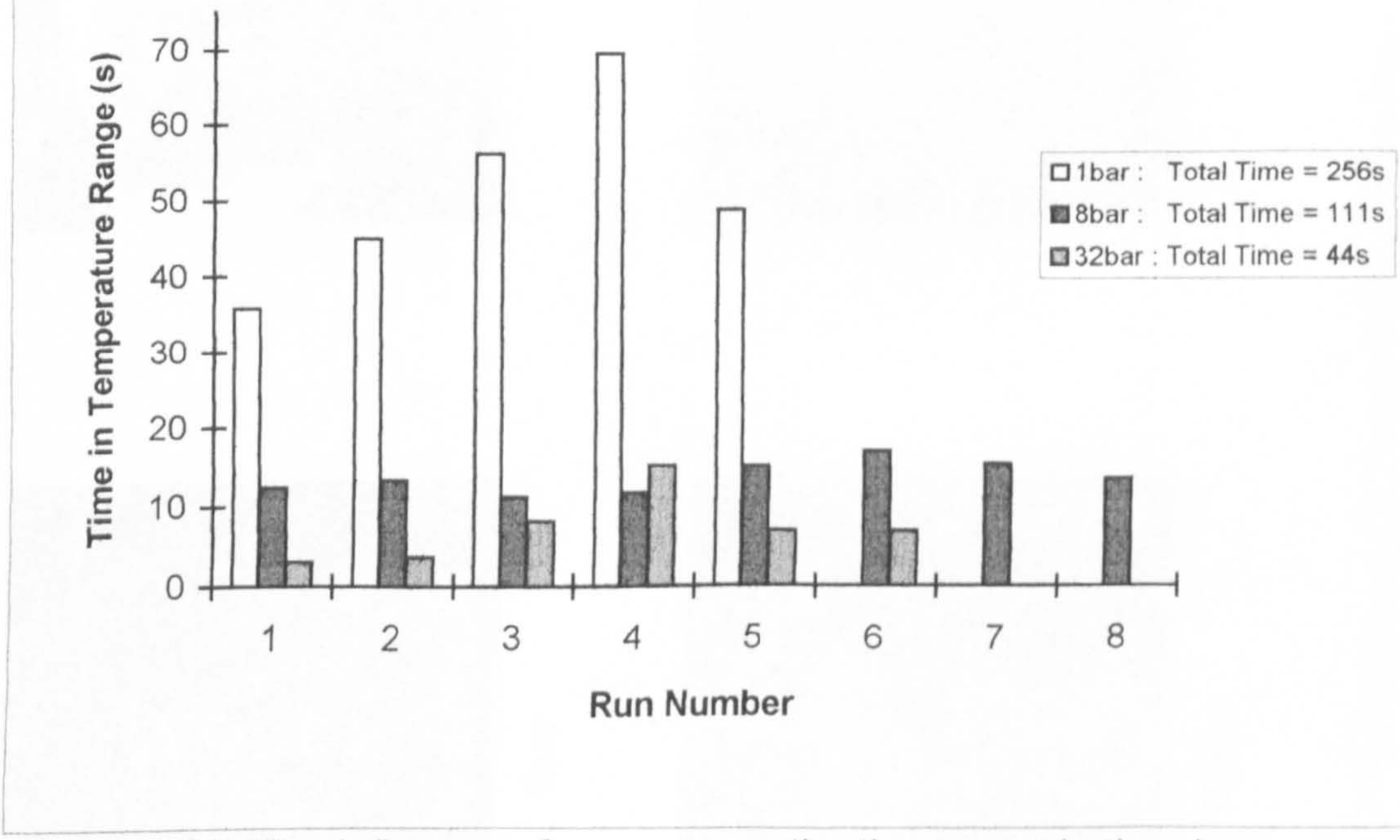

Figure 4.20: The influence of pressure on the time spent in the sigma phase forming temperature range for each weld pass for a duplex stainless steel weld.

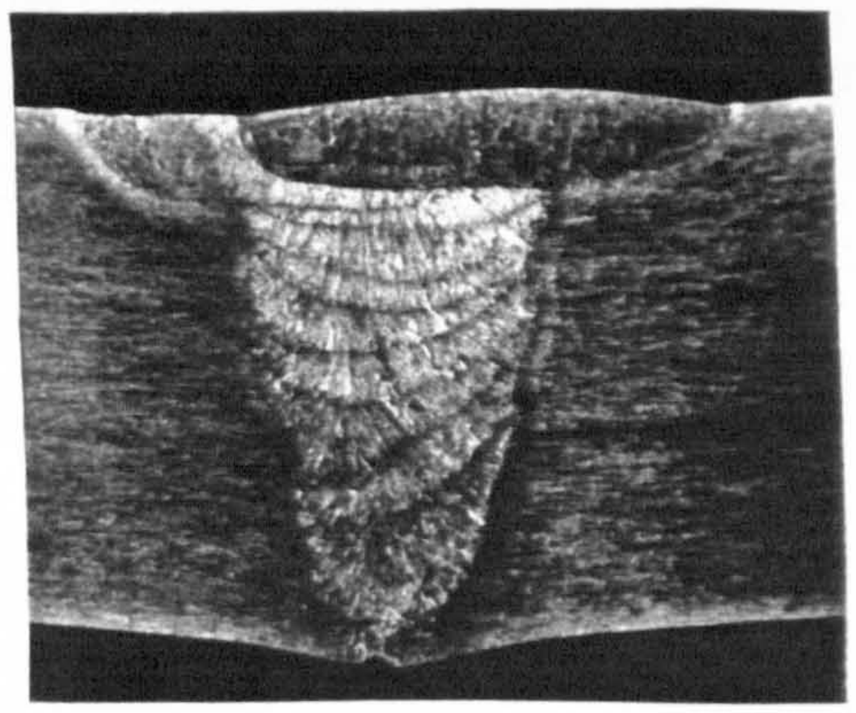

1bar

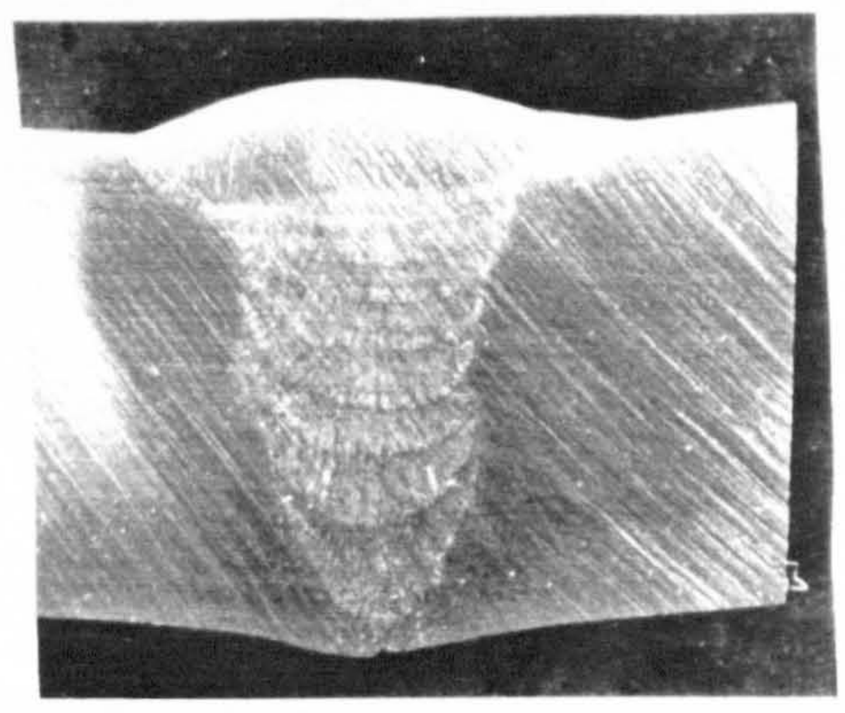

2bars

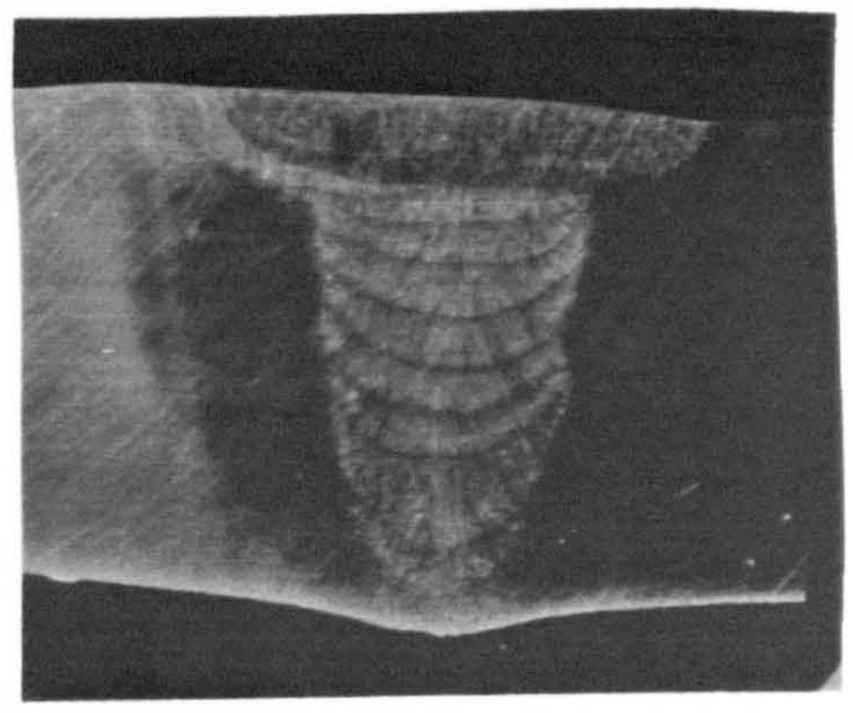

4bars

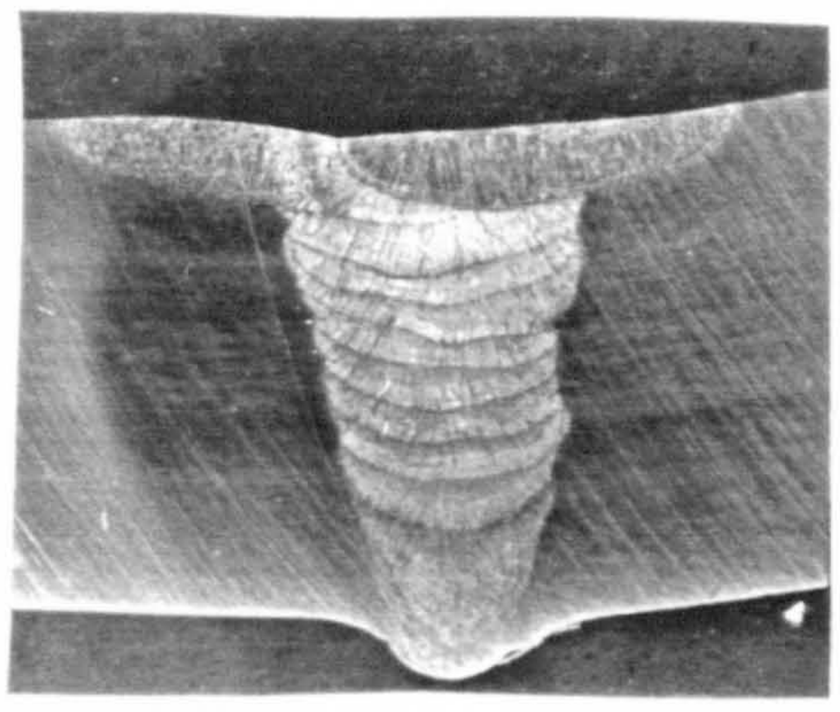

8bars

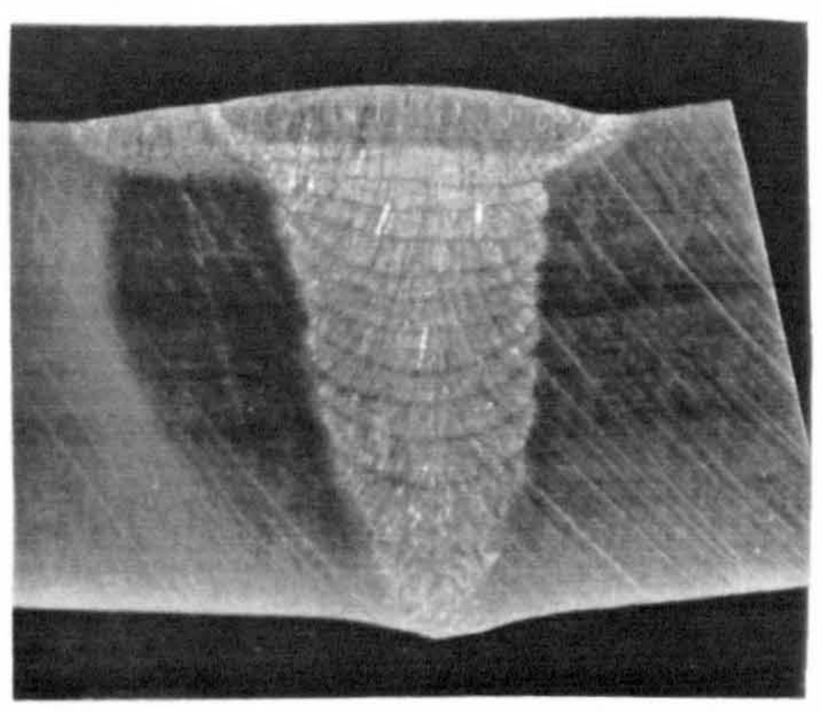

16bars

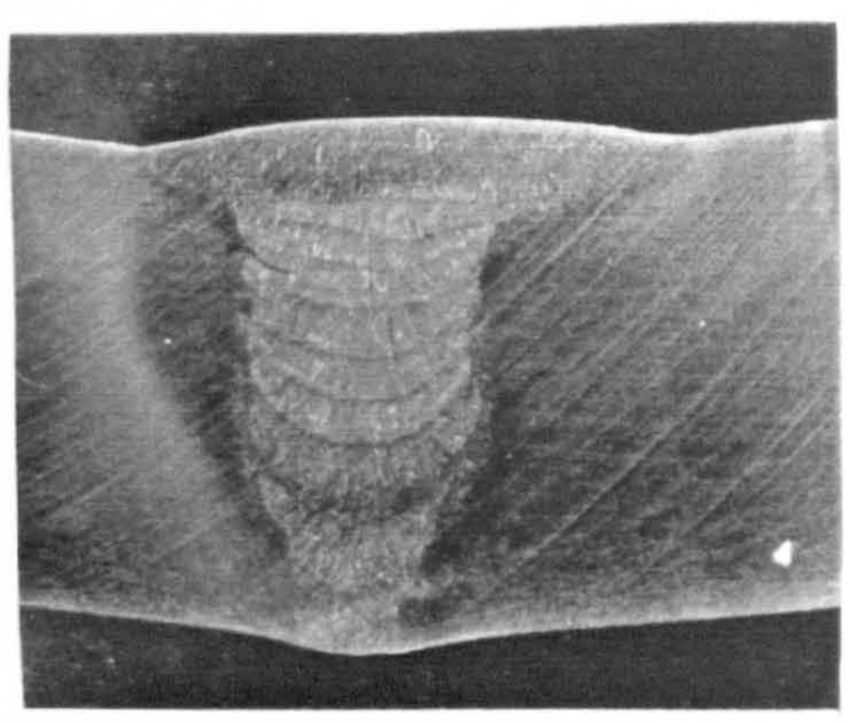

32bars

Figure 4.21: The profiles of the Avesta 2205 joints welded at pressures up to 32 bars (x2.5).

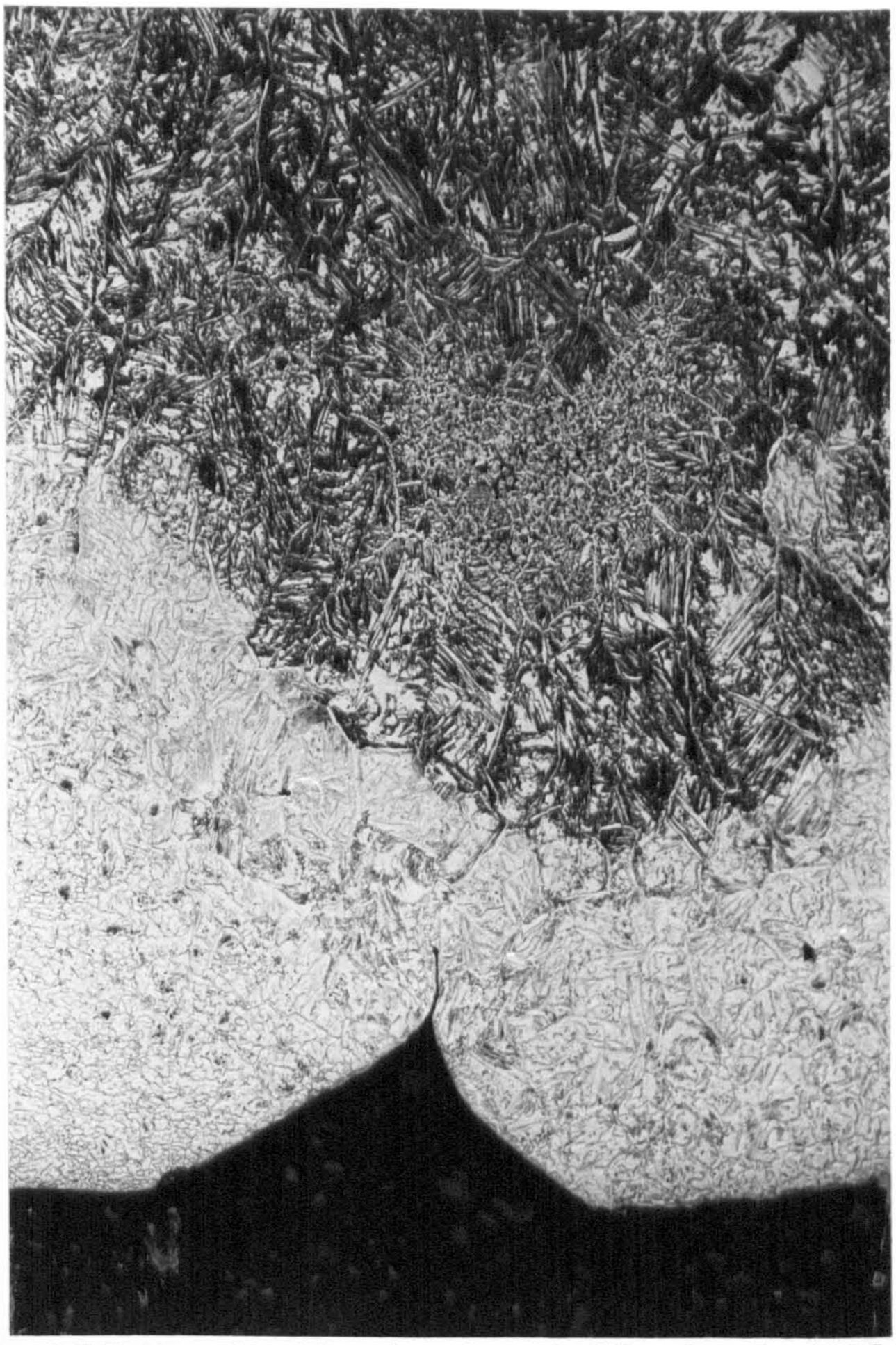

Figure 4.22: The 1.54kJ/mm heat input root weld of the Avesta 2205 joint welded at 1bar showing the fine grained weld metal (dark grey contrast) (x50).

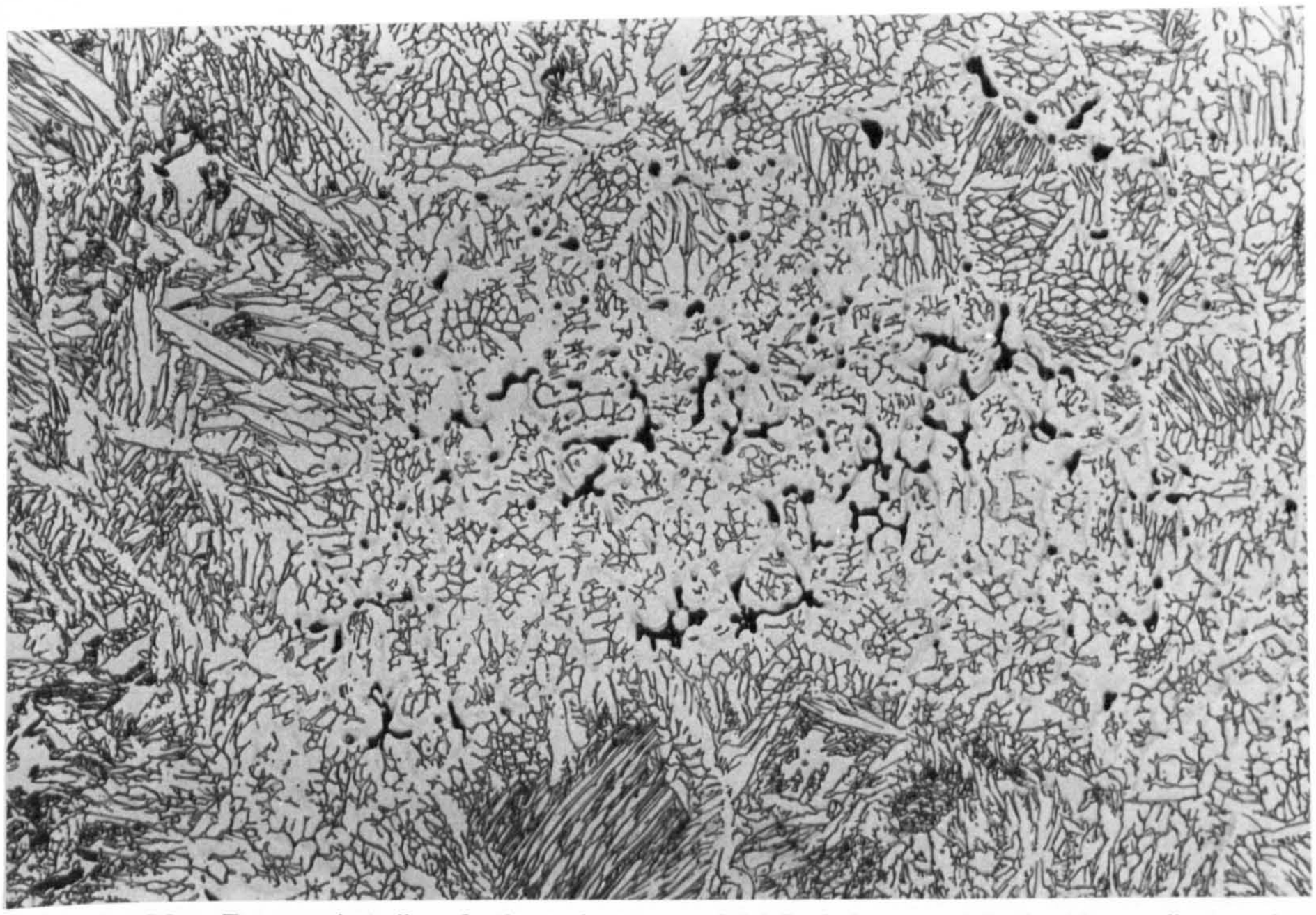

Figure 4.23: Root detail of the Avesta 2205 joint welded 1bar (heat input, 1.54kJ/mm) showing intergranular porosity between the austenite grains (x200).

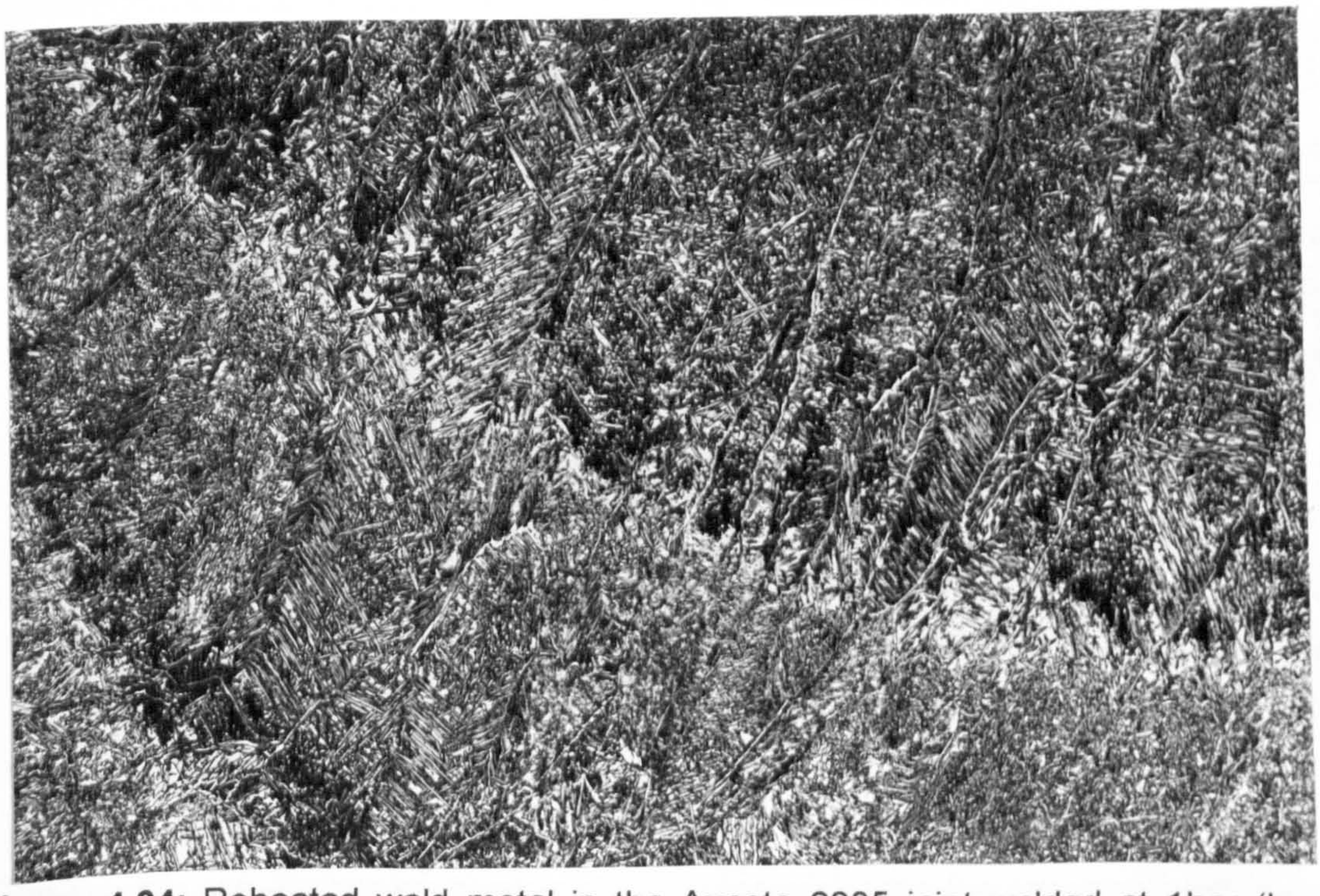

Figure 4.24: Reheated weld metal in the Avesta 2205 joint welded at 1bar (heat input, 1.00kJ/mm) (x50). The boundaries between passes are distinguished by the fine grained austenite material (dark contrast) and the region of ferrite growth (light contrast) formed as a result of reheating (x50).

Figure 4.25: Fine grained austenite in the reheated weld metal of the Avesta 2205 1.00 kJ/mm heat input joint welded at 1bar (x100).

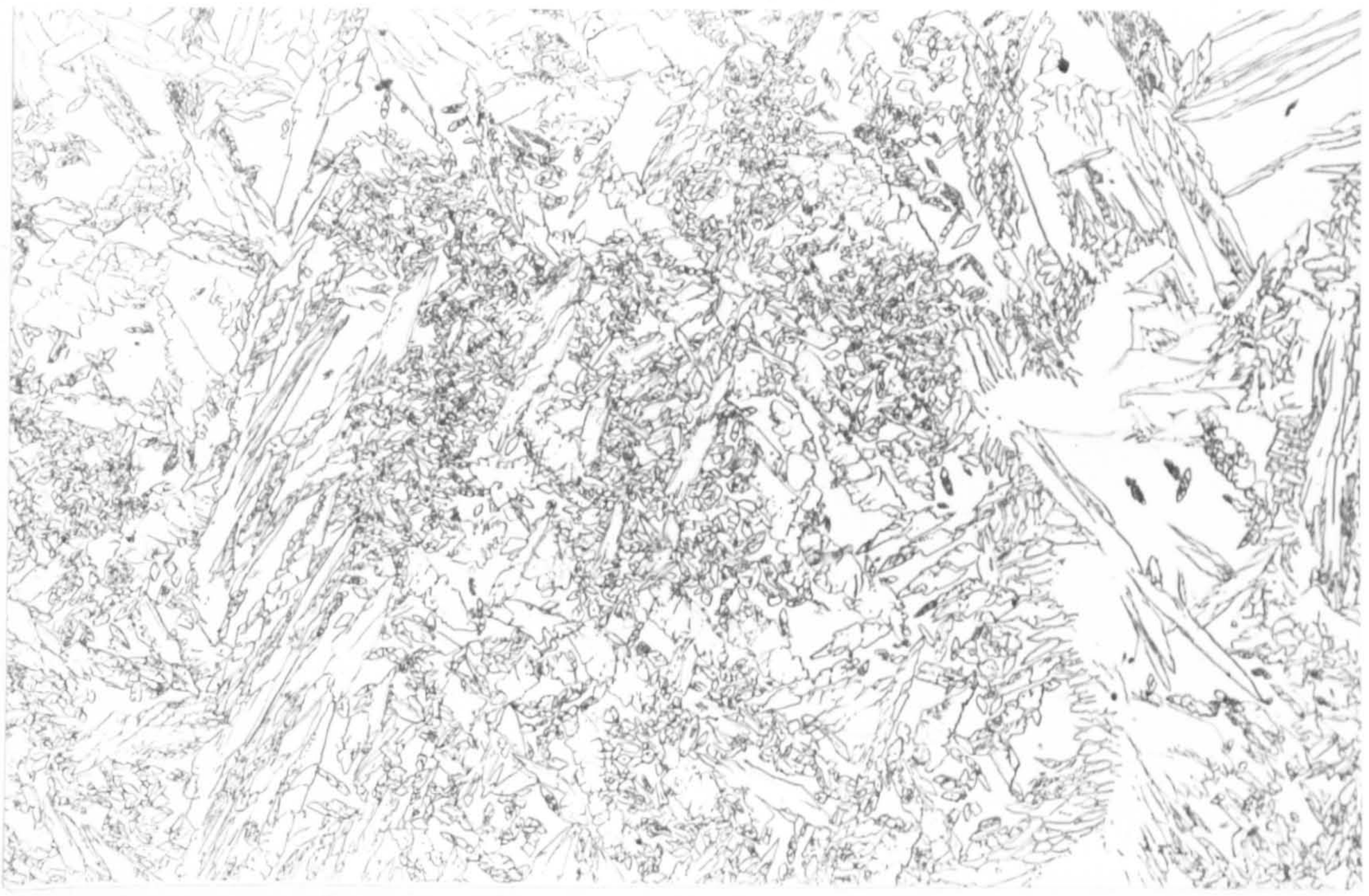

Figure 4.26: The Widmanstätten and acicular structure of the austenite in the reheated weld metal of the 1.00 kJ/mm heat input Avesta 2205 joint welded at 1bar (x400).

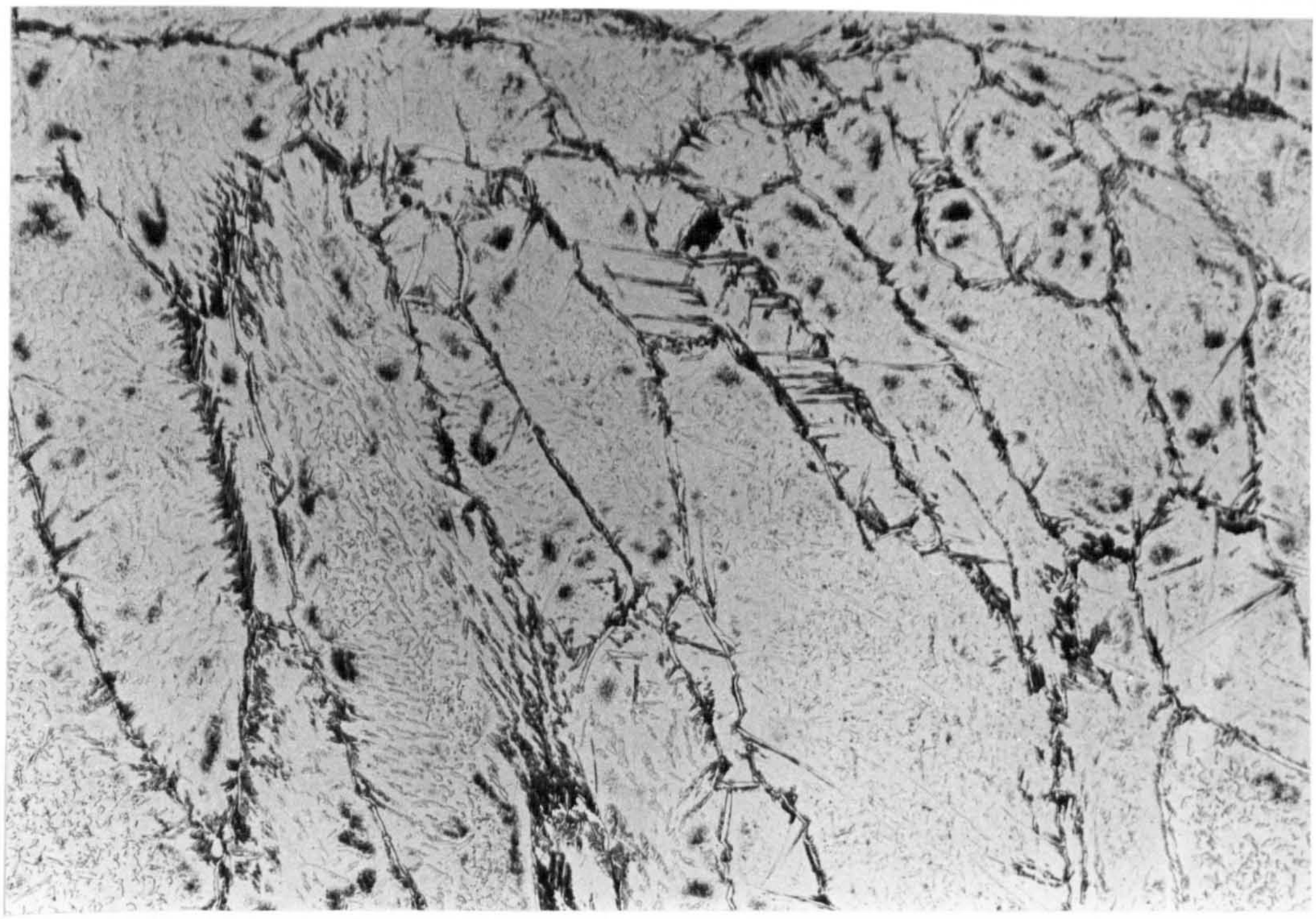

Figure 4.27: Large primary ferrite grains in the Sandvik 22.8.3L weld metal in the cap of the 1.00 kJ/mm heat input Avesta 2205 joint welded at 1bar (x100).

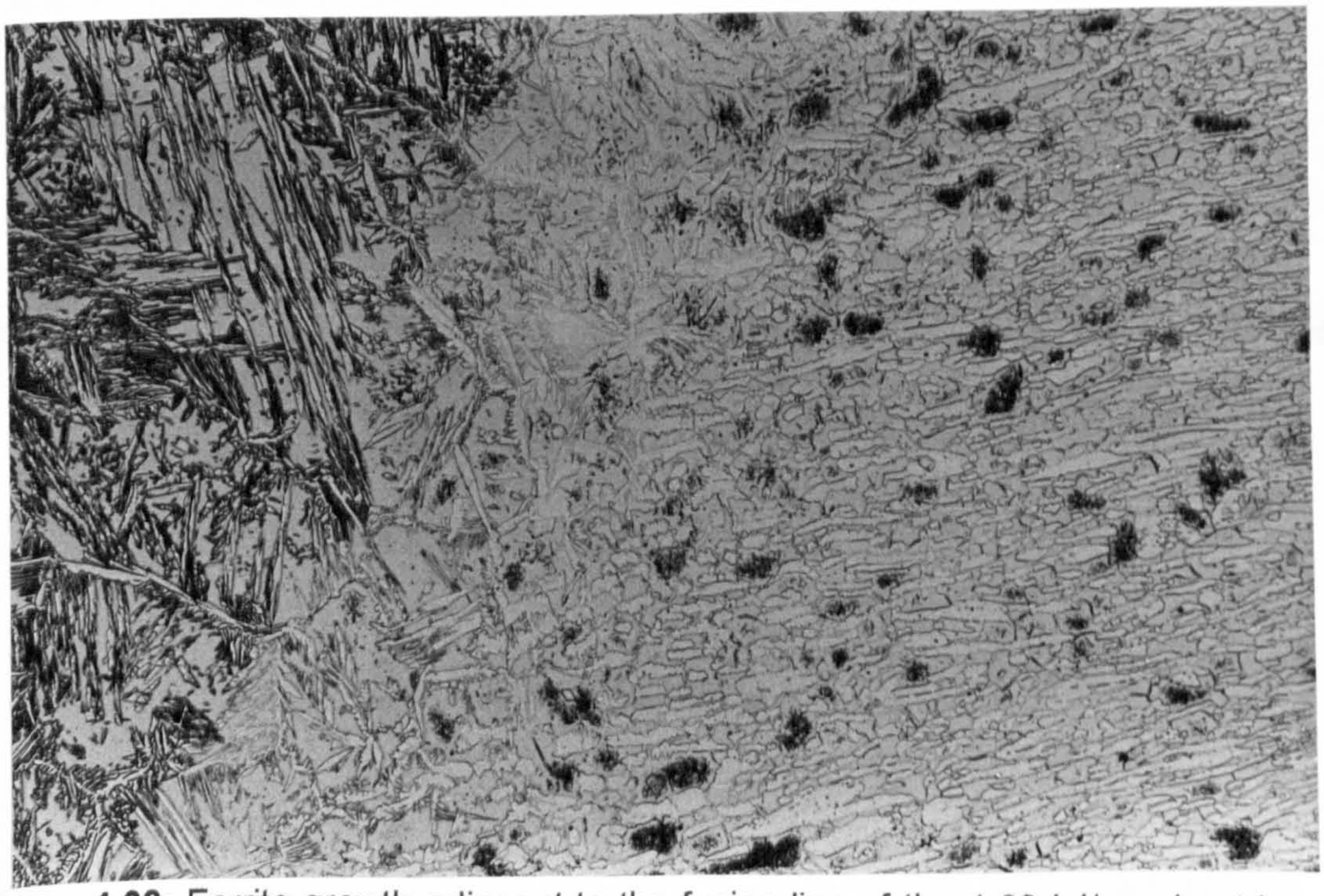

Figure 4.28: Ferrite growth adjacent to the fusion line of the 1.00 kJ/mm heat input Avesta 2205 joint welded at 1bar (x100).(The ferrite is the darker contrast of the two phases).

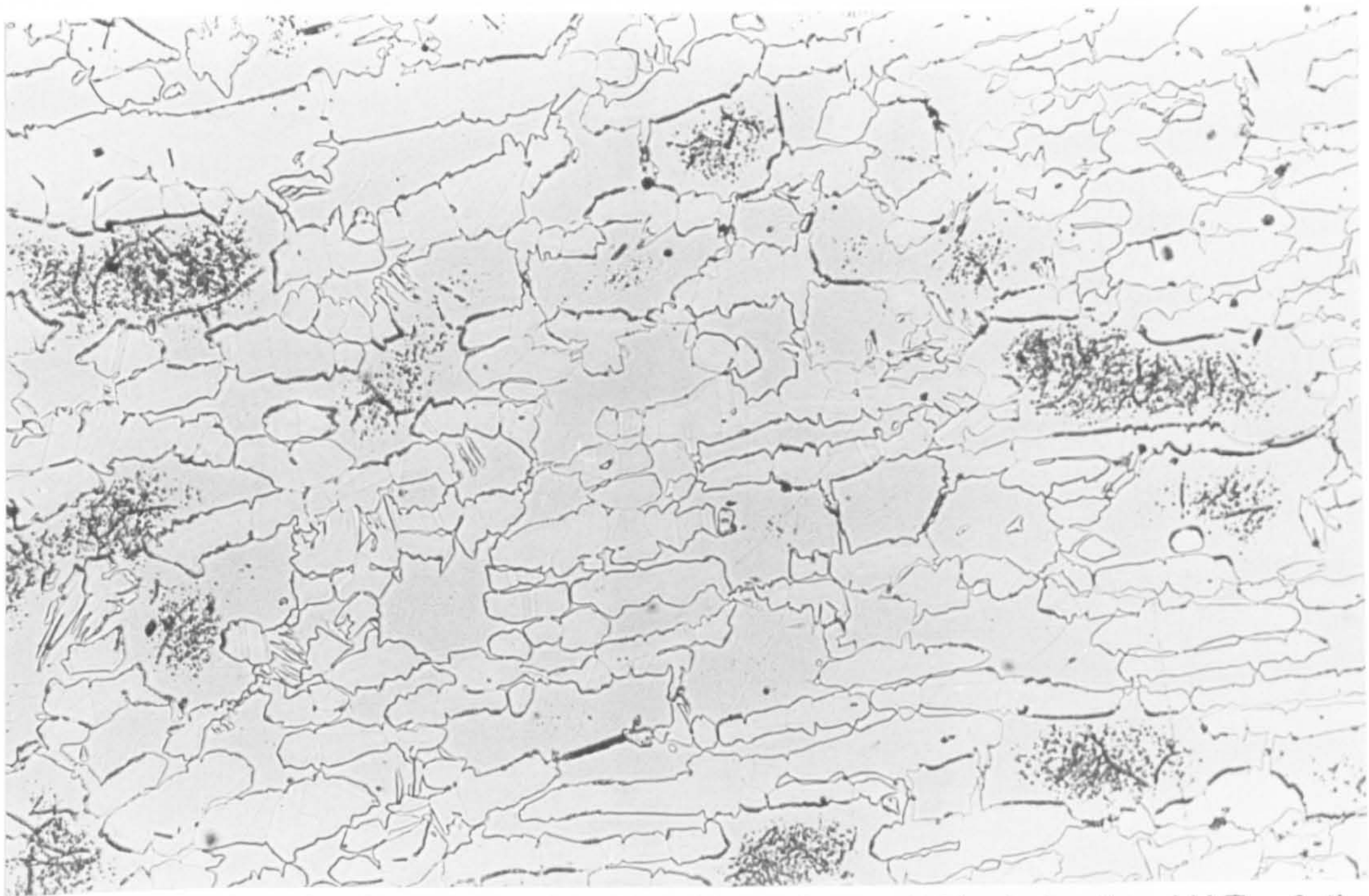

Figure 4.29: Detail of the precipitates (chromium nitrides) in the HAZ of the 1.00kJ/mm heat input Avesta 2205 joint welded at 1bar (x400).

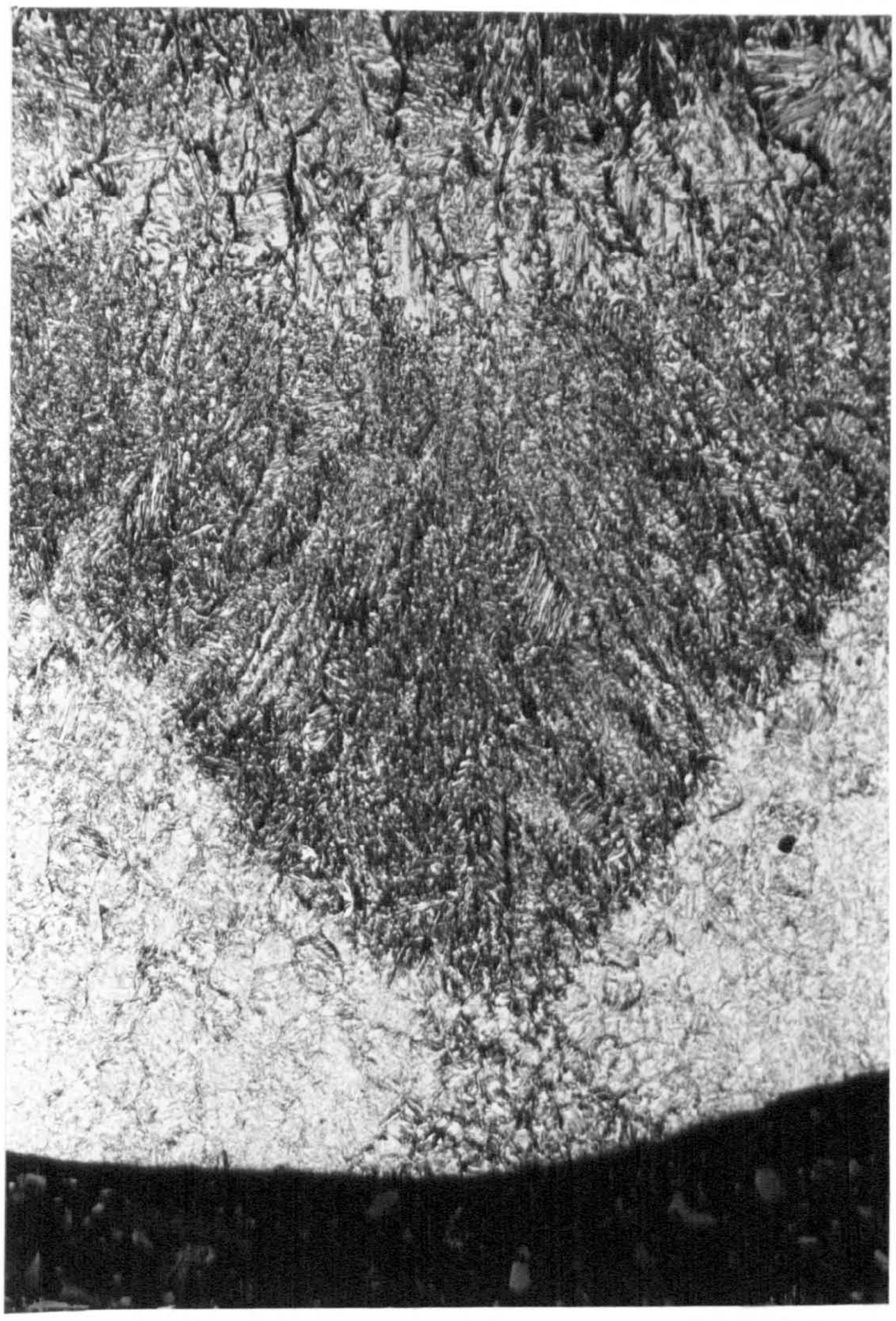

Figure 4.30: Complete penetration in the 0.27kJ/mm heat input root weld of the Avesta 2205 joint welded at 32bars (x50).

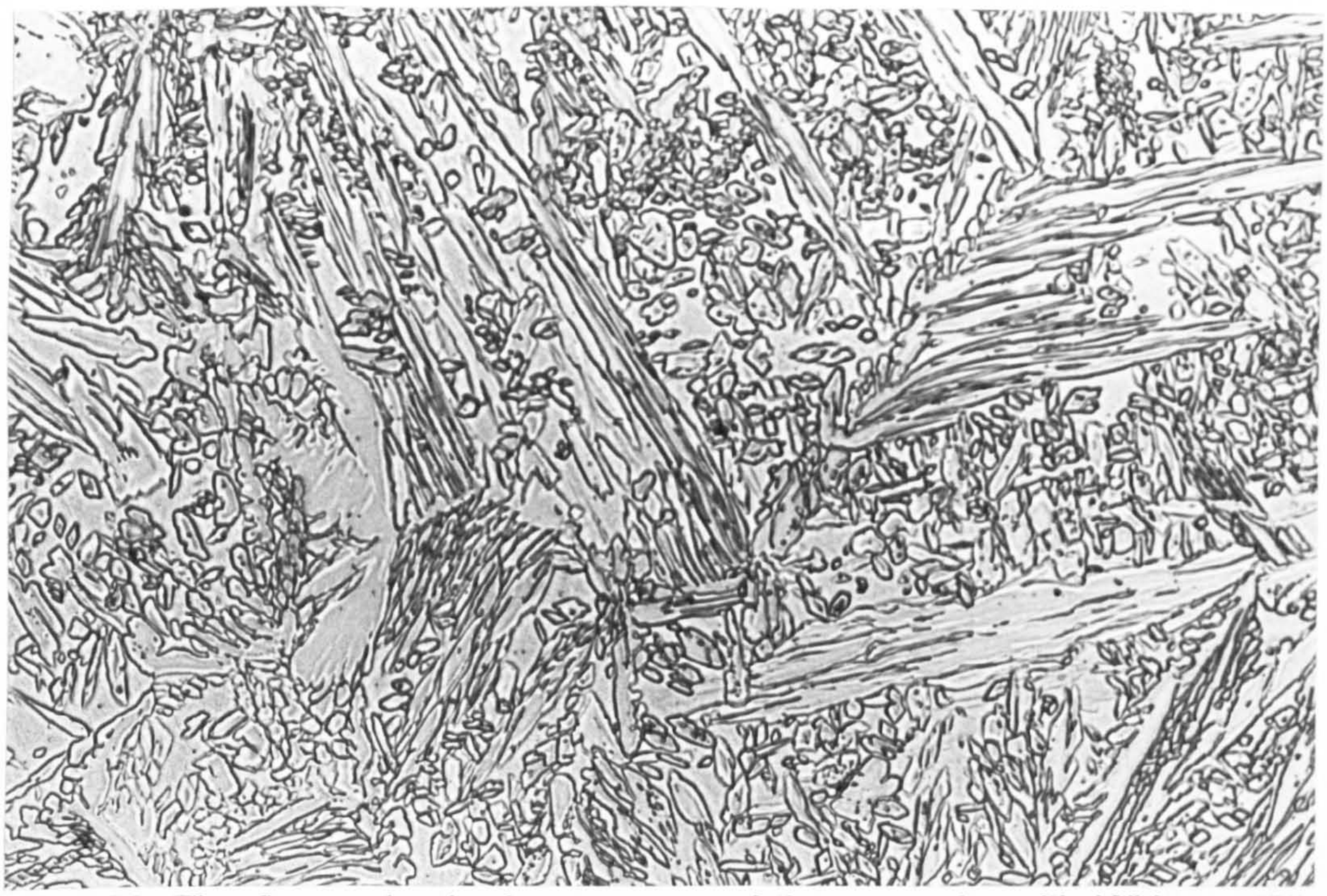

Figure 4.31: The fine grained microstructure of the austenite with Widmanstätten sideplates in the 0.27kJ/mm heat input root weld of the Avesta 2205 joint welded at 32bars (x400).

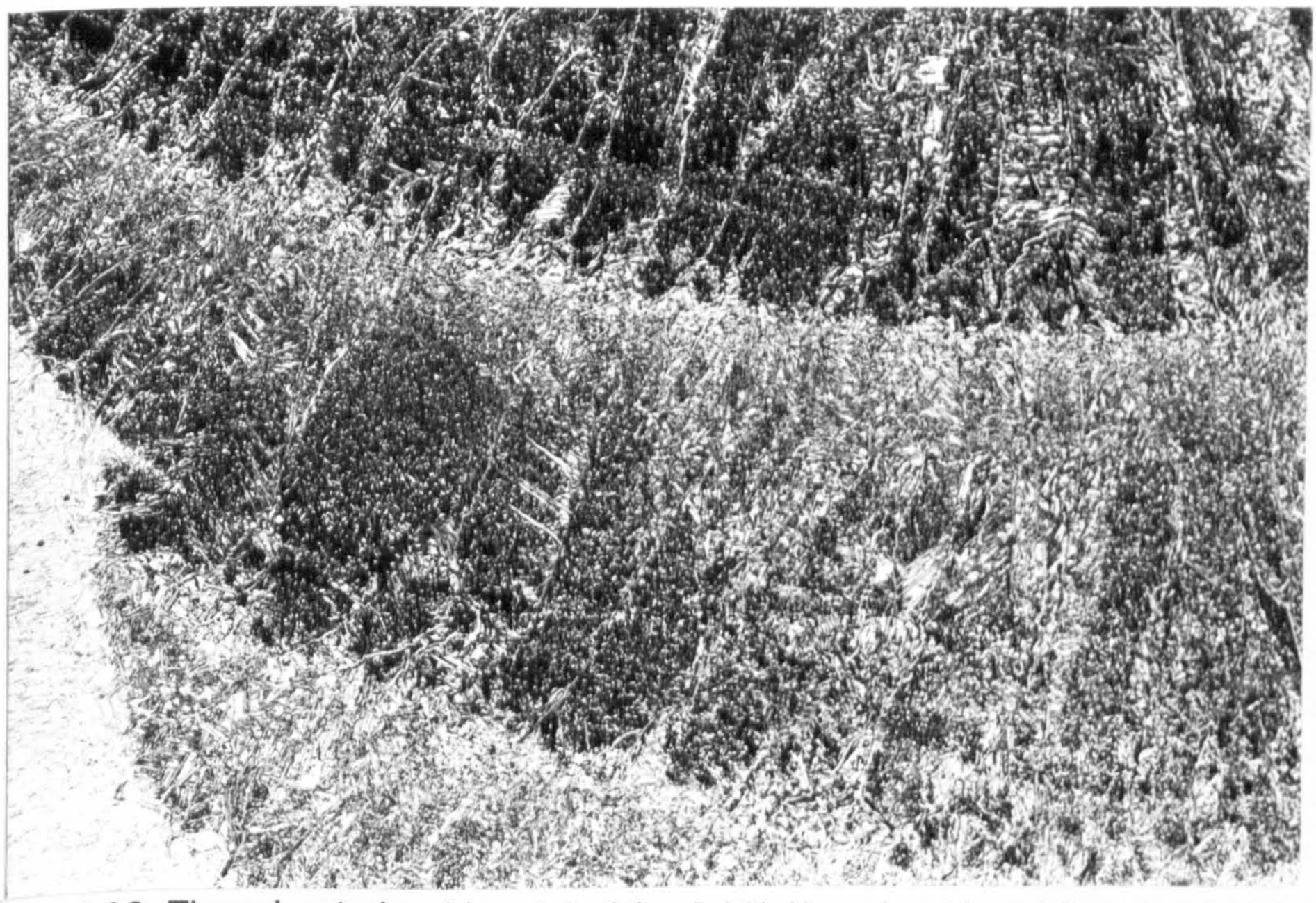

Figure 4.32: The reheated weld metal of the 0.66kJ/mm heat input Avesta 2205 joint welded at 32bars showing finer primary ferrite grains than in the joint welded at 1bar (x50).

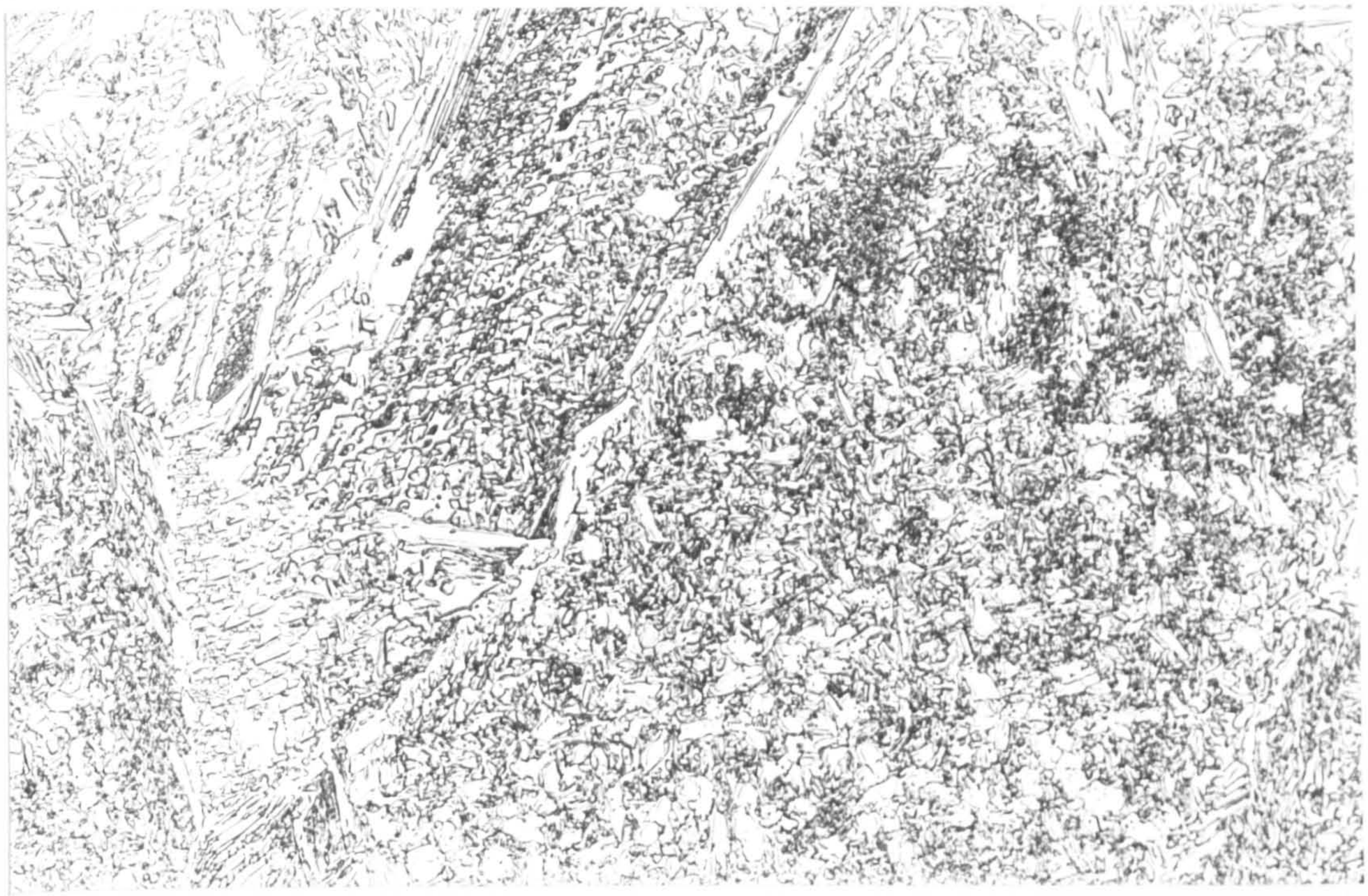

Figure 4.33: The predominantly fine grained acicular structure of the austenite in the reheated weld metal of the 0.66kJ/mm heat input Avesta 2205 joint welded at 32bars (x400).

Figure 4.34: Widmanstätten and acicular structure of the austenite in the cap weld metal of the 0.66kJ/mm heat input Avesta 2205 joint welded at 32bars (x400).

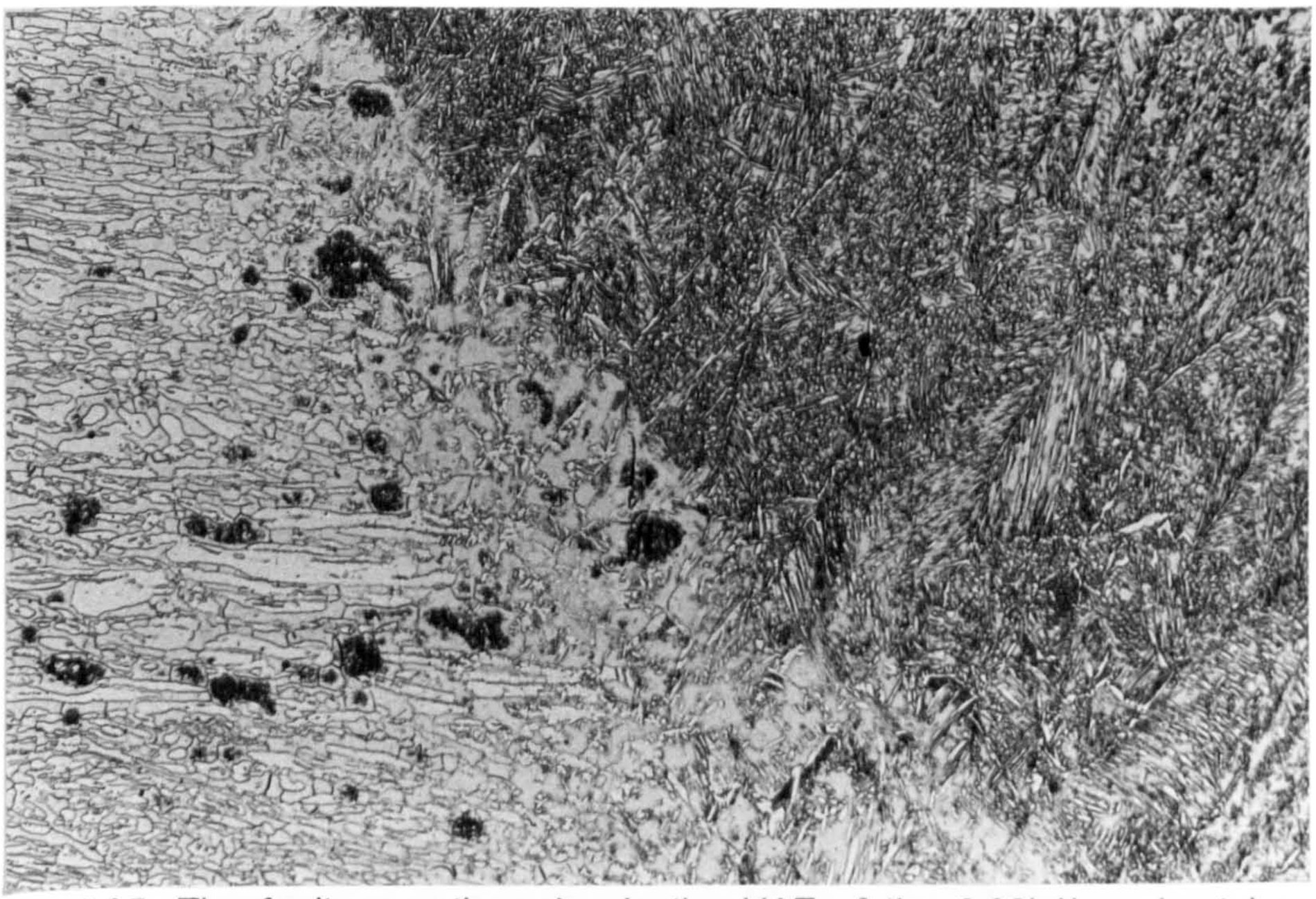

Figure 4.35: The ferrite growth region in the HAZ of the 0.66kJ/mm heat input Avesta 2205 joint welded at 32bars (x50).

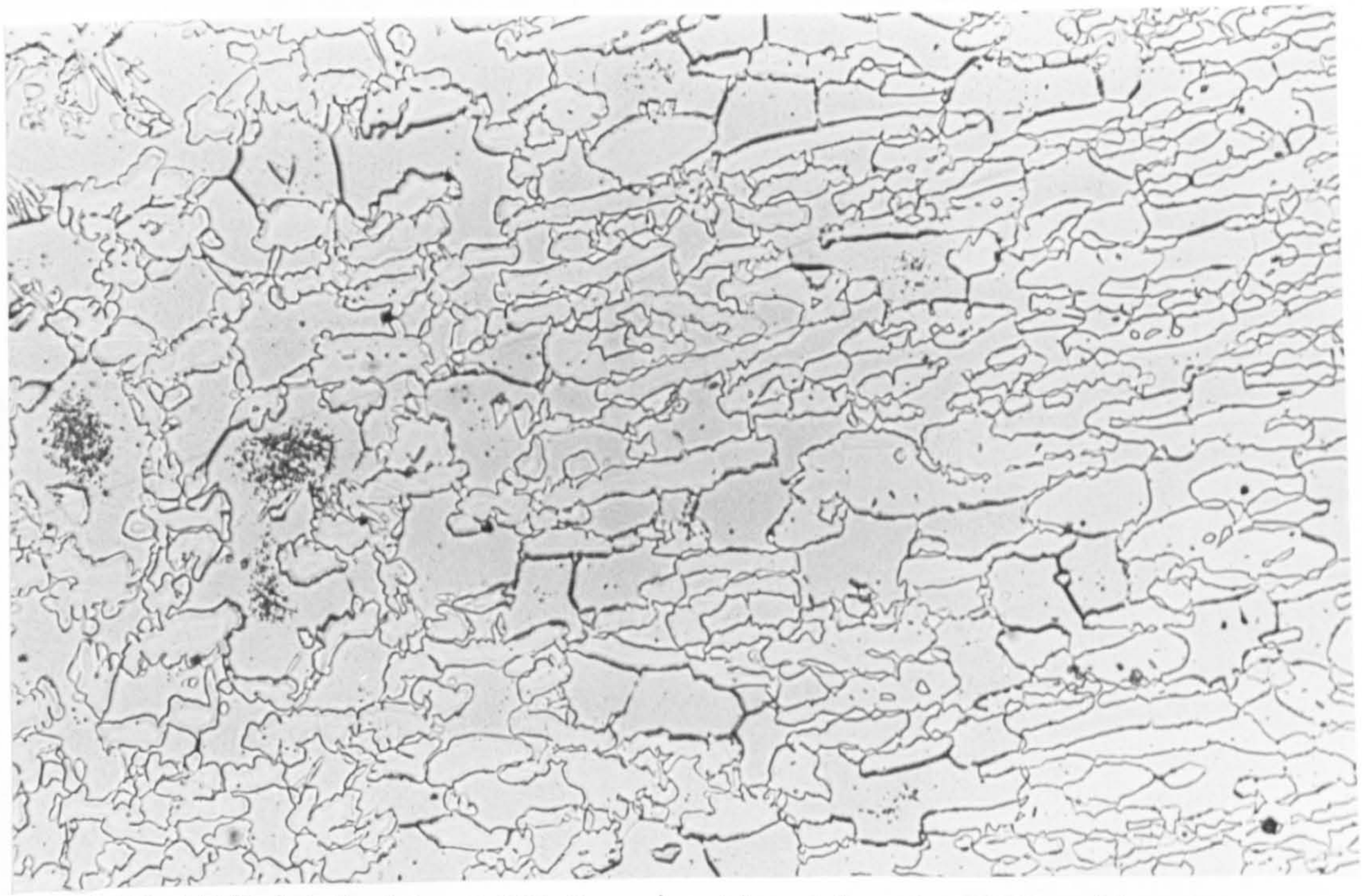

Figure 4.36: HAZ detail of the 0.66kJ/mm heat input Avesta 2205 weld performed at 32bars showing fewer precipitates than in the joint welded at 1bar (x400).

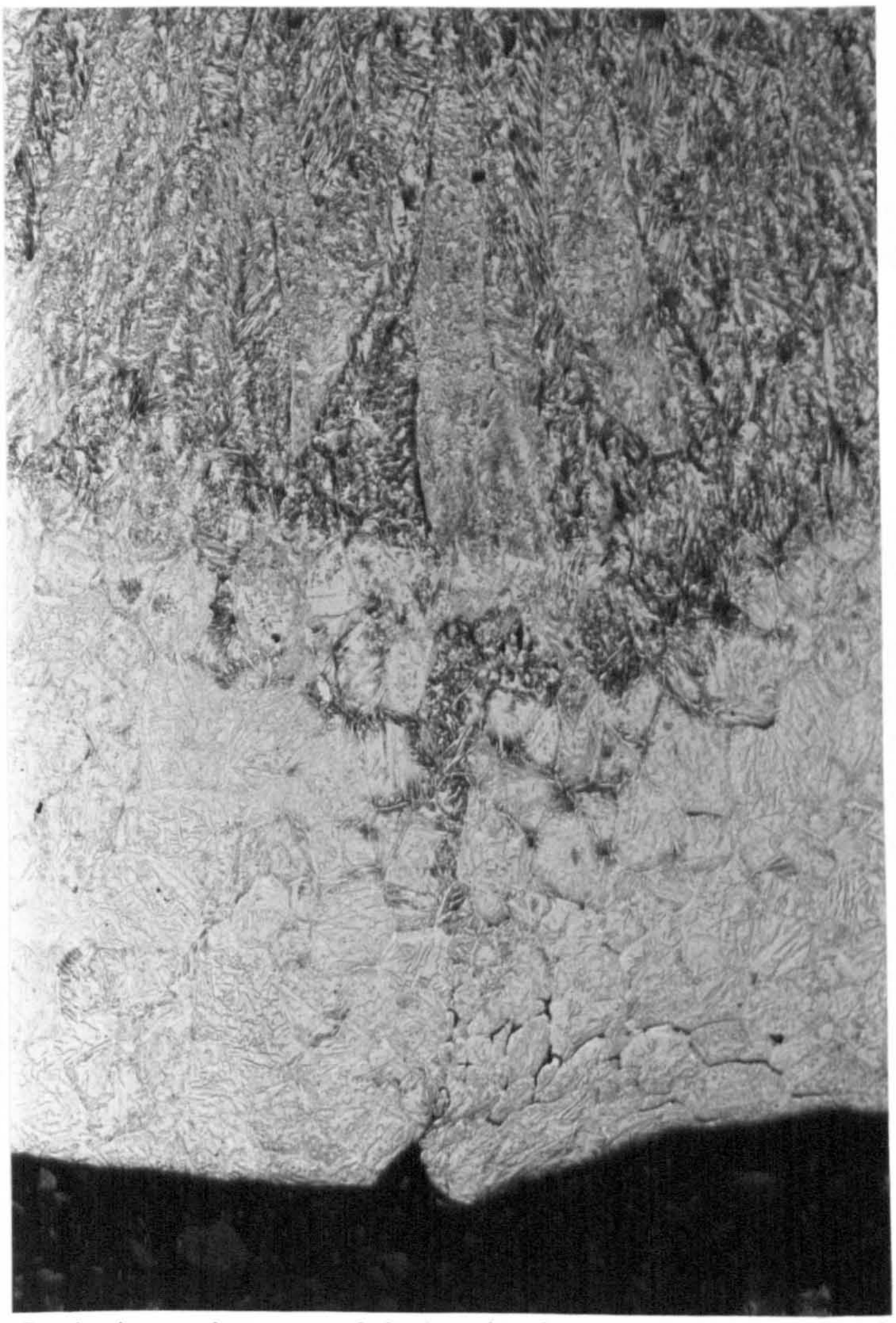

Figure 4.37: Grain boundary precipitates in the 1.30kJ/mm heat input root weld of the Avesta 2205 joint welded at 4bars (x50).

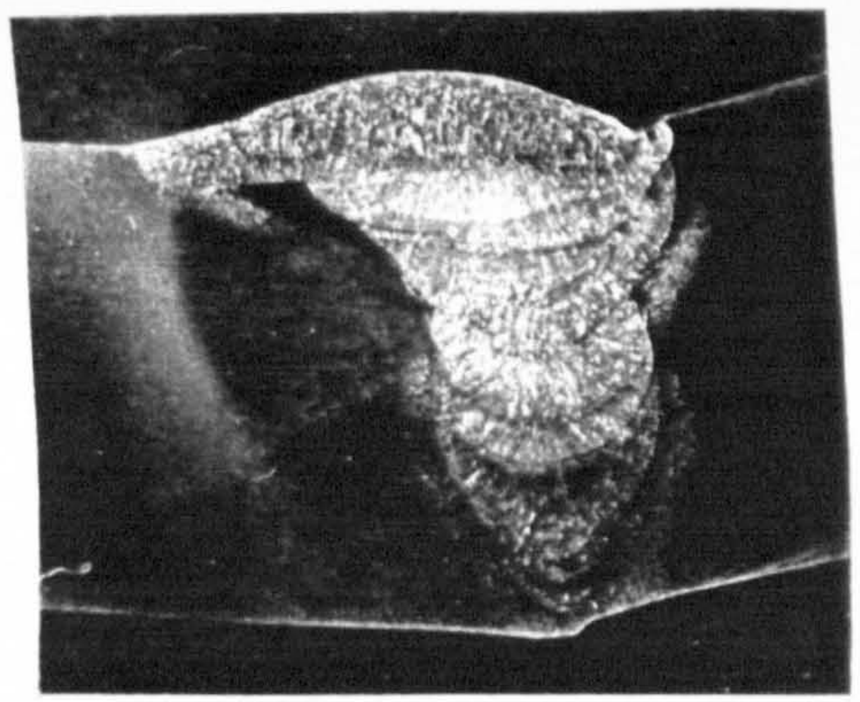

1bar

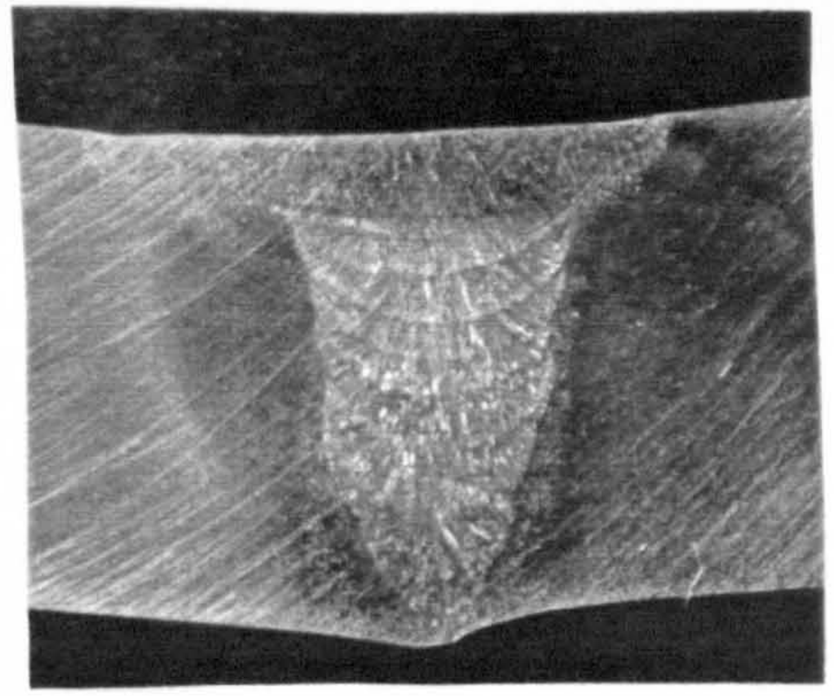

2bars

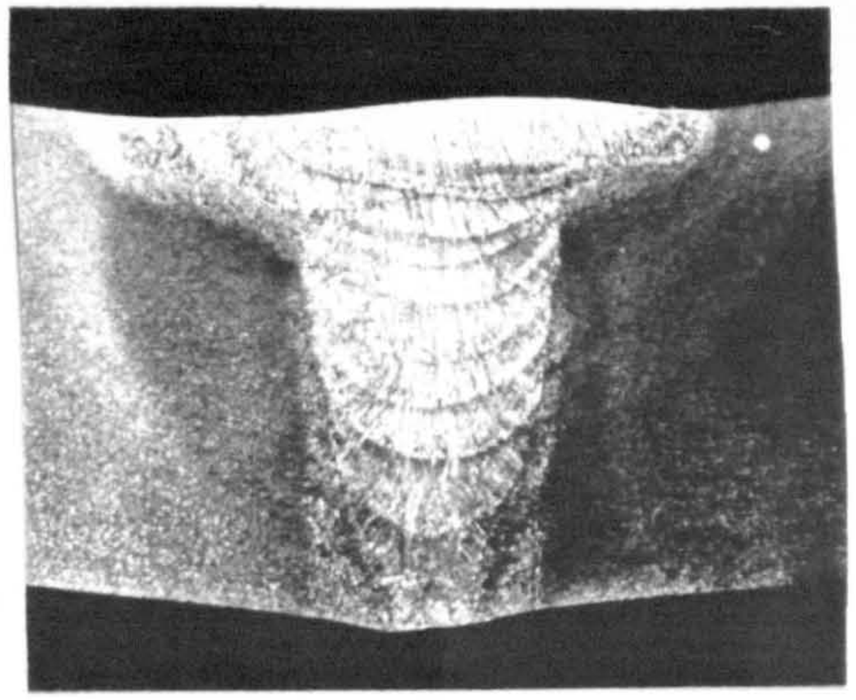

4bars

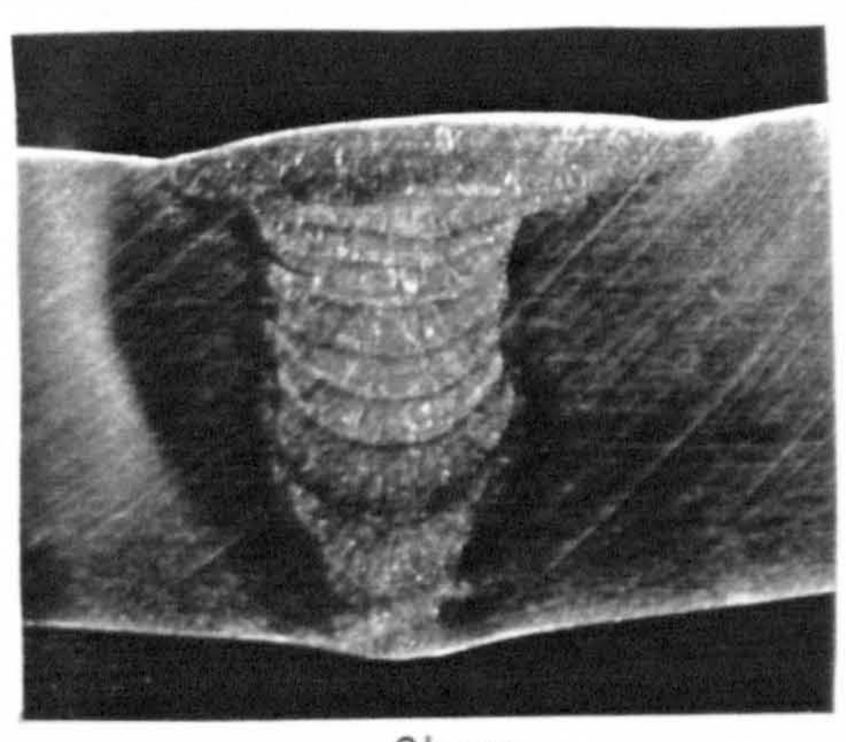

8bars

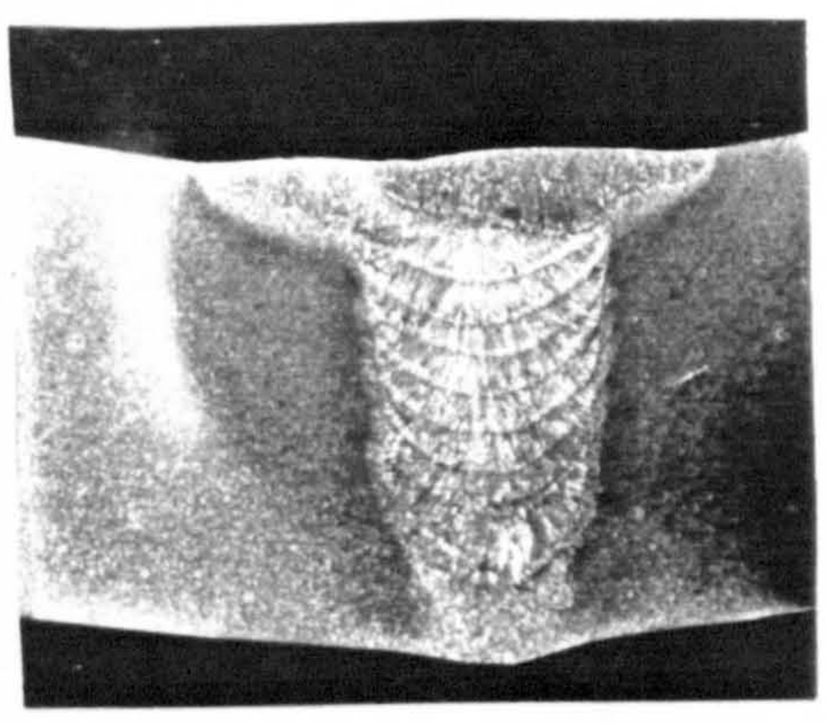

16bars

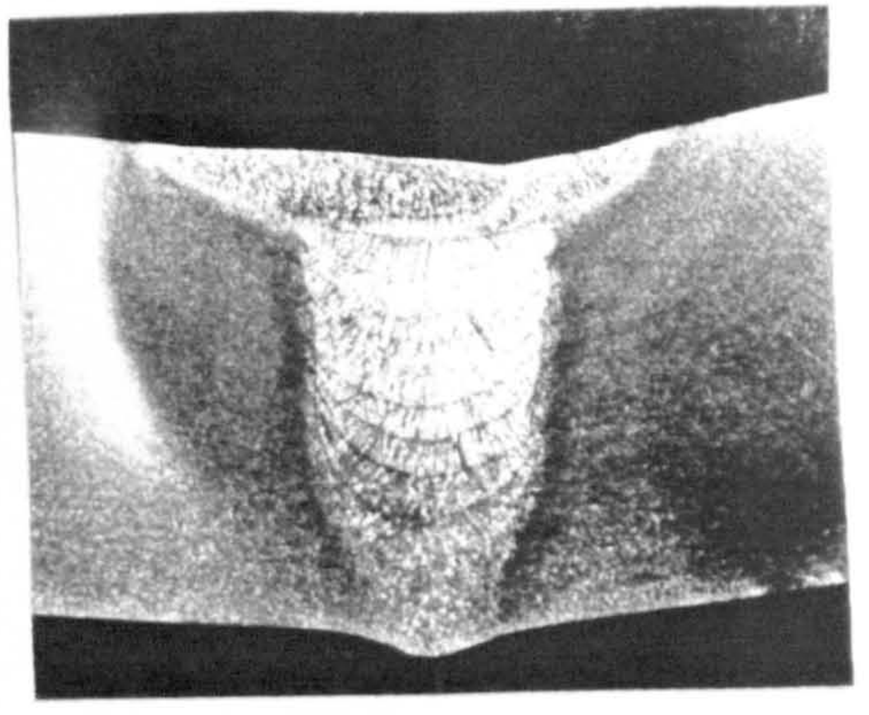

32bars

Figure 4.38: The profiles of the Sandvik SAF2507 joints welded at pressures up to 32 bars (x2.5).

Figure 4.39: Poor root penetration and large grained microstructure in the 1.50kJ/mm heat input root weld of the Sandvik SAF2507 joint welded at 1bar (x50).

Figure 4.40: Chromium nitride precipitates (dark contrast) in the 1.50kJ/mm root of the Sandvik SAF2507 joint welded at 1bar (x400).

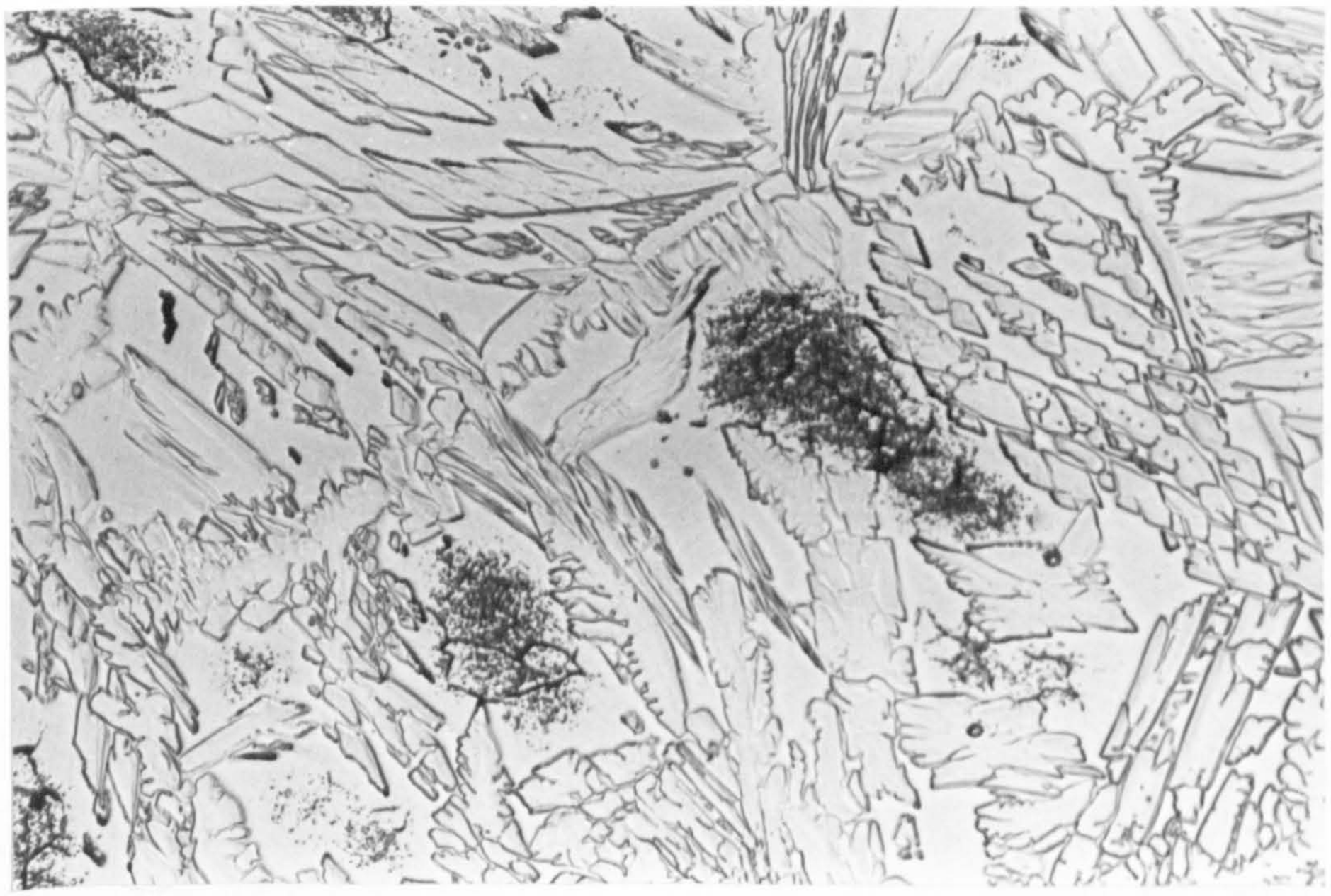

Figure 4.41: Chromium nitride precipitates (dark contrast) in the 1.50kJ/mm heat input root of the Sandvik SAF2507 joint welded at 1bar (x400).

Figure 4.42: Fine grained structure (black contrast) delineating the weld passes in the reheated weld metal of the 1.00 kJ/mm heat input Sandvik SAF2507 joint welded at 1bar (x50).

Figure 4.43: Austenite and chromium nitride precipitates (coloured black) in the reheated weld metal of the 1.00 kJ/mm heat input Sandvik SAF2507 joint welded at 1bar (x400).

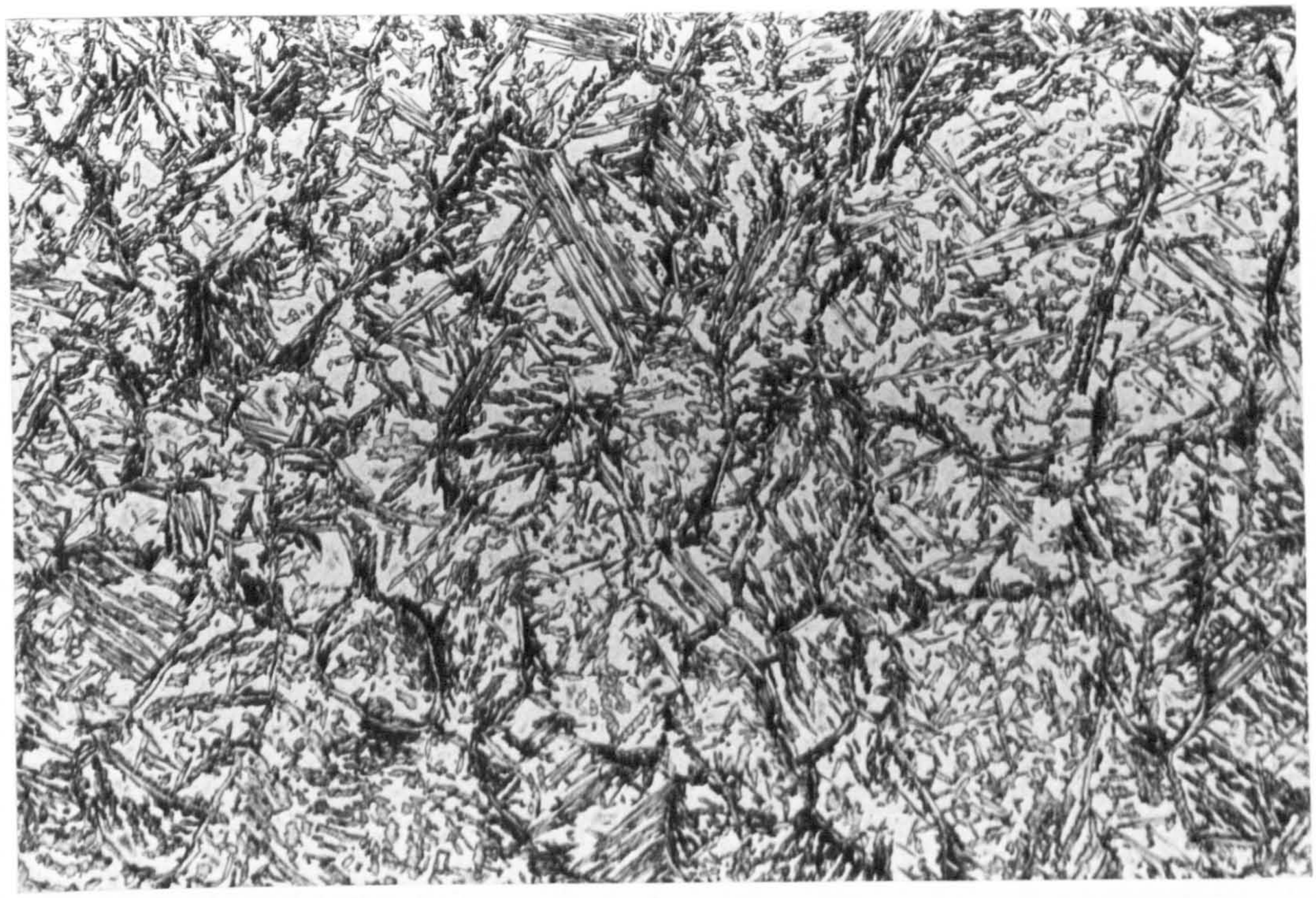

Figure 4.44: Sandvik 25.10.4L weld metal at the cap of the 1.00 kJ/mm heat input Sandvik SAF2507 joint welded at 1bar (x100).

Figure 4.45: Austenite formation in the cap weld metal of the 1.00 kJ/mm heat input Sandvik SAF2507 joint welded at 1bar (x400).

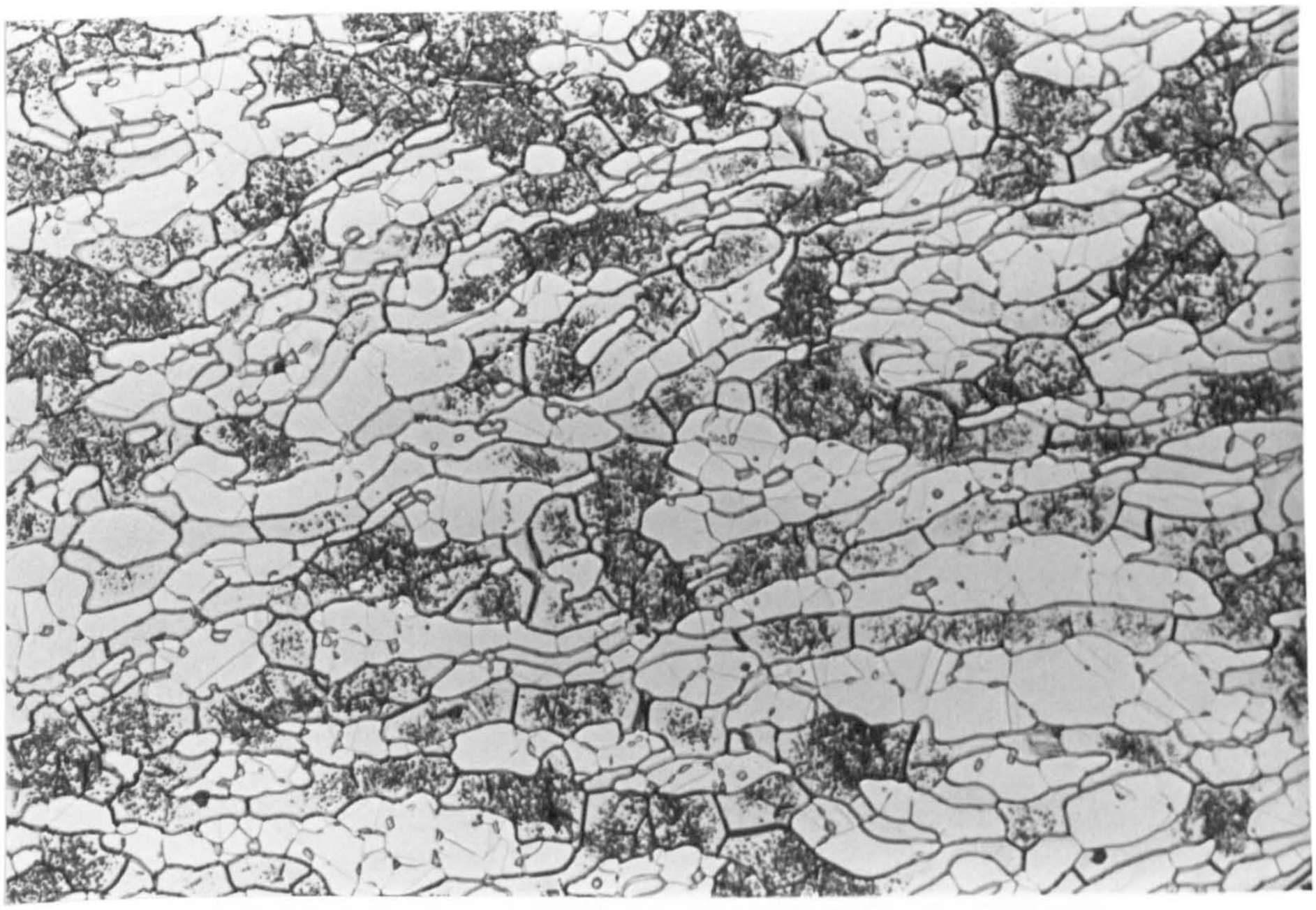

Figure 4.46: Significant chromium nitride precipitation in the HAZ of the 1.00 kJ/mm heat input Sandvik SAF2507 joint welded at 1bar (x400).

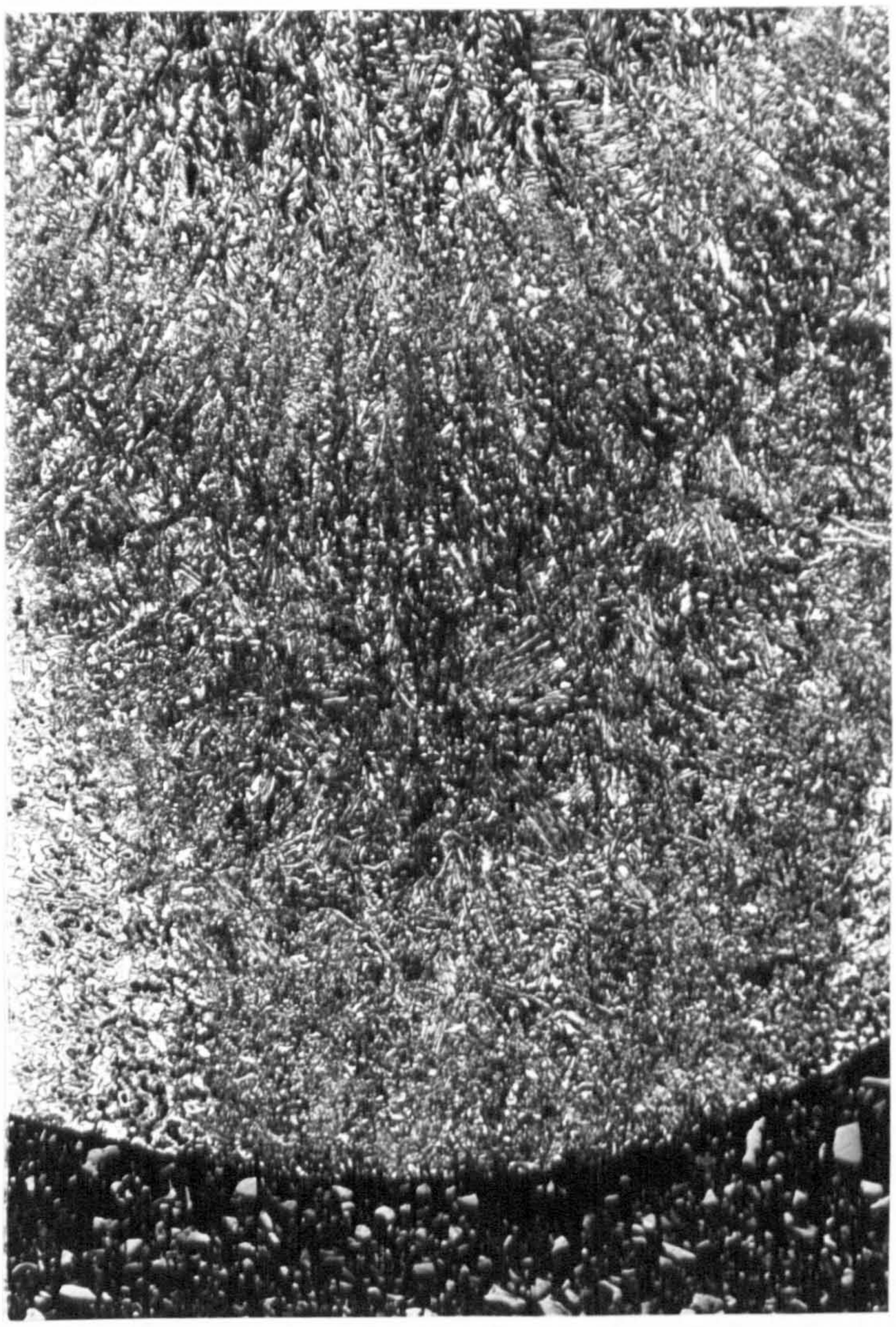

Figure 4.47: Complete penetration at the 0.34kJ/mm heat input root weld of the Sandvik SAF2507 joint welded at 32bars (x50).

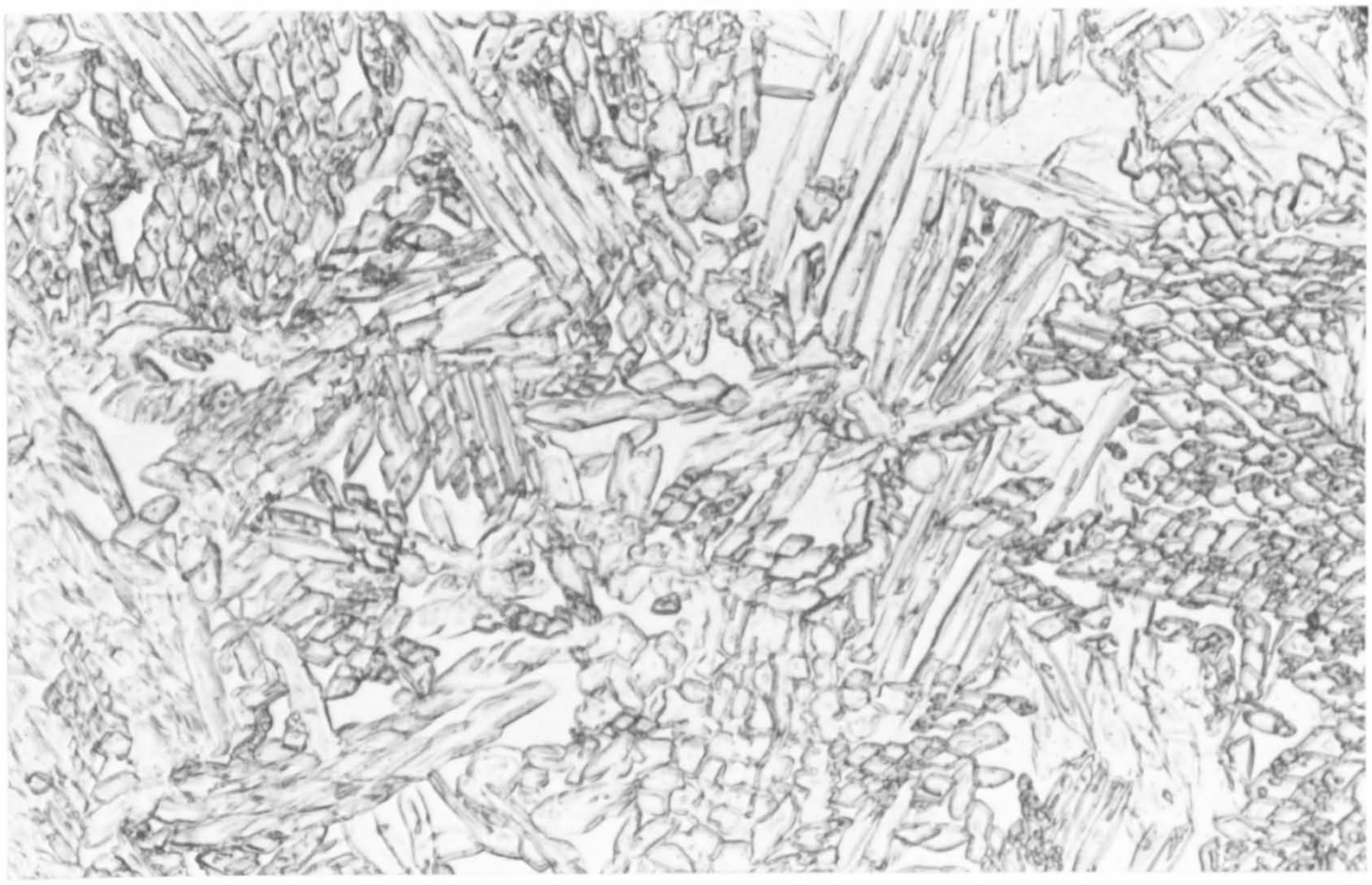

Figure 4.48: Fine grained microstructure free of defects in the 0.34kJ/mm heat input root weld of the Sandvik SAF2507 joint welded at 32bars (x400).

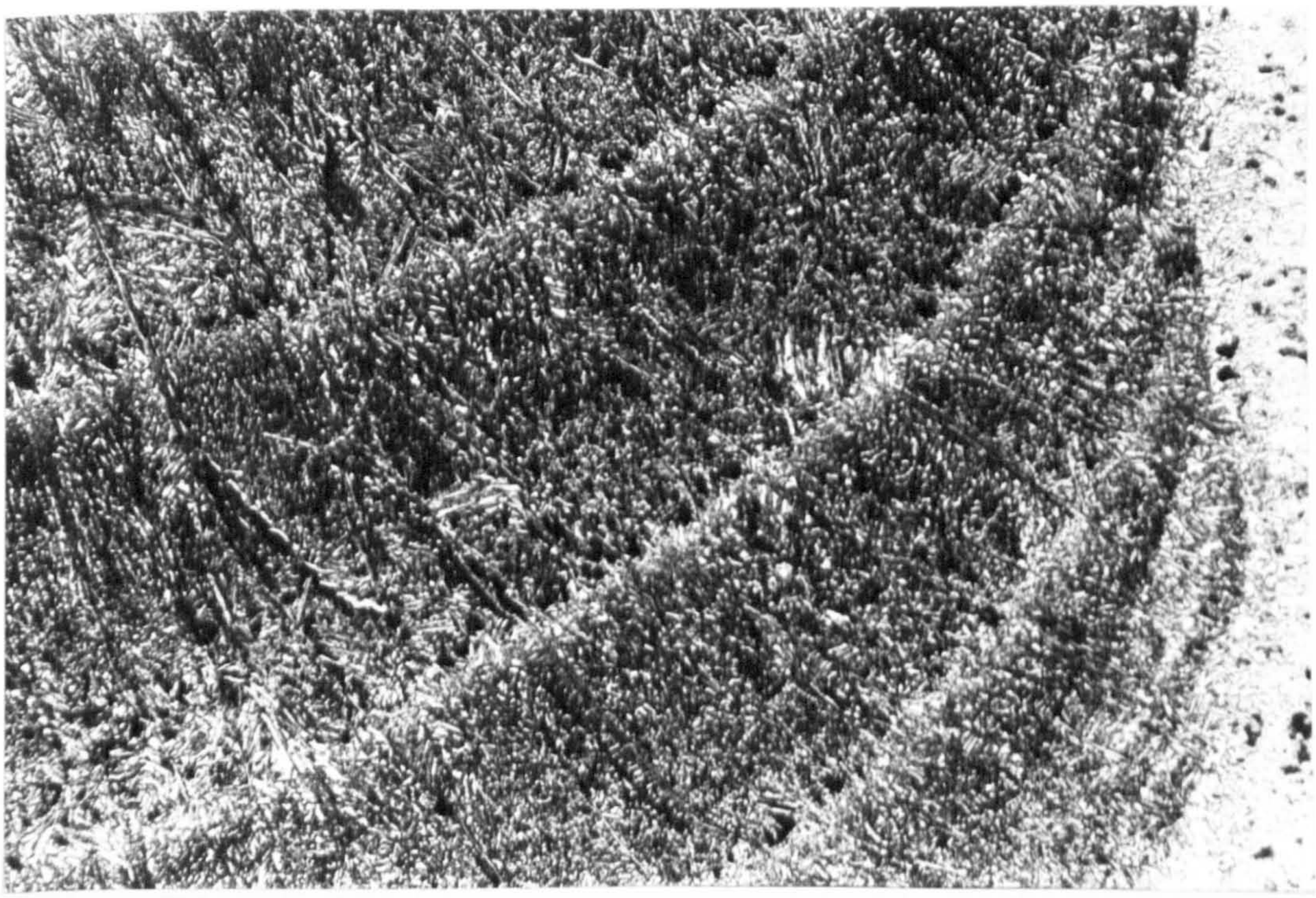

Figure 4.49: Weld passes delineated by the fine grained structure (black contrast) in the reheated weld metal of the 0.67kJ/mm heat input Sandvik SAF2507 joint welded at 32bars (x50).

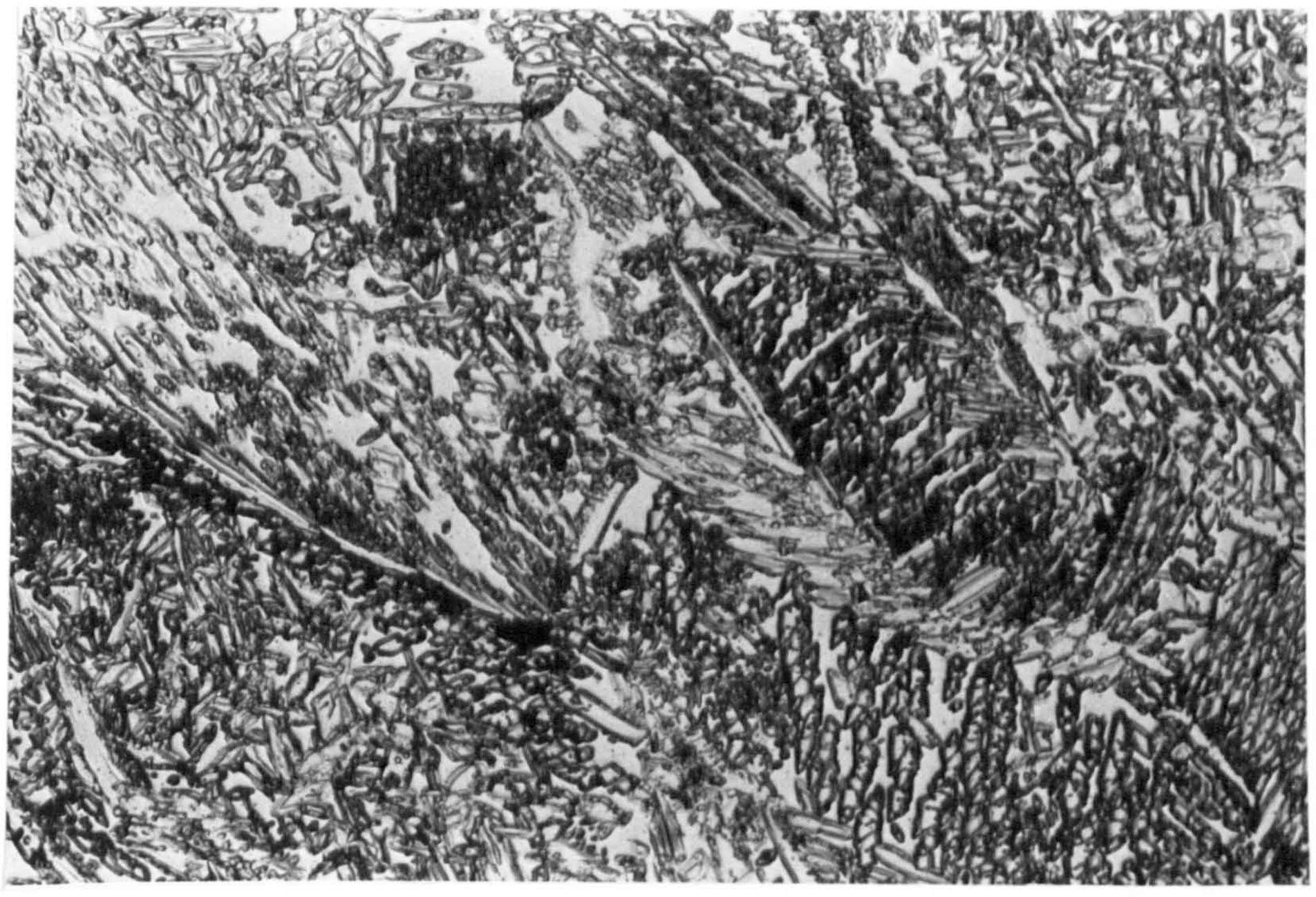

Figure 4.50: Fine austenite grains formed intragranularly in the reheated weld metal of the 0.67kJ/mm heat input Sandvik SAF2507 joint welded at 32bars (x400).

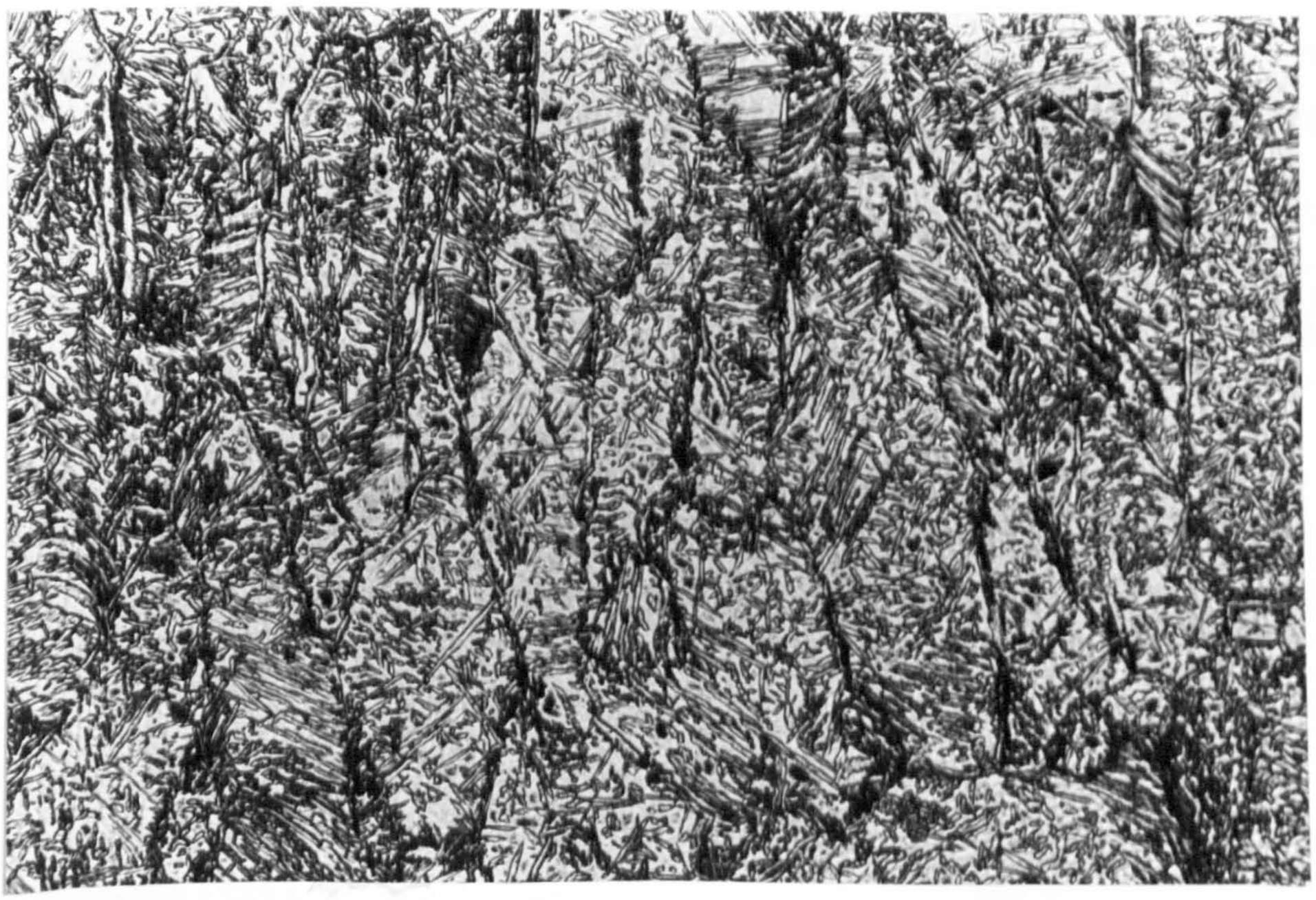

Figure 4.51: Sandvik 25.10.4L weld metal in the cap of the 0.67kJ/mm heat input Sandvik SAF2507 joint welded at 32bars (x100)

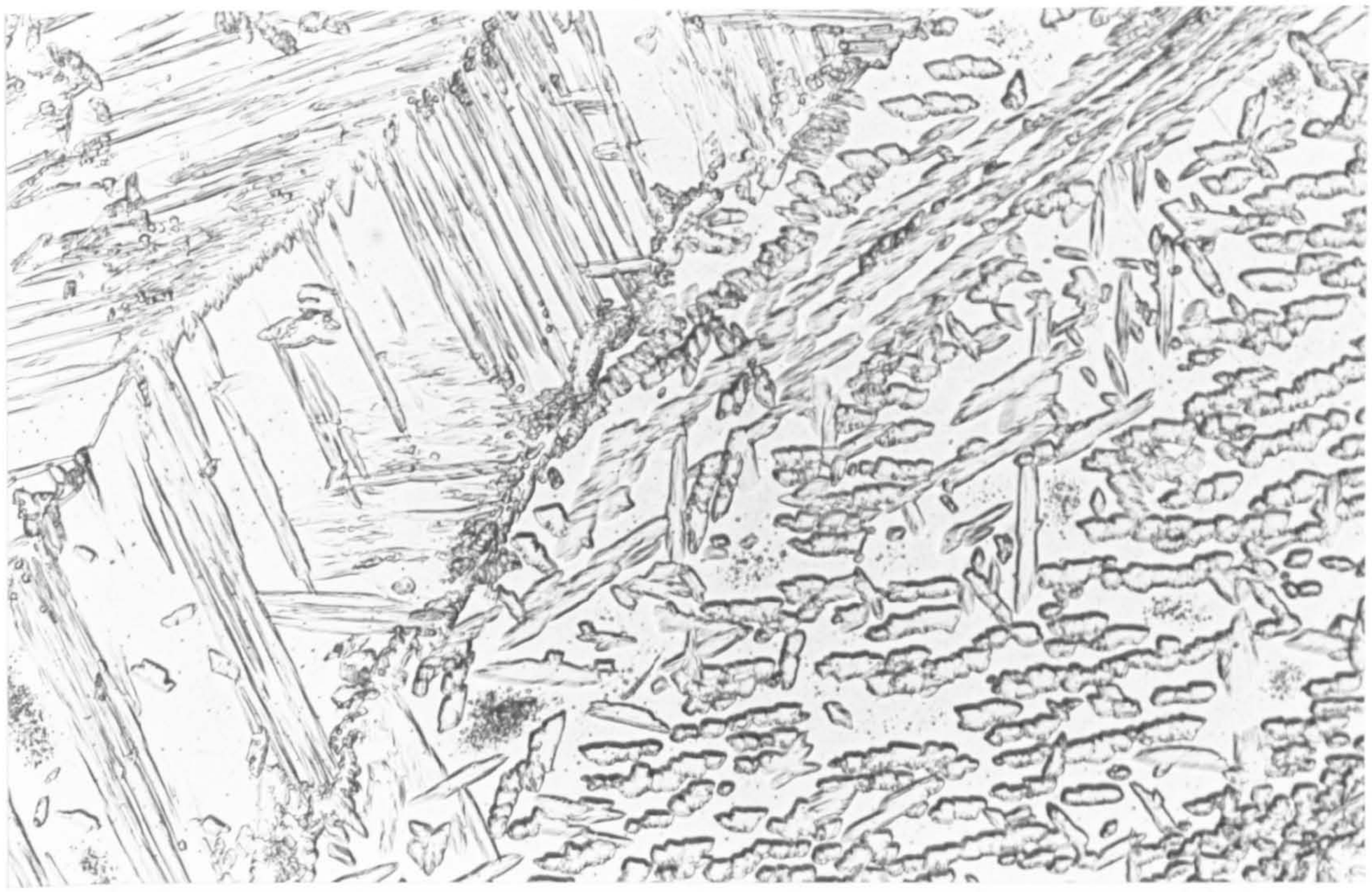

Figure 4.52: Austenite, both as Widmanstätten sideplates and fine grains in the cap of the 0.67kJ/mm heat input Sandvik SAF2507 joint welded at 32bars (x400).

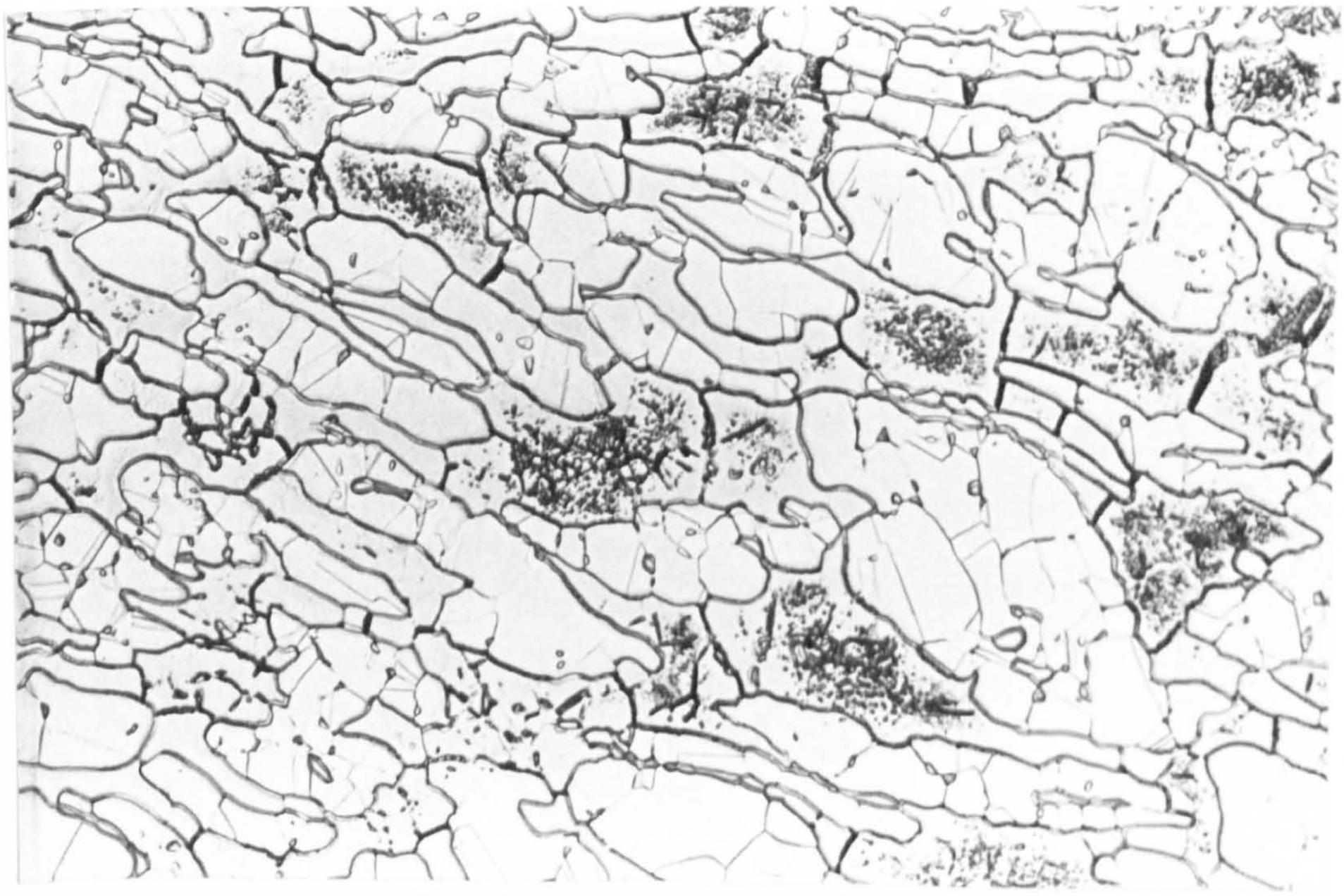

Figure 4.53: Chromium nitride precipitates in the HAZ of the 0.67kJ/mm heat input Sandvik SAF2507 joint welded at 32bars, despite a faster cooling rate (x400).

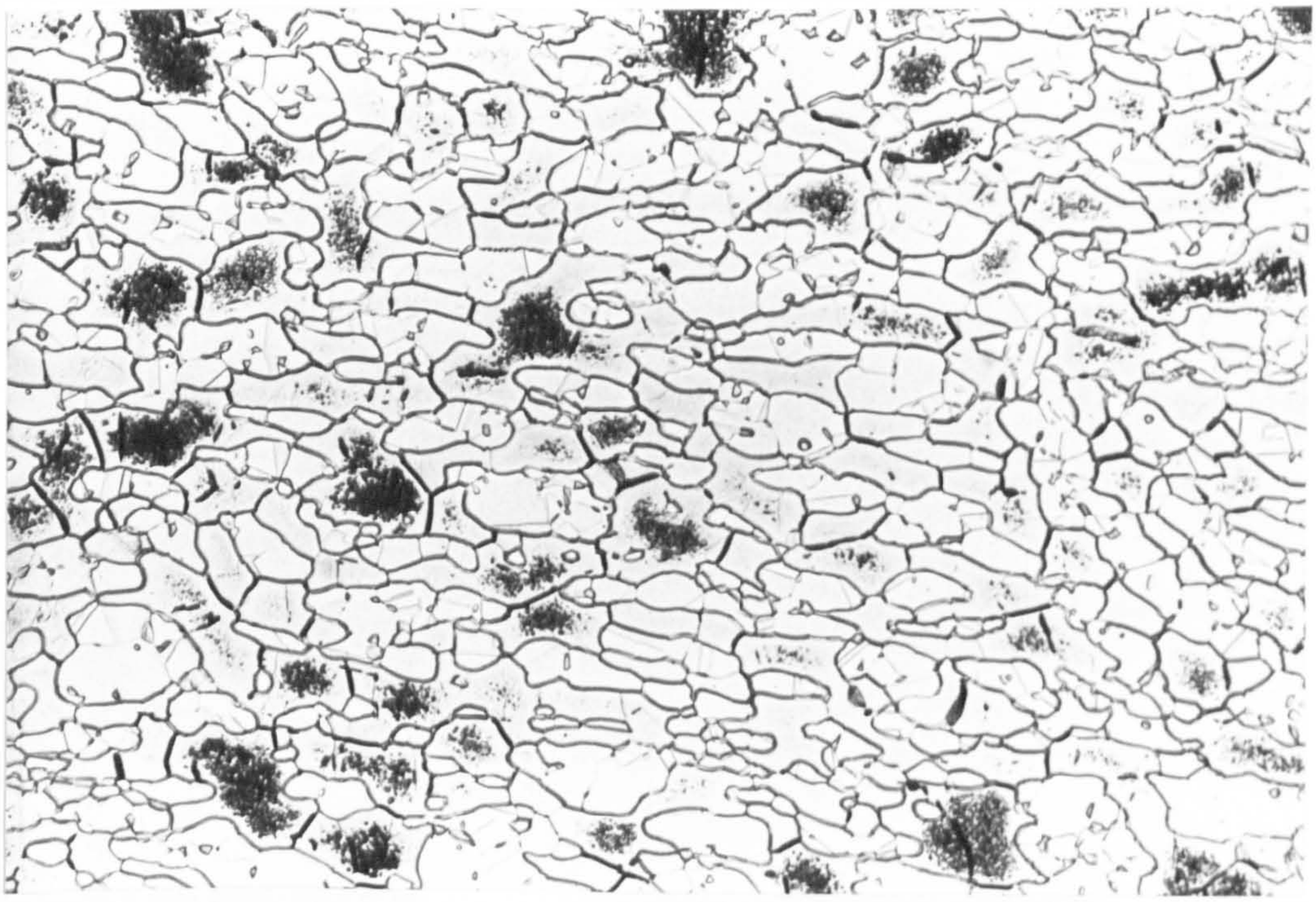

Figure 4.54: Chromium nitride precipitates in the HAZ around the cap of the 0.75kJ/mm heat input Sandvik SAF2507 joint welded at 16bars (x400).

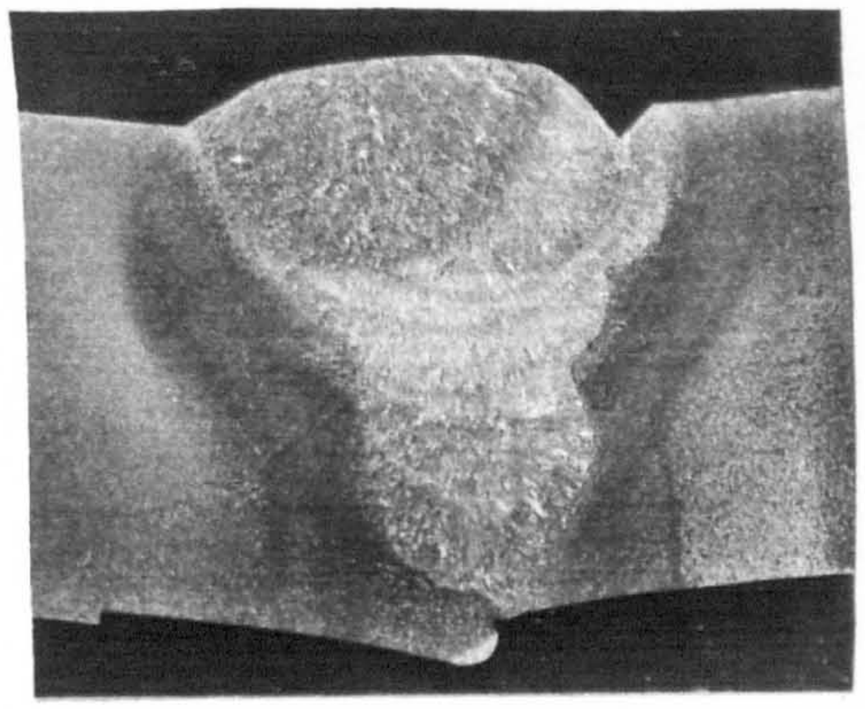

1bar

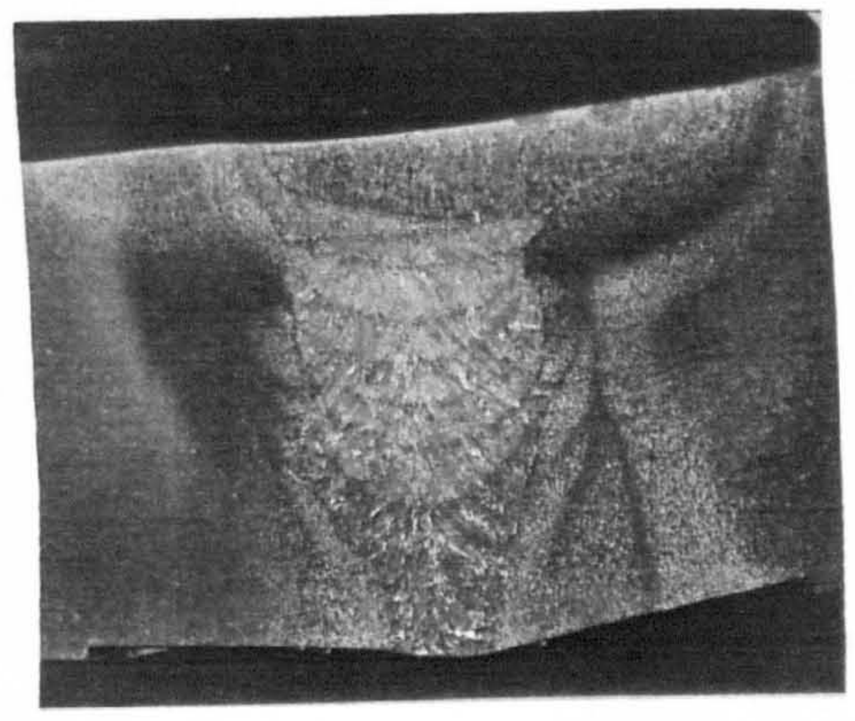

2bars

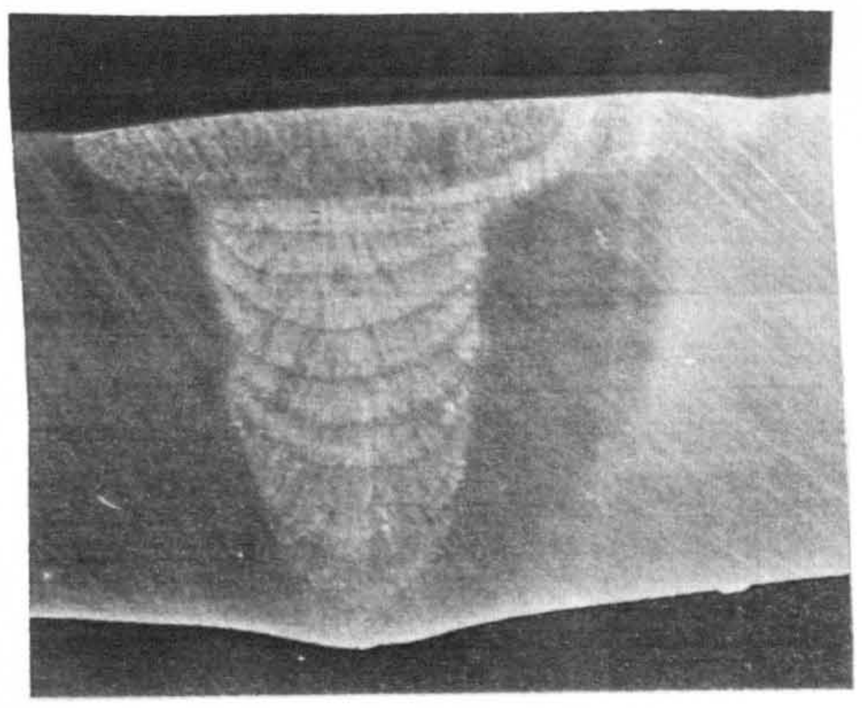

4bars

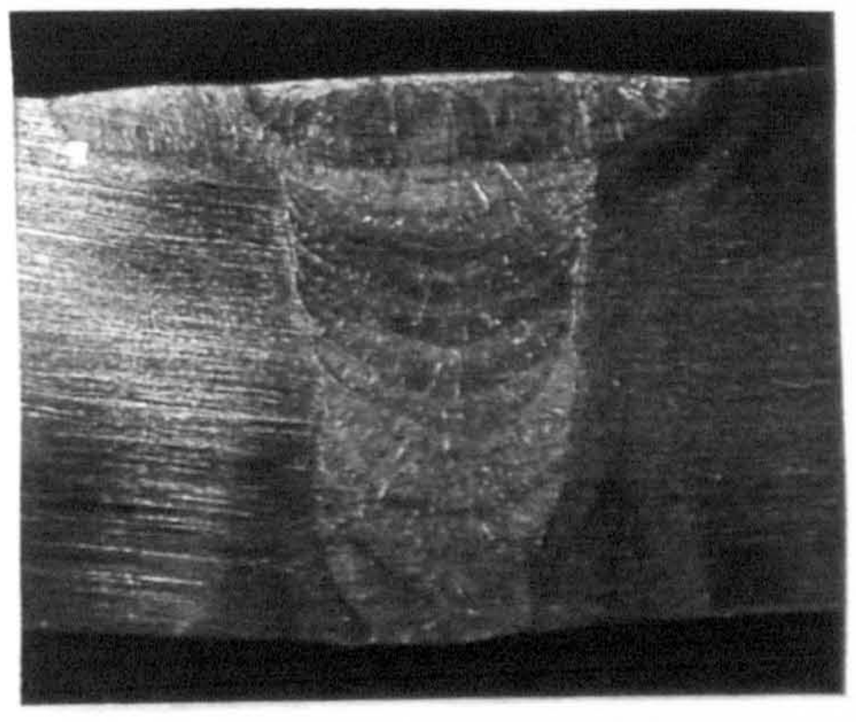

8bars

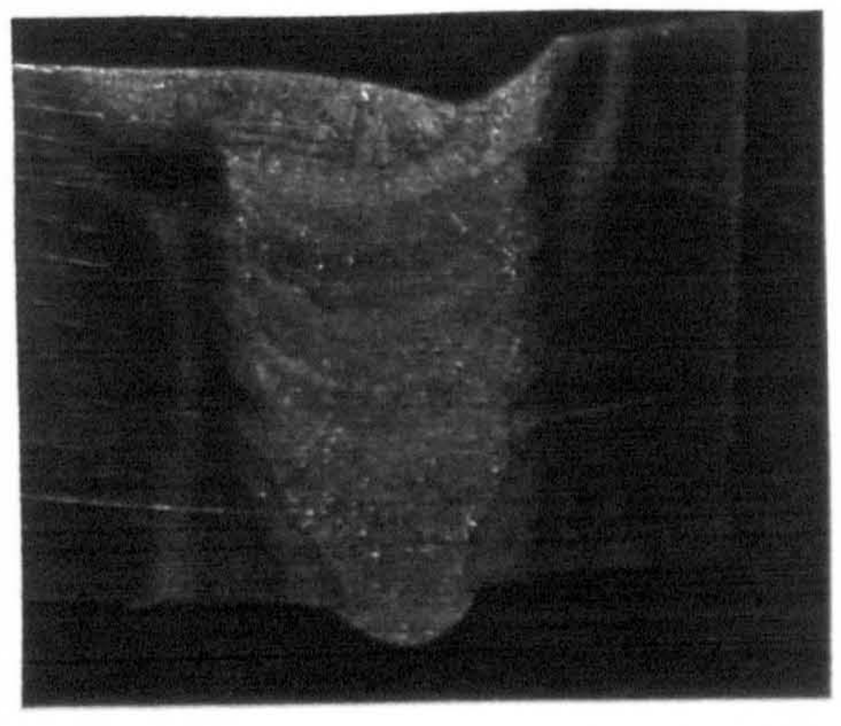

16bars

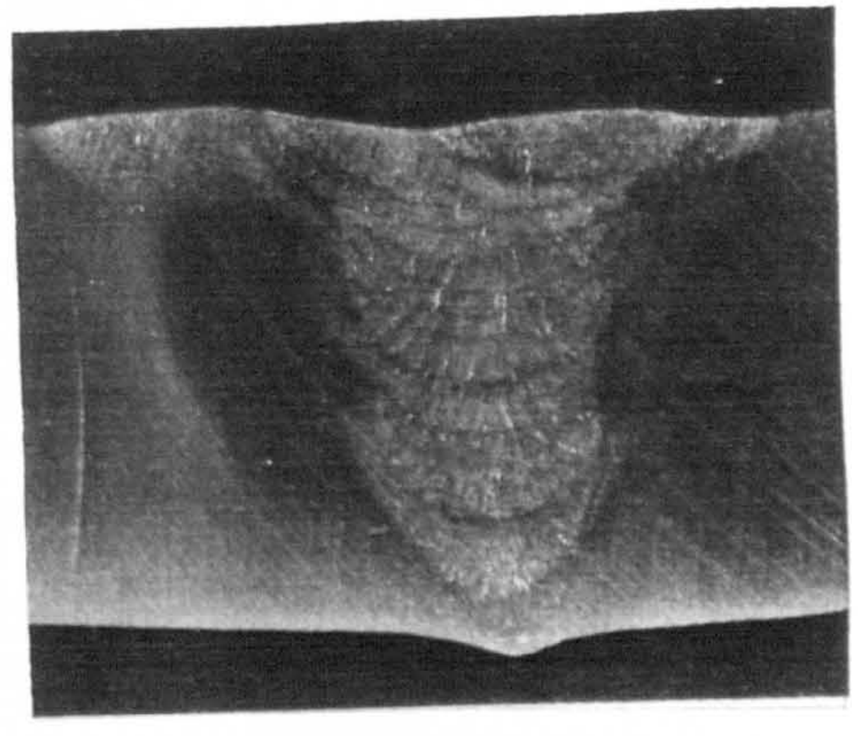

32bars

Figure 4.55: The profiles of the Zeron 100 joints welded at pressures up to 32 bars (x2.5).

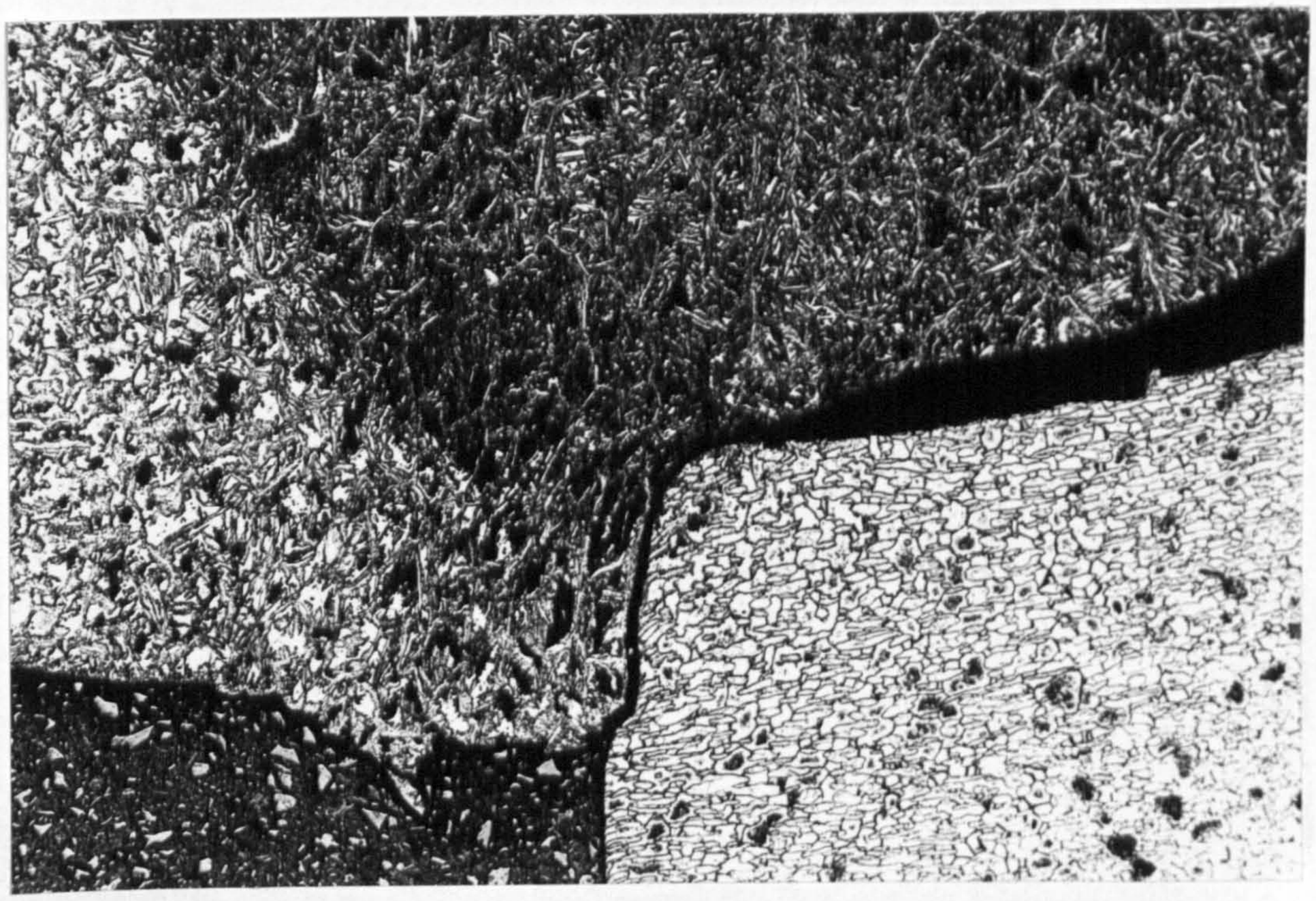

Figure 4.56: Poor joint fit up and lack of fusion in the 1.32kJ/mm heat input root weld of the Zeron 100 joint welded at 1bar (x50).

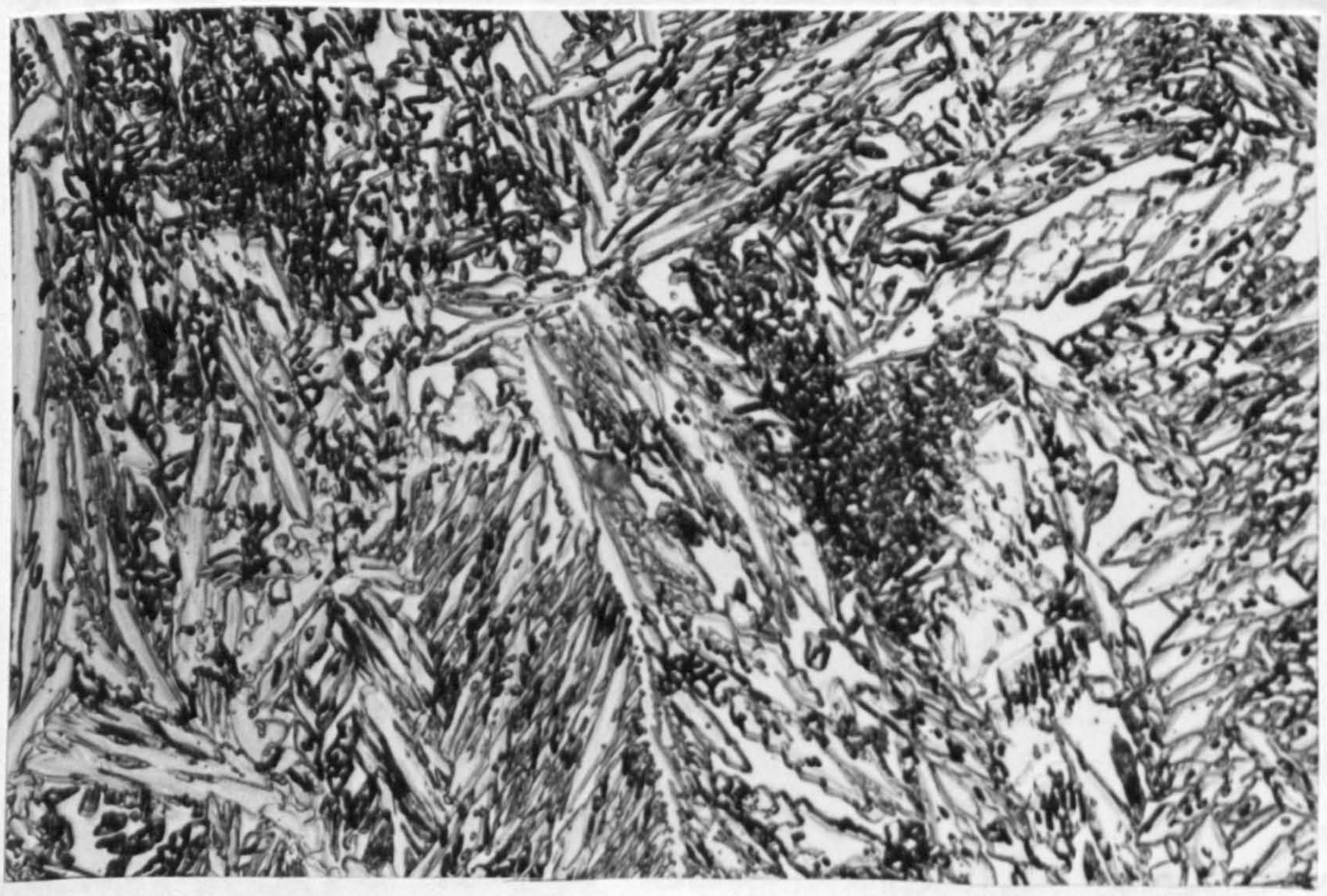

Figure 4.57: Widmanstätten and acicular austenite in the 1.32kJ/mm heat input root weld of the Zeron 100 joint welded at 1bar (x400).

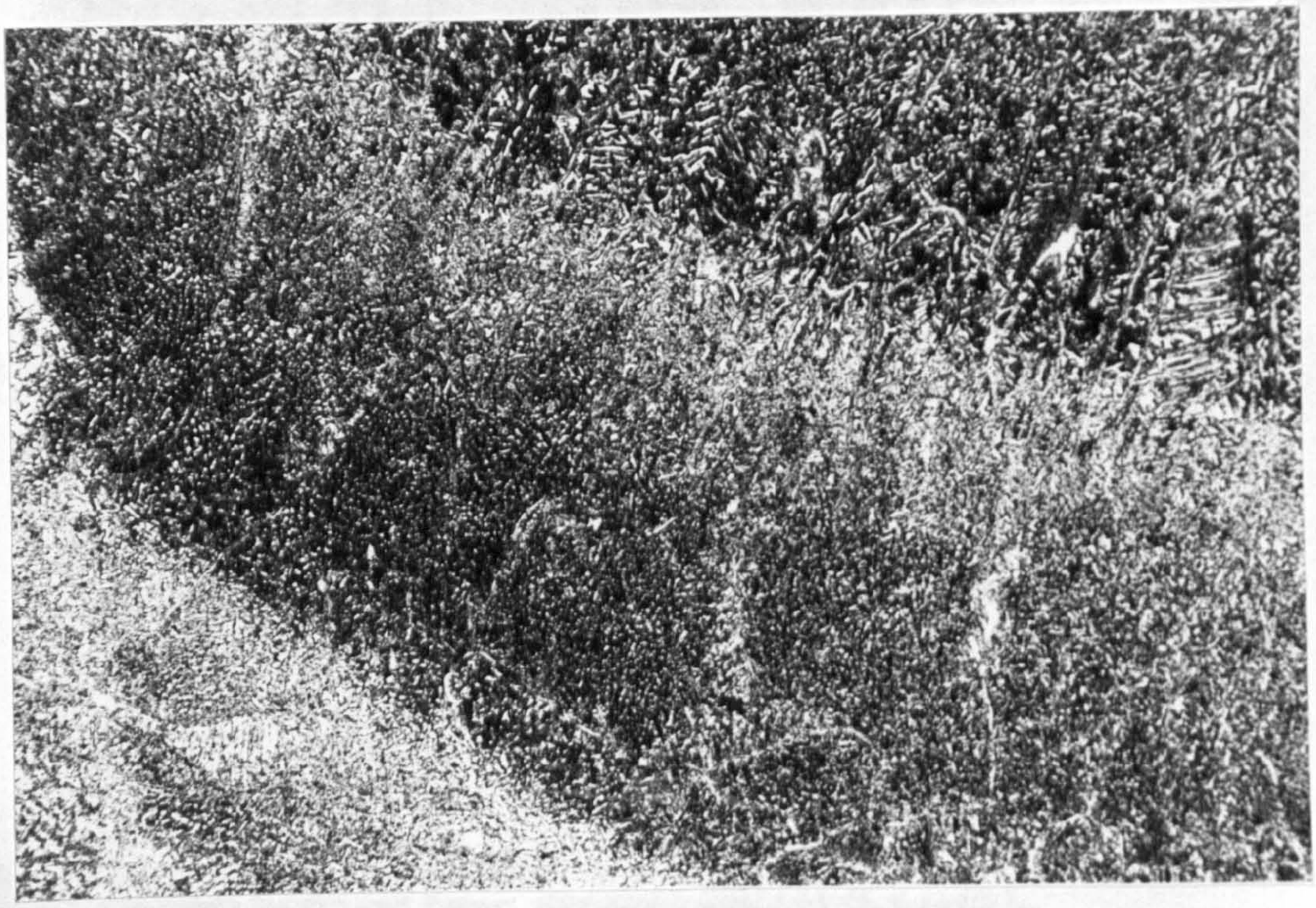

Figure 4.58: Fine grained austenite (dark contrast) and ferrite (light contrast) delineating the weld passes in the reheated weld metal of the 1.02kJ/mm heat input Zeron 100 joint welded at 1bar (x50).

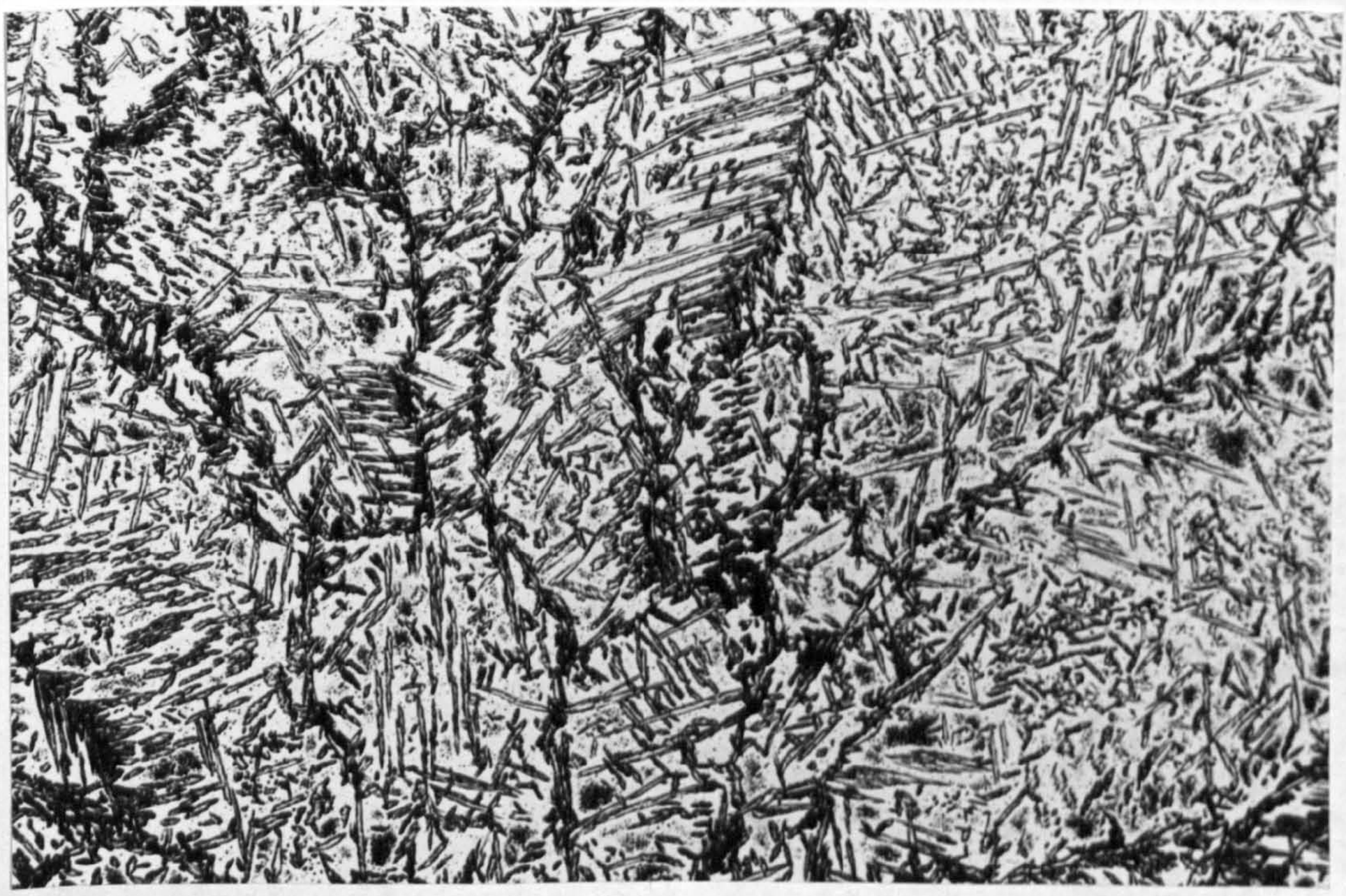

Figure 4.59: Austenite formation predominantly at the primary ferrite grain boundaries in the cap weld metal of the 1.02kJ/mm heat input Zeron 100 joint welded at 1bar (x100).

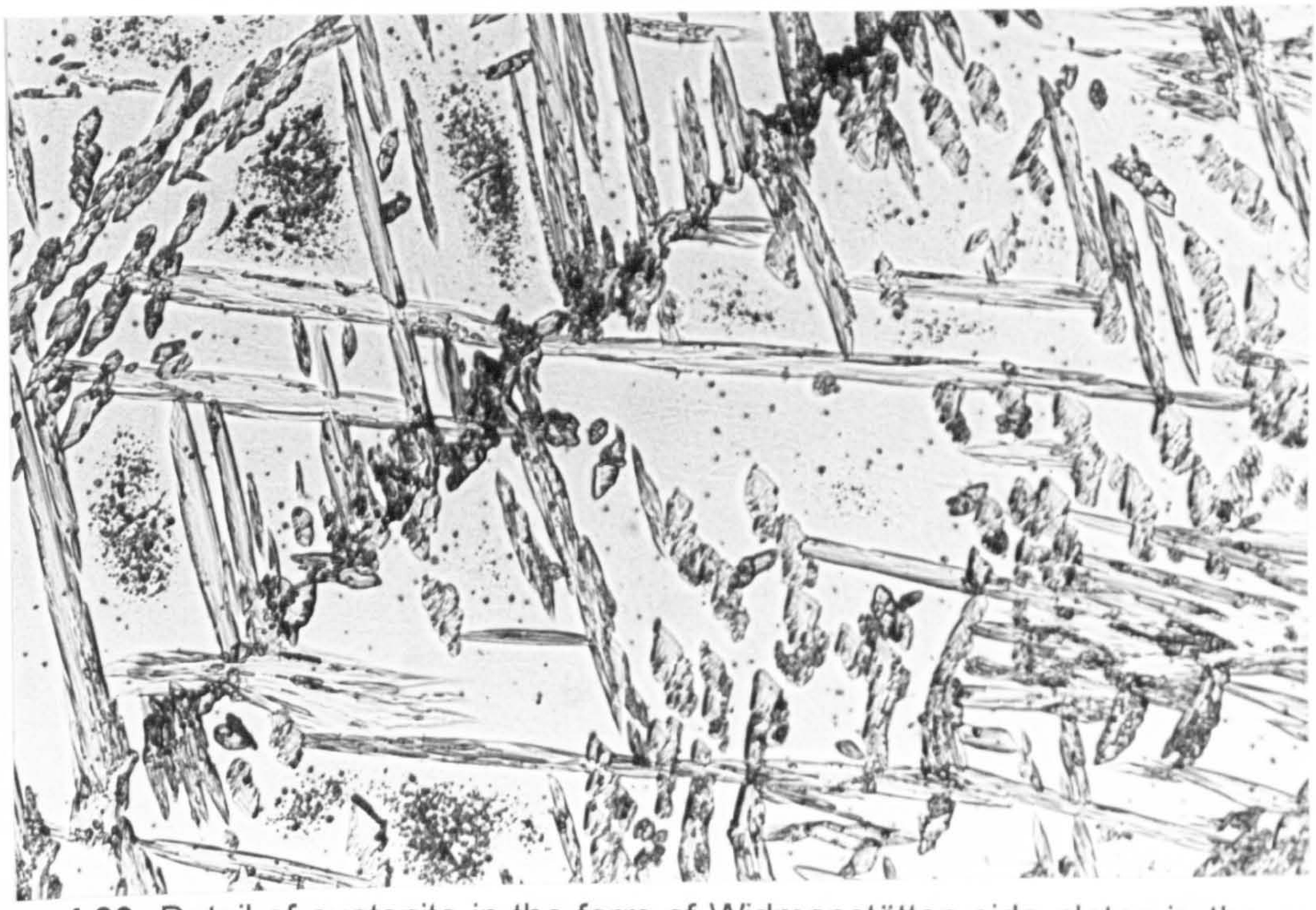

Figure 4.60: Detail of austenite in the form of Widmanstätten side plates in the cap of the 1.02kJ/mm heat input Zeron 100 joint welded at 1bar (x400).

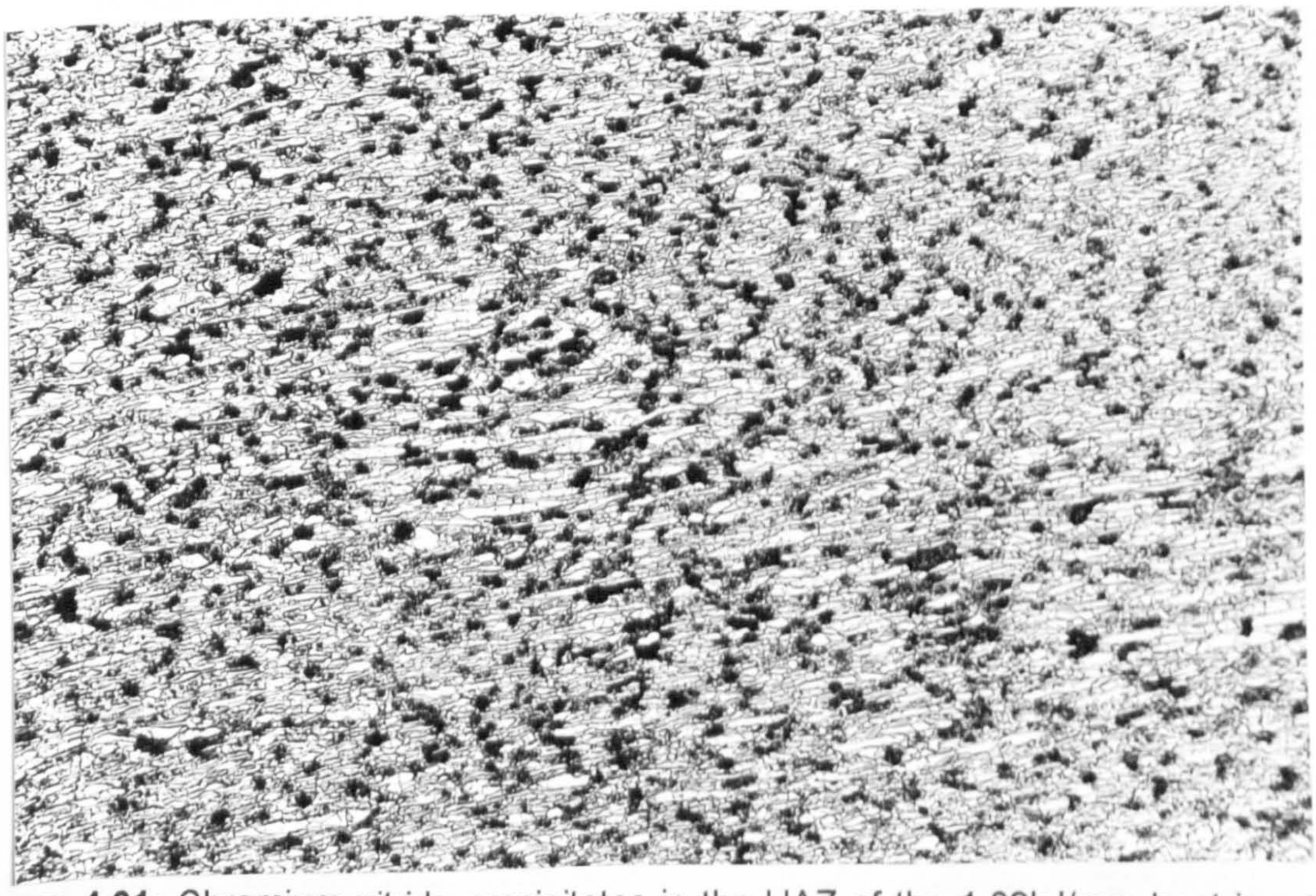

Figure 4.61: Chromium nitride precipitates in the HAZ of the 1.02kJ/mm heat input Zeron 100 joint welded at 1bar (x50).

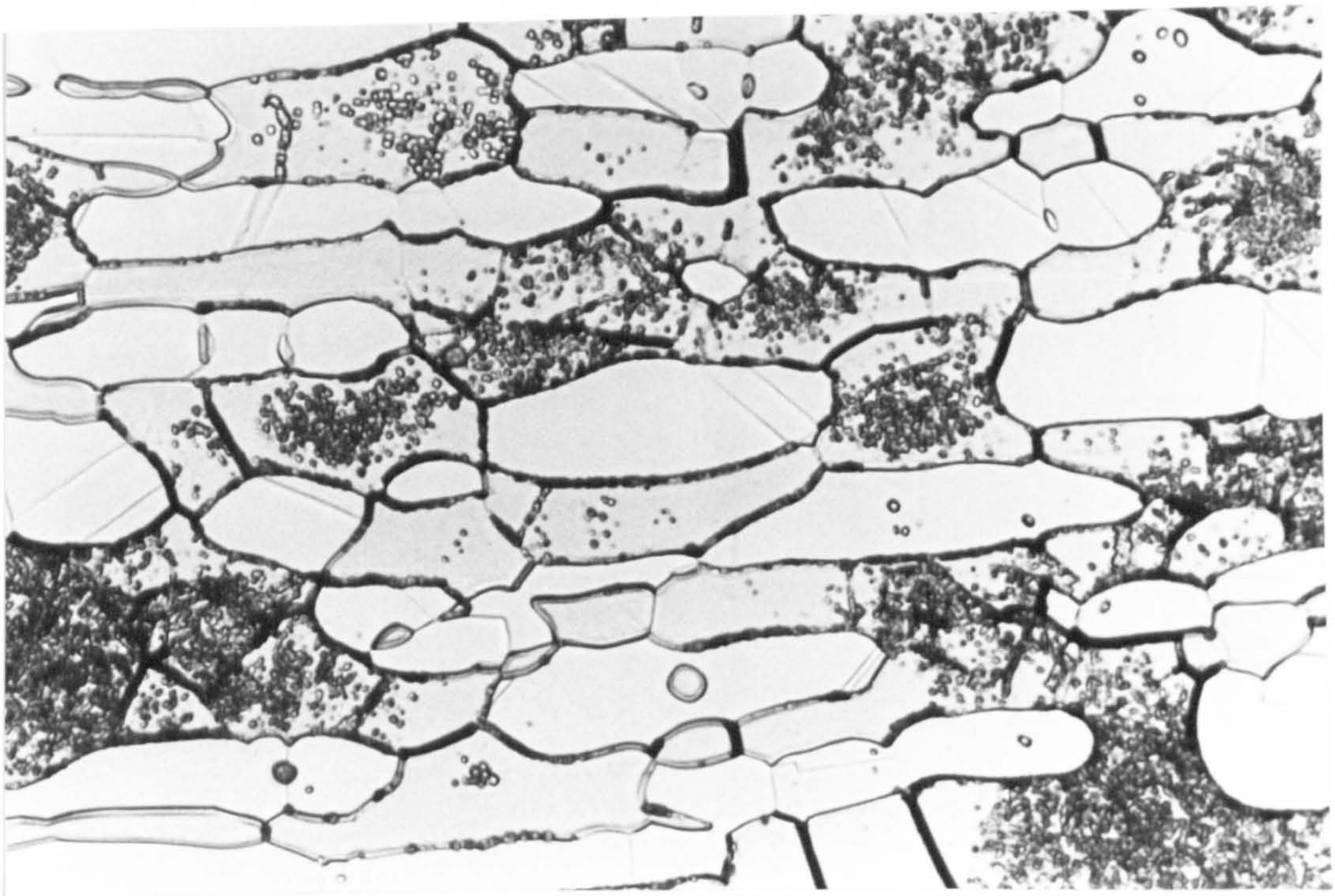

Figure 4.62: Chromium nitride precipitates and evidence of sigma phase formation at the grain boundaries in the HAZ of the 1.02kJ/mm heat input Zeron 100 joint welded at 1bar (x800).

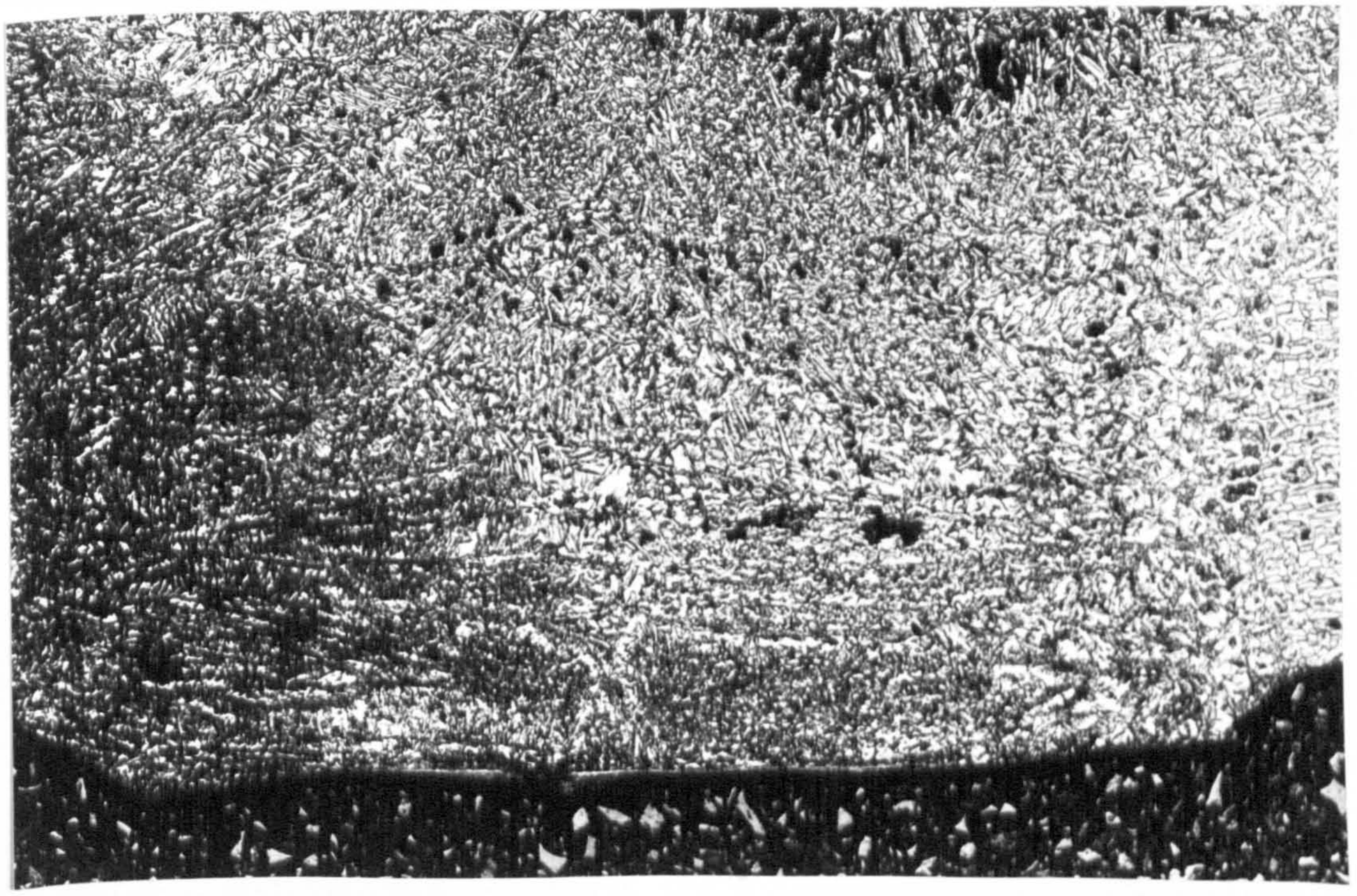

Figure 4.63: Complete penetration in the 0.27kJ/mm heat input root weld of the Zeron 100 joint welded at 32bars (x50).

Figure 4.64: Fine austenite grains within a ferrite matrix in the 0.27kJ/mm heat input root weld of the Zeron 100 joint welded at 32bars (x400).

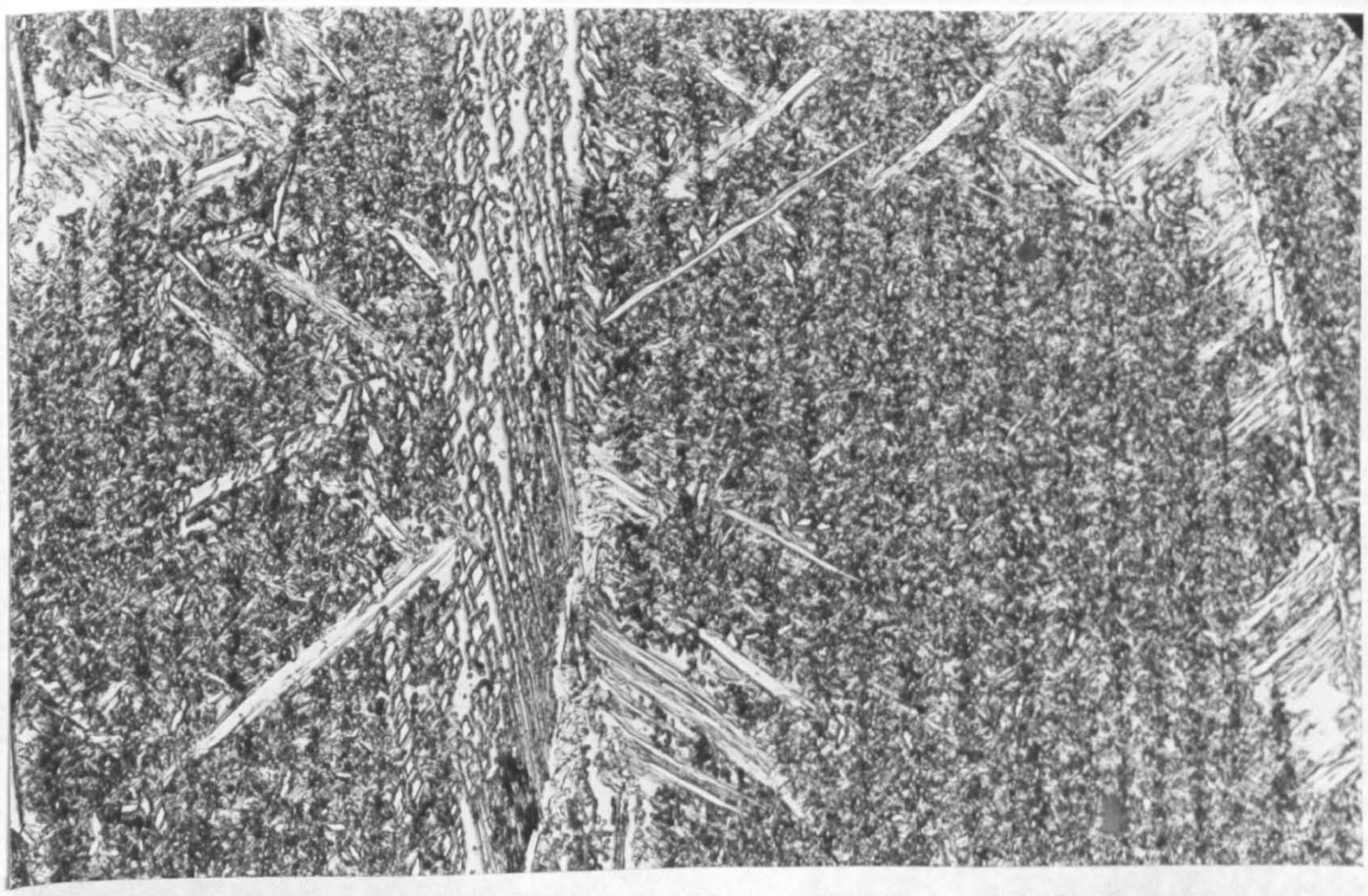

Figure 4.65: Austenite forming as fine grains rather than as Widmanstätten side plates in the reheated weld metal of the 0.27kJ/mm heat input Zeron 100 joint welded at 32bars (x400).

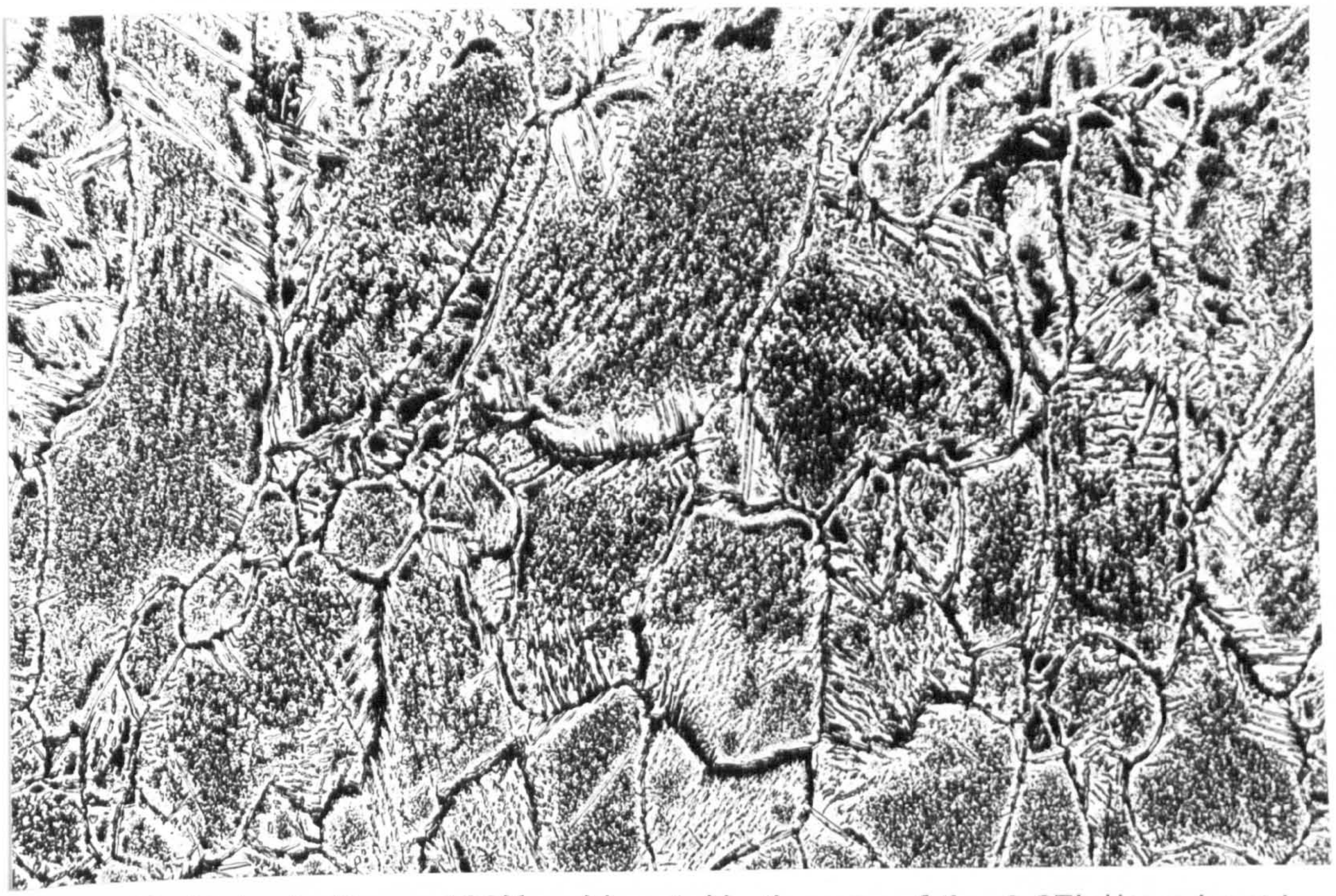

Figure 4.66: Metrode Zeron 100X weld metal in the cap of the 0.27kJ/mm heat input Zeron 100 joint welded at 32bars showing smaller primary ferrite grains than seen in the joint welded at 1bar (x100).

Figure 4.67: Acicular austenite in the primary ferrite grains in the cap of the 0.27kJ/mm heat input Zeron 100 joint welded at 32bars (x400).

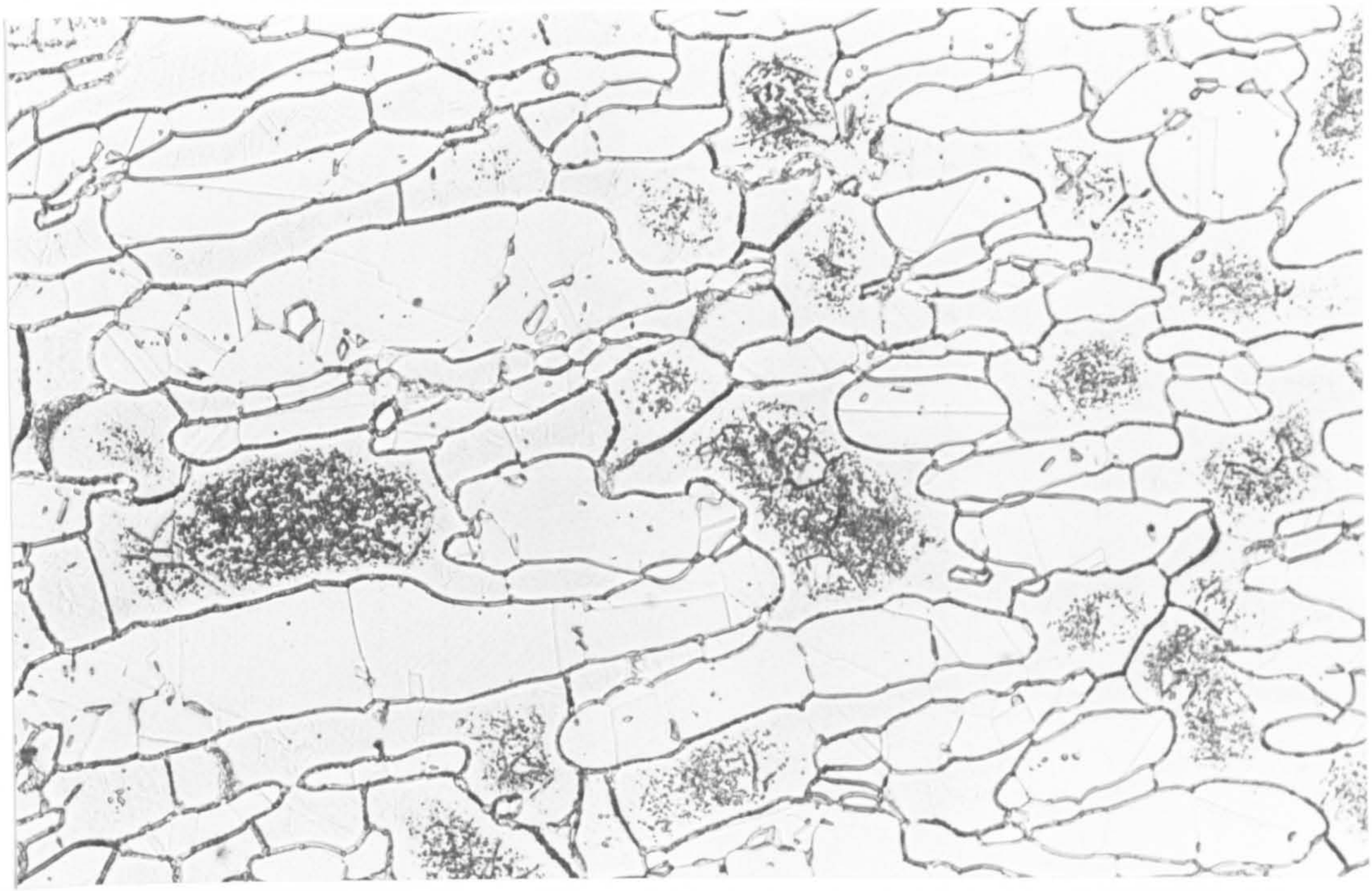

Figure 4.68: Limited chromium nitride precipitation in the HAZ of the 0.27kJ/mm heat input Zeron 100 joint welded at 32bars (x400).

Figure 4.69: Clusters of chromium nitride precipitates in the 0.99 kJ/mm heat input root weld of the Zeron 100 joint welded at 2bars (x400).

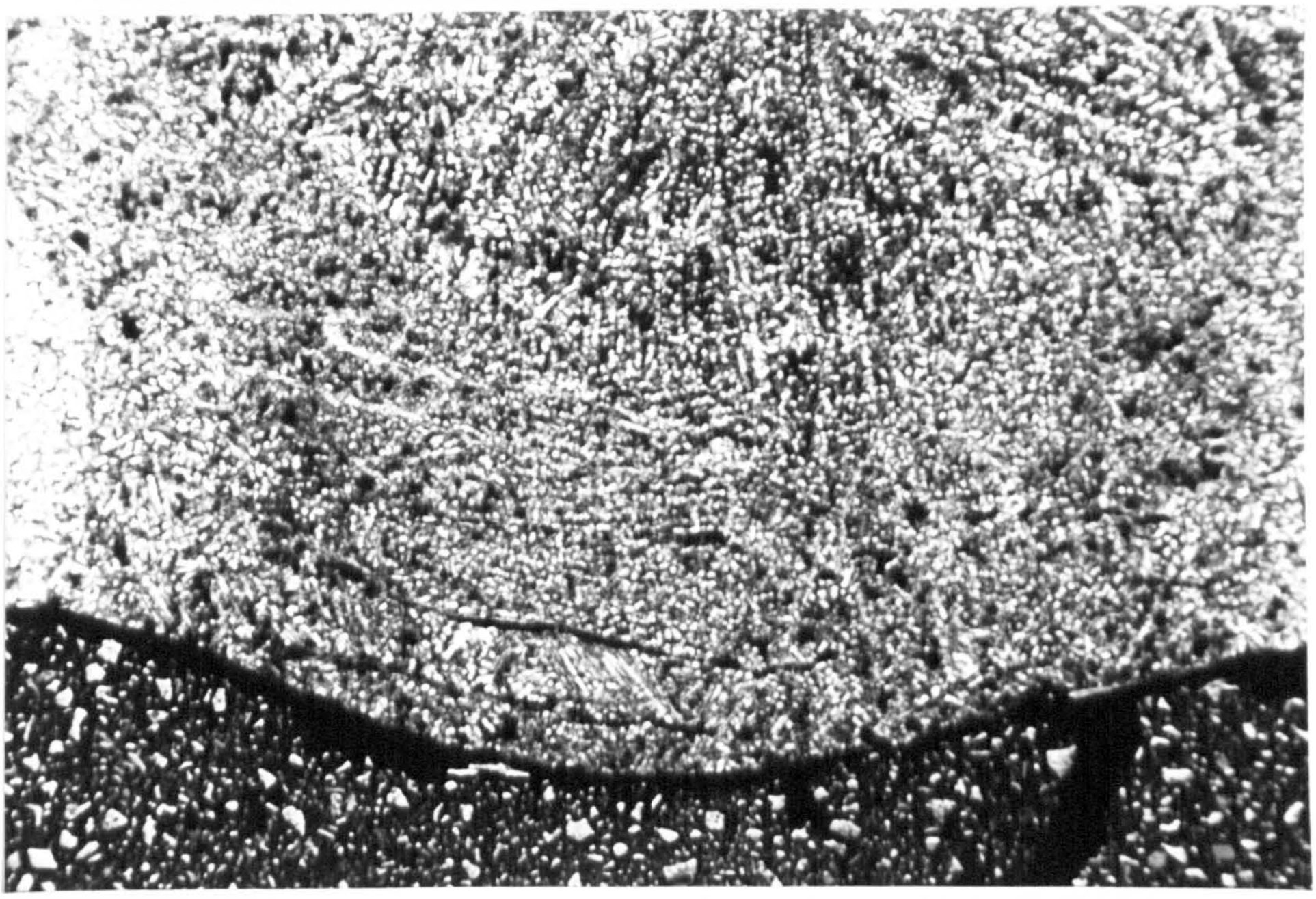

Figure 4.70: Apparent line of precipitates across the 0.39kJ/mm heat input root weld of the Zeron 100 joint welded at 8bars (x50).

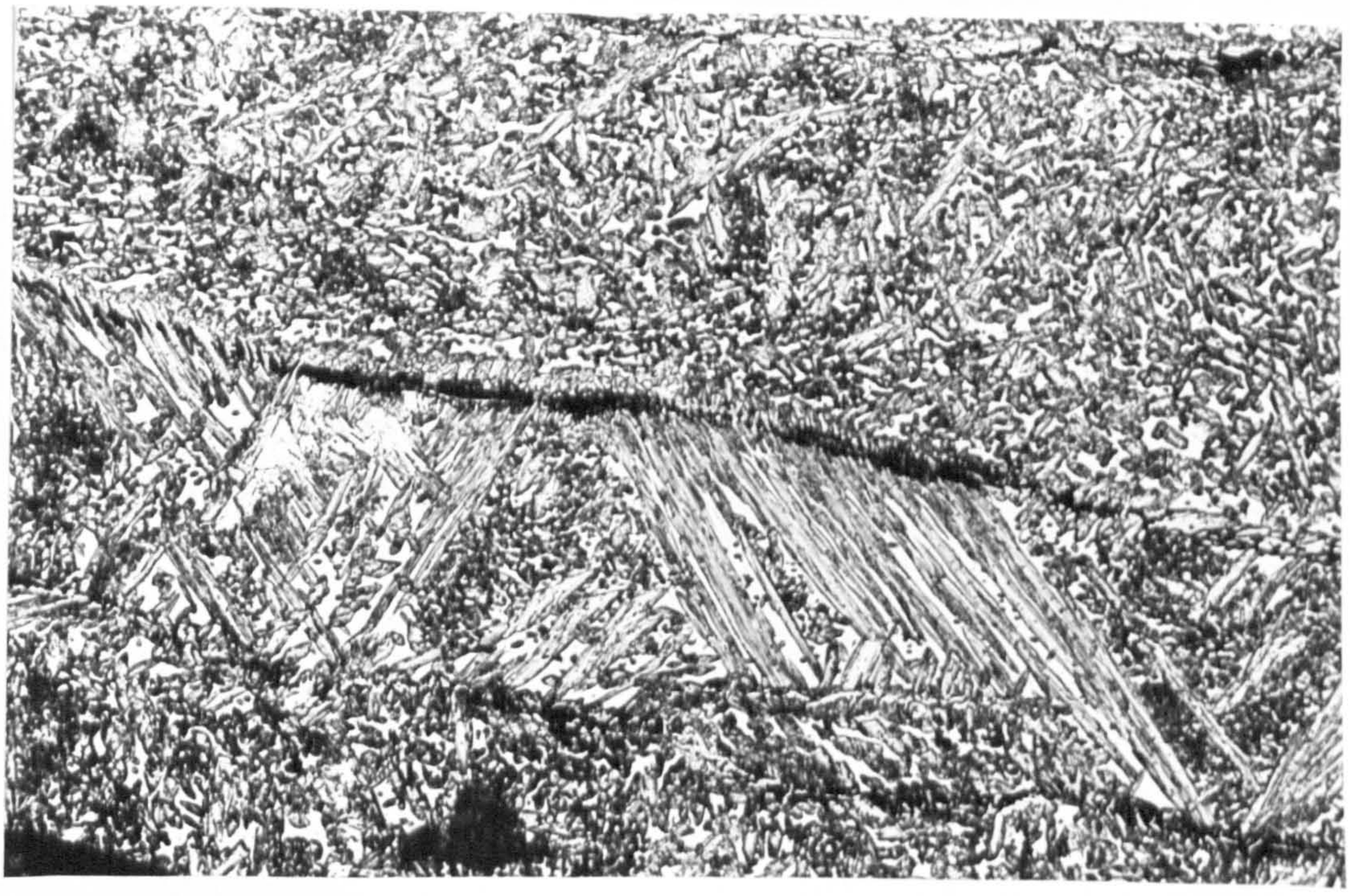

Figure 4.71: Precipitates formed at a prior ferrite grain boundary in the 0.39kJ/mm heat input root weld of the Zeron 100 joint welded at 8bars (x200).

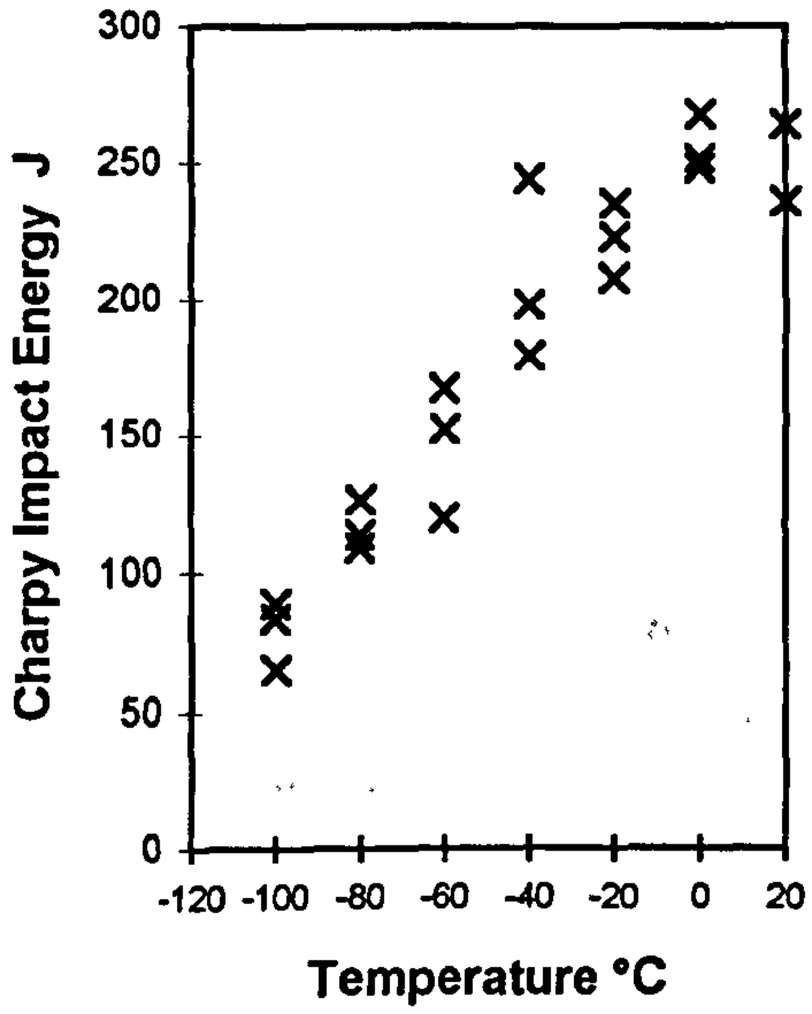

(a) Avesta 2205 Plate Material

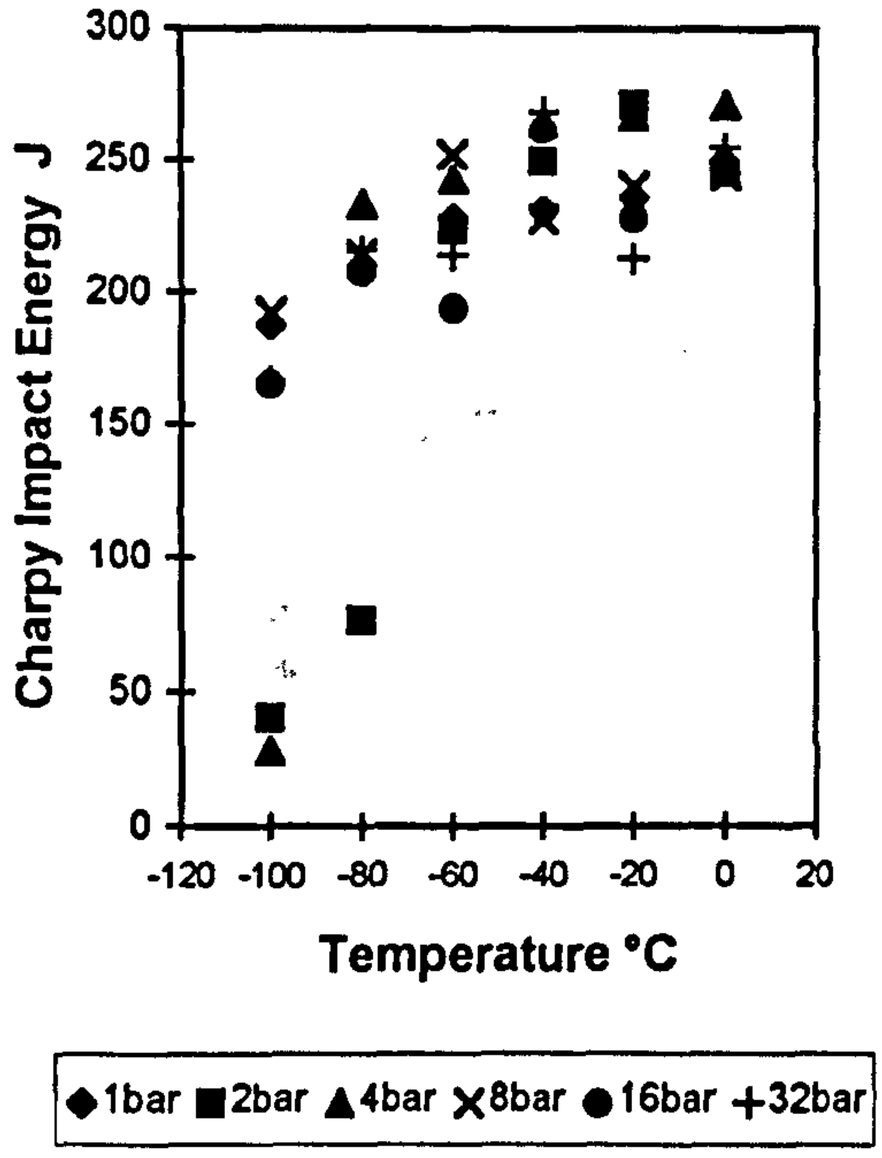

(b) Weld Metal (Sandvik 22.8.3L)

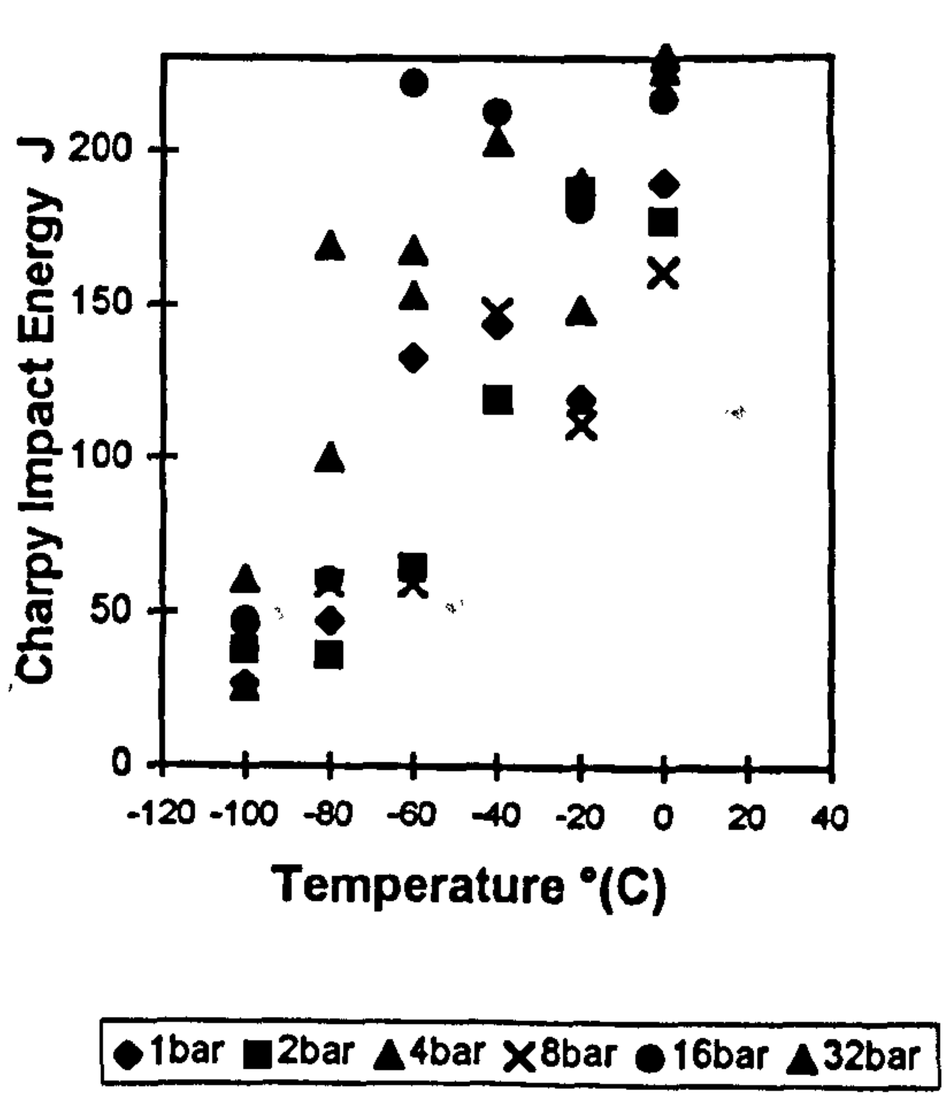

(c) Avesta 2205 HAZ (¾ size)

Figure 4.72: The Charpy impact results on Avesta 2205 duplex stainless steels.

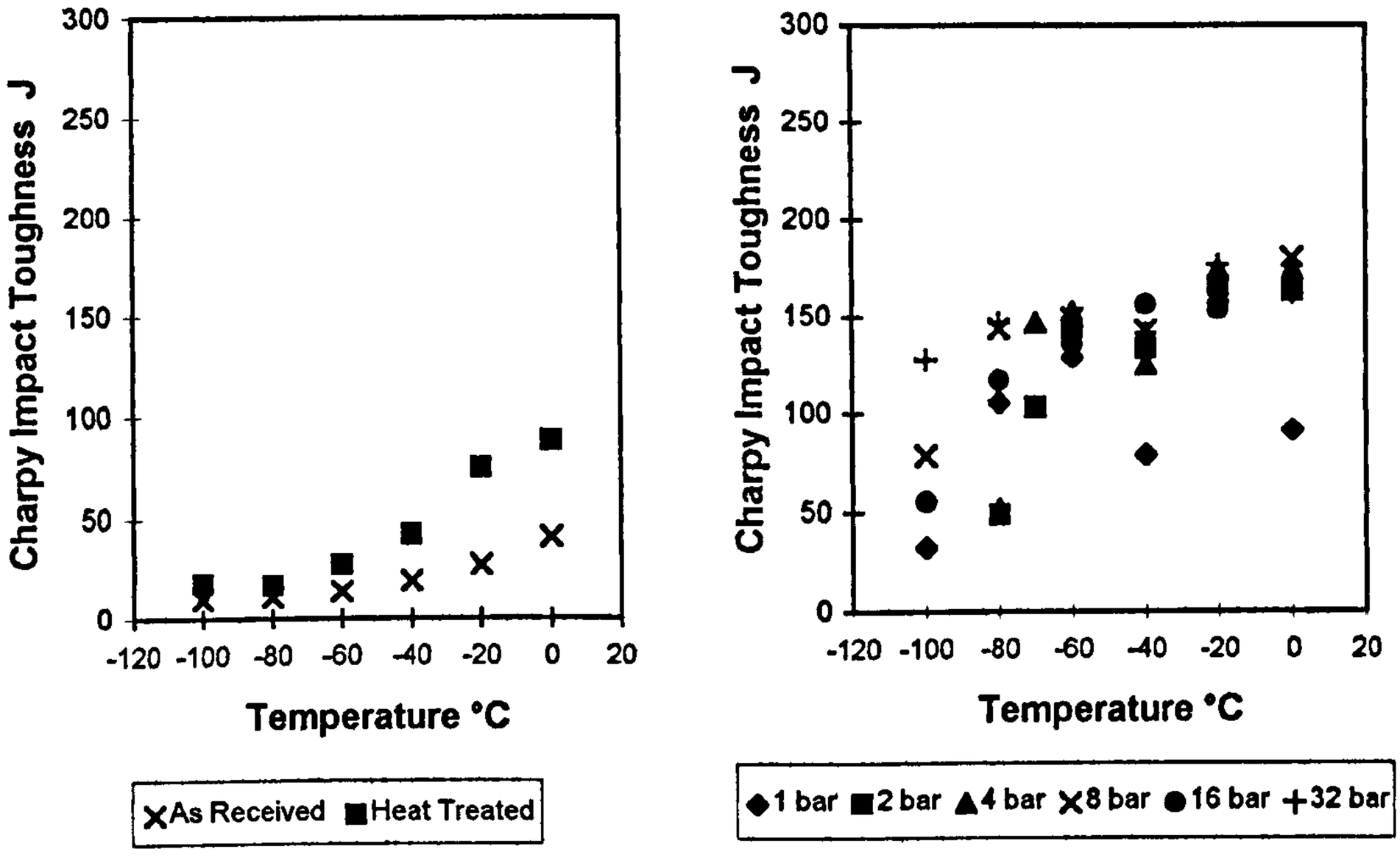

(a) Sandvik SAF2507 Plate Material

(b) Weld Metal (Sandvik 25.10.4L)

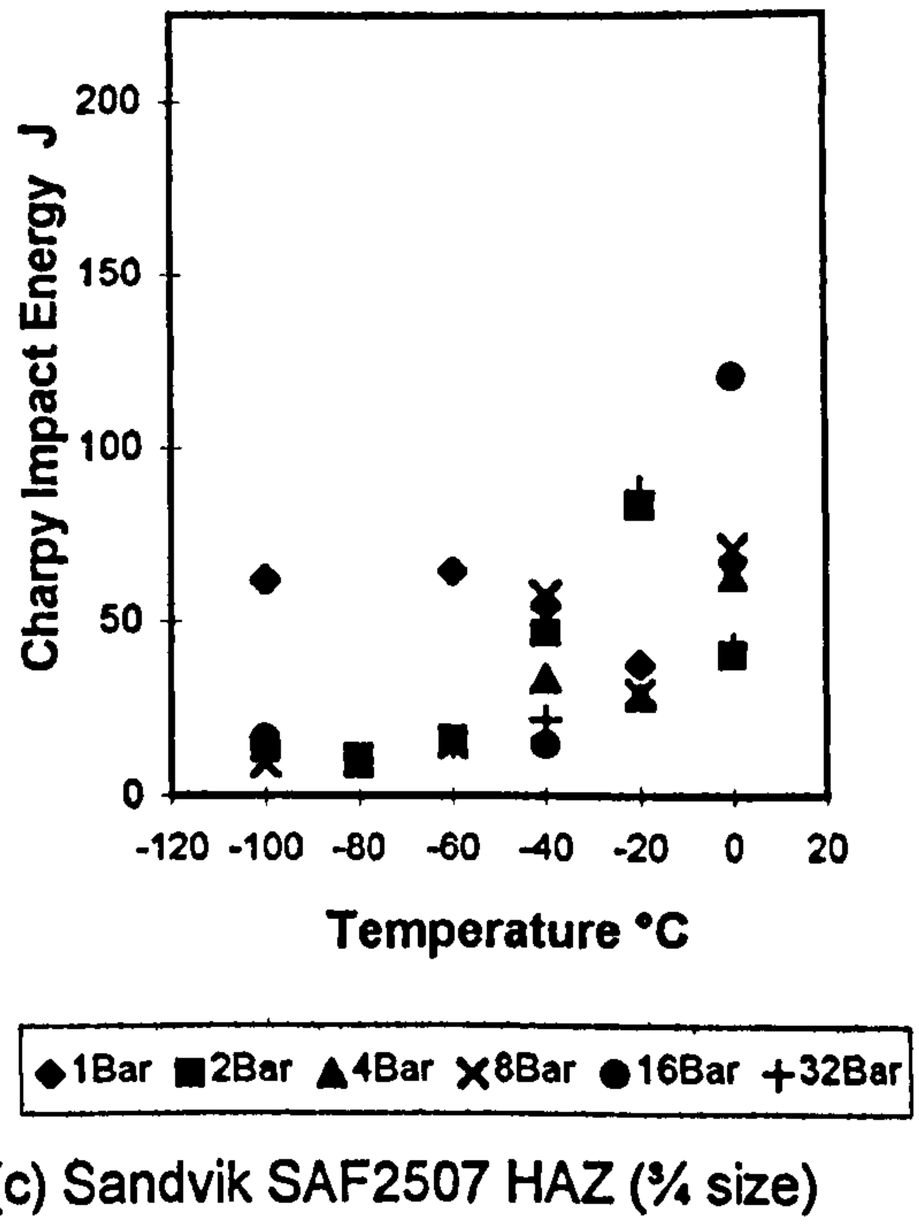

(c) Sandvik SAF2507 HAZ (¾ size)

Figure 4.73: The Charpy impact results on Sandvik SAF2507 super duplex stainless steels.

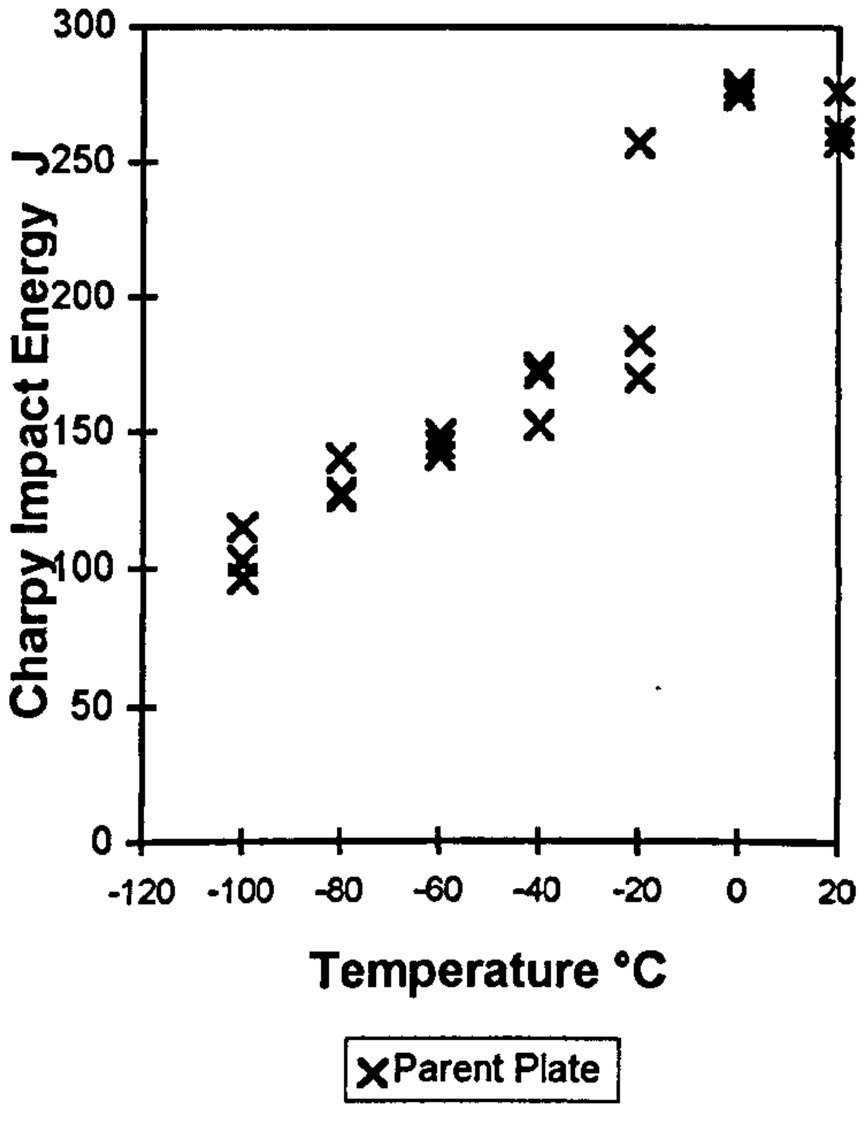

(a) Zeron 100 Plate Material

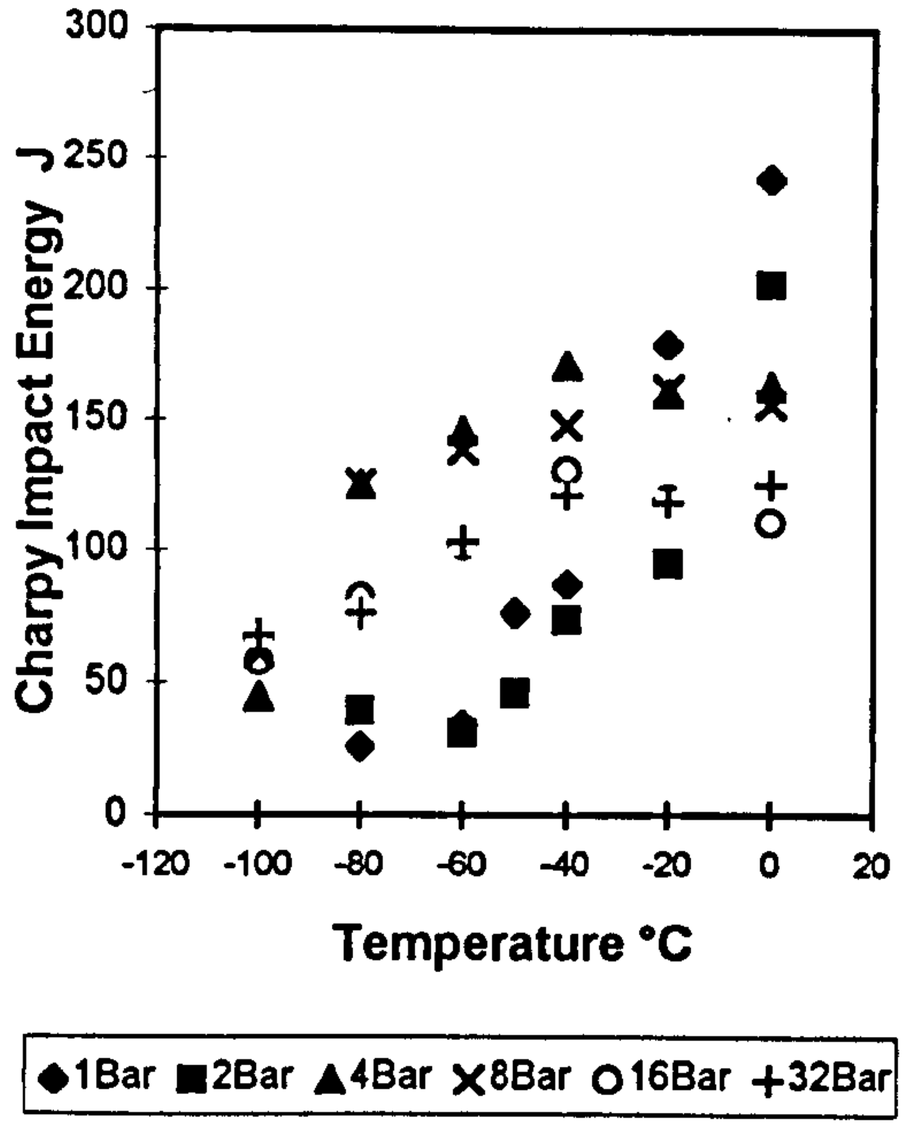

(b) Weld Metal (Metrode Zeron 100X)

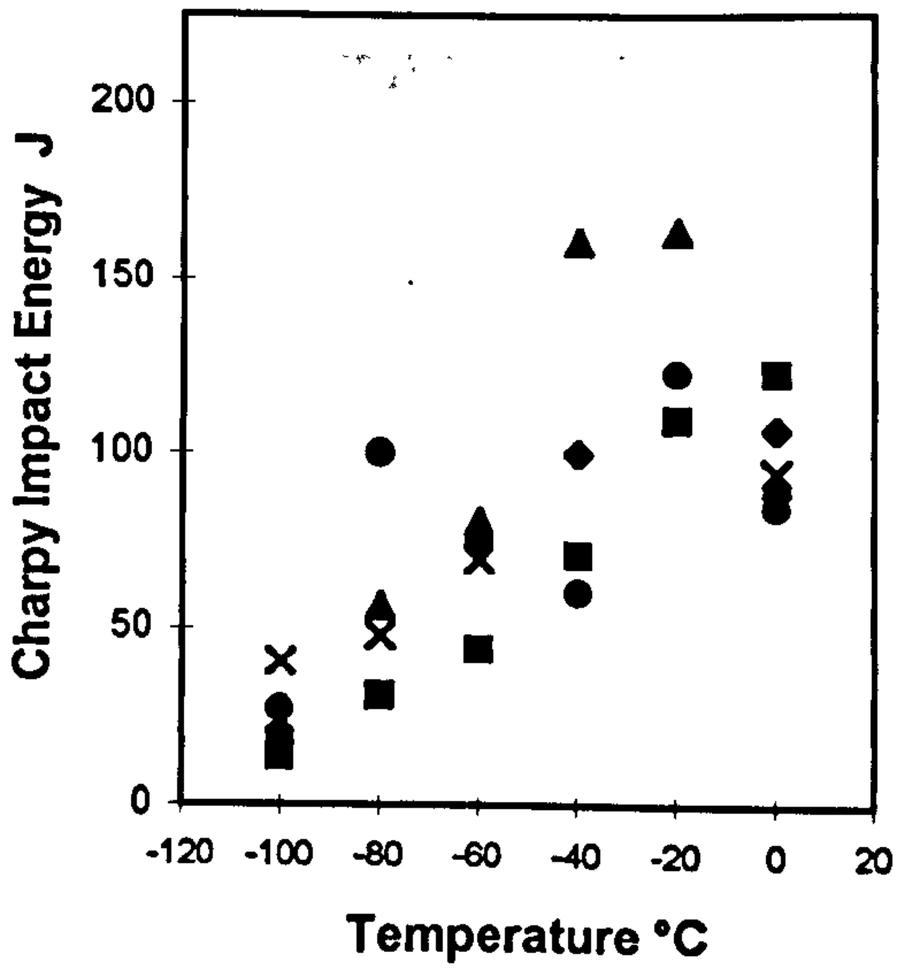

(c) Zeron 100 HAZ (¾ size)

Figure 4.74: The Charpy impact results on Zeron 100 super duplex stainless steels.

TABLES

Gas	Molecular Weight	Density g/l	Dissociation Energy kJ/mol	Ionisation Potential eV
Argon	39.9	1.78	4.7	15.75
Helium	4.0	0.18	3.8	24.59
Nitrogen	28.0	1.25	945.3	14.53
Hydrogen	2.0	0.09	436.0	13.60

Table 2.1: The properties of some shielding gases.

Tradename	Standard	% Alloying Elements					PRE
		Cr	Mo	Ni	N	Others	
SAF 2304 UR35N	UNS S32304	23	0.2	4	0.1	-	25
3RE60	UNS S 31500	18.5	2.7	5	0.07	1.5Si	29
UR45N SAF 2205 2205 FALC223 AF22 VS22	UNS S31803	22	3	5.3	0.17	-	35
10RE51	UNS S32900	25	1.5	4.5	-	-	30
DP 3	UNS S31260	25	3	6.5	0.16	0.5Cu 0.3W	37
UR52N Ferralium 255	UNS S32550	25	3	6.5	0.18	1.6Cu	38
UR47N	UNS S32200	25	3	6.5	0.18	-	38
Zeron 100	UNS S32760	25	3.6	7	0.25	0.7Cu 0.7W	41
UR52N^{+}	UNS S25500	25	3.8	6	0.26	1.5Cu	42
SAF 2507	UNS S32760	25	3.8	7	0.27	-	42

Table 2.2: The nominal compositions of some duplex stainless steels.

Chromium	Ferrite former. More than 13% required to maintain passive film.
Nickel	Austenite stabiliser, required to ensure sufficient austenite formation.
Molybdenum	Ferrite former. Stabilises the passive film.
Nitrogen	Austenite stabiliser. Increases strength and corrosion resistance of the austenitic phase.
Silicon	Ferrite former. Stabilises the passive film.
Copper	Austenite stabiliser.
Tungsten	Stabilises passive film.

Table 2.3: The rôle of the major alloying elements in duplex stainless steels.

Area of Use	Application	Alloy Type	Ref.
Oil and Gas Production	Pressure vessels	UNS S31803 UNS S32760 UNS S32750	20,39
	Pipelines	UNS S31803 UNS S32750	20,34
	Seawater piping	UNS S32760	34
	Wirelines in H_2S/Cl^- environments	UNS S32750	21
	Reactor coils	UNS S31803	22
	Cargo tanks	UNS S31803	26
	Manifolds	UNS S32760	37
Chemical Plant	Wet Phosphoric acid production	UNS S31803	41
	Heat exchanger	UNS S32750	24
Food Industry	Heat Exchanger (Wine Production)	UNS S32304	20
	Margarine Coolers	UNS S31803	20
	Pasta Production	UNS S32304	27
	Heat exchangers (Sugar Production)	UNS S32304	27
Miscellaneous	Flue Gas Desulphurisation	UNS S32550	27
	Soil Reinforcement	UNS S32304	27,40
	Paper Production	UNS 31803 UNS S32304	29,30
	Washing Machine Drums	UNS S32304	27
	Domstic Hot Water Heaters	UNS S32304	41
	Lamp Posts	UNS S31803	41

Table 2.4: Examples of use of duplex stainless steels.

Phase	Formation Temperature	References
Sigma Phase (σ)	650-950°C	42-52
Chromium Nitrides	700-900°C	50
Secondary Austenite (γ')	Up to 900°C	56
Chi (χ)	700-900°C	52
R	550-700°C	53,54
π	Around 600°C	54
Carbides (M_7C_3, $M_{23}C_6$)	Up to 1050°C	43,51
475°C Embrittlement (α')	350-550°C	42,47,57

Table 2.5:A summary of precipitates found in duplex stainless steels.

Alloy	PRE	0.2% Proof Stress Nmm^{-2}	U.T.S. Nmm^{-2}	% Elongation
UNS S43000	18	880	1100	3
UNS S 31600	25	200	480	40
UNS S32304	25	400	600	25
UNS S31803	35	450	680	25
UNS S32550	38			
UNS S32760	41	550	750	25
UNS S32750	42	550	800	25

Table 2.6: A comparison of the tensile properties of some ferritic (UNS S43000) and austenitic (UNS S31600) stainless steels with duplex grades.

Material	Standard	Form	Heat No.
Avesta 2205	UNS S31803	12.00mm plate	821049
Sandvik SAF2507	UNS S32750	219.08mm dia. pipe 12.70mm wall thickness	466063
Zeron 100	UNS S32760	13.00mm plate	61071

Table 3.1 The form and heat numbers of the materials used.

Material	0.2% Proof Stress MPa	U.T.S. MPa	Elongation %
Avesta 2205	549	772	45
Sandvik SAF32750	552	883	30
Zeron 100	658	808	29

Table 3.2 The mechanical properties of the materials (as supplied by manufacturer).

Material	Heat No.	% Alloying Elements										
		C	Si	Mn	P	S	Cr	Ni	Mo	Cu	W	N
Avesta 2205	821049	0.018	0.43	1.53	0.24	0.001	21.9	5.7	2.99	-	-	0.17
Sandvik SAF2507	466063	0.075	0.28	0.47	0.015	0.001	24.99	6.92	3.83	0.075	-	0.28
Weir Materials Zeron 100	61071	0.015	0.336	0.792	0.027	0.001	25.069	7.086	3.594	0.603	0.634	0.22

Table 3.3 : The composition of the materials investigated.

Consumable	Batch/ Heat	% Alloying Elements											
		C	Si	Mn	P	S	Cr	Ni	Mo	Co	Cu	W	N
Sandvik 22.8.3.L	465234	0.015	0.48	1.62	0.014	0.001	22.51	8.72	3.11	0.034	0.088	-	0.131
Sandvik 25.10.4.L	765521	0.015	0.32	0.41	0.018	0.001	25.03	9.49	4.01	0.028	0.098	-	0.28
Metrode Zeron 100X	FW2439	0.016	0.40	0.70	0.030	0.002	25.1	9.2	3.85	-	0.57	0.60	0.23

Table 3.4 : The compositions of the welding consumables used.

Consumable	$Ni_{(eq)}:Cr_{(eq)}$	PRE
Sandvik 22.8.3.L	0.528	34.9
Sandvik 25.10.4L	0.623	42.7
Metrode Zeron 100	0.573	41.5

Table 3.5 : The $Ni_{(eq)}:Cr_{(eq)}$ ratios and PRE values for the welding consumables.

Polarity	D.C. electrode negative
Welding Position	Downhand
Welding Direction	Leading
Nozzle Diameter	9.5mm
Electrode Composition	2% thoria
Electrode Diameter	2mm
Electrode Geometry	50° included
Workpiece Preparation	Ground and cleaned with propanone
Electrode Preparation	Ground and cleaned with propanone
Arc Ignition	Programmed touch strike
Chamber Gas	Argon
Shielding Gas	75%Helium, 25%Argon

Table 3.6 : The welding parameters common to all the welding operations.

Pressure (bar)	Welding Current (A)	Welding Speed (mm/s)	Arc Length (mm)	Shielding Gas Flow Rate (l/min)
1	100, 150	3.0	2.5	14.03
2	100, 150	3.0	2.5	9.92
4	100,150	3.0	2.5	7.02
8	100,150	3.0	2.5	4.96
16	100,150	3.0	2.5	3.51
32	100,150	3.0	2.5	2.48

Table 3.7 The variable welding parameters for the initial autogenous bead on plate welds.

Welding Current (A)	Welding Speed (mm/s)	Arc Length (mm)	Shielding Gas Flow Rate (l/min)
100, 150	1.0, 1.5, 2.0	2.5	14.03

Table 3.8 : The welding parameters for the autogenous bead on plate welds at one atmosphere.

Pressure (bar)	Welding Current (A)	Welding Speed (mm/s)	Arc Voltage (V)	Shielding Gas Flow Rate (l/min)	Heat Input (kJ/mm)
1	100	1.37	12.4-13.7	14.03	0.91-1.01
	150	1.13	13.0-14.2	"	1.73-1.89
2	100	1.48	13.9-16.0	9.92	0.95-1.09
	150	1.13	13.5-14.4	"	1.79-1.91
4	100	1.59	15.1-17.0	7.02	0.96-1.08
	150	1.13	16.2-17.2	"	2.15-2.28
8	100	1.70	17.5-19.4	4.96	1.03-1.14
	150	1.36	18.0-19.4	"	1.99-2.14
16	100	2.13	22.6-25.3	3.52	1.05-1.18
	150	1.78	24.0-26.3	"	2.02-2.22
32	100	2.93	28.2-31.2	2.48	0.96-1.06
	150	2.48	28.0-35.4	"	1.69-2.13

Table 3.9 : The welding parameters used for the autogenous bead on plate thermal cycle experiments.

Pressure (bar)	Welding Current (A)	Arc Voltage (V)	Welding Speed (mm/s)	Wire Feed Rate (m/min)	Heat Input (kJ/mm)	Shielding Gas Flow Rate (l/min)
1	123	13.2	1.13	3.00	1.436	14.03
2	123	15.0	1.28	3.00	1.441	9.92
4	123	16.5	1.57	3.00	1.292	7.02
8	123	18.4-18.9	2.05	3.00	1.104-1.134	4.96
16	124	24.2-24.8	2.87	3.00	1.046-1.071	3.51
32	124	30.8-31.5	3.50-4.26	3.00-3.50	0.896-0.917	2.48

Table 3.10 : The welding parameters used for the weld joint design evaluation experiments.

Pressure (bar)	Pass Number	Shielding Gas Flow Rate	Welding Current (A)	Arc Voltage (V)	Welding Speed (mm/s)	Wire Feed Rate (m/min)	Heat Input (kJ/mm)
1	Root	14.03	155/78	14.1/13.3	1.05	1.59-1.65	1.535
	2-9	14.03	176-177	13.9-14.3	2.50	1.98-2.04	0.979-1.012
2	Root	9.92	155/78	15.8/15.4	1.31	1.50	1.381-1.411
	2-10	9.92	177	15.8-16.2	2.83	1.97-2.00	0.988-1.013
4	Root	7.02	145/78	17.1/15.0	1.40	1.50	1.302
	2-11	7.02	177	17.2-17.8	3.10	1.98-2.04	0.976-1.016
8	Root	4.96	107/58	17.1/17.1	3.50	2.04	0.367
	2-12	4.96	119	19.4-20.2	3.00	1.96-2.04	0.770-0.801
16	Root & 2	3.51	74/49	23.1/23.3	4.00	1.98-2.01	0.321
	3-15	3.51	100	23.2-25.6	3.31	1.97-2.04	0.701-0.764
32	Root	2.48	74/49	30.4/29.4	6.00	2.50	0.254-0.283
	2-15	2.48	80-81	31.0-32.0	3.81	1.97-2.01	0.651-0.672

Table 3.11 : A summary of the welding parameters used for the Avesta 2205 welded joints.

Pressure (bar)	Pass Number	Shielding Gas Flow Rate	Welding Current (A)	Arc Voltage (V)	Welding Speed (mm/s)	Wire Feed Rate (m/min)	Heat Input (kJ/mm)
1	Root	14.03	146/78	13.8/13.3	1.05	1.22-1.48	1.499
	2-10	14.03	177	13.6-14.2	2.50	1.96-2.01	0.963-1.005
2	Root	9.92	146/78	15.4/14.1	1.31	2.02	1.280
	2-9	9.92	177	15.6-16.1	2.83	1.98-2.00	0.976-1.019
4	Root	7.02	146/78	16.6/15.1	1.40	1.49	1.289
	2-10	7.02	177	16.8-17.2	3.10	1.98-2.01	0.965-0.993
8	Root	4.96	109/59	19.1/17.6	3.00	2.00	0.464
	2-11	4.96	119	19.2-19.8	3.00 (2.30)	1.99-2.02	0.762-1.019
16	Root & 2	3.51	74/49	23.0/22.6	4.00	1.97	0.306-0.323
	3-12	3.51	100	23.3-24.9	3.31	1.97-1.99	0.740-0.755
32	Root & 2	2.48	74/49	31.0-30.6	4.00-6.00	1.50-2.00	0.280-0.409
	3-13	2.48	3.81	1.98-2.04	3.81	1.98-2.04	0.659-0.674

Table 3.12 : A summary of the welding parameters used for the Sandvik SAF2507 welded joints.

Pressure (bar)	Pass Number	Shielding Gas Flow Rate	Welding Current (A)	Arc Voltage (V)	Welding Speed (mm/s)	Wire Feed Rate (m/min)	Heat Input (kJ/mm)
1	Root	14.03	145/78	13.9/12.5	1.13	1.50	1.323
	2-4	14.03	149	13.4-13.5	2.00	0.68	0.998-1.006
	5-9	14.03	177-178	13.8-14.2	2.50	1.97-1.991	0.977-1.005
2	Root	9.92	146/78	15.7/14.1	1.13-1.28	1.50-1.64	1.342-1.481
	2-9	9.92	177-178	15.7-16.1	2.83	1.96-2.01	0.982-1.019
4	Root & 2	7.02	106/59	17.5/17.5	3.50	2.00	0.377
	3-12	7.02	176-177	17.1-17.50	3.10	2.00	0.971-0.999
8	Root	4.96	106/59	18.9/17.5	3.50-3.60	2.00	0.386
	2-13	4.96	119	19.0-19.9	3.00	1.98-2.04	0.754-0.785
16	Root & 2	3.51	74/49	22.2/22.3	4.00	2.00-2.02	0.304-0.311
	3-12	3.51	99-100	24.7-25.0	3.31	1.99-2.01	0.736-0.755
32	Root & 2	2.48	74/49	31.1/30.0	6.00	2.50	0.264-0.281
	3-13	2.48	80-81	30.5-31.7	3.81	1.47-2.00	0.651-0.712

Table 3.13 : A summary of the welding parameters used for the Zeron 100 welded joints.

Pressure (bar)	Welding Current (A)	Arc Stability	Arc Voltage (V)	Heat Input (kJ/mm)
1	100	Stable	11.5	0.383
	150	Stable	10.5	0.525
2	100	Stable	12.6	0.420
	150	Stable	13.0	0.650
4	100	Stable	13.5	0.450
	150	Stable	13.4	0.670
8	100	Stable	15.7	0.523
	150	Stable	18.0	0.900
16	100	Stable	18.3	0.610
	150	Stable	19.3	0.965
32	100	Stable	26.2	0.873
	150	Stable	Not recorded	Not recorded

Table 4.1 : The arc stabilities and arc voltages for the initial autogenous bead on plate welds on Avesta 2205.

Pressure (bar)	Welding Current (A)	Arc Stability	Arc Voltage (V)	Heat Input (kJ/mm)
1	100	Stable	11.5	0.383
	150	Stable	10.9	0.545
2	100	Stable	12.6	0.420
	150	Stable	11.8	0.590
4	100	Stable	12.5	0.416
	150	Stable	13.1	0.655
8	100	Stable	17.1	0.570
	150	Stable	19.5	0.975
16	100	Stable	20.0	0.666
	150	Stable	21.2	1.060
32	100	Stable	25.4	0.846
	150	Stable	28.5	1.425

Table 4.2 : The arc stabilities and arc voltages for the initial autogenous bead on plate welds on Sandvik SAF 2507.

Pressure (bar)	Welding Current (A)	Arc Stability	Arc Voltage (V)	Heat Input (kJ/mm)
1	100	Stable	11.7	0.390
	150	Stable	11.6	0.580
2	100	Stable	12.7	0.423
	150	Stable	12.6	0.630
4	100	Stable	13.7	0.456
	150	Stable	14.4	0.720
8	100	Stable	Not recorded	Not recorded
	150	Stable	18.5	0.925
16	100	Stable	20.0	0.666
	150	Stable	20.9	1.045
32	100	Stable	27.3	0.910
	150	Stable	28.5	1.425

Table 4.3 : The arc stabilities and arc voltages for the initial autogenous bead on plate welds on Zeron 100.

Element	Partition Coefficient (δ/γ)					
	Avesta 2205		Sandvik SAF2507		Zeron 100	
	P.P.	W.M.	P.P.	W.M.	P.P.	W.M.
Cr	1.137	1.010	1.098	1.011	1.124	1.007
Mo	1.827	0.941	1.674	1.071	1.588	0.998
Ni	0.646	1.001	0.630	0.924	0.649	0.977
Cu	-	0.143	0.158	1.407	0.692	0.659
W	1.129	1.292	0.941	12.333	2.144	1.229
Si	1.037	0.909	1.722	0.298	0.672	0.810
Mn	1.032	1.025	0.858	0.983	1.002	0.914

Table 4.4 : The partition coefficients for the parent plate (P.P.) and autogeneous weld metal (W.M.)of the three materials.

Pressure	Vickers Hardness, Hv_{10}		
	Root	Mid-Weld	Cap
1	289	262	270
2	282	271	271
4	285	286	286
8	280	267	267
16	297	272	272
32	285	279	279

Table 4.5 : The hardness survey results for the Sandvik 22.8.3L (Avesta 2205) weld metals.

Pressure	Vickers Hardness, Hv_{10}		
	Root	Mid-Weld	Cap
1	296	290	280
2	283	279	286
4	294	292	290
8	298	294	286
16	274	285	276
32	286	295	279

Table 4.6 : The hardness survey results of the Sandvik 25.10.4L (SAF 2507) weld metals.

Pressure	Vickers Hardness, Hv_{10}		
	Root	Mid-Weld	Cap
1	282	282	289
2	288	302	302
4	285	304	305
8	303	300	302
16	297	299	302
32	278	303	296

Table 4.7 : The hardness survey results for the Metrode Zeron 100X (Zeron 100) weld metal.

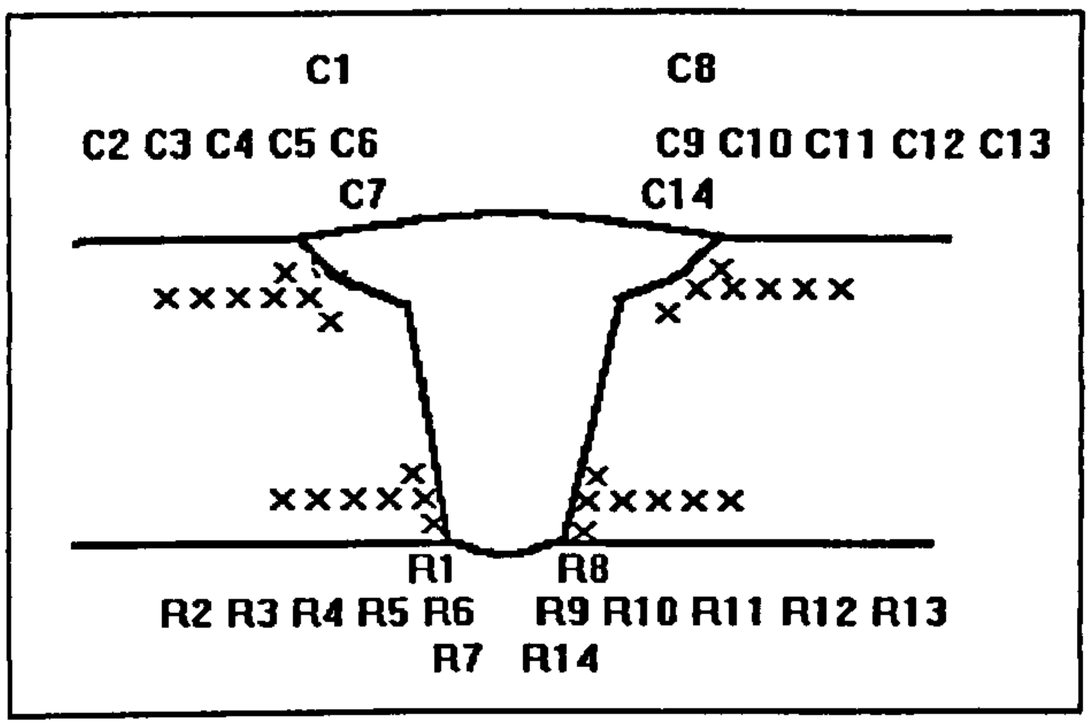

Position	Pressure (bar)					
	1bar	2bar	4bar	8bar	16bar	32bar
R1	283	277	291	284	284	280
R2	262	271	273	269	269	264
R3	262	267	272	273	269	273
R4	274	271	279	274	274	282
R5	278	273	284	283	260	274
R6	279	258	286	289	271	275
R7	270	271	283	280	273	274
R8	274	275	285	308	274	280
R9	282	280	273	292	277	283
R10	279	283	256	280	270	281
R11	280	278	278	288	256	275
R12	270	268	279	279	269	270
R13	250	265	279	267	256	258
R14	275	295	290	281	281	290
C1	243	260	264	258	255	274
C2	241	262	248	254	250	255
C3	246	258	257	278	251	254
C4	251	253	256	264	259	250
C5	246	254	255	259	258	263
C6	254	258	255	256	264	262
C7	252	262	278	252	261	254
C8	270	274	264	252	268	263
C9	269	260	255	247	247	251
C10	269	258	255	254	249	253
C11	266	263	250	249	251	265
C12	265	253	254	254	252	259
C13	272	260	247	246	246	248
C14	244	253	250	252	262	257

Table 4.8 :The hardness survey results for the Avesta 2205 welds.

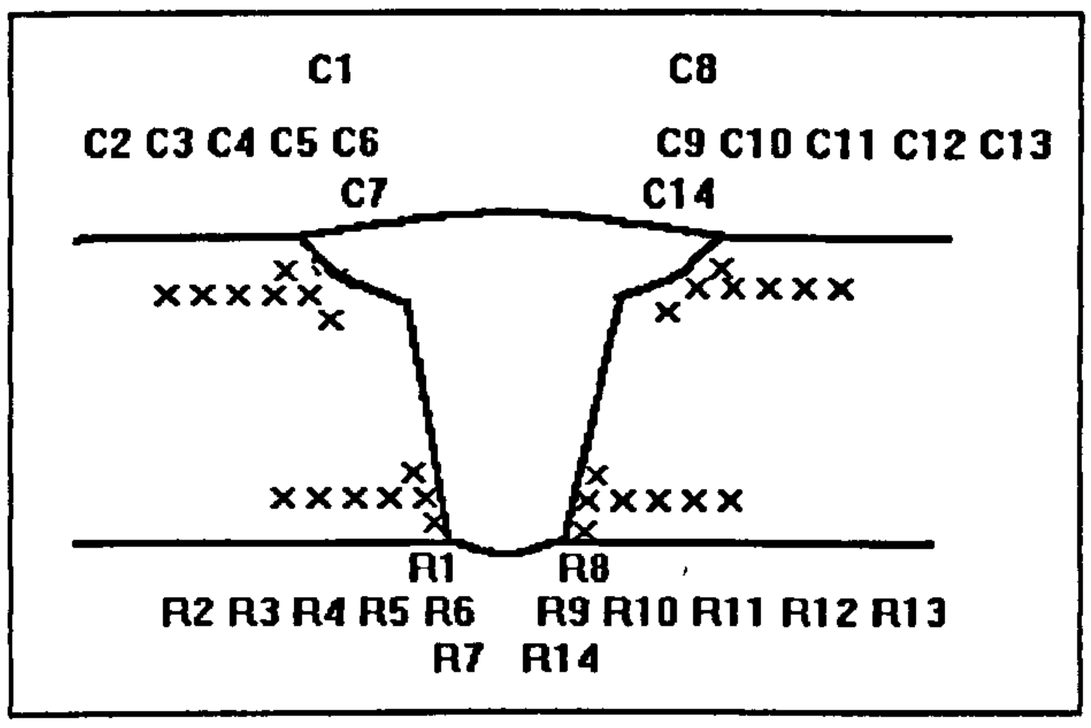

Position	Pressure (bar)					
	1bar	2bar	4bar	8bar	16bar	32bar
R1	297	302	319	306	313	313
R2	303	272	301	280	287	283
R3	295	276	302	287	295	287
R4	295	287	306	283	301	298
R5	305	302	316	297	307	311
R6	312	293	327	303	314	304
R7	309	289	322	306	303	322
R8	309	292	329	291	313	310
R9	317	307	325	301	304	320
R10	309	296	313	287	297	298
R11	306	281	307	278	279	294
R12	301	285	308	278	282	286
R13	288	280	310	278	278	279
R14	332	300	313	297	310	321
C1	307	287	310	294	290	303
C2	322	281	307	285	286	255
C3	325	277	314	293	288	259
C4	324	275	314	293	274	267
C5	316	275	320	291	252	290
C6	307	270	312	291	228?	289
C7	317	271	320	289	254	274
C8	330	291	316	295	280	293
C9	322	265	314	291	271	290
C10	321	288	331	286	277	290
C11	329	284	308	283	275	293
C12	322	279	308	293	275	282
C13	321	284	307	283	273	278
C14	326	283	309	288	272	292

Table 4.9 : The hardness survey results for the SAF 2507 welds.

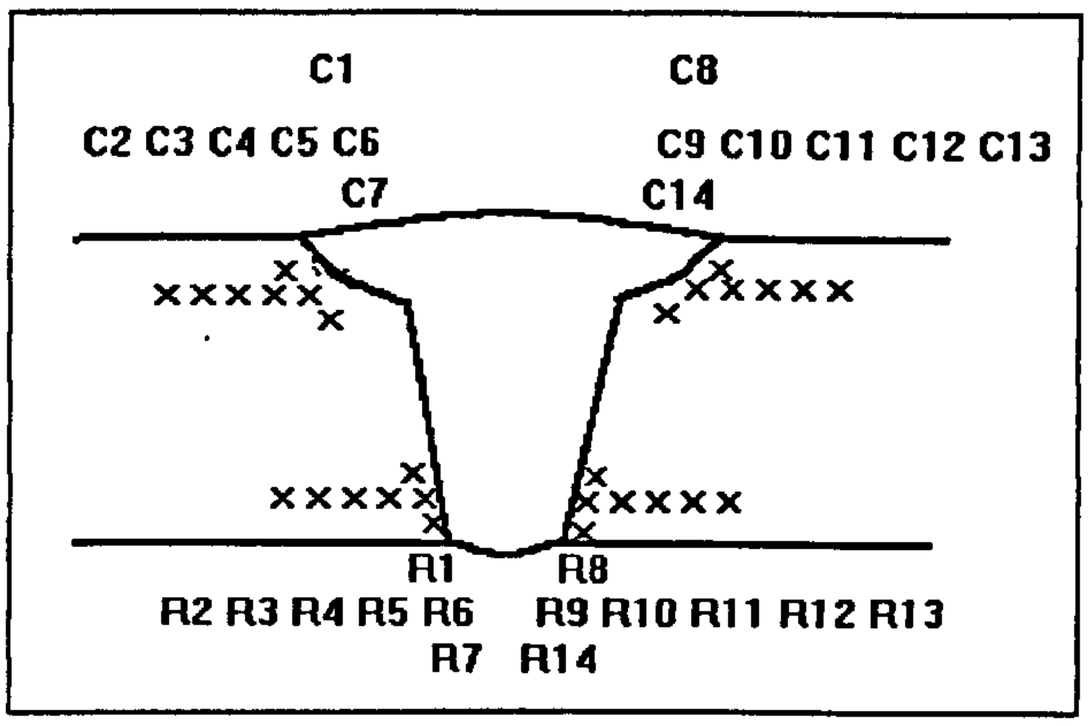

Position	Pressure (bar)					
	1bar	2bar	4bar	8bar	16bar	32bar
R1	287	335	300	288	297	285
R2	275	234	272	269	282	269
R3	275	296	277	258	279	272
R4	279	259	278	273	283	271
R5	270	310	271	276	291	284
R6	281	309	298	292	287	289
R7	289	279	288	285	293	288
R8	278	317	309	303	304	297
R9	285	304	307	295	297	282
R10	286	291	293	291	287	267
R11	290	282	282	278	289	255
R12	269	282	283	280	294	270
R13	284	296	278	285	286	275
R14	287	273	293	303	306	282
C1	289	325	282	286	286	287
C2	273	304	284	283	279	282
C3	264	297	278	281	278	272
C4	277	295	282	288	282	272
C5	271	307	285	280	278	283
C6	293	298	276	286	284	228
C7	288	302	293	283	279	278
C8	281	303	277	288	282	295
C9	284	321	293	291	297	276
C10	275	313	285	301	282	275
C11	274	306	280	281	287	297
C12	272	307	285	280	294	288
C13	273	299	286	283	283	283
C14	281	300	288	289	282	282

Table 4.10: The HAZ hardness survey results for the Zeron 100 welds.

APPENDIX

The Welding Parameters Used for the Welded Joints

Avesta 2205
1bar (LHS)

Pass Number	Welding Current (A)	Pulse Duration (ms)	Arc Voltage (V)	Welding Speed (mm/s)	Wire Feed Rate (m/min)	Heat Input (kJ/mm)
Root	155	500	14.1	1.05	1.65-1.59	1.535
	78	500	13.3			
1	177		13.9	2.50	2.00	0.984
2	176		14.2	2.50	2.02-2.01	1.000
3	176		13.9	2.50	2.03	0.979
4	177		14.3	2.50	2.04	1.012
5	177		14.1	2.50	1.99	0.998
6	177		13.9	2.50	1.98	0.984
7	177		13.9	2.50	1.98	0.984
8	177		14.1	2.50	1.99	0.998

Avesta 2205
2bar (LHS)

Pass Number	Welding Current (A)	Pulse Duration (ms)	Arc Voltage (V)	Welding Speed (mm/s)	Wire Feed Rate (m/min)	Heat Input (kJ/mm)
Root	155	500	15.7	1.31	1.50	1.381
	78	500	15.2			
1	177		15.9	2.83	1.98	0.994
2	177		16.0	2.83	1.98	1.001
3	177		16.0	2.83	1.97	1.001
4	177		16.0	2.83	1.96	1.001
5	177		15.8	2.83	1.97	0.988
6	177		15.8	2.83	1.96	0.988
7	177		15.9	2.83	1.98	0.994
8	177		15.8	2.83	1.96	0.988
9	177		16.2	2.83	1.97	1.013

Avesta 2205
2bar (RHS)

Pass Number	Welding Current (A)	Pulse Duration (ms)	Arc Voltage (V)	Welding Speed (mm/s)	Wire Feed Rate (m/min)	Heat Input (kJ/mm)
Root	155	500	16.0	1.31	1.49	1.411
	78	500	15.6			
1	177		15.8	2.83	1.96	0.988
2	177		15.9	2.83	2.00	0.994
3	177		15.9	2.83	1.97	0.994
4	177		15.9	2.83	1.96	0.994
5	177		16.0	2.83	1.97	1.001
6	177		16.0	2.83	1.98	1.001
7	177		16.0	2.83	1.98	1.001
8	177		15.8	2.83	1.98	0.988
9	177		15.9	2.83	1.98	0.994

Avesta 2205
4bar (LHS)

Pass Number	Welding Current (A)	Pulse Duration (ms)	Arc Voltage (V)	Welding Speed (mm/s)	Wire Feed Rate (m/min)	Heat Input (kJ/mm)
Root	145	500	17.2	1.40	1.50	1.295
	78	500	14.5			
1	177		17.2	3.10	1.98	0.982
2	177		17.2	3.10	1.98	0.982
3	177		17.3	3.10	1.98	0.988
4	177		17.2	3.10	1.98	0.982
5	177		17.2	3.10	2.00	0.982
6	177		17.1	3.10	2.04	0.976
7	177		17.2	3.10	2.00	0.982
8	177		17.7	3.10	1.99	1.011
9	177		17.7	3.10	2.01	1.011
10	177		17.5	3.10	1.98	0.999

Avesta 2205
4bar (RHS)

Pass Number	Welding Current (A)	Pulse Duration (ms)	Arc Voltage (V)	Welding Speed (mm/s)	Wire Feed Rate (m/min)	Heat Input (kJ/mm)
Root	145	500	17.0	1.40	1.49	1.309
	78	500	15.4			
1	177		17.6	3.10	1.98	1.005
2	177		17.8	3.10	1.98	1.016
3	177		17.6	3.10	1.98	1.005
4	177		17.7	3.10	2.00	1.011
5	177		17.8	3.10	1.97	1.016
6	177		17.2	3.10	1.98	0.982
7	177		17.5	3.10	1.98	0.999
8	177		17.8	3.10	2.01	1.016
9	177		17.3	3.10	1.99	0.988

Avesta 2205
8bar (RHS)

Pass Number	Welding Current (A)	Pulse Duration (ms)	Arc Voltage (V)	Welding Speed (mm/s)	Wire Feed Rate (m/min)	Heat Input (kJ/mm)
Root	107	350	17.1	3.50	2.04	0.367
	58	650	17.1			
1	119		20.0	3.00	2.02	0.793
2	119		19.5	3.00	2.03	0.774
3	119		19.7	3.00	2.04	0.781
4	119		19.7	3.00	2.00	0.781
5	119		19.3	3.00	2.03	0.766
6	119		19.6	3.00	2.04	0.777
7	119		19.5	3.00	2.04	0.774
8	119		19.5	3.00	2.04	0.774
9	119		20.2	3.00	1.96	0.801
10	119		19.9	3.00	2.01	0.789
11	119		19.4	3.00	2.01	0.770

Avesta 2205
16bar (LHS)

Pass Number	Welding Current (A)	Pulse Duration (ms)	Arc Voltage (V)	Welding Speed (mm/s)	Wire Feed Rate (m/min)	Heat Input (kJ/mm)
Root	74	250	23.1	4.00	1.98	0.326
	49	750	23.8			
1	74	250	23.1	4.00	1.98	0.321
	49	750	23.3			
Wash	100		24.5	3.31		0.740
2	100		24.6	3.31	2.01	0.743
3	100		25.0	3.31	2.00	0.755
4	100		24.6	3.31	2.00	0.743
5	100		24.5	3.31	1.97	0.740
6	100		25.0	3.31	2.02	0.755
7	100		23.2	3.31	2.02	0.701
8	100		25.0	3.31	2.03	0.755
9	100		24.4	3.31	2.01	0.737
10	100		24.5	3.31	2.00	0.740
11	100		25.0	3.31	1.98	0.755

Avesta 2205
16bar (RHS)

Pass Number	Welding Current (A)	Pulse Duration (ms)	Arc Voltage (V)	Welding Speed (mm/s)	Wire Feed Rate (m/min)	Heat Input (kJ/mm)
Root	74	250	22.9	4.00	2.01	0.308
	49	750	22.0			
1	74	250	23.3	4.00	2.00	0.329
	49	750	24.1			
Wash	100		24.6	5.00		0.492
2	100		24.6	3.31	2.02	0.743
3	100		25.3	3.31	2.04	0.764
4	100		25.1	3.31	!	0.758
5	100		25.2	3.31	2.01	0.761
6	100		25.0	3.31	2.04	0.755
7	100		24.1	3.31	2.02	0.728
8	100		25.3	3.31	2.02	0.764
9	100		25.6	3.31	2.04	0.773
10	100		24.5	3.31	1.99	0.740
11	100		24.8	3.31	1.98	0.749
12	100		25.0	3.31	1.98	0.755
13	100		25.0	3.31	1.99	0.755
14	100		25.0	3.31	2.01	0.755

Avesta 2205
32bar (LHS)

Pass Number	Welding Current (A)	Pulse Duration (ms)	Arc Voltage (V)	Welding Speed (mm/s)	Wire Feed Rate (m/min)	Heat Input (kJ/mm)
Root	74	200	31.9	6.00	2.50	0.283
	49	800	31.3			
1	74	200	29.0	6.00	2.50	0.254
	49	800	28.0			
2	80		31.0	3.81	1.53	0.651
3	80		31.0	3.81		0.651
4	80		31.0	3.81	2.01	0.651
5	80		32.0	3.81	2.00	0.672
6	80		31.0	3.81	2.00	0.651
7	80		31.0	3.81	2.00	0.651
8	80		31.0	3.81	2.01	0.651
9	80		31.0	3.81	2.00	0.651
10	80		31.0	3.81	1.99	0.651
11	80		31.0	3.81	1.98	0.651
12	80		31.0	3.81	1.98	0.651
13	81		31.0	3.81	1.98	0.659
14	81		31.0	3.81	2.00	0.659

Avesta 2205
32bar (RHS)

Pass Number	Welding Current (A)	Pulse Duration (ms)	Arc Voltage (V)	Welding Speed (mm/s)	Wire Feed Rate (m/min)	Heat Input (kJ/mm)
Root	74	200	30.5	6.00	2.50	0.265
	49	800	29.0			
1	74	200	30.0	6.00	2.50	0.263
	49	800	29.0			
2	80		31.6	3.81	1.56	0.664
3	80		31.6	3.81		0.664
4	81		31.6	3.81	2.00	0.672
5	81		31.0	3.81	2.00	0.659
6	81		32.0	3.81	1.97	0.680
7	81		32.0	3.81	1.98	0.680
8	81		31.1	3.81	1.97	0.661
9	81		31.2	3.81	1.97	0.663
10	81		31.5	3.81	1.97	0.670
11	81		31.0	3.81	1.97	0.659
12	81		31.0	3.81	1.97	0.659
13	81		31.0	3.81	1.99	0.659
14	81		31.0	3.81	1.98	0.659

SAF 2507
1bar (LHS)

Pass Number	Welding Current (A)	Pulse Duration (ms)	Arc Voltage (V)	Welding Speed (mm/s)	Wire Feed Rate (m/min)	Heat Input (kJ/mm)
Root	146	500	13.8	1.05	1.48	1.439
	78	500	12.9			
1	177		13.6	2.50	1.97	0.963
2	177		13.7	2.50	1.97	0.970
3	177		13.7	2.50	1.97	0.970
4	177		13.8	2.50	1.97	0.977
5	177		14.2	2.50	1.97	1.005
6	177		13.9	2.50	1.50	0.984
7	177		13.7	2.50	1.97	0.970
8	177		13.8	2.50	1.96	0.977
9	177		14.0	2.50	1.97	0.991

SAF 2507
1bar (RHS)

Pass Number	Welding Current (A)	Pulse Duration (ms)	Arc Voltage (V)	Welding Speed (mm/s)	Wire Feed Rate (m/min)	Heat Input (kJ/mm)
Root	146	500	13.9	1.00	1.33 - 1.20	1.549
	78	500	13.7			
1	177		13.9	2.50	1.97	0.984
2	177		14.1	2.50	1.98	0.998
3	177		13.6	2.50	2.01	0.963
4	177		13.7	2.50	1.98	0.970
5	177		14.2	2.50	1.97	1.005
6	177		14.0	2.50	1.98	0.991
7	177		13.8	2.50	1.97	0.977
8	177		14.0	2.50	1.97	0.991

SAF 2507
2bar (LHS)

Pass Number	Welding Current (A)	Pulse Duration (ms)	Arc Voltage (V)	Welding Speed (mm/s)	Wire Feed Rate (m/min)	Heat Input (kJ/mm)
Root	146	500	15.4	1.31	2.04	1.281
	78	500	14.2			
1	177		15.6	2.83	1.99	0.976
2	177		16.0	2.83	2.01	1.001
3	177		15.8	2.83	2.00	0.988
4	177		15.8	2.83	2.00	0.988
5	177		16.3	2.83	2.00	1.019
6	177		16.1	2.83	2.00	1.007
7	177		15.8	2.83	2.00	0.988
8	177		15.9	2.83	2.00	0.994

SAF 2507
2bar (RHS)

Pass Number	Welding Current (A)	Pulse Duration (ms)	Arc Voltage (V)	Welding Speed (mm/s)	Wire Feed Rate (m/min)	Heat Input (kJ/mm)
Root	146	500	15.5	1.31	2.00	1.278
	78	500	13.9			
1	177		15.8	2.83	1.99	0.988
2	177		15.7	2.83	1.98	0.982
3	177		15.8	2.83	1.99	0.988
4	177		16.1	2.83	1.99	1.007
5	177		16.3	2.83	1.99	1.019
6	177		16.1	2.83	1.99	1.007
7	177		16.3	2.83	1.99	1.019
8	177		15.6	2.83	1.99	0.976

SAF 2507
4bar (LHS)

Pass Number	Welding Current (A)	Pulse Duration (ms)	Arc Voltage (V)	Welding Speed (mm/s)	Wire Feed Rate (m/min)	Heat Input (kJ/mm)
Root	146	500	16.8	1.40	1.49	1.299
	78	500	15.2			
1	177		17.1	3.10	2.01	0.976
2	177		16.8	3.10	1.98	0.959
3	177		16.8	3.10	2.01	0.959
4	177		17.1	3.10	2.01	0.976
5	177		17.3	3.10	2.01	0.988
6	177		17.4	3.10	2.01	0.993
7	177		17.0	3.10	2.01	0.971
8	177		17.2	3.10	2.00	0.982
9	177		17.0	3.10	2.00	0.971

SAF 2507
4bar (RHS)

Pass Number	Welding Current (A)	Pulse Duration (ms)	Arc Voltage (V)	Welding Speed (mm/s)	Wire Feed Rate (m/min)	Heat Input (kJ/mm)
Root	146	500	16.5	1.40	1.49	1.278
	78	500	15.0			
1	177		17.1	3.10	1.99	0.976
2	177		17.1	3.10	1.99	0.976
3	177		16.9	3.10	1.99	0.965
4	177		16.9	3.10	1.99	0.965
5	177		17.0	3.10	1.99	0.971
6	177		17.1	3.10	1.99	0.976
7	177		17.0	3.10	2.00	0.971
8	177		17.4	3.10	1.99	0.993
9	177		17.3	3.10	1.99	0.988

SAF 2507
8bar (LHS)

Pass Number	Welding Current (A)	Pulse Duration (ms)	Arc Voltage (V)	Welding Speed (mm/s)	Wire Feed Rate (m/min)	Heat Input (kJ/mm)
Root	107	350	19.8	3.00	2.00	0.472
	59	650	17.6			
1	119		19.7	3.00	2.00	0.781
2	119		19.7	2.30	2.01	1.019
3	119		19.2	3.00	2.01	0.762
4	119		19.2	3.00	2.00	0.762
5	119		19.5	3.00	2.01	0.774
6	119		19.2	3.00	2.01	0.762
7	119		19.4	3.00	2.01	0.770
8	119		19.4	3.00	2.01	0.770
9	119		19.5	3.00	2.02	0.774
10	119		19.8	3.00	2.01	0.785

SAF 2507
8bar (RHS)

Pass Number	Welding Current (A)	Pulse Duration (ms)	Arc Voltage (V)	Welding Speed (mm/s)	Wire Feed Rate (m/min)	Heat Input (kJ/mm)
Root	107 59	350 650	18.4 17.6	3.00	2.00	0.455
1	120		19.5	3.00	2.00	0.780
2	119		19.4	2.30	2.00	1.004
3	119		19.8	3.00	1.99	0.785
4	119		19.8	3.00	2.00	0.785
5	119		19.5	3.00	2.00	0.774
6	119		19.2	3.00	1.99	0.762
7	119		19.3	3.00	2.00	0.766
8	119		19.4	3.00	2.00	0.770
9	119		19.7	3.00	2.00	0.781
10	119		17.7	3.00	2.00	0.702

SAF 2507
16bar (LHS)

Pass Number	Welding Current (A)	Pulse Duration (ms)	Arc Voltage (V)	Welding Speed (mm/s)	Wire Feed Rate (m/min)	Heat Input (kJ/mm)
Root	74	250	22.4	4.00	1.97	0.306
	49	750	22.0			
1	74	250	23.6	4.00	1.98	0.323
	49	750	23.3			
2	100		25.0	3.31	1.99	0.755
3	100		24.9	3.31	1.98	0.752
4	100		24.6	3.31	1.98	0.743
5	100		24.5	3.31	1.98	0.740
6	100		24.5	3.31	1.98	0.740
7	100		24.5	3.31	1.97	0.740
8	100		24.5	3.31	1.98	0.740
9	100		24.5	3.31	1.97	0.740
10	100		24.7	3.31	1.97	0.746
11	100		24.7	3.31	1.98	0.746

SAF 2507
32bar (LHS)

Pass Number	Welding Current (A)	Pulse Duration (ms)	Arc Voltage (V)	Welding Speed (mm/s)	Wire Feed Rate (m/min)	Heat Input (kJ/mm)
Root	74	200	31.5	6.00	2.00	0.280
	49	800	31.0			
1	74	200	31.0	4.00	2.00	0.409
	49	800	30.0			
2	81		31.0	3.81	1.98	0.659
3	81		31.0	3.81	1.98	0.659
4	81		31.0	3.81	1.98	0.659
5	81		31.0	3.81	1.98	0.659
6	81		31.0	3.81	1.98	0.659
7	81		31.7	3.81	1.98	0.674
8	81		31.0	3.81	1.98	0.659
9	81		31.0	3.81	1.98	0.659
10	81		31.5	3.81	1.98	0.670
11	81		31.4	3.81	1.99	0.668
12	81		31.5	3.81	1.98	0.670

SAF 2507
32bar (RHS)

Pass Number	Welding Current (A)	Pulse Duration (ms)	Arc Voltage (V)	Welding Speed (mm/s)	Wire Feed Rate (m/min)	Heat Input (kJ/mm)
Root	74	200	31.5	5.5	2	0.306
	49	800	31.0			
1	74	200	30.0	4.00	1.50	0.409
	49	800	30.4			
2	81		31.0	3.81	1.98	0.659
3	81		31.0	3.81	1.98	0.659
4	81		31.0	3.81	1.99	0.659
5	81		31.0	3.81	1.99	0.659
6	81		31.0	3.81	2.01	0.659
7	81		31.0	3.81	2.00	0.659
8	81		31.0	3.81	1.99	0.659
9	81		31.0	3.81	2.00	0.659
10	81		31.0	3.81	2.04	0.659
11	81		31.0	3.81	1.99	0.659
12	81		31.0	3.81	1.99	0.659

Zeron 100
1bar (LHS)

Pass Number	Welding Current (A)	Pulse Duration (ms)	Arc Voltage (V)	Welding Speed (mm/s)	Wire Feed Rate (m/min)	Heat Input (kJ/mm)
Root	145	500	13.9	1.13	1.5	1.323
	78	500	12.5			
1	149		13.5	2.00	0.68	1.006
2	149		13.4	2.00	0.68	0.998
3	149		13.5	2.00	0.68	1.006
4	177		13.9	2.50	1.98	0.984
5	178		14.1	2.50	1.99	1.004
6	177		13.8	2.50	1.99	0.977
7	178		14.1	2.50	1.99	1.004
8	177		14.2	2.50	1.97	1.005

Zeron 100
2bar (RHS)

Pass Number	Welding Current (A)	Pulse Duration (ms)	Arc Voltage (V)	Welding Speed (mm/s)	Wire Feed Rate (m/min)	Heat Input (kJ/mm)
Root	146	500	15.5	1.13	1.64	1.481
	78	500	13.9			
1	178		16.2	2.83	2.00	1.019
2	178		16.0	2.83	1.97	1.006
3	177		15.7	2.83	1.95	0.982
4	177		15.7	2.83	1.99	0.982
5	177		15.7	2.83	1.96	0.982
6	177		15.6	2.83	1.97	0.976
7	177		15.8	2.83	1.97	0.988
8	177		16.0	2.83	2.00	1.001

Zeron 100
2bar (RHS)

Pass Number	Welding Current (A)	Pulse Duration (ms)	Arc Voltage (V)	Welding Speed (mm/s)	Wire Feed Rate (m/min)	Heat Input (kJ/mm)
Root	146	500	15.9	1.28	1.50	1.343
	78	500	14.3			
1	178		16.1	2.83	1.96	1.013
2	178		15.9	2.83	1.98	1.000
3	177		15.9	2.83	1.98	0.994
4	177		15.9	2.83	2.00	0.994
5	177		15.7	2.83	1.98	0.982
6	177		15.8	2.83	2.01	0.988
7	178		16.0	2.83	2.00	1.006
8	177		15.7	2.83	2.01	0.982

Zeron 100
4bar (LHS)

Pass Number	Welding Current (A)	Pulse Duration (ms)	Arc Voltage (V)	Welding Speed (mm/s)	Wire Feed Rate (m/min)	Heat Input (kJ/mm)
Root	106 59	350 650	17.50 17.50	3.5	2.00	0.377
1	106 59	350 650	17.50 17.50	3.5	2.00	0.377
2	177		17.50	3.1	2.00	0.999
3	176		17.10	3.1	2.00	0.971
4	176		17.10	3.1	2.00	0.971
5	176		17.10	3.1	2.00	0.971
6	176		17.40	3.1	2.00	0.988
7	176		17.20	3.1	2.00	0.977
8	176		17.10	3.1	2.00	0.971
9	177		17.30	3.1	2.00	0.988
10	177		17.10	3.1	2.00	0.976
11	177		17.00	3.1	2.00	0.971

Zeron 100
8bar (LHS)

Pass Number	Welding Current (A)	Pulse Duration (ms)	Arc Voltage (V)	Welding Speed (mm/s)	Wire Feed Rate (m/min)	Heat Input (kJ/mm)
Root	106	350	19.0	3.60	2.00	0.398
	59	650	19.0			
1	119		19.7	3.00	1.99	0.781
2	119		18.7	3.00	2.00	0.742
3	119		18.7	3.00	2.00	0.742
4	119		18.7	3.00	2.00	0.742
5	119		19.5	3.00	1.99	0.774
6	119		19.5	3.00	1.99	0.774
7	119		19.8	3.00	1.99	0.785
8	119		19.7	3.00	1.98	0.781
9	119		19.7	3.00	1.99	0.781
10	119		19.5	3.00	1.98	0.774
11	119		19.6	3.00	2.02	0.777
12	119		19.7	3.00	1.99	0.781

Zeron 100
8bar (RHS)

Pass Number	Welding Current (A)	Pulse Duration (ms)	Arc Voltage (V)	Welding Speed (mm/s)	Wire Feed Rate (m/min)	Heat Input (kJ/mm)
Root	106	350	18.7	3.50	2.00	0.374
	59	650	16.0			
1	119		19.0	3.00	2.00	0.754
2	119		19.0	3.00	2.00	0.754
3	119		18.7	3.00	2.00	0.742
4	119		19.8	3.00	2.03	0.785
5	119		19.9	3.00	2.04	0.789
6	119		19.5	3.00	2.03	0.774
7	119		19.9	3.00	2.00	0.789
8	119		19.8	3.00	1.98	0.785
9	119		19.3	3.00	2.00	0.766
10	119		19.9	3.00	2.01	0.789
11	119		19.6	3.00	2.00	0.775

Zeron 100
16bar (LHS)

Pass Number	Welding Current (A)	Pulse Duration (ms)	Arc Voltage (V)	Welding Speed (mm/s)	Wire Feed Rate (m/min)	Heat Input (kJ/mm)
Root	74	250	22.0	4.00	2.00	0.304
	49	750	22.0			
1	74	250	22.5	4.00	2.02	0.311
	49	750	22.5			
2	100		25.0	3.31	2.02	0.755
3	100		25.0	3.31	2.02	0.755
4	100		25.0	3.31	2.01	0.755
5	99		25.0	3.31	2.01	0.748
6	99		24.8	3.31	2.00	0.742
7	99		24.9	3.31	2.02	0.745
8	99		24.7	3.31	1.99	0.739
9	99		24.6	3.31	1.99	0.736
10	99		24.7	3.31	1.99	0.739
11	99		24.8	3.31	1.99	0.742
12	99		25.0	3.31	1.99	0.748

Zeron 100
16bar (RHS)

Pass Number	Welding Current (A)	Pulse Duration (ms)	Arc Voltage (V)	Welding Speed (mm/s)	Wire Feed Rate (m/min)	Heat Input (kJ/mm)
Root	74 49	250 750	22.5 22.5	4.00	2.00	0.311
1	74 49	250 750	22.0 22.0	4.00	2.02	0.304
2	100	25.0	3.31	2.00	0.755	
3	100	25.0	3.31	2.01	0.755	
4	99	24.8	3.31	1.99	0.742	
5	99	24.9	3.31	2.01	0.745	
6	99	25.0	3.31	2.01	0.748	
7	99	25.0	3.31	2.00	0.748	
8	99	24.8	3.31	2.01	0.742	
9	99	24.8	3.31	1.99	0.742	
10	99	24.7	3.31	1.99	0.739	
11	99	24.9	3.31	1.99	0.745	
12	99	24.7	3.31	1.99	0.739	

Zeron 100
32bar (LHS)

Pass Number	Welding Current (A)	Pulse Duration (ms)	Arc Voltage (V)	Welding Speed (mm/s)	Wire Feed Rate (m/min)	Heat Input (kJ/mm)
Root	74	200	31.3	6.00	2.50	0.276
	49	800	30.5			
1	74	200	32.0	6.00	2.50	0.281
	49	800	31.0			
2	80		31.0	3.81	1.47	0.651
3	80		31.5	3.81	1.98	0.661
4	80		31.0	3.81	1.98	0.651
5	80		31.0	3.81	1.97	0.651
6	80		31.0	3.81	1.97	0.651
7	80		31.0	3.81	1.98	0.651
8	80		31.0	3.81	1.96	0.651
9	81		31.0	3.81	1.98	0.659
10	81		31.0	3.81	1.99	0.659
11	81		31.0	3.81	1.97	0.659
12	81		31.0	3.81	1.47	0.659
13	81		31.0	3.81	1.47	0.659
Wash	81		33.5	3.81		0.712
14	81		32.0	3.81	1.98	0.680
15	81		31.7	3.81	1.98	0.674
16	81		30.5	3.81	1.98	0.648

Zeron 100
32bar (RHS)

Pass Number	Welding Current (A)	Pulse Duration (ms)	Arc Voltage (V)	Welding Speed (mm/s)	Wire Feed Rate (m/min)	Heat Input (kJ/mm)
Root	74	200	31.2	6.00	2.50	0.264
	49	800	28.6			
1	74	200	30.0	6.00	2.50	0.270
	49	800	30.0	3.81		
2	80		31.8	3.81	1.48	0.668
3	80		31.5	3.81	1.97	0.661
4	80		31.5	3.81	1.97	0.661
5	80		31.5	3.81	1.97	0.661
6	80		31.0	3.81	1.97	0.651
7	80		31.0	3.81	1.97	0.651
8	80		31.0	3.81	1.98	0.651
9	81		31.0	3.81	1.98	0.659
10	81		31.0	3.81	2.00	0.659
11	81		31.0	3.81	1.98	0.659
12	81		31.0	3.81	1.47	0.659
13	81		31.0	3.81	1.47	0.659
14	81		31.0	3.81	1.98	0.659
15	81		31.5	3.81	1.99	0.670
16	81		31.0	3.81	1.97	0.659